Improved rock physical models for the integration of core, log and seismic data

Jun Yan

Thesis submitted for the degree of Doctor of Philosophy

Department of Geology and Geophysics

University of Edinburgh

2003

ABSTRACT

The exploration for oil and gas requires a wide variety of professional skills, and knowledge of disciplines in earth science such as geology, geophysics, petrophysics and associated reservoir engineering. Techniques of data acquisition, processing and interpretation are being used more and more frequently for reservoir characterization. This makes it possible to establish models for the development and exploitation of oil and gas fields.

Reservoir characterization is essential in modelling hydrocarbon reservoirs. This has led to the development of special techniques and increased collaboration between experts from different subject areas or fields. Data and information derived from each of these subjects are complementary in nature, so it is necessary to integrate the data from different disciplines, such as geology, geophysics, logging and production engineering.

However, the data integration technology has not been fully developed and there are many acquisition related problems yet to be solved. The main focus of this thesis is to develop modelling techniques for reservoir characterization to find ways of establishing a satisfactory connection between petrophysical techniques (core analysis and well-logging) and geophysical techniques (especially borehole seismic surveying, VSP). The work includes core, log and seismic data analyses; calibration and matching for different data types, and integrated reservoir studies. By refining the approaches in predicting reservoir parameters and rock properties in both isotropic and anisotropic porous media, an improved understanding on reservoir characterization has been achieved.

In this thesis, I find

- The P- and S-wave velocities can be used to provide a suitable link between reservoir parameters and rock properties. Data integration plays a significant role in

the use of core, log and seismic data for the purpose of reservoir characterization.

- The pore aspect-ratios as the key parameters of rock geometry can be used to explain the different responses of elastic properties in clay-sand rocks (especially for thin and varying lithology formations). The use of fixed aspect-ratio for physical velocity models will result in obvious errors in the prediction of elastic moduli and velocities (in particular for formations at shallow depth, or in unconsolidated and thin layers).

- The time-average equation (Wyllie *et al.*, 1956) ignores the effects of pore geometry, degree of consolidation, fluid and clay content. It results in a hidden defect in the transformation between porosity (from core and well-log) and velocity (from seismic) for rocks with high clay content.

- The current available models of Gassmann (1951), Kuster and Toksöz (1974) and Xu and White (1995) have difficulties in calculating elastic moduli for rocks containing aligned pores and minerals in anisotropic formations.

For the aim of data integration and investigate these problems above, firstly, I use a method of multiple regression to combine with the results of artificial neural networks in order to establish an empirical correlation between reservoir parameters and P- and S-wave velocities. This correlation includes porosity, clay content, aspect-ratios and velocities. Hence, this method can be regarded as an extension of Han *et al.* (1986) model, and it is called improved empirical model or the semi-empirical model in this thesis.

Secondly, in order to overcome the weakness of my empirical model, the more realistic theoretical models are introduced firstly, and then, an isotropic dual porosity model is developed. The aim is to develop a practical rock physical model which can provide a satisfactory integrated approach for the evaluation and prediction of reservoir

parameters and rock properties in isotropic rocks. This model is called Isotropic Dual Porosity model (IDP).

Thirdly, because the IDP model ignores the effects of orientation of pores and inclusions in isotropic rocks, it cannot be used to predict rock properties and shear wave velocity in anisotropy rocks. To overcome the weakness, a refined Anisotropic Dual Porosity model (ADP) is then developed for anisotropic porous media.

Fourthly, a series of practical techniques are presented to match and calibrate different types of data for the purpose of data integration, which is a uniform body with the models I have developed in this thesis. These technique and approach include core data correction, log editing and seismic data analysis.

Finally, the comprehensive field data sets from the North Sea are analysed to demonstrate the application of techniques developed in this thesis to solve practical problems.

ACKNOWLEDGEMENTS

A PhD thesis such as this is never a one-man effort. Many people have helped me in different ways.

In 1998, when I began my PhD study in Edinburgh, I was very lucky to have supervisors in the University of Edinburgh and British Geological Survey (BGS). I would like to express my sincere gratitude to Dr. Enru Liu and Professor Xiang-Yang Li of the BGS. None of this research would have been possible without their enthusiasm, support and guidance. I am greatly indebted to both of them for their time, effort and patience through the years. I am grateful to Dr. Roger Scrutton, my university supervisor, for his guidance, invaluable suggestions and his borehole geophysics course that I attended. Without Roger, it would have been impossible to complete my PhD study.

I offer my heartfelt thanks to the following people:

* To Professor Colin MacBeth (Heriot-Watt University), who was one of my supervisors in my first year PhD study when he worked at the BGS.

* To a number of staff at the Edinburgh Anisotropy Project (EAP) at the BGS: much gratitude to Hengchang Dai, Mark Chapman, Frank Ohlsen and IT staff. In particular, the software and system problems were solved with the assistance of Dr. Hengchang Dai, who provided help on many occasions during the period of my thesis corrections.

* To my friends and fellow PhD students at BGS: Yi-Jie Liu, Jianxin Yuan, Peter Hanssen, Fabian Borocin, Anna Droujinina and Jack Wang. Both Yi-Jie and Jianxin shared with me for three years of PhD study, and many useful ideas and suggestions were obtained from our talking.

* To John Lovell, who read this thesis and provided very important corrections and useful suggestions.

* To Phillips Petroleum Company, Norway for providing some of the field data, and for permission to publish the data. This work was supported by the Natural Environment Research Council of UK and the industrial sponsors of the EAP: Agip, BGS, BP Amoco, Chevron, Conoco, Norsk Hydro, PGS, Phillips, Schlumberger, Shell, Texaco, Trade Partners UK and Veritas DGC.

* To my family, my wife Hong and my daughter Jie. Words cannot express...

Contents

Notations and conventions

The mathematical variables and other abbreviations that are used throughout the thesis are explained here. They are arranged by chapters in the order of their appearance.

General

Symbol	Meaning
ADP	Anisotropic Dual Porosity model
AR	Pores Aspect-Ratio
BPNN	Back Propagation Neural Network
CPI	Computer Process Interpretation for log data
DEM	Differential Affective Medium
IDP	Isotropic Dual Porosity model
K-T	Kuster-Toksöz model (1974)
PADP	Preliminary Anisotropic Dual Porosity model (or called IDP)
P- and S-wave	Compressional wave and Shear wave
SCA	Self Consistent Approximation
TIV	Transverse Isotropy with a Vertical symmetry axis
TVD	True Vertical Depth
VSP	Vertical Seismic Profiles
X-W	Xu-White model (1995)

Chapter 2

Symbol	Meaning	Unit
M	effective elastic modulus	GPa
M_v	average effective elastic modulus	GPa
K	effective bulk modulus	GPa
μ	effective shear modulus	GPa
K_m	bulk moduli of solid matrix	GPa
K_f	bulk moduli of fluid	GPa
ϕ	porosity	decimal
V_p	P-wave velocity	m/s
V_s	S-wave velocity	m/s
t	total travel-time	s
D	total constituents	
$\overline{V}$	average velocity	m/s
V_m	compressional velocity in rock matrix	m/s
V_f	compressional velocity in pore fluid	m/s
ρ	density	g/cm^3
ρ_b	bulk density	g/cm^3
ρ_m	matrix density	g/cm^3
ρ_f	fluid density.	g/cm^3

Symbol	Meaning	Unit
V_{cl}	clay content	decimal
V_{sh}	shale (clay) content	decimal
α	aspect-ratio	
f_1, f_2	volume fractions	
$T_{iijj}(\alpha_s)$	functions of the aspect-ratio for sand pores by K-T model	
$T_{ijij}(\alpha_c)$	functions of the aspect-ratio for clay pores by K-T model	
β	Biot coefficient 1	
δ	Biot coefficient 2	
ν	Poisson's ratio	
ε	crack density parameters	
S_{ijkl}	effective elastic compliance tensor	$(MPa)^{-1}$
β_{fl}	compressibility of pore fluid	
$S_{ijkl}^{(day)}$	effective elastic compliance tensor for dry rock	$(MPa)^{-1}$
$S_{ijkl}^{(sat)}$	effective elastic compliance tensor for saturated rock	$(MPa)^{-1}$
C^{SCA}	elastic effective stiffness tensor	MPa
σ_T^2	traveltime variance	
σ_S^2	slowness variance	
R_o	rock resistivity with 100% water	*ohm-m*
R_w	formation water resistivity	*ohm-m*

Symbol	Meaning	Unit
GR	gamma-ray log	api
GR_{ma}	value of gamma-ray log for clean sand	api
GR_{sh}	value of gamma-ray for clean shale	api
R_t	true formation resistivity	$ohm\text{-}m$
F	formation resistivity factor	
m	cementing factor	
I	resistivity index	
a	Archie's factor	
n	saturation exponent	
k	permeability	mD
ϕ_N	neutron log porosity	decimal
ϕ_D	density log porosity	decimal
ϕ_S	sonic log porosity	decimal
b	coefficient of Rider equation	
ε	Thomsen parameter by $(C_{11} - C_{33})/2C_{33}$, ($P$-wave)	
γ	Thomsen parameter by $(C_{66} - C_{44})/2C_{44}$, ($S$-wave)	
δ	Thomsen parameter by $\frac{(C_{13}+C_{44})^2-(C_{33}-C_{44})^2}{2C_{33}(C_{33}-C_{44})}$	
C_{ij}	elastic constant	

Chapter 3

Symbol	Meaning	Unit
ϕ	rock or formation porosity	decimal
V_p	P-wave velocity	m/s
V_s	S-wave velocity	m/s
V_f	velocity in the pore fluid	m/s
V_m	compressional velocity in matrix.	m/s
V_{cl}	clay content	decimal
$T(\alpha)$	aspect-ratio function	
V	velocity	m/s
x_i	inputs of neural network	
x_j	outputs of neural network	
$m_l^{[1]}$, $m_l^{[2]}$	linking weights of network	
Q	vector pair	
W^o, W^h.	weight matrices	
CAL	caliper log	$inch$
GR	gamma-ray log	api
DEN	density log	g/cm^3
DT	sonic log	$\mu s/m$
r^2	standard calculated error	

Chapter 4

Symbol	Meaning	Unit
ρ	density value	g/cm^3
GR	rock gamma-ray value	api
ϕ	total effective porosity	decimal
ψ	clay volume	decimal
T_s^p	P-wave transit time of sand grains	$\mu s/m$
T_s^s	S-wave transit time of sand grains	$\mu s/m$
T_{sh}^p	P-wave transit time of clay particles	$\mu s/m$
T_{sh}^s	S-wave transit time of clay particles	$\mu s/m$
α_s	aspect-ratio for sand related pores	decimal
α_c	aspect-ratio for clay related pores	decimal
K_d	bulk moduli for dry frame	$kg/m.s^2$
μ_d	shear moduli for dry frame	$kg/m.s^2$
K_m	bulk moduli for mixture	$kg/m.s^2$
μ_m	shear moduli for mixture	$kg/m.s^2$
V_p	P-wave velocity	m/s
V_s	S-wave velocity	m/s
V_m	compressional velocity in matrix.	m/s
$PADP$	or called as IDP model	

Symbol	Meaning	Unit
V_ψ	P-wave velocities in pure clay	m/s
V_{sa}	P-wave velocities in pure sand	m/s
V_f	velocity in the pore fluid	m/s
$T_{iijj}(\alpha)$	function of the aspect-ratio	
Δw_{ijk}	variation of weight connection in BPNN	
η	learning rate in BPNN	decimal

Chapter 5

Symbol	Meaning	Unit
m	anisotropic coefficient by $m = \frac{V_{s2}-V_{s1}}{\overline{V}}$	decimal
V_{sx}	velocities of shear-wave in X directions	m/s
V_{sy}	velocities of shear-wave in Y directions	m/s
$\overline{V}$	average velocity	m/s
σ_{ij}	linearly proportional to the strain ε_{ij}	
C_{ijlk}	fourth-rank tensor	
θ	propagating angle	*degree*
$V_p(\theta)$	phase velocity of a compressional wave	m/s

Symbol	Meaning	Unit
$V_p(\theta)$	phase velocity of a compressional wave	m/s
$V_{SH}(\theta)$	phase velocity of Vs polarization in horizontal direction	m/s
$V_{SV}(\theta)$	phase velocity of Vs polarization in vertical direction	m/s
$D(\theta)$	phase velocities of P- and SV waves	m/s
ε	anisotropic parameter by Thomsen 1986	
γ	anisotropic parameter by Thomsen 1986	
δ	anisotropic parameter by Thomsen 1986	
K^*	effective bulk moduli	GPa
μ^*	effective shear moduli	GPa
ρ	density value	g/cm^3
Q	geometric factor	
P	geometric factor	
$S_{ijkl}^{(dry)}$	elastic compliance tensor of dry rock	$(MPa)^{-1}$
$S_{ijkl}^{(sat)}$	elastic compliance tensor of saturated rock	$(MPa)^{-1}$
$S_{ij\alpha\alpha}^{0}$	elastic compliance tensor of mineral material	$(MPa)^{-1}$
β_{fl}	compressibility of pore fluid	
β_L, β_G	compressibility of the liquid phase	
β_L, β_G	compressibility of the gas phase	

Chapter 6

Symbol	Meaning	Unit
δ	angle of hole deviation	*degree*
h	depth	*metre*
dz	vertical distance of a deviated well	*metre*
dh	deviation distance of a deviated well	*metre*
$log*$	generated new log curves	log unit
Log_{nor}	normalized log value	log unit
σ	root-mean-square error	decimal
COR	the core value after filtering	
T_{H_0}	time of log starting depth	*s*
T_i	interval transit time from sonic log or dipole log	*s*
ΔH	depth sampling interval	m*etre*
T	dual transit time	*s*
Δt	acoustic transit time	*s*
$f(z)$	filtering factor	
α	filtering coefficient-1	
β	filtering coefficient-2	
γ	filtering coefficient-3	

Chapter 7

Symbol	Meaning	Unit
m	anisotropy coefficient by shear-wave	
DT	sonic log	$\mu s/m$
ρ	bulk density from density log	g/cm^3
ρ_{ma}	matrix density	g/cm^3
ρ_f	fluid density	g/cm^3
ΔGR	gamma-ray log index	
GR	measured value of gamma-ray log	api
GR_{sh}	gamma-ray value of shale formation	api
GR_{ma}	gamma-ray values of pure sand	api
V_{cl}	clay content	decimal
S_{sh}	shale content	decimal
K	permeability	mD
S_w	water saturation	decimal
R_0	rock resistivity containing 100% water	$ohm\text{-}m$
R_w	water resistivity	$ohm\text{-}m$
S_o	oil saturation	decimal
R_t	formation true resistivity	$ohm\text{-}m$

Chapter 1

INTRODUCTION

1.1 Objectives of the work

Data integration has been one of the most valuable ideas in the exploration and development of the oil-gas industry. Professionals of various disciplines, such as geology, geophysics, petrophysics and reservoir engineering, have been working together to search for synergy and to integrate their individual pieces of work.

Seismic surveys and sonic logging are based on the same laws of wave propagation but using different methodology. We often use seismic data to obtain P- and S-wave velocities and hence Vp/Vs ratios. These values in turn are used for lithology prediction and analysis of fluid substitution. Under certain conditions, seismic measurements can be used to improve knowledge of reservoir characteristics. In contrast, well-logging has a very different vertical and lateral range of investigation compared with seismic surveys (surface or borehole), and can be used to estimate reservoir parameters and velocities. One obvious benefit of using well-log data is its ability to link with core data. In order to understand the effects of fluid and lithology variation on elastic wave velocities, various theories and models have been proposed. This results in the possibility of relating geology with reservoir engineering to improve understanding of reservoir characterization.

Core analysis, well-log measurement and seismic survey cover different frequency bands (e.g. acoustic logs: in the order of 10 kHz; seismic: ranging from 10 to hundred Hz). A number of publications have shown that velocities can provide a direct and usable link between core data, well-log data and seismic data (VSP). However, rock velocities are affected by numerous geologic factors such as rock matrix, mineralogy, porosity, pore geometry, pore fluid, bulk density, effective stress, depth, type and degree of cementing, and orientation of fracturing. In order to understand how rock properties influence velocity and what their relationships are, the data integration is essential for reservoir studies.

Under certain conditions, we may use empirical or physical models to determine reservoir parameters, and rock properties as well. However, how can we use these parameters or properties to predict the lithology in an oil-gas reservoir? Can we do better than just predicting velocities, porosity and other parameters? Can we build the relationship between rock properties and reservoir parameters for the purpose of integrated reservoir studies? Can we consider the various effects such as pore geometry, pore orientation, fluid and clay contents? In order to answer these questions, an important matter is to find out approaches which suitable for various reservoir conditions and requirements so that the methods of data integration can be used effectively for reservoir characterization. Therefore, the ultimate aim of this study is to develop a set of methods which provide a satisfactory link between seismic, well log and core data to build relationships between rock properties and reservoir parameters for integrated studies in both isotropic and anisotropic porous media.

The broad theme of this thesis is to explore the response of different measurements using data integration methods and to understand how they relate to petrophysical parameters in reservoir studies. This understanding is the key to using core, well-log and seismic data. The unique aspect of this work is to focus on connecting measurements,

observations and velocities with rock physics for the purpose of reservoir characterization. Therefore, this study will establish usable rock physical models for various geological environments and highlight the most for the aspect of diagnostic. These principles will be carried through to their manifestations in measurements, borehole and VSP responses, in order to understand the role of experimental petrophysics and well-logs in constraining the seismic interpretation.

1.2 Current status

Outside the laboratory the most petrophysical properties cannot be measured directly, therefore they must be inferred from the measurement of other parameters, such resistivity, bulk density, interval transit time, spontaneous potential, natural radioactivity and hydrogen content of the reservoir rock. In order to achieve this goal, well-log data are often combined with core data, and then linked with seismic data for practical application purpose. A successful data integration can supply subsurface structural mapping, define the lithology, identify the productive zones and accurately describe their depths and thickness, distinguish between oil and gas, and permit a valid quantitative and qualitative interpretation of reservoir characteristics, such as fluid saturation, porosity, permeability and velocities.

To build a quantitative relationship between rock properties (e.g. velocities and elastic constants) and reservoir parameters (e.g. porosity, clay content, permeability, saturation etc.), various theories and approaches have been proposed since the pioneer work of Gassmann (1951); and Biot (1956a,b). In the 1980s, logging companies developed tools that record the entire seismic waveforms. These tools record the wave trains at more than one receivers, and then use some types of semblance processing algorithms to determine the arrival times of the wave trains. Full-waveform recordings contain information on the amplitude and phase of the signals. During this period,

owing to considerable technological and scientific advances, development of recording techniques removed a large number of assumptions and general corrections. For example, the dipole sonic log can now provide shear-wave information directly, which leads to a change from a correlation tool for geologists to an indispensable data source for reservoir studies.

During the 1990s, a number of theoretical models were published to analyze the relationship between reservoir parameters and rock properties. These can be divided into two types, the models for isotropic porous media, such as Xu and White (1995a, b; 1996), and the models for anisotropic rocks, such as Mukerji and Mavko (1994) and Hornby (1994). Note that the advantages and the limitations of these models above will be discussed in Chapter 2.

Up to now, various theoretical models have been proposed to study elastic wave propagation and reservoir parameters in isotropic and anisotropic porous rocks for the purpose of reservoir characterization. The theories and models mentioned above give a reasonably good estimation and correlation between rock properties and reservoir parameters. These approaches and models are very useful for the prediction of elastic moduli, velocities and reservoir parameters in different ways, however there are no suitable models that can be used for integrating core, well-log and seismic data. Most of the available models are strictly applicable only within certain conditions, such as in pure sand or pure shale rocks and single fluid phases. Accordingly, these models may be used for predicting reservoir parameters or rock properties only within a limited range of application, and some require specific parameters which can only be measured in the laboratory while others require more knowledge than what is possible to provide. Since it is well-known that the most rocks are found experimentally to be anisotropic. This anisotropy refers to different elastic properties in different directions, where the number of independent constants are controlled by the symmetry causing the anisotropy.

Therefore, it is needed for a further research to tackle these problems.

1.3 Main achievements of the research

New findings and achievements have been obtained in this thesis, and are briefly summarised below:

(a) Rock geometry parameters (e.g. aspect-ratios) have been introduced into empirical model to build the relationship between velocities, porosity, clay content and aspect-ratio.

Han's *et al.* (1986) model plays a significant role in establishing the relationship of porosity, clay and velocity, but the aspect-ratio (pore geometry parameter) may help us to explain the different rock response in clay-sand formations (containing fluid such as gas etc.).

(b) ***Two extended time-average formulae are developed to replace Wyllie et al. (1956) equation to link porosity with velocity.***

The time-average equation gives a useful relationship between total travel time (velocity) and porosity in the two-components system. This equation requires that the formation should be a clean sand rock; if clay is contained in the sand formation it will affect porosity and velocity. To overcome this weakness, I have defined the clay content as an independent component, so that the sand formation containing clay can be equivalent to a dual-porosity model, e.g. (1) the lithology property formula is used to calculate clay content; and (2) the physical property formula is used to calculate porosity considering clay influence.

(c) Two varying pore aspect-ratios derived from a neural network are used to replace the fixed aspect-ratios in Xu-White (1995) model. The accuracy with which elastic properties and velocities can be predicted is therefore enhanced.

Xu-White (1995) model has been shown that it is useful for predicting elastic wave properties in clay-sand mixtures, but the weak points of this model were identified, which ignores the effects of pore geometry, degree of consolidation, fluid, clay content etc. If Xu-White model is used for loose formations, it will result in an obvious error for the prediction of elastic moduli and velocities (In particular, in shallow depth or thin-bed formations). To overcome the weaknesses above, I have proposed two main improvements below: 1) Using my extended time-average equation for lithology and physics properties. 2) Using the varying aspect-ratio to replace the fixed aspect-ratio.

(d) The new physical models are developed for practical applications in isotropic and anisotropic rocks.

Based on the suggestions above (points a, b and c), the Isotropic Dual Porosity model (IDP) is developed, which provides a practical tool for modelling elastic wave velocities and rock properties. Due to the IDP model is still only suitable for clay-sand formations in isotropic rocks, it cannot be used in anisotropic rocks (in particular, there are obvious difficulties for calculating elastic moduli when rocks contain high clay or aligned minerals). To extend this model to anisotropic rocks, the Anisotropy Dual Porosity model (ADP) extended my previous IDP mode by means of the theories of Differential Effective Medium (DEM) and Self Consistent Approximate (SCA). The ADP model can be used for predicting elastic constants and velocities in anisotropy rocks, and for anisotropy evaluation as well.

(e) The procedure of data preparation and calibration is built as a uniform body of data integration.

To apply my empirical and physical models for the purpose of reservoir characterization, a set of approaches have been built for data preparation and calibration, which is a uniform body with the models I developed. The approach can be used to match or calibrate different types of data, and can be used to determine reservoir parameters as

the models' inputs.

1.4 Definition of the concepts

1.4.1 Fundamental problems

As mentioned above, this thesis presents an integrated technique from core, well-log and seismic data to determine reservoir parameters and rock properties. The results are then used to build the relationship between the rock geophysical properties and the reservoir parameters for the application in integrated reservoir studies.

The first problem in this study is calibration. The process by which measurements are compared with known standards for the purpose of enabling the quantitative extrapolation of measurements. It requires samples for which supposedly "true" values are known in order that "right" precision may be defined. A practical calibration procedure used in this thesis is to assume that one of the datasets represents "true" values and then to adjust others to create a best fit.

Log-seismic matching is another problem which involves establishing a velocity relationship to make well-log measurements consistent with the seismic survey results. In other words, the log measurements are recalculated to be compatible with variations in fluid and lithological composition, so the integrated travel time between two depth readings can be matched with the corresponding data from the well velocity survey. A well velocity survey is carried out by measuring the travel time of the first break from a vertical seismic profile (VSP), which usually covers only a section of the well bore. A high level of precision is required for the comparison of seismic and well logging datasets, particularly in the context of reservoir studies. It is therefore necessary to apply preliminary corrections before calibration of log data with well velocity survey.

Velocities are measured at different scales by log and seismic method. They were therefore chosen as the most representative geophysical property for analysis as an ex-

ample of the average rock property behaviour. Compressional velocity data for both log and seismic data are derived using different techniques. Well-log scale data are provided by sonic velocity logging, and seismic data are derived directly from the two way transit velocities by VSP. Even though the VSP data have a poorer vertical resolution compared with well logging and a restricted frequency range, they can be used to adjust profiles obtained from seismic reflection surveys carried out at the surface.

Elastic anisotropy refers to a material having different elastic properties, such as bulk and shear moduli and velocities in different directions. The number of different or unique constants is controlled by the symmetry of the features causing the anisotropy. The features or fabric causing anisotropy in sedimentary rock include typically a preferred alignment of anisotropic minerals such as clay and quartz, fractures, stresses and the orientation of pore aspect-ratios. One of the simplest and the most ubiquitous symmetries displaying these properties is hexagonal or transverse isotropy. The main reasons in exploration and production for understanding anisotropy are: 1) laterally misplaced targets below dipping wedges of anisotropic elastic sequences; 2) effect on logging response in deviated borehole or dipping layers; 3) effect on upscaling and down-scaling core observations; 4) influence on calculation of closure stresses; 5) effect on stress concentrations around a borehole, hence stability; and 6) time to depth conversion.

Finally, an integrated reservoir study is a complex process, which involves the integration of different disciplines and needs a clearly definite objective. In this thesis, some of these aspects of in a reservoir study, which are critical to the integration process will be discussed. Most of these aspects require a change of focus with respect to the traditional way of working. In the past, the approach has been a sequential one, where geophysicist, reservoir geologist, petrophysicist and reservoir engineer worked almost independently, while the results of each one are passed to the other without significant

feedback. At present, the process of integrating different disciplines to perform an integrated reservoir study requires a change of focus. Professionals work in an interrelated way, where the feedback from other disciplines is essential to the validation of the work.

1.4.2 Basic definitions

The following basic definitions are necessary and are often mentioned in this thesis.

- *Core analysis:* Core analysis is a highly specialized phase of petroleum reservoir engineering, which provides information on geology and reservoir engineering. Porosity, permeability, shale volume, clay content and water saturation are the most common parameters measured by core analysis in the laboratory,

- *Log data:* Well-logging provides an intermediate link between the small-scale, high-resolution sediment geological and stratigraphical features visible at outcrops and the large-scale data available from seismic profiling sections. Well-log data are obtained from tools running into a borehole at the end of a cable.

- *Seismic data:* The operation of Vertical Seismic Profiles (VSP) is very similar to a check shot survey (well velocity survey) at the operational level. The VSP is a down-hole seismic operation where a seismic signal emitted at surface is recorded by a geophone situated successively at different depths in the well.

- *Reservoir parameters:* Reservoir parameters are typically related to significant spatial heterogeneity in porosity, permeability, clay content, fluid saturation and other properties.

- *Rock properties:* The rock properties in this thesis include elastic constants, bulk moduli, shear moduli, aspect-ratios, P- and S-wave velocity and the ratio of V_p and V_s.

- *BPNN:* Back Propagation Neural Network (BPNN) is employed to estimate reservoir parameters and aspect-ratio from core and log data. This neural network consists of input layer, intermediate layer (hidden layer) and output layer.

- Aspect-ratio*:* Aspect-ratio is the ratio of the shorter axis to longer axis of a pore space. There is evidence showing that the aspect-ratio significantly controls the elastic behaviour of a sand and clay mixture.

- *IDP model:* Isotropic Dual Porosity (IDP) model is an extension of Xu and White model in isotropic porous rocks. It is also called 'preliminary anisotropic dual porosity model (PADP)' or 'improved Xu-White model' in this thesis.

- *ADP model:* Anisotropic Dual Porosity (ADP) model is a rock physical model developed in this thesis, which is basically an extension of the IDP model developed in anisotropic porous rocks.

1.5 Outline of the thesis

In this thesis, I concentrate mainly on the integration of core, log and seismic data from isotropic and anisotropic rock. This thesis can been divided into four parts as:

In the first part, the profile of this thesis was given and the current methods and theories are reviewed, and the approaches of Han *et al.* (1986) and Xu-White (1995a, b; 1996) are identified as the starting point for my study in this thesis

The second part, both the improved empirical model and the isotropic dual porosity model are developed for practical applications in isotropic formations, and the anisotropic dual porosity (ADP) model is developed for anisotropic formations.

The third part, the techniques of different types of data calibration and matching are described and gives the ways for implementation, this is a uniform body with my models for the aim of application.

In the final part, a field data set from the North Sea are used to validate the develop models, and to demonstrate the use of the proposed approaches.

In details, this thesis is sub-divided into eight chapters below:

Following this chapter, Chapter 2 gives an overview of the studies on the elastic properties of rock. I have collected a number of theoretical papers on rock physics and reservoir parameters studies, a literature review has been carried out and a few approaches have been selected as a starting point in the development of a strategy toward integrated studies using core, log and seismic data. These theoretical studies can be divided into the following subjects: (1) bounding methods; (2) empirical models; (3) physical models; (4) data matching and calibration; and (5) integrated reservoir studies.

Chapter 3 is concerned with the empirical and semi-empirical approaches with an aim of building a simple but useful relationship between seismic velocities (P- and S-waves), reservoir parameters (porosity, clay content) and rock properties (aspect-ratios). The traditional statistical techniques (multiple regression) are used to identify the relationship between formation and rock properties. A back propagation neural network is then introduced to estimate reservoir parameters. The artificial neural network is obviously different from traditional statistical techniques such as the linear or non-linear regression, especially in petrophysics and formation evaluation. The main goal of this chapter is to provide a practical approach for the prediction of the P- and S-wave velocities, porosity, clay content and pore aspect-ratio by empirical methods.

Chapter 4 discusses the widely used model developed by Xu and White (1995a, b; 1996). Several improvements to this model have been made. I firstly implemented Xu-White model and tested it using field data from sonic log to find out its weakness, and then developed an isotropic dual porosity (IDP) model. The goal of this chapter

is to develop a general rock physical model that can provide a satisfactory approach to evaluate and predict the reservoir parameters and rock properties. The improvements include: (1) development of an extended time-average equation to estimate porosity and clay content; (2) using a back propagation neural network to invert pore aspect-ratios; (3) the variable aspect-ratios are used to supersede the fixed values in order to consider the effects of thin formations and variable lithology on the seismic wave velocities.

Chapter 5 presents a new physical model for anisotropic rock, which is basically an extension of the model developed in Chapter 4. Although the isotropic dual porosity model presented in Chapter 4 is a practical model for simulating elastic wave velocities and predicting reservoir parameters, and is suitable for clay-sand formations, but it is only limited to isotropic model, that can only be used for isotropic rock. Therefore, this chapter is devoted to a new approach to estimate reservoir parameters and predict rock properties in anisotropic porous media. To achieve this, I use theories of self-consistent and differential effective medium to calculate effective elastic moduli and elastic constants in rocks with randomly oriented and aligned inclusions.

Chapter 6 focuses on the data conditioning and calibration of different types of data. Core, log and seismic data are obtained, using different measurement systems. If we predict rock properties and petrophysical parameters through an integration of these data, we must consider a suitable method for data correction in order to have a satisfactory estimation in data calibration and matching. A calibration procedure is to assume that one of the datasets is corrected and to adjust others to create a best fit for core-log calibration or log-seismic calibration. Note that whilst laboratory determinations are standard by which in situ log measurements are compared, each method must be examined carefully to determine experimental limitations, accuracy and precision during testing. Also, the fact that potential mineral alteration processes can occur when a rock is sampled.

In Chapter 7, I present an integrated case study using field data from the North Sea. The purpose of this chapter is to verify the developed methodology in the previous chapters. This chapter covers the practical techniques, methods and work flows for evaluating reservoir parameters, ranging from basic laboratory and theoretical results to practical 'recipes' that can be immediately applied to field data. Several examples are presented here to demonstrate the applications of the models developed in the previous chapters, which provide effectively the validation of these models.

Finally, in Chapter 8, discussion, conclusions and expectation about possible future work are presented. This study has demonstrated that data integration plays an important role in the oil industry, particularly, for the aspects of petrophysical study, formation evaluation and reservoir characterization.

1.6 Software

1.6.1 Software used

Processing of VSP data, well-log data and analysis of rock properties (including core) in this thesis was performed by the following software:

- **PROMAX** is used to process seismic data. In particular it was used to pick seismic velocity to obtain an accurate first break picking from a three-components zero-offset VSP.

- **ANISEIS** is used for modelling studies of synthetic seismic data for comparison with the real VSP data.

- **GEOLOG** is used to process well-log data and analyse the relationship between velocity and rock properties. It was also used to output the CPI (Computer Processing Interpretation) results.

- **PETROTOOLS** is used to process core data to build the various relationships between different data based on mathematical statistical methods such as linear or non-linear regression and multi-regression.

- The graphics were made by **GnuPLOT** and **CoreDRAW**, and all text processing was done by **LyX**.

1.6.2 Programs developed

In this thesis, I have developed the following main programs.

- **BPNN** includes two main programs, **BPTRAIN** and **BPPREDICT**. These programs were used to predict reservoir parameters based on core and log data, such as porosity, clay, aspect-ratio etc. **BPTRAIN** was developed to study and train the input and output data based on well logs and measured data. **BPPREDICT** was used to predict reservoir parameters based on the training results. Both programs were derived from the theory of the back propagation neural network (BPNN).

- **XWMODEL** was developed for the implementation of Xu-White (1995) model. Its function is to predict elastic moduli as well as P- and S-wave velocities.

- **IDP** was developed to calculate elastic moduli, P- and S-wave velocities in isotropic porous rocks. Well logs and varying aspect-ratios were used as inputs. Its output is the bulk and shear moduli, P- and S-wave velocities.

- **ADP** was developed to calculate the elastic tensor, P- and S-wave velocities in anisotropic rocks. This program can also be used to predict three anisotropic coefficients.

Chapter 2

REVIEW OF ROCK PHYSICAL MODELS

2.1 Introduction

Various approaches have been proposed to establish relationships between reservoir parameters and rock properties in porous media. These include the bounding methods, empirical models and physical methods. Strictly speaking, all theories on the elastic properties of porous media are effective medium theory. These cover a wide range of materials, such as cracked solids, porous media, and multicomponent composite materials. They are used mainly by earth scientists in solving exploration problems.

For many reasons we should model or estimate the effective elastic moduli of rocks in terms of the properties of various constituent minerals and pore fluids. Numerous theories and models exist in the literature describing elastic properties and velocity. These include the effect of reservoir parameters such as porosity, pore fluid type and clay content on the wave velocities. These theories and models can be grouped for convenience of description as bounding methods, empirical models and physical models.

Both the bounding and empirical methods provide theoretical limits for the acoustic velocities of multi-phase media, but they allow forward direct applications. They are also generally very simple.

Numerous effective medium theories exist which were developed mostly by material

scientists and mechanical engineers to study elastic properties of composite materials. Some of the theories give exact analytical solutions, others give the upper and lower bounds of elastic constants. The effective medium is anisotropic under either hydrostatic or unaxial pressure. For random packing of elastic spheres, the effective medium is anisotropic only under unaxial pressure. In consolidated rocks, orientation of either elongated grains or elongated pores in a rock will result in anisotropy. Furthermore, even if the grains or cracks are randomly distributed, the application of uneven or directional stresses to the rock will yield anisotropy.

A relatively successful, and certainly popular method was developed to incorporate both small and large concentrations of inclusions to allow for interactions among the inclusions. This approach extended these specific geometry methods to cover slightly high concentration of inclusions using the self-consistent approximation. The assumption of self-consistency is that the orientation average of the inclusion strain is set equal to the overall strain, each inclusion is assumed isolated in a uniform matrix, and they are treated as having the same elastic properties as the effective medium as a whole. The effective bulk and shear moduli are coupled together in self-consistent equations.

In this chapter, the review of theories and methods is divided into the following five sections: (1) the bounding methods, employed for the effective elastic moduli and velocities calculation, (2) the empirical models, studied the relationship between reservoir parameters and velocities, (3) the physical methods, including effective medium and self consistent theories, which are applied to study elastic properties for isotropic and anisotropic rock, (4) data matching and calibration, the practical approach to achieve the integration of core, log and seismic data, and (5) integrated reservoir studies, especially for the reservoir characterization.

2.2 Effective elastic moduli: Bounding methods

The bounding methods are powerful and robust tools. They give rigorous upper and lower limits on the moduli with given composition. Generally, the gap between bounds is quite large if the phases are characterized by very different elastic moduli. Bounds find application in the estimations of the elastic moduli of rock matrices when the ratios between the elastic moduli of the individual grain phases are not too large.

2.2.1 Upper and lower bounds

Voigt (1928) proposed an initial model for studying the elastic properties, which uses the averaging method of the stress in each individual crystal in terms of a given strain. The following expression for the average elastic modulus (M_v) is given:

$$M_v = \sum_{i=1}^{n} \phi_i M_i \,, \tag{2.1}$$

where M_v is the Voigt effective modulus, which can be either the bulk modulus K_v or the shear modulus μ_v, ϕ_i and M_i are the volume fraction and the modulus of the ith component, respectively. The Voigt modulus is an algebraic average, which represents the upper bound; the measured modulus is always lower. This model assumes that the strain is uniform throughout the aggregate.

Reuss (1929) proposed a different model using the harmonic average. This model assumes uniform stress in the aggregate and is an iso-stress model. The calculated effective modulus using the Reuss model is a lower bound and the effective elastic modulus (M_r) can be expressed as

$$\frac{1}{M_r} = \sum_{i=1}^{n} \frac{\phi_i}{M_i} \,, \tag{2.2}$$

where M_r may be either the bulk modulus K_r or the shear modulus μ_r, ϕ_i and M_i are

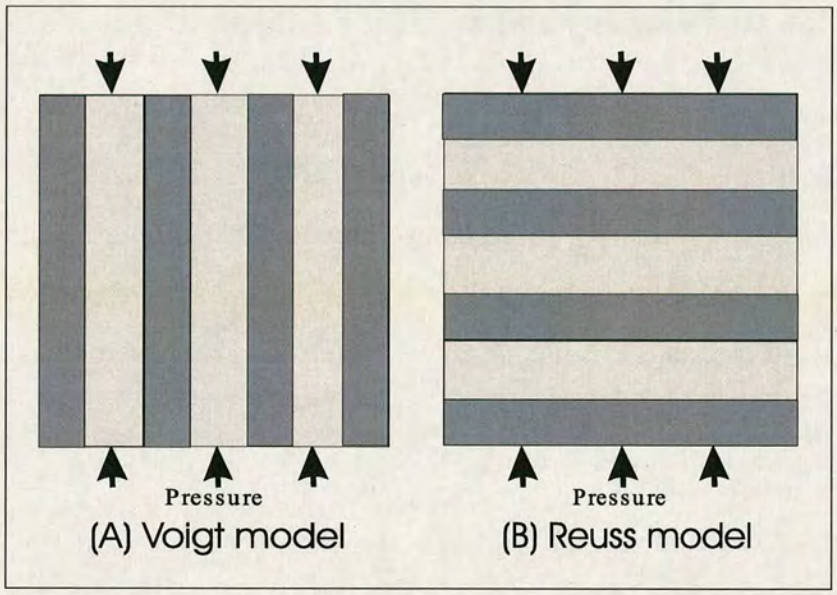

Figure 2.1: The geometric interpretations of Voigt (iso-strain) and Reuss (iso-stress) models.

the volume fraction and the modulus of the ith component, respectively.

The stress and strain are generally unknown in the composite and are expected to be nonuniform. The upper bound (Voigt) is found assuming that the strain is everywhere uniform and that stress add in parallel. The lower bound (Reuss) is found assuming that the stress is everywhere uniform and the strain add in perpendicular. The geometric interpretations are shown as Figure 2.1. This figure shows a graphic illustration of Voigt (iso-strain) and Reuss (iso-stress) models for a two-component effective medium.

Since Voigt's and Reuss's models are the upper and lower bounds respectively, an estimation of the actual value is sometimes taken as the average of the two. Thus, the Voigt and Reuss averages are interpreted as the ratio of average stress and average strain within the composite. Hill (1952) has suggested their averaging method to provide a more practical estimate of the effective moduli of rocks.

$$M_{vrh} = \frac{M_v + M_r}{2}. \tag{2.3}$$

This approach is useful for estimating the elastic moduli of a rock matrix composed of different minerals. Hill's average can also be used to estimate the bulk modulus of water saturated rocks. However it should not be used to calculate the effective moduli of gas saturated rocks and it does not provide reliable estimates for the effective shear modulus of fluid (both liquid and gas) saturated rocks (Wang and Nur, 1990).

2.2.2 Hashin and Shtrikman bounds

Hashin and Shtrikman (1963) established a set of upper and lower bounds for the effective moduli of composite materials. The inclusions can be multi phase with arbitrary geometry (not necessarily spherical or spheroidal). The materials considered are described as mechanical mixtures of a number of different isotropic and homogeneous elastic phases of arbitrary geometry. The effective media are also considered as quasi-isotropic and quasi-homogeneous.

The narrowest possible bounds on moduli that we can estimate for an isotropic material, knowing only the volume fractions of the constituents, are the Hashin-Shtrikman bounds (because Voigt-Reuss bounds are wider range), so for a mixture of two materials we have:

$$K^{HS\pm} = K_1 + \frac{f_2}{\frac{1}{(K_2-K_1)} + f_1 \cdot (\frac{1}{K_1+\frac{4}{3}\mu_1})}, \tag{2.4}$$

$$\mu^{HS\pm} = \mu_1 + \frac{f_2}{\frac{1}{(\mu_2-\mu_1)} + \frac{2f_1(K_1+2\mu_1)}{5\mu_1(K_1+\frac{4}{3}\mu_1)}}, \tag{2.5}$$

where subscript 1= shell, 2= sphere, f_1 and f_2 are the volume fractions.

These give upper bounds when K_1, μ_1 are for the stiff material and lower bounds, when K_2, μ_2 are for the soft materials. The geometric interpretations of bulk modulus

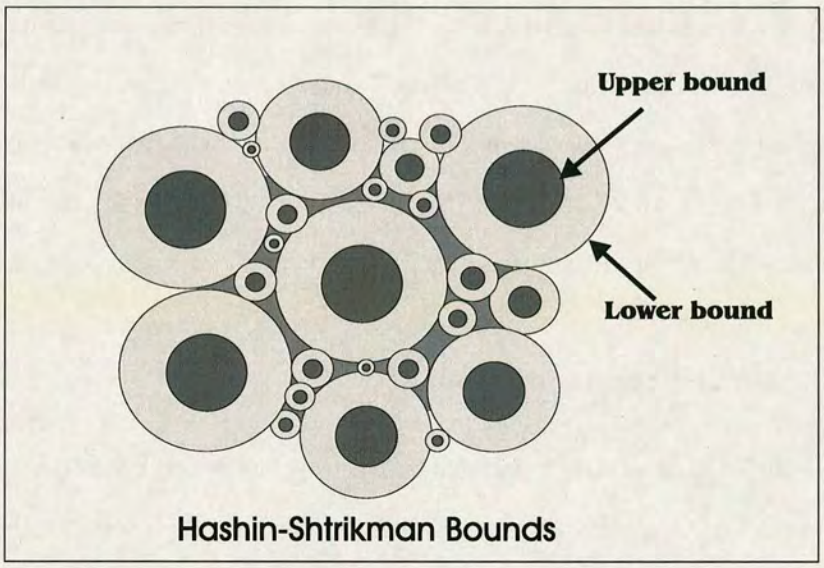

Figure 2.2: The geometric interpretations of Hashin and Shtrikman upper and lower bounds.

are shown in Figure 2.2.

According to Hashin and Shtrikman, the elastic moduli calculated by their model is closer to the measured data than the Voigt-Reuss values. In the limiting case of the highest possible upper bound and the lowest possible lower bound, the HS equations become the Voigt equation for the upper bound and the Reuss equation for the lower bound.

Generally, when the ratios between the elastic moduli of the component phase are not too large, the Hashin-Shtrikman upper and lower bounds are close to each other. Hence, this model is useful for estimating the effective moduli of the rock matrix once the mineralogical data are available.

2.2.3 Suspension models

Wood's (1930) model was derived on an isostress 'zero-frequency' basis. An understanding of the significance of Reuss's averaging method of the bulk modulus can be

gained by this equation, therefore it can be used to evaluate the bulk modulus of dilute suspensions (no physical contacts among the particle grains). In general, Wood's model can be used to estimate the bulk modulus of shallow marine sediments. However, where the particle grains of the sediments are in contact, it only provides the lower bound of the bulk modulus (Wang and Nur, 1990).

In a study of the elastic properties of physical mixtures of one or more fluids, Wood (1930) noted that the adiabatic compressibility of the mixture is equal to the sum of the individual component compressibility weighted by their proportional volumes in the total volume. In terms of bulk moduli (K), this relation can be expressed as:

$$\frac{1}{k} = \sum_{i=1}^{n} \frac{\phi_i}{K_i}, \tag{2.6}$$

where k is the bulk modulus of the suspension, K_i are the bulk moduli of the individual components and ϕ_i are the fractional volumes of each component.

The compressional velocity (V_p) can be calculated by using Wood's equation since the bulk densities are also known. However, the calculated velocities will be affected by the fluctuation of bulk density (Dunn *et al.*, 1986, Shumway, 1960 and Hamilton *et al.*,1956). These are two possible causes for the discrepancy between the laboratory measured values and prediction from Wood's equation. Firstly, the porosity and density are often measured with high uncertainties due to the nature of the core samples. Secondly, most laboratory data are measured at high frequencies (about 100 kHz), but the Wood's equation is derived as a low or 'zero-frequency', so that velocity dispersion may have arisen.

2.2.4 Composite materials

Nur *et al.* (1995) presented a critical porosity model as an extension of the models of Voigt (1928), Reuss (1929) and Wood (1930). According to Nur *et al.* (1995), when

the critical porosity for a particular material is known, it is possible to describe the relationship between porosity and velocity. At one extreme case for porosity exceeding the critical porosity value, the material behaves as a suspension and the effective bulk and shear moduli are given by the Reuss (1929) average:

$$\frac{1}{K} = \frac{(1-\phi)}{K_m} + \frac{\phi}{K_f}\,, \tag{2.7}$$

$$\mu = 0\,,$$

where K_m and K_f are the bulk moduli of the solid matrix and fluid. K and μ are the effective bulk and shear moduli and ϕ is the porosity. If the porosities are smaller than the critical porosity, the moduli rapidly increase from the suspension values at critical porosity toward the mineral values at zero porosity. This variation is approximated by Nur *et al.*(1995) as a linear trend when expressed as modulus versus porosity.

For water saturated rock:

$$K = K_m(1 - \frac{\phi}{\phi_c}) + \frac{\phi}{\phi_c}K_c\,, \tag{2.8}$$

$$\mu = \mu_m(1 - \frac{\phi}{\phi_c})\,, \tag{2.9}$$

where K_c is the Reuss average given by equation (2.7) and evaluated at the critical porosity (ϕ_c).

As described above this model does not predict a smooth behaviour of the elastic moduli in the vicinity of the critical porosity value, but it presents continuous and smooth behaviour of the P- and S-wave velocities over the entire range of porosities.

2.3 Empirical models

Empirical and semi-empirical models have the advantage of being generally very simple to use, thus allowing direct applications to be made, so that they are very popular in reservoir characterization.

2.3.1 Porosity and velocity relationship

Wyllie *et al.* (1956) found that the travel time through water saturated, consolidated rock could be approximately described as the volume weighted average of the travel time through the constituents. This empirical equation is a transformation of P-wave velocity to porosity, and it is widely used to estimate porosity from P-wave sonic logs.

The Wyllie time average equation was formulated on the fact of that the total travel-time t through alternating disks of Lucite (a plastic) and aluminium fitted very well. The equation is:

$$t = t_1 + t_2 + t_3\,, \tag{2.10}$$

because $t = \frac{D}{\overline{V}}$

$$\frac{D}{\overline{V}} = \frac{D_1}{V_1} + \frac{D_2}{V_2} + \frac{D_3}{V_3}\,, \tag{2.11}$$

so

$$\frac{1}{\overline{V}} = \frac{d_1/D}{V_1} + \frac{d_2/D}{V_2} + \frac{d_3/D}{V_3}\,, \tag{2.12}$$

$$\frac{1}{\overline{V}} = \frac{f_1}{V_1} + \frac{f_2}{V_2} + \frac{f_3}{V_3}\,, \tag{2.13}$$

where t is the total travel time, D is the total constituents, $\overline{V}$ is the average velocity in

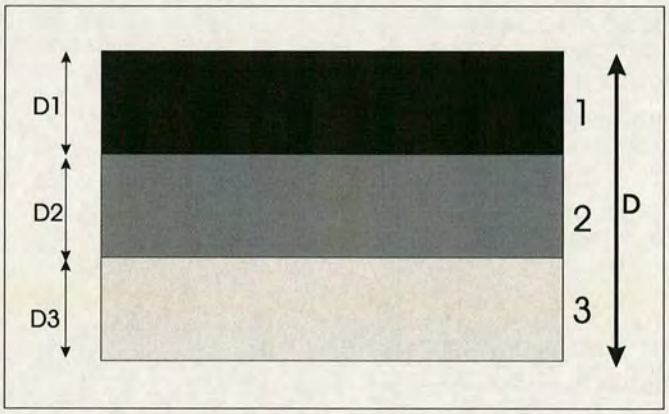

Figure 2.3: The geometric interpretations of the Wyllie (1956) *et al.* time-average model, which describes the volume weighted average of the travel time through the constituents.

total rock and f_1, f_2 and f_3 are the volume fractions. The geometric interpretation of these relationship may be shown in Figure 2.3.

For a fluid-saturated porous rock, the above equation has been reformulated as

$$\frac{1}{V_p} = \frac{\phi}{V_f} + \frac{1-\phi}{V_m}, \tag{2.14}$$

where ϕ is the porosity, V_p is the resulting average compressional velocity through the stack of disks, V_f is the velocity in the pore fluid, and V_m is the compressional velocity in the rock matrix.

Since its inception, the Wyllie time average relationship has been used to derive porosity from sonic log measurements. Generally, Wyllie's equation works well for (1) water-saturated rocks, (2) consolidated rock and (3) high external stress. But its limitations are: (1) the rock should be isotropic, (2) the rock must be fluid-saturated under high effective pressure (external stress), (3) it works well for primary porosity or at intermediate porosity, however we must be careful about mixed mineralogy (such as shale and clay).

The Wyllie time average equation is heuristic and cannot be justified theoretically.

It is based on ray theory which requires that the wavelength is smaller than grain and pore size, and that the minerals and pores are arranged in flat layers.

The model of Raymer *et al.* (1980) is a modification of Wyllie *et al.*'s (1956) equation. This model can be extended to a sand-shale system by estimating the effective moduli of the solid matrix. In a similar way to the Wyllie *el al'*s (1956) model, the Raymer *et al.* (1980) model is also a P-wave velocity to porosity transformation, i.e.:

$$V_p = (1-\phi)^2 V_m + \phi V_f \ \ (\phi < 37\%), \tag{2.15}$$

$$\frac{1}{\rho V_p} = \frac{\phi}{\rho_f V_f^2} + \frac{1-\phi}{\rho_m V_m^2} \ \ (\phi > 47\%), \tag{2.16}$$

$$\frac{1}{V_p} = \frac{0.47-\phi}{0.1} \cdot \frac{1}{V_{37}} + \frac{\phi - 0.27}{0.1} \cdot \frac{1}{V_{47}} \ (37 < \phi < 47\%). \tag{2.17}$$

Raymer *et al.* (1980) claim that these equations are still strictly empirical relations, but their relations are valid for sands and sand-shale systems, and the porosity range is larger than the Wyllie *et al'*s model.

The Wyllie and Raymer equations assumed a mono-mineral rock. They identified porosity as the pore factor controlled by velocity. Both of them neglect the influence of factors such as pore shape, lithology, pressure, degree of consolidation and cementing.

2.3.2 Bulk density and *Vp* relationship

As the bulk density can be expressed by porosity, matrix and fluid density, they have the following relationship:

$$\rho = (1-\phi)\rho_m + \rho_f \,, \tag{2.18}$$

where ϕ is the porosity, ρ is the bulk density, ρ_m is matrix density and ρ_f is the fluid density.

Density is a required parameter when seismic data are inverted for velocities. Therefore if the density is unavailable, the velocity to density relationship can be expressed by useful empirical equation of Gardner *et al.* (1974) as

$$\rho = c \cdot V_{p,}^{0.25} \tag{2.19}$$

where ρ is the bulk density (g/cm^3), V_p is P-wave velocity (ft/s) and c is the constant due to used system (here, 2.5 for V_p in ft/s and 0.31 for V_p in m/s).

This empirical relationship is based on field data and laboratory measurements of saturated sedimentary rock from a wide range of basins and depths. According to Gardner *et al.* (1974), the velocity equation shows that the increase in velocity is not caused by the higher density, but by a much greater increase in the bulk modulus or the rigidity modulus. Thus, this relationship is essentially an average of the fits for sandstone, shale and carbonates. The Gardner *et al.* (1974) equation can be reformulated as a function of porosity and densities of two components, and this relationship may be used as the transformation of P-wave velocity-density using a density log and seismic velocity. The equation has a reasonable solid phase velocity, and it can be reliably used for cemented sandstones having the primary and intermediate porosity range. However neither the Wyllie *et al.* (1956) nor the Gardner *et al.* (1974) equations provide an adequate prediction for unconsolidated sand and therefore they must not be used with these rocks.

Lindseth (1979) used Gardner's empirical data to derive the following relationship between density and P-wave velocity:

$$\rho V = (V - 3460)/0.308\,, \tag{2.20}$$

where ρ is the bulk density (g/cm^3), V is P-wave velocity (ft/s). Lindseth's (1979) results shown that detailed velocity measurements could be used to predict rock type.

2.3.3 Bulk density and *Vs* relationship

There are many empirical relationships that describe P-wave velocity as a function of density, such as the empirical equations of Gardner *et al.* (1974) and Linseth (1979), but they are very few models that treat S-wave velocity as a function of density. Robertson *et al.* (1987) suggested that the S-wave velocity gives a very good approximation to Gardner's relationship:

$$\rho = 0.37 \cdot V_s^{0.22} \tag{2.21}$$

According to their results, the variance or scatter about the best-fit line for predicting densities in both Gardner's and Lindseth's relationship is lower for S-wave than for P-wave velocities.

2.3.4 Transformation of *Vp* and *Vs*

Castagna *et al.* (1985) proposed an empirical P-wave velocity to S-wave velocity transformation. This equation was called the mud-rock line. The S-wave velocity of water saturated clastic silicate rock is related to the P-wave velocity by

$$V_p = 1.16V_s + 1.36\,, \tag{2.22}$$

where velocities are expressed in km/s, the mud-rock trend seems to describe accurately the P- and S-wave velocity relation for shaly rocks.

2.3.5 Influence of shale (clay content)

Han *et al.*(1986) observed that the models of both Wyllie *et al.* (1956) and Raymer *et al.* (1980) significantly overestimate porosity in shales and shaly sands, so suggested that they should not be used with these lithologies. Han *et al.*(1986) proposed the following empirical equations to relate velocities, porosity and clay content by

$$V = a + b \cdot \phi + c \cdot V_{sh}\,, \tag{2.23}$$

where V can be either P or S-wave velocity, ϕ is the porosity, V_{sh} is clay content, a, b and c are the coefficients calculated through least square regression. The data of Han *et al.* (1986) measured at the confining pressure of 40 MPa and a pore pressure of 1.0 MPa, suggesting a relationship between P- and S-wave velocity, porosity and clay content expressed as:

$$V_p = 5.59 - 6.3\phi - 2.18V_{sh}, \tag{2.24}$$

$$V_s = 3.52 - 4.91\phi - 1.89V_{sh}. \tag{2.25}$$

The Han *et al.* (1986) equations show that the porosity and clay have a larger influence on velocities. P- to S-wave velocity ratio is also a function of porosity and clay content, increasing with an increase of porosity or clay content. The different results in the regression are obtained by different authors and the extrapolation of this type of approach to other datasets does require calibration to be made along with a reasonable number of measurements.

2.4 Further study of elastic properties: Physical methods

Several physical models based on wave-theory will be reviewed in this section. These fundamental theories of wave propagation in porous media have been used to establish practical and physical models in studying the velocities and rock properties for isotropic and anisotropic rocks.

2.4.1 Effective medium theories

2.4.1.1 *Fluid substitution: Gassmann model*

Gassmann (1951) model is the most often used model in the studying the effect of fluid saturation on seismic velocities in porous rocks. It can be used as a P-wave velocity to S-wave velocity transformation if a relationship between the elastic moduli of the dry framework is available.

This model related the elastic moduli of a fluid saturated porous rock to the elastic moduli of the rock in the dry state (rock frame), the moduli of solid grain matrix and pore fluids. The fluid saturated bulk modulus K is given by:

$$K = K_m \frac{K_d + Q}{K_m + Q}, \tag{2.26}$$

where

$$Q = K_f \frac{K_f(K_m - K_d)}{\phi(K_m - K_f)}. \tag{2.27}$$

where K is the bulk modulus, the subscripts m, f and d are related to the matrix, pore fluid and dry rock frame, ϕ is the porosity. The shear modulus μ is unaffected by fluid saturation because

$$\mu = \mu_d$$

The above equations are normally used together with the auxiliary equations expressing the P- and S-wave velocities in terms of the elastic moduli. Also the bulk density ρ and porosity ϕ are related:

$$\rho = (1 - \phi)\rho_m + \rho_f \,, \tag{2.28}$$

for velocities, have

$$V_p = \sqrt{\frac{K + 4/3\mu}{\rho}}, \tag{2.29}$$

$$V_s = \sqrt{\frac{\mu}{\rho}}. \tag{2.30}$$

In the original derivation of the Gassmann equation, a limited number of assumptions were explicitly made, they are

(1) The pores are interconnected.

(2) The pores are filled with a frictionless fluid.

(3) The relative movement between the solid and the fluid is negligible small.

(4) The pore fluid does not interact with the solid matrix in a way that would change the shear rigidity of the frame.

Assumption (1) means that the porosity and permeability of the rock is generally high and that there are no isolated pores. Assumption (2) means that the saturating fluid has low viscosity. Assumption (3) implies that the wavelength is large compared to the pore size(low frequency). Assumption (4) requires that there is no chemical or physical interactions between the fluid and the rock frame (for example hardening or softening).

The Gassmann (1951) equations can be used to predict the elastic moduli and hence velocities under water saturation conditions. Rather more common is the situation in

which the properties of the water saturated rock are known. To use equation (2.26), the following input parameters are required; the parameters K_d and μ_d can be obtained through laboratory velocity measurements on dry rocks or through formation evaluation; porosity (ϕ) and densities (ρ) can be measured in the laboratory or logs; K_m can be calculated by the effective medium theories when the mineralogical analysis data are available or to be assumed (in general, K_m can be assumed in the following table).

Lithology	sandstone	limestone	dolomite	shale	shaly sandstone
K_m **(GPa)**	38	72	80	35	35

Based on the data from Wang and Nur, 1990, The Gassmann-calculated V_p in Figure2.4 is lower than the measured V_p in all the carbonate samples, where it varies by about 10 percent. The Gassmann-calculated V_s is generally lower than the measured V_s, but fits within 10 percent of the most of the measured V_s (Wang and Nur, 1990). The difference between the calculated and measured velocities decreases as the effective pressure increases. The misfits between the Gassmann-calculated and measured velocities are caused by: (1) the presence of cracks or micro-fractures in the rock samples, (2) uncertainties in the input parameters to the Gassmann equation, (3) velocity dispersion and (4) non-conformance of real rocks to Gassmann's assumptions.

Real rock and fluid may not always conform to Gassmann's assumptions. For example, a rock sample inevitably contains some isolated or poorly connected pores; water and oil are not really frictionless; and some pore fluids certainly interact with the rock matrix in such a way as to change the internal surface energy level of the rock. Hence, the difference between the Gassmann calculated value and measured value should be considered as a correction for practical purposes.

In general, the Gassmann equations can be used to predict the S-wave velocity from the P-wave velocity if a relationship between the bulk and shear moduli in the dry

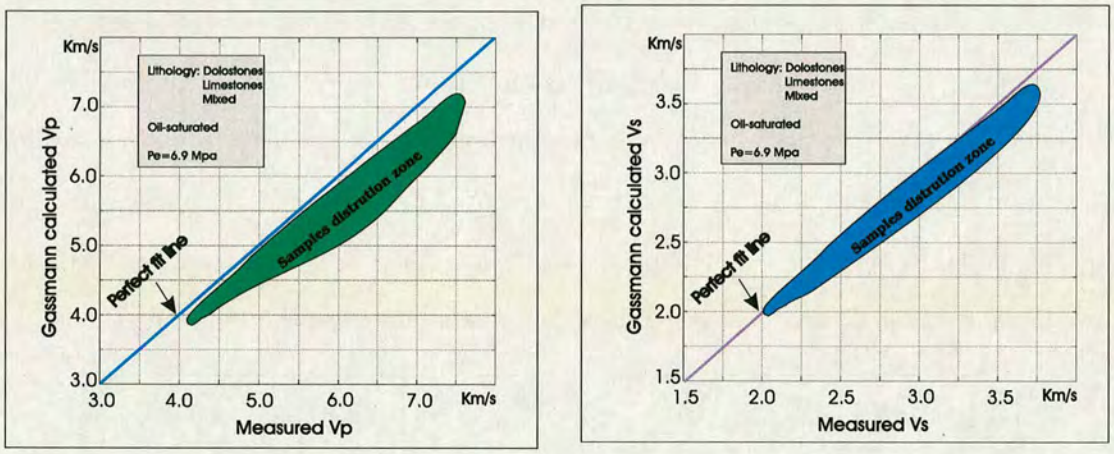

Figure 2.4: Comparison between laboratory measured and calculated compressional velocities (left plot), and shear (right plot) wave velocities (data from Wang and Nur, 1990).

state is assumed. This assumption is consistent with experimental data from different authors. Hence, the Gassmann equation can provide theoretical justification for the use of seismic attributes, which measure estimation of Vp and Vp/Vs as hydrocarbon indicators.

2.4.1.2 *Biot theory*

Biot (1962) developed a theory to model the behaviour of a fluid-saturated poroelastic system. The difference of Biot method comparing with the Gasmmann's method is that Biot (1962) theory covers the whole frequency range for rock properties and velocities. The main assumptions of Biot are that the rocks are saturated in isotropic, and all minerals making up the rocks have the same bulk and shear moduli. The low-frequency limited velocities are the same as those predicted by Gassmann's relations, but the high frequency limited velocities Vp and Vs are given by

$$V_{p\infty} = \left\{ \frac{1}{\rho_o(1-\phi) + \phi\rho_{fl}(1-a^{-1})} \left[(K_{kf} + \frac{4}{3}\mu_{fr}) + \frac{\phi\frac{\rho}{\rho_{fl}}a^{-1} + (1-\frac{K_{fr}}{K_o})(1-\frac{K_{fl}}{K_o} - 2\phi a^{-1})}{(1-\frac{K_{fr}}{K} - \phi)\frac{1}{K} + \frac{\phi}{K}} \right] \right\}^{\frac{1}{2}}, \tag{2.31}$$

$$V_{s\infty} = \left(\frac{\mu_{fr}}{\rho_o(1-\phi) + \phi\rho_{fl}(1-a^{-1})} \right)^{\frac{1}{2}}, \tag{2.32}$$

where K_{fr}, μ_{fr} are bulk and shear moduli of dry rock frame, K_o is bulk modulus of mineral, K_{fl} is effective bulk modulus of pore fluid. ϕ is porosity, ρ_o is mineral density, ρ_{fl} is fluid density, ρ is low frequency density of saturated composite ($\rho = (1-\phi)\rho_o + \phi\rho_{fl}$) and a^{-1} is a factor.

The two solutions given above for the high-frequency limited P-wave velocity, correspond to the "fast" and "slow" waves. The fast wave is the compression body-wave, which most easily observed in the laboratory and the field. It corresponds to overall fluid and solid movements that are in phase. The slow wave is a highly dissipative wave in which the overall solid and fluid movements are out of phase.

Biot's theory can be used for estimating saturated rock velocities from dry rock velocities, but the rock should be completely saturated (fluid-bearing rock) and all minerals making up the rock have the same bulk and shear moduli.

2.4.1.3 *Kuster*-Toksöz *theory*

Kuster and Toksöz (1974) derived their model using the scattering theory. They have formulated a widely used model for two-phase medium, which relates the porosity and pore aspect-ratios to P- and S-wave velocities. According to their model, the porous rock is characterized by its solid elastic matrix, assumed to be isotropic as a whole, with randomly distributed pores and saturating pore fluids, the pores are assumed to be spheroidal with their shape characterized by their aspect-ratio.

For a porous rock characterized by pores with a single aspect-ratio, the effective

elastic moduli of the rock are related to the elastic moduli of the solid phase, and bulk modulus of the fluid and the pore aspect-ratios by the following equations:

$$K_d = \frac{K_m + 4A\mu_m}{1 - 3A}, \tag{2.33}$$

$$\mu_d = \mu_m \frac{1 + B(9K_m + 8\mu_m)}{1 - 6B(K_m + 2\mu_m)}, \tag{2.34}$$

K_d and K_m are the bulk moduli of the dry frame and mixture, μ_d and μ_m are the corresponding shear moduli. A is a function of the pore aspect-ratio (the ratio of short semi-axis to long semi-axis in pore space).

The Kuster and Toksöz model assumes that (1) the effective medium is composed of two phases with different properties, (2) one phase (the matrix) forms a continuum and the other phase is the inclusion embedded randomly, (3) the inclusions (pores) are so dilute that they do not interact or overlap with each other and (4) the wavelength is much larger than the size of the inclusions.

Apart from the already quoted assumption about the pores' elliptical shape and their random distribution, another important hypothesis was made in formulating the model, namely that the pore distribution is diluted:

$$\frac{\phi}{\alpha} \ll 1,$$

where ϕ is porosity, and α is pore aspect-ratio. This clearly limits the practical applications of the model to low porosity rocks, where the interaction between different pores can be ignored.

Kuster and Toksöz model for the effective bulk modulus, if all pores are spherical (aspect-ratio is one), reduces to the Gassmann equation. Moreover for an aspect-ratio equal to one, the effective shear modulus becomes independent of the saturating fluid

like the Gassmann equation. However when pores with small aspect-ratios are present the effective shear modulus for dry rocks can be significantly smaller than the modulus in the case of water saturation.

Generally, Kuster and Toksöz (1974) model shows that the effective elastic moduli of a two-phase medium depend not only on the intrinsic moduli and the concentration (porosity for rocks) but also on the shape of the inclusions. A small concentration of low aspect-ratio pores in a rock can greatly reduce the effective moduli.

2.4.1.4 *Krief et al. model*

Krief *et al.* (1990) reformulated the Gassmann equation as a function of β (the Biot coefficient) and M (the fluid-frame interaction modulus). The two parameters are defined in the theory of Biot (1962) on the consolidation of fluid in hydraulic pressure and the variation $\delta(V_{fm})$ in the volume of the formation as:

$$\delta(V_{ft}) = \frac{\delta(p)}{M} + \beta\delta(V_{fm}), \tag{2.35}$$

where β is the Biot coefficient which is a function of porosity. It measures the change in porosity relative to the bulk volume when a confining pressure is applied to the rock and fluid pressure is allowed to be constant. M is a modulus, it measures the variation of hydraulic pressure needed to force an amount of water into the formation without any change in formation volume.

The relation between these two parameters, the porosity and the bulk moduli is:

$$\beta = 1 - K_d/K_m, \tag{2.36}$$

whilst the fluid-frame interaction modulus:

$$\frac{1}{M} = \frac{(\beta - \phi)}{K_m} + \frac{\phi}{K_f}, \tag{2.37}$$

then, the equation reduces to

$$K = K_d + \beta^2 M = K_m(1 - \beta) + \beta^2 M\,. \tag{2.38}$$

Krief *et al.*(1990) found experimentally that a relationship exists between β and ϕ below:

$$(1 - \beta) = (1 - \phi)^{\frac{3}{(1-\phi)}}\,. \tag{2.39}$$

This model provides a single smooth and continuous behaviour of the P- and S-wave velocities. Krief *et al.*(1990) successfully illustrate that this relationship can be used in practise both for lithology and pore fluid identification, and also as a tool for quality control and edition of P- and S-wave sonic logs.

2.4.1.5 *Xu and White model*

Xu and White (1995a, b; 1996) provided a practical tool for simulating elastic wave velocities, which was developed from the Kuster-Toksöz (KT) model, differential effective medium (DEM) and Gassmann's theories. The model accurately simulates the combined effect of lithology, porosity, clay content, water saturation and fluid type in laboratory and logging P- and S-wave velocities.

The model divides the total pore space into two parts, one associated with sand grains and the other associated with clay. Pores associated with clay minerals tend to be characterized by smaller aspect-ratios than those associated with sand grains. Because of their geometry, pores associated with clay are more compliant than pores associated with the sand fraction. Therefore, the effect of clay on elastic wave velocities

can be divided into effects from (a) mineralogy, since clay particles are normally softer than sand grains, and (b) pore geometry, since pores associated with clays from flatter pores than sands.

The key feature of Xu and White model is that the dry rock-frame is calculated by the Kuster-Toksöz (1974) and differential effective medium theories, this overcomes the limitation of Kuster-Toksöz theory (dilute concentration of pores). Another feature is that Gassmann (1951) equation is used for velocity prediction in fluid saturated rocks, this is because Gassmann's equations (1951) relate the elastic moduli of a fluid saturated porous rock to the elastic moduli of the rock in the dry state as well as the moduli of the solid grain matrix and the pore fluids.

In Xu and White model, the aspect-ratios are usually determined by the best fitting velocity predictions with the sonic log measurements. Because direct measurements were extremely impractical, the aspect-ratios of 0.1 for sand related pores and 0.04 for clay related pores were often used for velocity prediction.

Xu-White model requires inputs, such as density, elastic moduli for sand grains, clay particles and pore fluid, and two aspect-ratios as well. The output results include intermediate elastic properties (bulk and shear moduli) and the final outputs, P-wave and S-wave velocities. The more details and improvements to Xu-White model will be presented again in Chapters 4.

2.4.2 Theoretical models in anisotropic rocks

In order to understand the theoretical model in anisotropic rocks, it is helpful to restate certain basic concepts. The intention here is not to present those concepts in a rigorous and complete way but to invoke those aspects, which are most useful for the task at hand.

2.4.2.1 *Basic equations*

Considering an elastic homogeneous medium, the elastic coefficients vary in different directions. Hooke's law for a general anisotropic, linear elastic solid states that the stress σ_{ij} is linearly proportional to the strain ε_{ij} as expressed by

$$\sigma_{ij} = C_{ijkl}\varepsilon_{kl}, \quad (i, j, k, l = 1, 2, 3) \tag{2.40}$$

C_{ijlk} is a fourth-rank tensor obeying the laws of tensor transformation and has a total of eighty-one components. However, not all eighty-one components are independent. The symmetry of stresses and strains implies that

$$C_{ijkl} = C_{jikl} = C_{ijlk} = C_{jilk},$$

reducing the number of independent constants to 36. Also the existence of an unique strain energy potential requires that

$$C_{ijkl} = C_{klij},$$

further reduces the number of independent constants to 21. This is the maximum number of elastic constants that any medium can have. Additional restrictions imposed by symmetry considerations reduce this number even further. Isotropic, linear elastic materials, which have the maximum symmetry, are characterized by two independent constants, whereas materials with the lowest symmetry require all 21 constants (Appendix B). In transversely isotropic media, there are 5 independent elastic stiffnesses, as shown in equation (2.41) below:

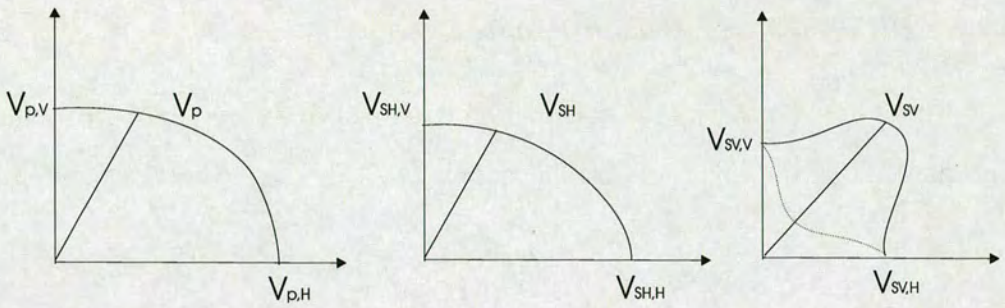

Figure 2.5: The relationship of velocity and propagation angle (Winterstein,1990).

$$C = \begin{bmatrix} C_{1111} & C_{1122} & C_{1133} & 0 & 0 & 0 \\ C_{1122} & C_{1111} & C_{1133} & 0 & 0 & 0 \\ C_{1133} & C_{1133} & C_{3333} & 0 & 0 & 0 \\ 0 & 0 & 0 & C_{2323} & 0 & 0 \\ 0 & 0 & 0 & 0 & C_{2323} & 0 \\ 0 & 0 & 0 & 0 & 0 & \frac{C_{1111}-C_{1122}}{2} \end{bmatrix}. \tag{2.41}$$

After obtaining 5 independent elastic constants. we can calculate the velocities in any propagation direction. Because of the symmetry, in fact, the wave velocity only depends on the angle (θ) between the propagating direction and symmetry axis (ox_3). So we have:

$$V_{p,V} = \sqrt{\frac{C_{3333}}{\rho}}, \quad V_{p,H} = \sqrt{\frac{C_{1111}}{\rho}},$$
$$V_{SV,V} = \sqrt{\frac{C_{2323}}{\rho}}, \quad V_{SV,H} = \sqrt{\frac{C_{2323}}{\rho}},$$
$$V_{SH,V} = \sqrt{\frac{C_{2323}}{\rho}}, \quad V_{SH,H} = \sqrt{\frac{C_{1111}-C_{1122}}{2\rho}}.$$

The wave surfaces are shown schematically in Figure 2.5 after Winterstein (1990).

2.4.2.2 *O'Connell and Budiansky model*

O'Connell and Budiansky's (1974) model is developed for a medium with randomly orientation cracks; the equations are shown below:

$$\frac{K_{sc}^*}{K} = 1 - \frac{16}{9}\left(\frac{1-\nu_{sc}^{*2}}{1-2\nu_{sc}^*}\right)\varepsilon, \tag{2.42}$$

$$\frac{\mu_{sc}^*}{\mu} = 1 - \frac{32}{45}\left[\frac{(1-\nu_{sc}^*)(5-\nu_{sc}^*)}{(2-\nu_{sc}^*)}\right]\varepsilon, \tag{2.43}$$

$$\varepsilon = \frac{45}{16}\frac{(\nu-\nu_{sc}^*)(2-\nu_{sc}^*)}{(1-\nu_{sc}^{*2})(10\nu-3\nu\nu_{sc}^*-\nu_{sc}^*)}, \tag{2.44}$$

K and μ are the bulk and shear moduli of the un-cracked medium, ν is the Poisson's ratio, and ε is the crack density parameters.

Assuming small aspect-ratios ($\alpha \rightarrow 0$), the calculations are simplified by the approximation:

$$\nu_{sc}^* \approx \nu(1 - \frac{16}{9}\varepsilon), \tag{2.45}$$

O'Connell and Budiansky (1974) find two characteristic frequencies in their theory near which wave attenuation is the largest and the effective moduli change rapidly with frequency. This theory can adequately explain the large velocity dispersions in some rocks that the Biot's theory (1956, 1962) fails to explain. It also establishes a theoretical basis for the fact that whenever a hard, well consolidated rock shows a large compressional velocity increase (often accompanied by a shear velocity increase) when

saturated with a viscous fluid, this rock must contain thin cracks or micro-fractures.

2.4.2.3 *Berryman model*

Berryman (1980, 1995) extends Kuster-Toksöz (1974) model to accommodate both small and large concentrations of inclusions. Although the Berryman model is derived for rocks with a uniform pore shape (aspect-ratio), it does allow for range of pore aspect-ratios with slight modifications. The assumption in Berryman model appears to imply that the model is valid for low frequencies. In fact, it is a high frequency model in terms of pore fluid flow like the Kuster-Toksöz model, due to the assumption of isolated pores. Berryman (1980, 1995) gives a more general form of the self-consistent approximations for N-phase composites:

$$\sum_{i=1}^{N} x_i(K_i - K^*_{sc})P^{*i} = 0\,, \tag{2.46}$$

$$\sum_{i=1}^{N} x_i(\mu_i - \mu^*_{sc})Q^{*i} = 0\,, \tag{2.47}$$

for three-phase composites, these may be expressed as

$$K^*_{sc} = \frac{(x_1K_1P^{*1} + x_2K_2P^{*3} + x_3K_3P^{*3})}{(x_1P^{*1} + x_2P^{*2} + x_3P^{*3})}, \tag{2.48}$$

$$\mu^*_{sc} = \frac{(x_{11}\mu_1Q^{*1} + x_2\mu_2Q^{*3} + x_3\mu_3Q^{*3})}{(x_1Q^{*1} + x_2Q^{*2} + x_3Q^{*3})}, \tag{2.49}$$

where i refers to the ith material, x_i is its volume fraction, P and Q are geometric factors, and superscript $*i$ on P and Q indicates that the factors are for an inclusion of material i in a background medium with self-consistent effective moduli K^*_{sc} and

μ^*_{sc}. These equations are coupled and must be solved by simultaneous iteration. Although Berryman's self-consistent method does not converge for fluid disks ($\mu_2 = 0$), the formulae for penny-shaped fluid-filled cracks are generally not singular and converge rapidly. However, his estimation for needles, disks, and penny-shaped cracks should be used cautiously for fluid-saturated composite materials. Dry cavities can be modelled by setting the inclusion moduli to zero, fluid saturated cavities are simulated by setting the inclusion shear modulus to zero.

2.4.2.4 *Hornby model*

Hornby *et al.* (1994) used a combination of anisotropic formulations of self-consistent (SCA) and differential effective-medium (DEM) theories. They have developed a theoretical framework to predict the effective elastic properties of shales in anisotropic rocks. The model considers that the solid phase is generally comprised of several mineral components and forms an intricate and anisotropic micro-structure, including the shape, orientation and connection of the two phases controlling the anisotropic elastic properties of the composite solid. For the use of self-consistent effective medium theory, the following equation is used to calculate the elastic effective stiffness tensor:

$$\underline{\mathbf{C}}^{SCA} = \sum_{n=1}^{N} \nu_n \underline{\mathbf{c}}^n (\underline{\mathbf{I}} + \hat{\underline{\mathbf{G}}}(\underline{\mathbf{c}}' - \underline{\mathbf{c}}^{SCA}))^{-1} \times \left\{ \sum_{p=1}^{N} \nu_p \left[\underline{\mathbf{I}} + \hat{\underline{\mathbf{G}}}(\underline{\mathbf{c}}^p - \underline{\mathbf{c}}^{SCA}) \right]^{-1} \right\}^{-1} . \quad (2.50)$$

where $\boldsymbol{I}$ is the unit tensor, $\boldsymbol{G}$ is the tensor related to the pore geometry (Nishizawa,1982). $c^{p,} = \sigma^p, /e^p$, and σ^p is the stress tensor, e^p is the local stress tensor, v is the volume of a material, v_n is the volume of the nth constituent.

The equation above agrees with the expression derived by the self-consistent approximation of the overall properties of a polycrystalline solid. For the use of differential effective-medium theory, which considers the anisotropic versions, a final equation for

an anisotropic composite is given as

$$\frac{d}{dv}(\underline{\mathbf{c}}^{DEM}(v)) = \frac{1}{(1-v)}(\underline{\mathbf{c}}^{i} - \underline{\mathbf{c}}^{DEM}(v)) \times \left[\underline{\mathbf{I}} + \underline{\hat{\mathbf{G}}}(\underline{\mathbf{c}}^{i} - \underline{\mathbf{c}}^{DEM}(v))\right]^{-1}. \tag{2.51}$$

where $c^i = \sigma^i/e^i$, and σ^i is the stress tensor, e^i is the local stress tensor, $v = V_n/V$, and V is the volume of a material, V_i is the volume of the ith constituent, $\boldsymbol{I}$ is the unit tensor, $\boldsymbol{G}$ is the tensor related to the pore geometry (Nishizawa,1982).

2.4.2.5 *Fluid substitution: Brown and Korringa model*

Brown and Korringa (1975) developed their theory describing the relationship between the effective elastic moduli of an anisotropic dry rock and the effective moduli of the same rock containing fluid:

$$S_{ijkl}^{(dry)} - S_{ijkl}^{(sat)} = \frac{(S_{ij\alpha\alpha}^{(dry)} - S_{ij\alpha\alpha}^{0})(S_{kl\alpha\alpha}^{(dry)} - S_{kl\alpha\alpha}^{0})}{(S_{\alpha\alpha\beta\beta}^{(dry)} - S_{\alpha\alpha\beta\beta}^{0}) + (\beta_{fl} - \beta_0)\phi}, \tag{2.52}$$

where $S_{ijkl}^{(dry)}$ is the effective elastic compliance tensor of dry rock, $S_{ijkl}^{(sat)}$is the effective elastic compliance tensor of dry rock saturated with pore fluid, $S_{ij\alpha\alpha}^{0}$ is the effective elastic compliance tensor of mineral material making up the rock, β_{fl} is the compressibility of pore fluid, and β_0 is the compressibility of the mineral material.

2.5 Integration: Data matching and calibration

Integration has probably been the most fashionable word in the exploration and production domain recently. Many papers, conferences and technical meetings have focused on this concept and its advantages in practice. This is because multi-disciplinary integration such as core, log and seismic measurements provide crucial independent information about subsurface reservoir. The application of new numerical methods for

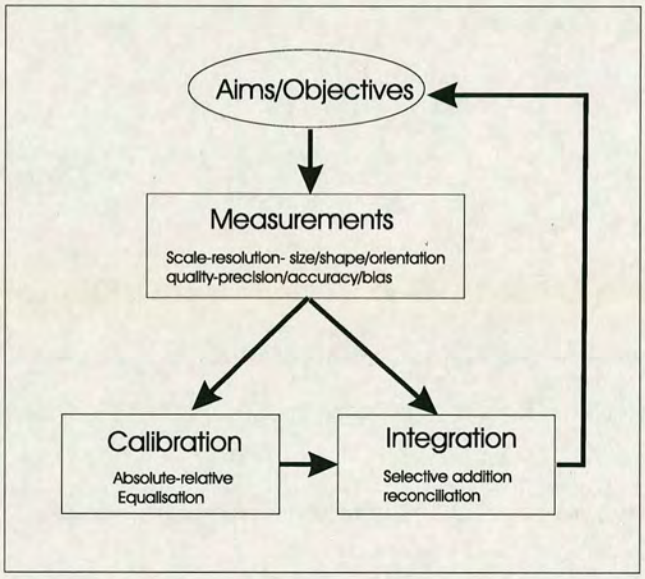

Figure 2.6: The calibration and integration of core and log data (Lovell and Jackson, 1991).

analyzing and modelling them provides a framework for the development of new and exciting approaches.

2.5.1 Calibration of core and log data

Core-log interpretation requires the reconciliation of datasets from different measurements. Measurement process, resolution, scale and quality must be appreciated for each dataset. Calibration of measurements involves the use of standards to enable quantitative comparison locally or globally.

Lovell and Jackson (1991) summarized the relationship between measurements, calibration and integration. The choice and specification of the measurement should be dictated by the aims and objectives of the study, and should dictate both whether there is a need for calibration and the route to integration.

For different data, the resolution concerns the minimum separation between two features which can be identified individually rather than as one combined feature (Sheriff

and Geldart, 1982). In terms of log measurements, this relates to the physical separation of two features along the length of the well (usually in a vertical sense assuming a vertical drill-hole). With respect to core measurements this definition applies equally, although it may be complicated by the consideration of lateral variations or heterogeneities visible in the core sample, whilst the concept of resolution is easily described.

Theys (1991) provided a theoretical definition of the vertical resolution of a log. The full width at half maximum of the response of the measurement to an infinitesimally short event. He then included other non-attributable definitions from elsewhere in the literature, the vertical resolution is the minimum distance, and the logging tool is able to resolve distinct events separated by this distance. Therefore, the vertical resolution is the minimum bed thickness for which in the bed.

Clark (1979) showed that the scale may be defined quantitatively with precise descriptions of the size and shape of the measurements, and it is linked to the measurement technique and hence the design of the tool. Excepting for isotropic and homogeneous media, the different aspects of scale will be important, and they will contribute to the measurement data value. The scale may also be linked to the resolution of the measurement.

Skopec (1992) pointed out that the core measurement calibration, meanwhile, is well-documented and generally involves the use of standards of a similar scale to the samples under test. These small volume local standards can be readily controlled and related to national or international standards.

2.5.2 Up-scaling and cross-scaling for seismic data

Jensen *et al.* (1997) defined the terms up-scaling and cross-scaling as follows:

Up-scaling: The determination of an effective (or pseudo) property at a scale is larger than that of the original measurement. An example is the layer permeability of

a composite layered media. The issue of measurement scale for the same petrophysical property is the process of up-scaling. Reservoir engineers are familiar with the up-scaling of permeability for reservoir simulation. Cross-scaling is a much less familiar concept and may be defined as follows:

Cross-scaling: The determination of a relationship between two different physical properties. Using regression to summarize the relationship between porosity and permeability for a suite of core plugs is a simple example. Comparing compressional wave transit time with porosity is a cross-scaling procedure.

Corbett *et al.* (1998) summarized that: (a) measurement scale and how it relates to the 'true' of 'required' petrophysical properties of the formation is defined as 'up-scaling', and (b) measurement physics and how we relate the physics of one measurement (e.g. porosity) to that of another (e.g. velocity or other properties) is termed 'cross-scaling'.

Marion *et al*, (1998) illustrated how to relate measurements at different scales for up-scaling as:

Lab (core samples) $\rightarrow$ Log (curves) $\rightarrow$Crosswell $\rightarrow$VSP$\rightarrow$Surface seismic.

From the laboratory rock physics to the field measurements, we should consider the following key issues: (1) frequency differences, (2) sample size differences, and (3) wavelength differences.

Seismic velocity depends not just on the rock and fluid properties, but also on the measurement scale relative to the geological scale. The waveforms show that both the travel time and amplitude/frequency depend on the ratio of wavelength to layer thickness. The velocities in the two limits are described well by ray theory and effective medium theory respectively. Warren (1961) proposed that the short wavelength behaviour, the variance of the travel time fluctuations around the mean travel-time, can be related to the variance of the slowness fluctuations. For plane waves in a heteroge-

neous medium:

$$\sigma_T^2 = \sqrt{\pi} \cdot L \cdot a \cdot \sigma_s^2, \tag{2.53}$$

where L is the path-length, a is the spatial correlation length, σ_T^2 is the travel-time variance and σ_T^2 is the slowness variance.

2.5.3 Data environment correction

Borehole logging provides quasi-continuous in situ measurements of a complete range of physical properties, and logging measurements also represent measurement of a much larger volume of rock than conventional core samples. It may be more representative of the lithology being logged. In contrast, core measurements do have a much higher accuracy than most log data, due to a less hostile acquisition environment. To match seismic data so as to obtain the same resolution, the requirements are not only to allow the log resolution to match the seismic wave, but also keep their physical characteristics. The benefit is that it will choose the true values rather than the average values in data alignment, so that the different properties among different rock layers will be maintained.

Lofts (1993) asks the question why it is necessary to carry out data environment correction for data integration. The answer is a combination of the following factors:

(1) To calibrate logging data, and to understand the source of the measurements being made. Without any reference to core data we would be uncertain about the log value that is most representative of a particular lithology or fluid.

(2) To acquire as much information as possible about a particular geological environment, a lithological or a petrophysical property such as porosity, or even permeability. The most thorough assessments of the subsurface reservoirs have been derived from joint core and log studies.

(3) Integration of core, log and seismic data enables engineer to predict the likely lithology in a cored sequence where core recovery is incomplete with reference to the logging data.

(4) To evaluate the potential lithologies that exist in the acquisition of cores.

Worthington (1989) proposed that techniques such as selection of core sampling can reduce matching error. For example, in the slab-bed core sample taken along the axis of the core over a length of up to 0.5m, core has been homogenized into a bulk sample, where the laboratory measurement is made. This procedure helps to minimize the disparity in the volume and vertical resolution of core and log data and makes them more suitable for integration. It is not a valid technique however for volumetric measurements such as porosity and permeability.

Nelson (1994) pointed out that well log data are identified by wireline depths and core data by driller depths. Both of these are usually different, but have to be integrated. This process of depth matching is very complicated where there is incomplete core recovery, which often is the case. Log data from different logging runs must be free from depth mismatch.

Parmmer *et al.* (1996) showed that borehole resistivity log is a well established technique for the study of sedimentary features down to a scale of less than 20mm. It has followed a rapid evolution from a 2 pad tool (where 56 small electrical buttons produced a high resolution image covering roughly 20% of the borehole by measuring micro-resistivity change in a formation) to a 4 pad, 4 flap device, boasting 196 electrode buttons, which obtains a micro-resistivity image with almost 100% coverage in a 15.6 cm borehole.

2.6 Reservoir parameter prediction

The integration study is a challenging task to perform, and the reservoir is a very complex object itself. It has to be characterized with a large number of parameters, to a remarkable degree of accuracy. It is well-known that one of the most important aspect in reservoir study is how to properly integrate data into a consistent model. Therefore, a review of approaches for reservoir parameter prediction is necessary.

2.6.1 Porosity estimation

The nature of reservoir rock dictates the quantities of fluids (oil and gas) trapped within the rock void space, the ability of fluids flow through the rock, and other related properties. The measurement of the void space is defined as the porosity; and methods for measuring porosity have been published frequently in the technical literature for the oil industry. Sand grains and particles of carbonate materials that make up sandstone and limestone reservoirs have never fit together a relationship perfectly. The space between grains, called pore space or interstices, is usually occupied by fluids. The porosity of a reservoir rock is defined as pore space fraction of the bulk volume of the reservoir formation. This can be expressed in a mathematical form as

$$\phi = \frac{V_b - V_{gr}}{V_b} = \frac{V_{por}}{V_b}, \tag{2.54}$$

where ϕ is porosity (volume fraction), V_b is the bulk volume of the reservoir rock, V_{gr} is the grain volume and V_{por} is pore volume. According to this definition, the porosity of porous materials may have any different values, but the porosity of most sedimentary rocks is generally lower than 50%. In fact, the porosity of oil and gas reservoirs ranges from 5% to 40%, but most frequently lies between 15% and 30% (Pirson, 1963). The factors governing the magnitude of porosity in clastic sediments are:

- **Uniformity of grain size:** uniformity or sorting is the gradation of grains. If small particles of silt or clay are mixed with larger sand grains, the effective (intercommunicating) porosity will be considerable reduced.

- **Degree of cementing or consolidation:** the highly cemented sandstones have low porosities, whereas the soft, unconsolidated rocks have high porosities.

- **Degree of compaction:** compaction during and after deposition tends to close voids and squeeze fluid out to bring the mineral particles closer together. Generally, porosity is low in deeper, older rocks, but exceptions to this basic trend are common. Many carbonate rocks show little evidence of physical compaction.

- **Methods of packing:** with increasing overburden pressure, poorly sorted angular sand grains show a progressive change from random packing to a closer packing. Some crushing and plastic deformation of the sand particles may occur.

The role played by the visual description of pore spaces in porous rocks has changed considerably since the development of a method for classifying carbonate reservoir rocks in 1942 by Archie. Development of well logging technology has provided the petroleum industry with effective and direct methods to measure the in-situ porosity of formations. Thus porosity can be estimated from a single borehole measurement when lithology is given, or from two or more logs otherwise. The density, sonic and neutron logs are considered particularly suitable for porosity estimation.

For the aim of data calibration and integration, the regression technique can be used to establish relationship between core porosity and log porosity derived from logs mentioned above. The complex considerations necessary for extracting reservoir parameters from logs require data on lithological fractions, core and those from experimental laboratory such as properties of the grain matrix and pore fluids.

The equation (2.55) shows an example to use a linear regression building the relationship between core porosity and log density:

$$\rho = -m \cdot \phi + a, \tag{2.55}$$

where ϕ is the total effective porosity from core in the laboratory, ρ is the bulk density from density log, expressed in g/cm^3 and both m and a are lithological coefficients to be determined on the basis of the least squares regression. In the same way, the correlation of core porosity and sonic log can be written as

$$\phi = b \cdot \Delta t + c, \tag{2.56}$$

where Δt is the interval transit time from sonic log in $\mu s/m$, similar to the density formulae, both b and c are both lithological coefficients to be determined.

Considering the effect of shale, the porosity value should be corrected to remove the influence of shale content. We know that the gamma-ray readings most likely reflect shale content of the formations, and they can therefore be used as a measurement of shale volume. When shale value is more than a certain level (for example, larger than 15%) a cutoff will be used to correct porosity below (Schlumberger, 1994):

$$\Phi^* = \frac{\rho_{ma} - \rho}{\rho_{ma} - \rho_w} - (V_{sh} - V_{cutoff})\frac{\rho_{ma} - \rho_{sh}}{\rho_{ma} - \rho_w}, \tag{2.57}$$

where $\Phi^*$is the corrected porosity, ρ_{sh} is the shale density, V_{sh} is the shale content, ρ_{ma} is the matrix density, ρ_w is the fluid density and V_{cutoff} is the shale cutoff. Note that estimation of porosity from density measurements requires the prior knowledge of lithology and fluid type. Furthermore, if the formation is saturated with gas or light hydrocarbons, the measured bulk density will be affected, therefore the computed

porosity will be far away from the true value.

Similarly porosity can be estimated from sonic and neutron logs, once the properties for the grain matrices and pore fluid are given. The reason of using resistivity logs to estimate porosity is because that the most of the common minerals except clays are electrically resistive. In clean, fully water saturated sands, porosity is related to the porous rock resistivity by the Archie (1942) equation:

$$R_0 = \frac{aR_w}{\phi^m}, \tag{2.58}$$

where R_0 is the rock resistivity in 100% pure formation, R_w is the formation water resistivity, ϕ is porosity, m is the parameter known as the cementing factor, which depends on the rock type and texture, a is a constant.

The Archie equation is not valid for shaly sands because the conductivity of clay minerals is not negligible, so a number of theoretical models and empirical laws have been proposed to describe the electrical properties of shaly sands.

2.6.2 Shale content determination

The presence of shale affects the response of all borehole measurements. Therefore, in theory, the responses from different measurements can be jointly used to produce an estimation of the clay volume in the rock. In practice, the evaluation method of shale volume estimation simultaneously takes into account more than one measurement. Far more commonly, in log analysis and formation evaluation, the volume of shale content in sedimentary rocks is estimated from one measurement only. The gamma-ray counts are certainly the most widely used measurement to estimate the shale fraction. Gamma-ray log provides a measure of the natural radioactivity in rocks, the total gamma-ray value is a measurement of the cumulative radioactivity from three elements, while potassium, thorium and uranium gamma-ray (spectral gamma-ray) logs provide measurements of

the radioactivity of each element.

The gamma-ray curve is used to calculate compute the gamma-ray index to calibrate the core value of shale volume using equation (2.59);

$$\Delta GR = \frac{GR - GR_{sh}}{GR_{ma} - GR_{sh}}. \tag{2.59}$$

where ΔGR is gamma-ray index, GR is the measured value of gamma-ray log, GR_{sh} and GR_{ma} are the gamma-ray values associated with clean shale and sand, often corresponding to the minimum and maximum recorded values of gamma-ray counts. The standard gamma-ray unit is API unit (American Petroleum Institute), defined from a standard well in the grounds of University of Houston, Texas.

Core data are available to be used to convert the gamma-ray index to shale volume, each of which will give significantly different estimates (Heslop, 1974). Heslop observed a linear relationship between gamma-ray response and clay volume as determined by x-ray diffraction data from core samples. The shale volume may be obtained in the laboratory. The relationship between shale volume (V_{sh}) and gamma-ray log (GR) is determined using a nonlinear regression, in a similar way to porosity equations based on a geostatistical method:

$$V_{sh} = 10^{c*\Delta GR+d}, \tag{2.60}$$

where both c, d are the nonlinear regression coefficients, the gamma-ray index (ΔGR) can be estimated by gamma-ray log (GR) in turn to estimate shale value, the method is similar to calculate shale volume. A correction to this relationship has been proposed by Rider (1986):

$$V_{sh} = a(2^{\Delta GR} - 1)\,, \tag{2.61}$$

where V_{sh} is the shale volume, and ΔGR is given by equation (2.59). The coefficients a and b depends on consolidated rocks. In general, a is 0.33 and b is 2 for normal rocks; and a is 0.083 and b is 3.7 for older consolidated rocks.

The weakness of this approach is that radioactivity is not associated with sands and is only attributable to the shale fraction, therefore, this method can be applied where radioactive isotopes are not present in the non-shaly fraction. To overcome this weakness, a combination of the neutron and density logs has been used by Rider (1996), once the density and neutron logs are taken, the shale volume may be determined, and this result will not be affected by the radioactive isotopes from gamma-ray measurements.

2.6.3 Clay content determination

Based on X-ray diffraction data, Kukal and Hill (1986) confirmed that the most shales contain about 60 percent clay. In general, these having grain size less than 0.03 mm is defined as clay content. Using the method similar to calculate the shale volume, the clay content (V_{cl}) is found by using

$$V_{cl} = 10^{e*\Delta GR+f}, \tag{2.62}$$

where both e, and f are nonlinear regression coefficients to be determined, and the gamma-ray index (ΔGR) can be estimated by the gamma-ray log (GR). The value of clay gamma-ray (GR_{cl}) is similar to that derived from equation (2.59).

Considering the effects of radioactive isotopes mentioned earlier, the volume of the shale volume and clay content can be estimated from other logs if porosity and lithology are given or have been estimated through other means. As an example, we know that it is possible to estimate the shale or clay content from the sonic log, further more, if the porosity is not available, both shale (clay) volume and porosity can also be simultaneously estimated from two borehole measurements, commonly a combination

of the neutron and density logs. This is because the response of both logs varies linearly with the shale content. The expression of this relationship is below:

$$\rho = \phi\rho_f + V_{cl}\rho_{cl} + (1 - V_{cl} - \phi)\rho_s, \tag{2.63}$$

where ϕ is porosity, and ρ_f, ρ_{cl} and ρ_s are the densities of the pore fluid, clay and sand mineral matrix. Once the density and porosity for sand, clay matrix and pore fluid are given, the equation can be inverted to yield the clay content.

2.6.4 Water saturation estimation

The pore space of reservoir rocks is filled with fluid, normally water and hydrocarbons. The relative spatial distribution of these fluids depends on a number of factors that are related to the physical properties of rock, fluid, as well as rock-fluid interactions. Determination of the saturation conditions of the reservoir formation is one of the most important tasks in reservoir study. In fact, not only these conditions affect the calculation of hydrocarbon in place, but also the fluid mechanics hence, the expected production performance of the reservoir. Unfortunately, fluid saturation is more difficult to determine than porosity, as in most cases its evaluation is subject to different sources of uncertainty.

The common practice of evaluating water saturation for a given field is through the interpretation of log resistivity curves. The principle behind this methodology is that the electrical conductivity of the formation is entirely controlled by water present in pore spaces, since both rock matrix and hydrocarbons are perfect insulators. Evaluation of the amount of hydrocarbons present in the reservoir is based on the ability of the log analyst to estimate the volume of water present in the pore space. This requires the solution of some form of Archie's equation for the water saturation parameters S_w. Because of its simplicity and worldwide use, the method of formation resistivity

for determining S_w is one of the most important approaches. The value of R_0/R_w is defined as the formation resistivity factor (F), and it can be represented by a well-known equation (2.64), Archie in 1942:

$$F = \frac{R_0}{R_w} = \frac{a}{\phi^m}, \tag{2.64}$$

where F is formation resistivity factor, R_0 is the rock resistivity containing 100% saturated with water, R_w is the water resistivity of formation, a is lithology factor (ranges from 0.4 to 1.5). The value of the cementing exponent m reflects the interconnected pore spaces and normally ranges between 1 and 2.3. Historical relationships for the formation factor are given by Charlez (1999) below:

- for limestone: $F = \phi^{-2}$
- for sandstone: $F = 0.81\phi^{-2}$
- for sandstone (deep depth): $F = 0.62\phi^{-2.15}$

The method for calculating water saturation is based on the ratio of the resistivity of the formation hydrocarbons (R_t) to the resistivity if 100% saturated with formation water (R_o) under the same porosity conditions. This ratio is defined as resistivity index (I) in equation (2.65) by Archie, (1942):

$$I = \frac{R_t}{R_o}, \tag{2.65}$$

based on equations (2.64) and (2.65), we can link the resistivity index (I) to the water saturation (S_w), and obtain a relationship as

$$I = \frac{R_t}{R_o} = \frac{b}{S_w^n}, \tag{2.66}$$

where b is the formation factor, n is saturation factor, and S_w is water saturation. Based on equation (2.64) to (2.66), we can obtain a new water saturation equation below:

$$S_w = \sqrt[n]{\frac{a \cdot b \cdot R_w}{R_t \cdot \phi^m}}, \tag{2.67}$$

because

$$S_w = 1 - S_o,$$

so we have

$$S_o = 1 - \sqrt[n]{\frac{a \cdot b \cdot R_w}{R_t \cdot \phi^m}}, \tag{2.68}$$

where S_w is water saturation, S_o is oil-gas saturation and R_w is the resistivity of formation water, which can be determined independently from the water-testing data or self-potential (SP) log method.

2.6.5 Permeability estimation

A reservoir rock must have the ability to allow fluids to flow through its interconnected pores. This rock property is termed permeability. Obviously, the permeability is affected by the rock grain size, grain shape, grain size distribution (sorting), grain packing and the degree of consolidation and cementing. On the other hand, the permeability is also affected by the type of clay present, especially where fresh water is present. The most common way to estimate permeability profiles in an un-cored well is through some permeability predictor. There are three types of permeability predictors that will be reviewed here.

(a) Porosity-Permeability plot

The most used permeability predictor is the porosity-permeability relationship; it can be used to recognize the most reservoir rocks, and shows a reasonably linear rela-

tionship between these parameters in a semi-log scale, which allows for the estimation of permeability if a porosity profile is available. Therefore, there is evidence that a clear porosity-permeability relationship exists in most reservoir and they can easily be constructed by means of a simple linear regression method.

(b) Multiple linear regressions

Multiple linear regression represents a complex estimation technique with respect to the simple k/ϕ plots and usually allows for a fast and reliable permeability estimation in most reservoirs. The methodology is based on the estimation of coefficients as

$$Logk = c_0 + c_1x_1 + c_2x_2 + ... + c_nx_n.$$

The estimation is performed using one or more key wells, where core permeability profiles are available. The resulting equation can then be applied to any other wells, where the independent variables x_1,x_2... are known.

(c) Empirical equations

A number of authors have been proposing empirical correlations to predict permeability. In general, these equations make use of readily available parameters, like porosity or water saturation, to derive a permeability profile at well locations.

In most cases, the empirical equations can only provide rough estimates of permeability. The main problem of this approach is that permeability is dependent on the size and distribution of pore spaces within rock framework. These proposed empirical correlations can be found from a number of publications, such as Carman (1956), Timur (1968) and Berg (1970) etc. Generally, studies have proved that two major factors are believed to control the permeability in most reservoir rocks. They are porosity and shale (clay) content. Thus, the permeability estimates often rely upon porosity and clay content as

$$K = G \cdot 10^4 \frac{\phi^g}{V_{sh}^h}, \tag{2.69}$$

where k is permeability (mD), V_{sh} is shale content (%), ϕ is effective porosity, G, g, and h are permeability coefficients.

2.6.6 Lithology indicator using *Vp/ Vs*

P-wave velocity alone is not a good lithology indicator because of the overlap in *Vp* for various rock types. The additional data provided by *Vs* can reduce this ambiguity. Pickett (1963) demonstrated the potential of using *Vp/Vs* as a lithology indicator through his laboratory research. Using core measurements Pickett determined *Vp/Vs* values of 1.9 for limestone, 1.8 for dolomite, 1.7 for calcareous sandstone, and 1.6 for clean sandstone. Subsequent research has generally confirmed these values, and has also indicated that *Vp/Vs* in mixed lithology varies linearly between the limits of *Vp/Vs* defined by these values (Nations, 1974; Rafavich *et al.*, 1984; Wilkens *et al.*, 1984; Miller and Stewart, 1990).

The correlations established from core and well log data have been successfully applied to surface seismic survey. *Vp/Vs* has been used to interpret sandstone channels encased in shales (McCormack *et al*, 1984). Pardus *et al.*(1990) described a field study in the Scipio field in Michigan, in which *Vp/Vs* was used to delineate reservoir dolomite encased in limestone. Rafavich *et al.* (1984) used the results of laboratory analysis to interpret porosity and lithology variation in seismic data from a carbonate sequence. The interpretation agreed well with well log data. As a lithology indicator using *Vp/Vs*, Rafavich *et al.* (1984) suggested a range of *Vp/Vs* values in typical sedimentary rocks as listed in Table 2.1.

Rock Type	Vp/Vs
Sandstone	1.59-1.76
Calcareous sandstone	1.67-1.76
Dolomite	1.78-1.84
Limestone	1.84-1.99
Shale	1.70-3.00

Table 2.1: The lithology indicator using Vp/Vs by Rafavich *et al.* (1984).

2.7 Summary

This chapter discussed current theories and models on the aspects of reservoir parameters and rock properties studies for the aim of data integration. A brief summary is given below for some of the most frequently used theories and methods in terms of their applications and limitations.

- Hill's (1952) model can be used to estimate the bulk modulus of water saturated rocks. However it should not be used to calculate the effective moduli of gas saturated rocks and it does not provide reliable estimates for the effective shear modulus of fluid (both liquid and gas) saturated rocks.

- Wyllie *et al.*'s (1956) time-average equation is widely used to estimate porosity from P-wave velocity; the weakness is that this equation can only be used for fluid-saturated rock having a high effective pressure with primary porosity or at intermediate porosity, and can cause an obvious error when used for mixed mineralogy (such as shale and clay).

- Han *et al.*'s (1986) equations provide empirical relationships between velocities, porosity and clay content that can be used to predict P- and S-wave velocities based on reservoir parameters (porosity and clay content). These equations are based on empirical relationship, so they should be used with caution.

- Gassmann's (1951) model is most often used to model the effect of fluid saturation on seismic velocities in rock. Its limitation is that the relationship between the elastic moduli of dry framework has to be assumed, and it works well only for medium porosity in isotropic media.

- Biot's theory (1962) can be used to estimate elastic moduli and velocities of fluid-saturated rocks from dry rock velocities. The low frequency limited velocities are the same as those predicted by Gassmann's relationship. For very high permeability materials using Biot's theory alone will lead to poor predictions of high-frequency saturated velocities.

- Kuster and Toksöz (1974) method is used to model two phase media. This method can be used to calculate elastic bulk moduli in dry and saturated rocks. Its limitation is that pore aspect-ratios must be known and it can only be used for isotropic rocks.

- Xu and White (1995a, b; 1996) model provides a practical tool for simulating elastic wave velocities. Their model is developed from the theories of Kuster-Toksöz model, differential effective medium (DEM) and Gassmann's equation. The model accurately simulates the combined effect of lithology, porosity, clay content as well as P- and S-wave velocities (Keys *et al.* 2002). This model does not take into account of the clay platelet alignment, which gives transverse isotropy with a vertical symmetry axis.

- Hornby *et al.* (1994) combined anisotropic formulations of self-consistent approximation (SCA) and differential effective-medium (DEM), developed a theoretical framework to predict the effective elastic properties of shales in anisotropic rocks.

- Brown and Korringa (1975) extended Gassmann's (1951) model to cover anisotropic

media. It is regarded as an anisotropic fluid substitution model.

- Data calibration is the key for reservoir integrated studies, which is a uniform body with empirical or physical models. The application of new numerical methods for analyzing and modelling core, log and seismic data, currently provides a framework for the development of new and exciting approaches in this area.

- Integrated reservoir study is a challenging task in the oil and gas industry. The reservoirs are very complex, which need to be characterized with a large number of parameters and to a remarkable degree of accuracy. It has been proved that one of the most important aspect of a reservoir study which is to properly integrate data into a consistent model.

Chapter 3

EMPIRICAL AND SEMI-EMPIRICAL MODELS

3.1 Introduction

This chapter presents a simple, but powerful empirical approach on the basis of geostatistical method, artificial neural network and the Han *et al.* (1986) model. This model can be used to derive reservoir parameters and rock properties from core and well-log data for the purpose of predicting seismic velocities. As a result of this, the developed relationship between different datasets may be established for the practical use in field data.

As we know, well-logging technology was introduced into the oil industry by Marcel and Conrad Schlumberger in 1927 in France. Since then, due to considerable technological advances, the techniques have undergone through a constant and significant change. The development of novel recording techniques has cleared a large number of earlier assumptions and general estimation for well-log computations. This results in a change of well-logging from a correlation tool for geologists to an indispensable data source in the oil industry. A successful logging program, along with core analysis, can supply data for subsurface structural mapping, define the lithology, identify the productive zones and accurately describe their depth and thickness. It can also distinguish between oil and gas, and permit a valid quantitative and qualitative interpretation

of reservoir characteristics, such as fluid saturation, porosity, and permeability. Because these petrophysical properties cannot be measured directly, therefore, they must be inferred from the measurement of other parameters in reservoir rock, such as the resistivity of rock, bulk density, interval transit time, spontaneous potential, natural radioactivity and hydrogen content of the rock. In order to achieve this goal, well-log data should be combined with other types of data (e.g. core data and seismic data) or other methods (e.g. theoretical and empirical techniques) for the practical case.

For this purpose, a Back-Propagation Neural Network (BPNN) approach will be used to estimate rock parameters. This artificial neural network is obviously different from the traditional statistical techniques, which has been widely applied in recent years in various fields for oil industry, especially in the areas of petrophysics and formation evaluation. Since it can process and learn in a parallel and distributed fashion, it is able to discover highly complex relationships between several variables. The key point of the application of a neural network is that it needs to observe, recognize and define problems in such a way that they will be addressable by neural nets. Their applications have proved that it is possible to solve the problems found in modelling, prediction, assessment, recognition, classification and image processing. Note that a good representative data set (or sub-dataset) is usually required to train the neural network, otherwise, obvious errors will occur to affect the predicted results.

In order to achieve this goal, the implementation can be divided into the following steps:

- A geostatistical method based on core and well-log data is used to derive porosity and clay content (including to use the methods of log interpretation or BPNN)

- BPNN is employed as a tool to estimate aspect-ratios to characterize pore geometry of rock.

- Using a multi-regression method, a new semi-empirical model can be obtained for velocity prediction.
- The application of this approach is in a similar way to the model of Han *et al.* (1986).

3.2 Empirical approach with neural network

As discussed in Section 2.3.5, Han *et al.* (1986) used the empirical method for the formation with a loose matrix (unconsolidated rocks), even with a suspension of particles in fluids. However there is a sacrifice in accuracy. This is because there is a complex relationship between velocity and the pore geometry. To overcome this weakness, pore aspect-ratios are introduced into the isotropic pore model of Han *et al.* (1986) for the consideration of the effect of pore geometry. As a result of this, an improved semi-empirical model may be built to identify the relationship between velocities and rock parameters for the purpose of petrophysical interpretation, which allows us to estimate porosity, clay content and aspect-ratios as well as compressional and shear wave velocities. We only consider to have random distributed pore spaces with varying aspect-ratio, resulting to an isotropic medium, for anisotropy case, a detailed discussion will be carried out in Chapter 5.

3.2.1 Methodology

The varying pore aspect-ratios over the entire reservoir formation depth are inverted using a back-propagation neural network, and these aspect-ratios are combined with the model of Han *et al.* (1986) by means of a multiple regression method. Because aspect-ratios cannot be directly measured from field data, so that the fixed value of aspect-ratio was used in most applications, and these fixed values were often expected to fit depth intervals up to the whole depth of the well. However, in reality, the rock

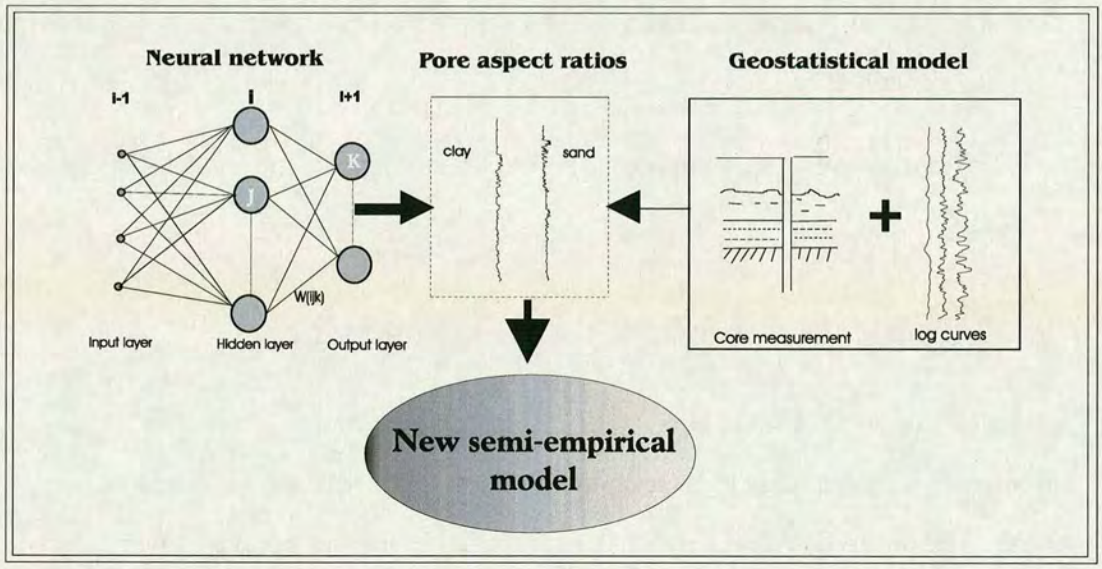

Figure 3.1: The work flow of the improved semi-empirical model based on the Han *et al.*(1986) model with the depth-varying aspect-ratios obtained from an artificial neural network.

pore aspect-ratios are not evenly distributed, and their values vary with lithology, fluid and other factors.

In this chapter, this restriction (fixed aspect-ratio) is relaxed by the construction of an inversion procedure using an artificial neural network. This is based on a linear processing element and interacts with complex non-linear behaviour, therefore it can learn and recognize patterns in data to develop its own generalizations. This new approach is shown in Figure 3.1.

In this approach, we use a forward segmentation multiple regression to extend Han's model, and combined it with aspect-ratios as the following function:

$$V = f\,[\phi,\, V_{cl},\, \alpha_s\, \alpha_c], \tag{3.1}$$

where V is the effective P or S-wave velocity, ϕ is the porosity, V_{cl} is the clay content, α_s and α_c is the aspect-ratio for sand pores and clay pores, and assuming aspect-ratio

is random orientation.

3.2.2 Parameters used in empirical model

The following parameters will be used in my empirical model, they are:

***Velocities (Vp and Vs)*:** The rate at which a wave travels through a medium (rock or formation). Velocity can be determined from laboratory measurements, acoustic logs, vertical seismic profiles or from velocity analysis model.

Porosity (POR): Porosity is defined as the ratio of pore volume to total volume. The percentage of pore volume or void space, or that volume within rock that can contain fluids. Be careful of different definitions of porosity, they include total porosity (total porosity is the total void space in the rock whether or not it contributes to fluid flow total non-mineral space), connected porosity also called effective porosity (pore space connected to the exterior of sample, which is the interconnected pore volume in a rock that contributes to fluid flow in a reservoir. It excludes isolated pores) and disconnected or trapped porosity (space not well connected). In this chapter the porosity that I used means total porosity, which will not consider whether pores are connected or disconnected. Porosity may be determined using well-logging such as density log, neutron log and sonic log (refer to Chapter 7) or a neural network based on core porosity samples and input logs.

Shale (Vcl): The presence of shale affects the response of measurements and predictions of velocities. Shale is a fine-grained, fissile, the sedimentary rock formed by consolidation of clay- and silt-sized particles into thin, relatively impermeable layers. Its typical fine grain size and lack of permeability, a consequence of the alignment of its platy or flaky grains, allow shale to form a good cap rock for hydrocarbon traps. Normally, the shale fine-grained sediments less than 0.03 mm in size can be defined as clay. The shale content can be determined using well-logging (refer to Chapter 7).

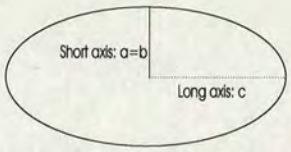

Figure 3.2: Aspect-ratio: The ratio of the short axis to the long axis in the pore space.

aspect-ratio ***(α):*** The aspect-ratio is one of the important parameters of rock geometry, which describes the shape of pore geometry. In this thesis, the aspect-ratio is defined as the ratio of the short axis to the long axis of ellipsoidal pore. Pore is assumed as a spheroid or ellipsoidal characterised in 3-dimension by its three axes a, b and c, where c is the long axis, a and b are short axes. We assume $a = b$, the quantity $\alpha = b/c = a/c$, which is called the aspect-ratio as illustrated in Figure 3.2.

Note that the aspect-ratio cannot be determined from well-log data directly, and the usual methods are used, such as (1) core data (special rock properties analysis), and (2) empirical relationship (Sams & Andrea 2001) or (3) theoretical approaches (refer to Appendix A).

3.2.3 Artificial neural network

The key point of empirical model in this study is to employ a neural network to improve the model of Han *et al.* (1986). As we know, the neural network is a powerful pattern recognition tool, it can utilize the knowledge obtained by experience, and it has a number of performance characteristics in common with human brain neural networks. In fact, the neural network can simulate a nervous system or living animal. It works in a way differently from conventional computing and analysis, and it is capable to compute and solve complex practical problems. Studies show that a neural network can be used to solve a large number of practical problems in geophysics and petrophysics. According to the algorithms, architectures and function, the neural networks can be divided into

three categories as follows:

- Feed-forward neural network: the output of each layer feeds the next layer of units.
- Feed-back propagation neural network: the input data defines the initial activity state of a system. The first output of the system is taken as the new input, which produces a new output.
- Self-organizing neural network: where neighbouring cells compete in their activation by means of mutual lateral interactions, and develop adaptively into specific detectors of different signal patterns.

In this thesis, the network used is the second one above, which is called Back Propagation Neural Network (BPNN). The benefit of BPNN is that this approach attempts to find the most suitable solution (numerical values of weights and thresholds) for parameter prediction between the desired output and its actual value for all of the training examples. In the learning procedure, the first pattern is presented as input to a randomly initialized network, and the weights and thresholds are then adjusted in all the links. Other patterns are then presented in succession, and the weights and thresholds adjusted from the previously determined values. This process continues until all patterns in the training set are exhausted (an iteration). The final solution is generally accepted to be independent of the order, in which the example patterns are presented. A final check can be performed by looking at the error, which is defined as the square of the mismatch errors, to determine whether the final network solution satisfies all the patterns presented to it within a certain error threshold. The set of weights and thresholds in the network are now specifically tailored to "remember" each input and output pattern, and can consequently be used to recognize or generate new patterns given an unknown input.

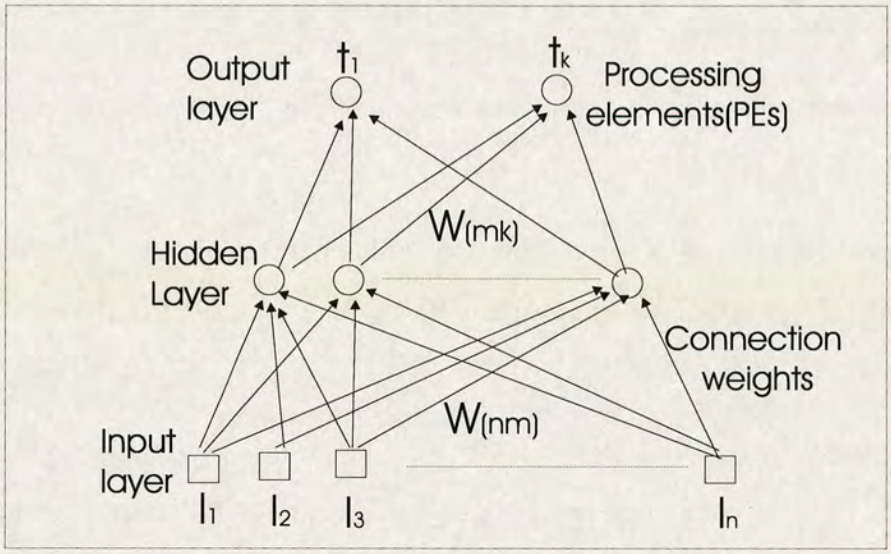

Figure 3.3: Schematic representation of a neural network. It is especially suitable for application to the problems in which some results are already known, but the manner these results have been achieved is not known.

The individual computational elements of a network are usually referred to as neurons or Processing Elements (PE). Each neuron consists of a vector of modifiable weights or connection strengths; the task of a neuron is to map a given input vector into a single output which will then be transmitted to other neurons. In the neuron model, each element of a given input vector is multiplied by a corresponding weight, then added together to produce a net input. The neuron uses an activation function to the transform. An activation function is commonly used in a network. This function has a linear transition part that exponentially reaches one of the two states. For the case of back propagation, training begins when a Processing Element (PE) receives some external stimulation that is passed to the hidden-layer of PE. The signals coming from the PE in the input layer are multiplied by the synaptic connection weights and summed over all connections leading into each PE in the first hidden layer (see Figure 3.3).

3.2.4 Basic concepts

Suppose that we have a set of Q vector pairs (X^1, Y^1) (X^2, Y^2),...,(X^q, Y^q),...,(X^Q, Y^Q) and assume that each X vector has N elements and each Y vector has M elements. We want to train a network to approximate an output for each of the input vectors. Considering a three-layer network such as the one shown in Figure 3.3, we have the following equation (Chiaruttini and Salemi, 1993).

$$a_j^q = f^h(\sum_{i=1}^{N} w_{ji}^h X_i^q + b_j), \tag{3.2}$$

where a_j^q is the net response of the jth neuron in the hidden layer to the qth input vector, $j = 1, ..., L$, L is the number of neurons in the hidden layer, w_{ji} is the ith weight of neuron j, the superscript h refers to the hidden layer, and b_j is a translation term of the activation function f^h. The activation function can take several forms and one that is commonly used is the sigmoid function.

$$f(x) = \frac{1 - e^{-2Hx}}{1 + e^{2Hx}}, \tag{3.3}$$

where H is a parameter which controls the steepness of the function near $x = 0$. The function above represents a general simplification (refer to Chiaruttini and Salemi, 1993). In a similar way, the equations for the output nodes are given by

$$O_k^q = f^o(\sum_{j=1}^{N} w_{kj}^o a_j^q + c_k), \tag{3.4}$$

where O_k^q is the kth output of the network, $k = 1, ..., M$, w_{kj}^o is the jth weight of output neuron k, and c_k is the kth translation term of the activation function f^o which is also defined by equation (3.3). The measure of the error is given by

$$E = \frac{1}{2} \sum_{q=1}^{Q} \cdot \sum_{k=1}^{M} (y_k^q - o_k^q)^2. \tag{3.5}$$

In the back-propagation method, the direction in which the weights are updated is given by the negative of the gradient of E with respect to every element of the weight matrices W^o and W^h. Note that weight updates starts in the output layer and proceed towards the first layer, hence called 'back-propagation'. Minimization of the error results in the following equations for updating the output and the hidden layer weights (Demuth and Beale, 1993):

$$w_{kj}^o(l+1) = w_{kj}^o(l) + \eta \sum_{q-1}^{Q} \delta o_k^q a_j^q, \tag{3.6}$$

and

$$w_{ji}^h(l+1) = w_{ji}^h(l) + \eta \sum_{q-1}^{Q} \delta h_j^q x_j^q, \tag{3.7}$$

respectively, where

$$\delta o_j^q = (y_k^q - o_k^q) f^{o'}, \tag{3.8}$$

and

$$\delta h_j^q = f^{h'} \sum_{k-1}^{M} \delta o_k^q w_{kj}^o, \tag{3.9}$$

in these equations, f' is the derivative of f, and the factor η is known as the learning rate parameter and is usually a small number, say between 0.0 and 0.5. In our implementation, we add a fraction of the weight perturbations from a previous iteration, also called the momentum term, to the right-hand sides of equations 3.6 and 3.7 to improve convergence during training.

3.2.5 Error discussion

BPNN can calculate standard error for the output results from training data. This allows the use of a quantitative means for comparing training results. The standard error can be expressed as:

$$\varepsilon = \sqrt{\frac{SSE}{n-2}}, \tag{3.10}$$

$$SSE = \sum_{i=1}^{n}(Y_i - Y_i^*)^2, \tag{3.11}$$

where Y_i is the measured output at point i, Y_i^* is the synthetic output at point i and n is the number of samples. The standard error also can be formulated by

$$\varepsilon^2 = \left(\frac{SY^*Y}{\sqrt{SY^* \cdot SY}}\right)^2 \tag{3.12}$$

where

$$SY^* = \sum_{i=1}^{n}(Y_i^* - \overline{Y^*})^2 \tag{3.13}$$

$$SY = \sum_{i=1}^{n}(Y_i - \overline{Y})^2 \tag{3.14}$$

and

$$SY^*Y = \sum_{i=1}^{n}(Y_i^* - \overline{Y^*})(Y_i - \overline{Y}) \tag{3.15}$$

3.2.6 Work flows

A small number of recordings are used to train the network, and the rest are used to test the performance of the trained network. The performance of a trained neural network

depends on the training data sets. The output error propagated backward through the network, modifying the link weights of the network, and mapping relationship between the input and desired output vectors are encoded in the weights with a distributed form. Figure 3.4 shows the work flow for the prediction of reservoir parameters. The main procedure may be summarised as follows:

•**Data preparation:** We have a field or study area and we need to obtain porosity, clay content or other parameters for the wells. We have full suites of logs or core data.

•**Create neural network:** Select one of the wells which has both the required input logs and output target recorded data (such as core or modelling results) to train the neural network and to create a neural network project.

•**Testing:** After obtaining an acceptable neural network solution from the training well, and to select those recorded data with the required input and output as application wells. To run the network generated synthetic curve against the recorded output in these confirmation wells.

3.3 Application to field data

3.3.1 Implementation of empirical model

The relationship between velocities and rock parameters (porosity, clay content and aspect-ratios) is built by the empirical model using a multi-linear regression approach, the format generally is given by

$$V_p = a_p + b_p \cdot \phi + c_p \cdot V_{cl} + d_p \cdot \alpha_s, + e_p \cdot \alpha_c\,, \tag{3.16}$$

$$V_s = a_s + b_s \cdot \phi + c_s \cdot V_{cl} + d_s \cdot \alpha_s + e_s \cdot \alpha_c, \tag{3.17}$$

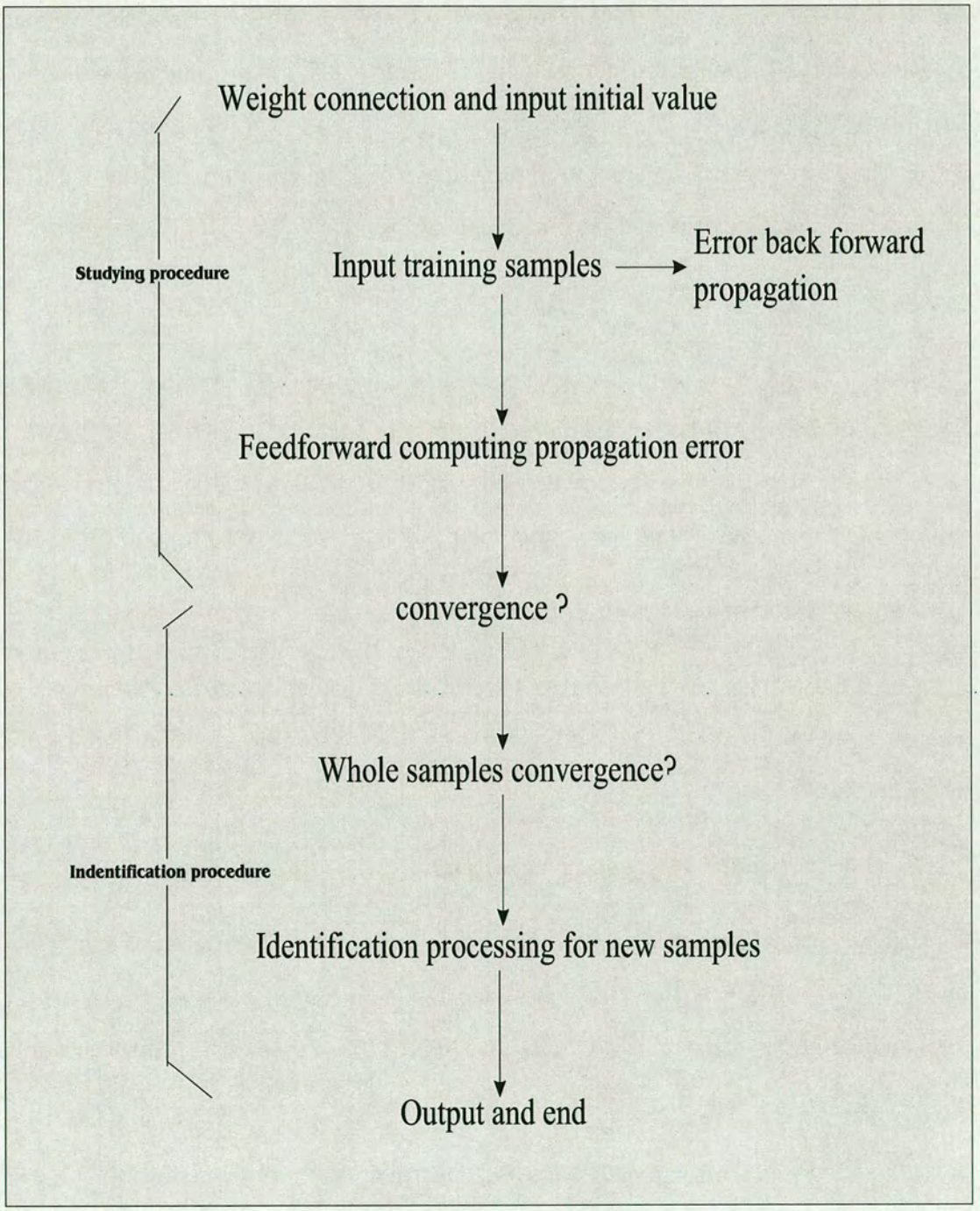

Figure 3.4: Work flow of a neural network for reservoir parameters prediction. Once items such as the data of input content, layer number of network, the number of neuron nodes, conversion function and connection weight after training are fixed, the whole system model may be obtained and will start to predict parameters.

where V_p and V_s are P- and S-wave velocities, ϕ is the porosity, V_{cl} is the clay content, α_s and α_c are the aspect-ratios for sand and clay (the explicit expression of aspect-ratio is given in Appendix A). The coefficients a_p,b_p,c_p,e_p and a_s,b_s,c_s,e_s are to be determined empirically by the multi-linear regression method. The implementation of the empirical models can be roughly divided into the following steps:

Step 1: Estimation of porosity (ϕ)

Using cross plot of neutron and density logs, the porosity can be estimated by normal log interpretation. Also, if the the porosity from core analysis is available, a BPNN can be used to predict the porosity for the whole depth in the same well or the second well in the same area (they should have the similar geological and lithology conditions etc.).

Step 2: Determination of clay content (V_{cl})

Using the *GR* log or *DEN* and *NEU* logs, the clay content can be determined by single or several log data. The methods will be discussed in detail in Section 3.3.3 of this Chapter.

Step 3: Estimation of aspect-ratio (α)

The aspect-ratio samples may be obtained from core properties analysis or physical modelling. Using BPNN to build the relationship (solution) between aspect-ratio samples and log data (such as *CAL, GR, DEN, BEU, RT*), so that the aspect-ratio can be estimated for the whole depth (refer to Chapter 4.4.2).

Step 4: Prediction of velocities (V_p ***and*** V_s)

Using a multi-linear regression, we can establish the relationship between porosity, clay content, aspect-ratio and velocity, therefore, an empirical model can be built to predict velocities using porosity, clay and aspect-ratio.

CNL	DEN	RT	DT	GR	POR_c	POR_p	CNL	DEN	RT	DT	GR	POR_c	POR_p
%	g/cm^3	$\Omega.m$	m/s	API	(%)	(%)	%	g/cm^3	$\Omega.m$	m/s	API	(%)	(%)
19.93	2.31	7.57	260.43	0.405	20.3	21.167	23.42	2.32	9.47	265.47	0.809	17.5	17.072
12.51	2.33	12.22	255.20	0.765	17.2	18.300	22.95	2.31	8.96	266.53	0.815	17.9	17.713
19.94	2.29	8.06	267.68	0.534	17	17.451	15.88	2.39	11.84	296.35	0.355	18.8	19.041
19.89	2.30	8.33	266.14	0.405	15.5	16.584	14.92	2.40	13.21	289.71	0.330	15.5	15.092
19.81	2.30	8.30	264.21	0.293	15.7	16.000	14.88	2.41	13.96	289.02	0.333	14.3	15.106
19.94	2.30	7.08	261.53	0.132	15	15.798	14.99	2.41	14.51	290.91	0.342	15.1	15.450
21.79	2.25	7.84	271.74	0.144	21	20.536	14.69	2.46	14.57	292.51	0.332	14.8	15.360
24.25	2.31	9.07	262.27	0.548	18	17.050	19.00	2.31	7.45	256.90	0.134	15.3	16.100
14.88	2.41	13.96	289.02	0.333	14.7	15.106	24.20	2.36	11.01	260.00	0.710	18	18.30

Table 3.1: Predicted porosity using a back-propagation neural network, which gives both core measured porosity and predicted porosity by BPNN (last two columns).

3.3.2 Porosity estimation

A major advantage of using a BPNN is that we do not need to know the physical relationships between inputs and outputs, The priori knowledge of the rock materials and pore fluid will help to constrain the BPNN.

Figure 3.5 describes a three-layer, back propagation network architecture for porosity prediction, which uses gamma-ray (GR), density (DEN), neutron (NUE), resistivity (RT) and sonic (DT) logs as input data to predict porosity (POR). This network begins the learning process by randomly assigning initial interconnection weights between the layers. The resulted output value (POR) is then compared to the recorded values for the output data in the training well. The differences are then back propagated through the network and used to adjust the interconnection weights. The process is repeated until the differences are small enough to satisfy the conditions set by users (for example, the error of porosity smaller than 2% is supplied normally for formation evaluation). Table 3.1 shows the predicted porosity results from this neural network.

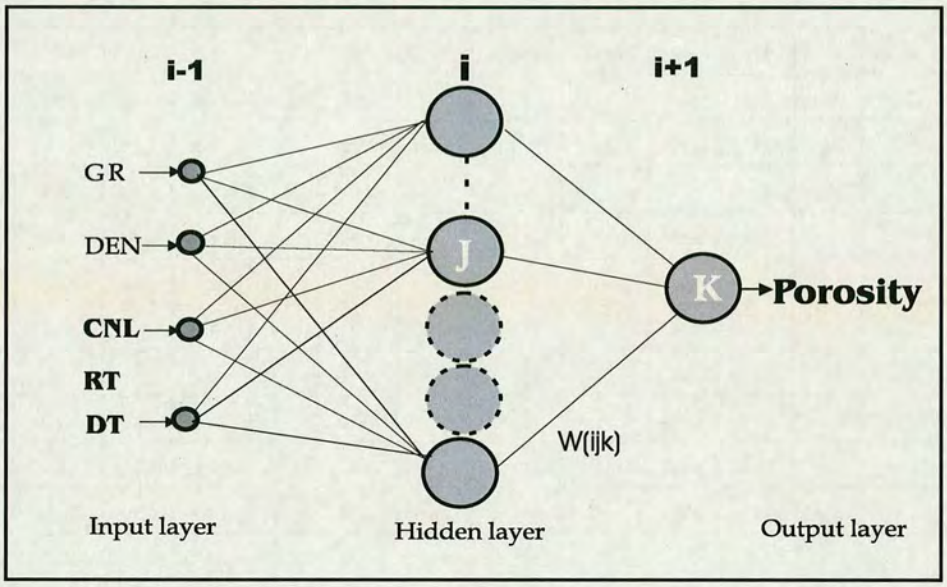

Figure 3.5: The structure of training for porosity using BPNN, which shows that *GR, DEN, CNL, DT* logs as inputs, after choosing a suitable number for hidden layer, the training formation will be outputted to compare with the sample data (measured porosity) until obtaining a ideal output (predicted porosity).

3.3.3 Clay content calculation

Gamma-ray log provides a measurement of the natural radioactivity in rocks, which is used to estimate clay content by:

$$V_{cl} = (GR - GR_{cl})/(GR_{ma} - GR_{cl}), \tag{3.18}$$

where V_{cl} is gamma-ray index, which responds to the clay volume, GR is the measured value of gamma-ray log, GR_{cl} and GR_{ma} are the gamma-ray values associated with clean clay and sand.

If radioactive isotopes are present in the non-shaly fraction, a combination of the neutron and density logs can be used by:

$$\phi_N = \phi_D \phi_{Nf} + V_{cl}\phi_{Ncl} + (1 - V_{cl} - \phi_D)\phi_{Nma}\,, \tag{3.19}$$

where ϕ_N is the total neutron log response, ϕ_D is the porosity from density log, ϕ_{Nf} is the response of pore fluid, ϕ_{Ncl} is the neutron responses of clay, ϕ_{Nma} is the response of sand matrix, and V_{cl} is the clay volume.

3.3.4 Aspect-ratio determination

As for the prediction of aspect-ratios using a neural network (I will give a further discussion in Chapter 4), an example is shown in Figure 3.6. In the figure, we can see that the aspect-ratio curve can be divided into different blocks based on logs. These blocks can provide an independent estimation of aspect-ratios block by block according to well-log data.

Using a linear regression method, a correlation of effective porosity and aspect-ratio has been given by Sams and Andrea (2001) in equation (3.20). Using this correlation of porosity and aspect-ratio, a modelling result has been given in Figure 3.7. The modelling result indicates that Figure 3.7 can be used to check the result of BPNN for the purpose of QC control. This correlation also gives a replacement for the case of the core properties analysis for aspect-ratio is invaluable.

Note that this linear relationship is able to use for isotropic rocks. Because the range of pore aspect-ratio is normally between 0.09 and 0.14 for sand formation (Sams & Andrea, 2001), this relationship will be suitable for the porosity between 15 and 33%.

$$\alpha_{AR} = 0.187 - 0.277\phi, \tag{3.20}$$

where α_{AR} is pore aspect-ratio, and ϕ is effective porosity.

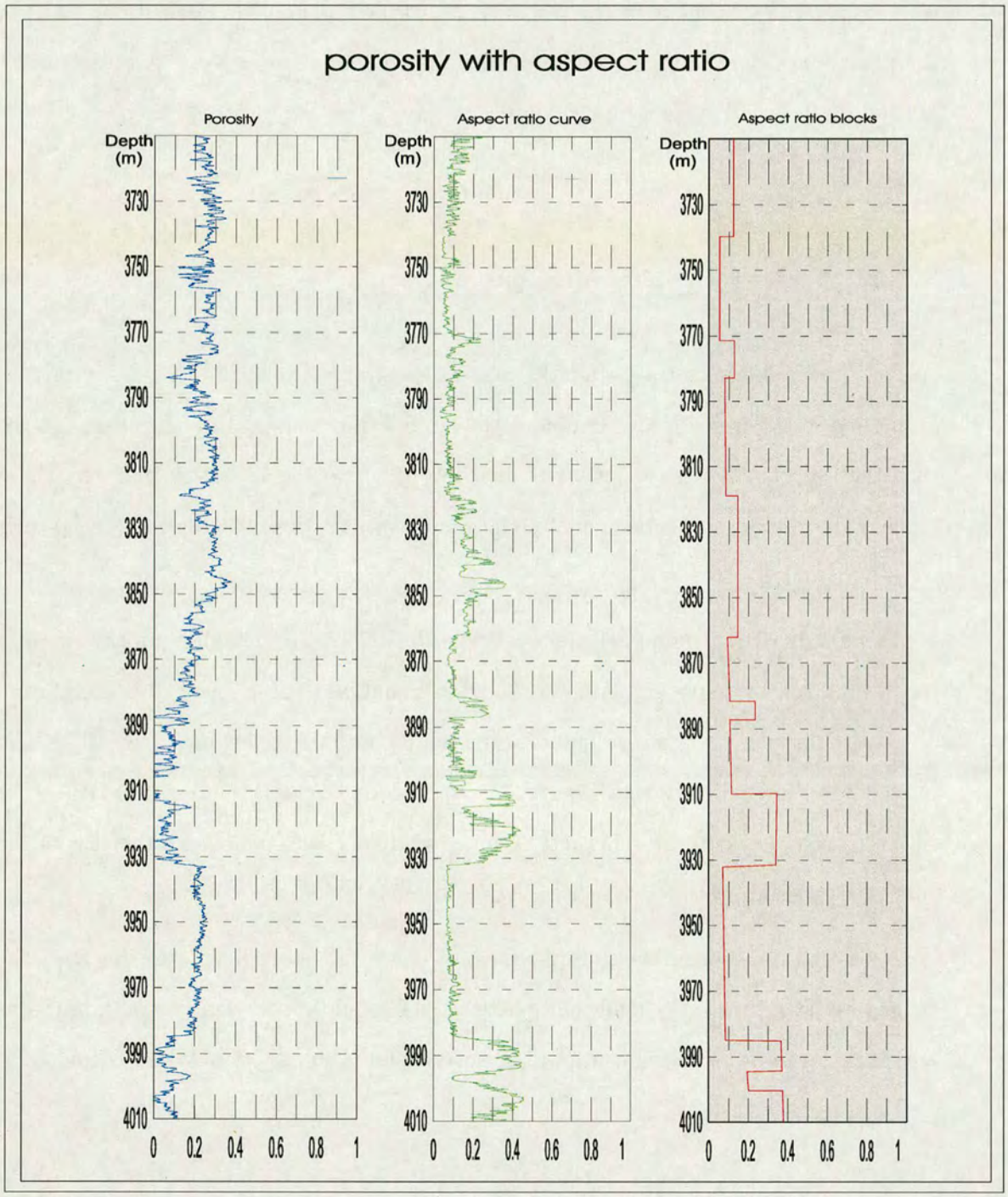

Figure 3.6: Prediction of aspect-ratios using well-log data and neural network. This figure shows the curves of porosity (panel 1) and predicted aspect-ratio (panel 2) by BPNN, also shows an independent estimation of aspect-ratios block (panel 3).

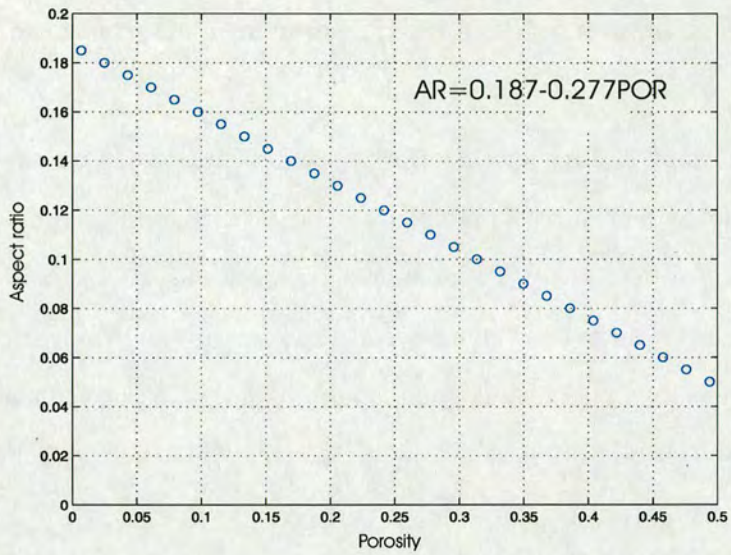

Figure 3.7: The modelling relationship of aspect-ratio and effective porosity for sand formation by equation (3.20) (Sams & Andrea, 2001). The result shows the changed tendency of porosity and aspect-ratio from 0 to 0.45 and 0 to 0.2 respectively.

3.3.5 Model results and validation

Using field data from the North Sea as inputs (caliper log, gamma-ray log, density log, self-potential log and sonic log, and aspect-ratio samples as well), the porosity(ϕ) and clay content (V_{cl}) can be obtained, and the equations (3.16) and (3.17) can be derived for velocity prediction, have

$$V_p = 4.198 - 4.17\phi - 1.64V_{cl} + [2.99\alpha_s - 4.05\alpha_c], \tag{3.21}$$

$$V_s = 3.199 - 3.24\phi - 1.42V_{cl} + [2.64\alpha_s - 3.32\alpha_c]. \tag{3.22}$$

The predictions using this semi-empirical approach are shown in Figure 3.8. The Figure 3.9(left) is a comparison of the predicted and measured porosity, which shows a good consistency, while Figure 3.9(right) shows the error distribution. They proved that this approach is successful in predicting velocities in study data set from the North Sea.

The error analysis between prediction and measurement also confirmed this conclusion.

The condition of validity for the application indicates that this improved empirical model can improve the results of predicted velocities because of a key control parameters (aspect-ratios) has been used. This model shows that the P- and S-wave velocity are the functions of porosity, shale content and aspect-ratio, and porosity having a larger influence on velocity than shale content, and it is far than the influence from aspect-ratios. The application of this model is based on the following assumptions:

1) Rock is consolidated without loose matrix.

2) Rock does not contain vugular pores or fractures.

3) It does not work for rock which contains very low velocity (such as gas).

This indicates that the results from this model will depend on the formation condition and assumption. Since the unconsolidated sands is certainly lower than that for the consolidated sands for main aspect-ratio, and higher than main porosity, therefore, the application of equations (3.21) and (3.22) to other wells assume that they have a similar condition, such as the lithology, minerals, cementing and pressure etc.

If we achieve an acceptable matching between the neural network generated results and the target values in the confirmation wells, this means that we have already achieved a robust solution. Therefore, we may then apply this solution to the remaining depth intervals or wells which have not target data. However, we should note if an incorrect or inconsistent data is used for the training data, we cannot expect it to give a correct predicted result.

For a second dataset, this empirical model may be used to build the relationship between velocity and reservoir parameters, but we also should keep in mind that this empirical model is only suitable for the similar lithology in the same formation or the same area with the first dataset. Otherwise, an obvious error will appear so that this

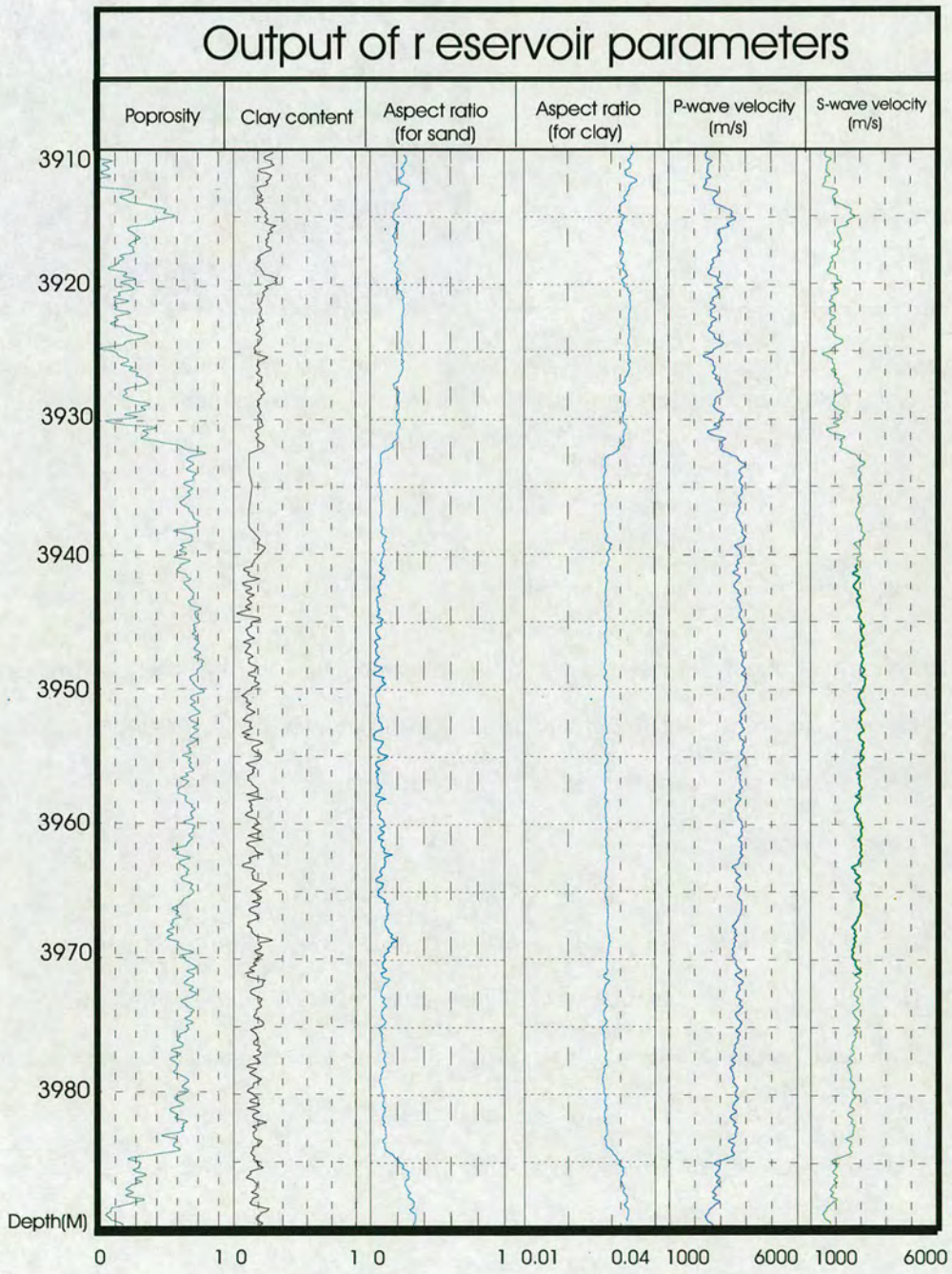

Figure 3.8: The relationship of velocity and reservoir parameters derived by semi-empirical approach (data from the North Sea).

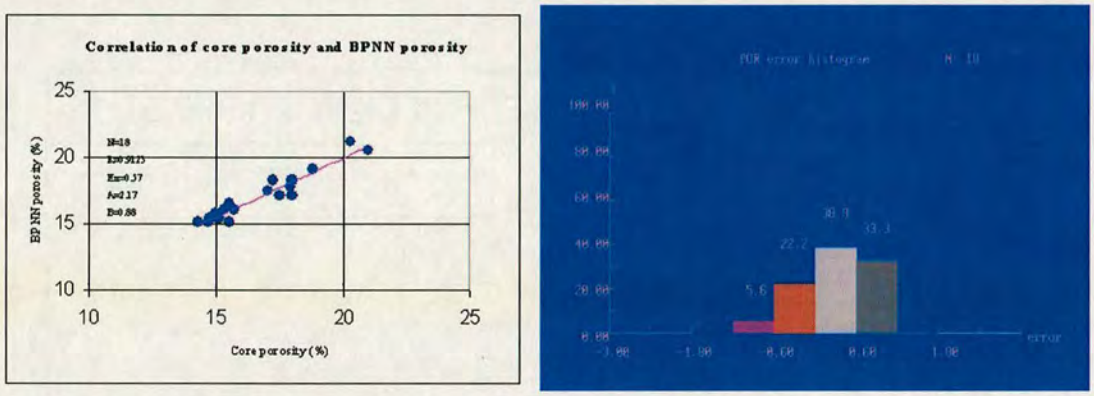

Figure 3.9: The plots of error analysis. Based on the data in Table 3.1. The left figure shows the comparison of core porosity and predicted porosity using BPNN. The right figure shows the error distribution of porosity by a histogram. The main porosity error is distributed between -0.6 and 0.8.

empirical model has probably been misused.

Note that as the differences in the multi-linear regression obtained by different authors proved, the extrapolation of this type of approach to other datasets does demand calibration with a reasonable quantity of measurements.

Like any other data processing, neural network processing mechanism and neural network technology can be misused. There must exist a good relationship between predictors and target values and the range of these values has to be represented in the training examples. The neural network relationship can only be trusted to the extent that it can be confirmed, both laterally and vertically by recorded data from other wells. The design of the neural network and the selection of training examples in current study, are best performed by an analyst who understands the correlative relationships between the logs and the rocks.

3.4 Weakness of semi-empirical approach

Generally speaking, the most empirical models based on statistical methods may not give an accurate prediction for the general case. The choice of a particular empirical model will depend on the objectives of application. Although the methods of geo-statistics usually give a very accurate prediction for the formation parameters such as velocities, porosity etc., special conditions are required in this case.

On the other hand, it is well-known that neural networks are ideally suitable for situations, where the manner that results are derived is unknown or is difficult to implement. Each of them has been used to solve different types of problem. Neural network used in this study is defined as nonlinear, multi layer, feed-forward, category, which has been trained by the back-propagation of error. This is the most popular type of artificial neural network in use for pattern recognition due to its learning ability. However, one of its major disadvantages is that it looks like a 'black-box' and provides no insight into its processing mechanism. Its performance is affected by many factors, such as the network structure itself (the numbers of input nodes, output nodes, hidden layers, hidden nodes and learning rate etc.), and training parameters (lithology, minerals, fluids and pressure etc.) which form the components of the generalized delta rule.

In addition to these weaknesses, there are also other limitations which have been encountered. These are:

(1) They do not provide insight into the physical mechanism governing the rock properties of the effective media.

(2) Application to datasets other than the one which has been used for their formulation usually requires calibration using a large quantity of data and a detailed analysis.

(3) Their conditions of validity may not be well defined.

(4) In the use of the neural network, the performance depends on the training data, and its ability to generate solutions cannot lie too far outside its experience.

3.5 Discussion and summary

This chapter presented an integration technique from well-log and core data to determine reservoir parameters using an empirical method to build the relationship between seismic velocities and reservoir parameters such as porosity, clay content and aspect-ratio.

The approach used in this chapter is an improved semi-empirical model, which is a combination of the empirical model of Han *et al.*(1986) and a neural network through a multi-regression method. As a result of this, a new relationship between velocity and reservoir parameters has been built. This semi-empirical approach is particularly suitable for solving problems where results are known but standard algorithms cannot be used due to uncertainty of the mathematical relationship. Artificial neural networks can offer significant advantages over traditional regression techniques. Linear regression requires the user to know the exact mathematical relationships between the predictors and the target values. In other words, we have to propose an algorithm. Neural networks do not require a proposed solution, only an intelligent selection of input curves and training examples. The tools in neural networks facilitate these selections. Regression techniques also force predicted values to lie near the mean values (having a smoothed-out solution) and thereby fail to preserve original data variability.

The pore aspect-ratios are used to characterize the compliances of the sand and clay components. Through the case study, we demonstrated that this approach provides a satisfactory result. This method can also be applied for the analysis of consolidated and unconsolidated formations, and it is suitable for isotropic and anisotropic reservoirs, this is because the relationship is derived from the real data itself in isotropic or anisotropic rocks. The application procedures are summarized below as:

(1) To establish the correlation between core and log data, the log and core should be

initially calibrated to ensure that the log and core data can be matched and integrated successfully (see Chapter 6 for details).

(2) The selection of geostatistical methods (different regression techniques) will affect the accuracy of parameter prediction (to compensate for the effects of lithology and other factors).

(3) The combination of reservoir parameters and seismic velocity will extend the use of well-log, core and seismic data for reservoir characterization.

(4) In practice, there are two important aspects that should be considered carefully, they are:

- How many sample data do we need to use for building a semi-empirical model ?
- What is the optimum number of hidden layer in the neural network for data training?

Chapter 4

ISOTROPIC DUAL POROSITY MODEL

4.1 Introduction

Xu and White (1995a, b; 1996) have proposed a model to predict elastic wave properties in clay-sand mixtures. This was identified as the starting point in the development of a strategy towards a powerful physical model in this study. In this chapter, I will present a modified model that circumvents some difficulties and weaknesses in constructing physically representative models of sandstone, by simulating certain geological processes. As a result, the key of reservoir parameters may be extracted directly from this approach. The elastic properties can then be calculated for the model without recourse to additional measurements. Prediction of velocity can enhance their interpretation for estimating reservoir parameters. The improvements in Xu-White model include the use of core-log calibration in order to integrate well-log, core and seismic data; development of an extended time-average equation to estimate porosity and clay content, and the use of a back propagation neural network to invert pore aspect-ratios. In order to understand the effects of fluid and lithology variation on the seismic wave velocities, following Xu and White approach (1995a, b; 1996), Kuster-Toksöz and DEM theories are used to calculate elastic properties, then the Gassmann's equations are employed to predict velocities for saturated rocks.

The impact of different reservoir parameters in isotropic rocks such as porosity, clay content, aspect-ratios, velocity and V_p/V_s ratio are analysed through field data analysis and modelling. Results derived from applying this model to the data from the North Sea have met our need satisfactorily. This has been further confirmed by error and sensitivity analysis.

4.2 Xu and White model

An overview of Xu-White model has been given in the previous chapter (Section 2.4.1.5) Figure 4.1 shows a flowchart of Xu-White model. This model requires inputs such as density and gamma-ray logs, rock elastic constants, and two fixed aspect-ratios for clay and sand formations. For log analysis, the clay content is usually approximated by the shale content. Because aspect-ratios are usually determined by the best fitting velocity predictions from sonic log measurement, also direct measurement is extremely impractical, Xu and White (1995, 1996) suggested a pore aspect-ratio of approximate 0.1 for sand related pores, and approximate 0.03 or 0.04 for clay related pores. The presence of even small number of fine cracks, or pores with very small aspect-ratios have a profound effect on the dry rock frame and its response to the introduction of pore fluids. It has already been mentioned that a significant drop in velocity occurs when even small amounts of air (or gas) are introduced into porous rock. Details of input parameters are listed in Table 4.1. Table 4.2 presents the outputs of Xu-White model, including elastic properties and predicted P- and S-wave velocities.

4.3 Starting point

Wyllie *et al.*'s (1956) time-average equation is used to build the relationship between porosity and velocity in Xu-White model, this equation is well at large burial depth. However, it has been suggested that it is clay that introduces scatter into the porosity-

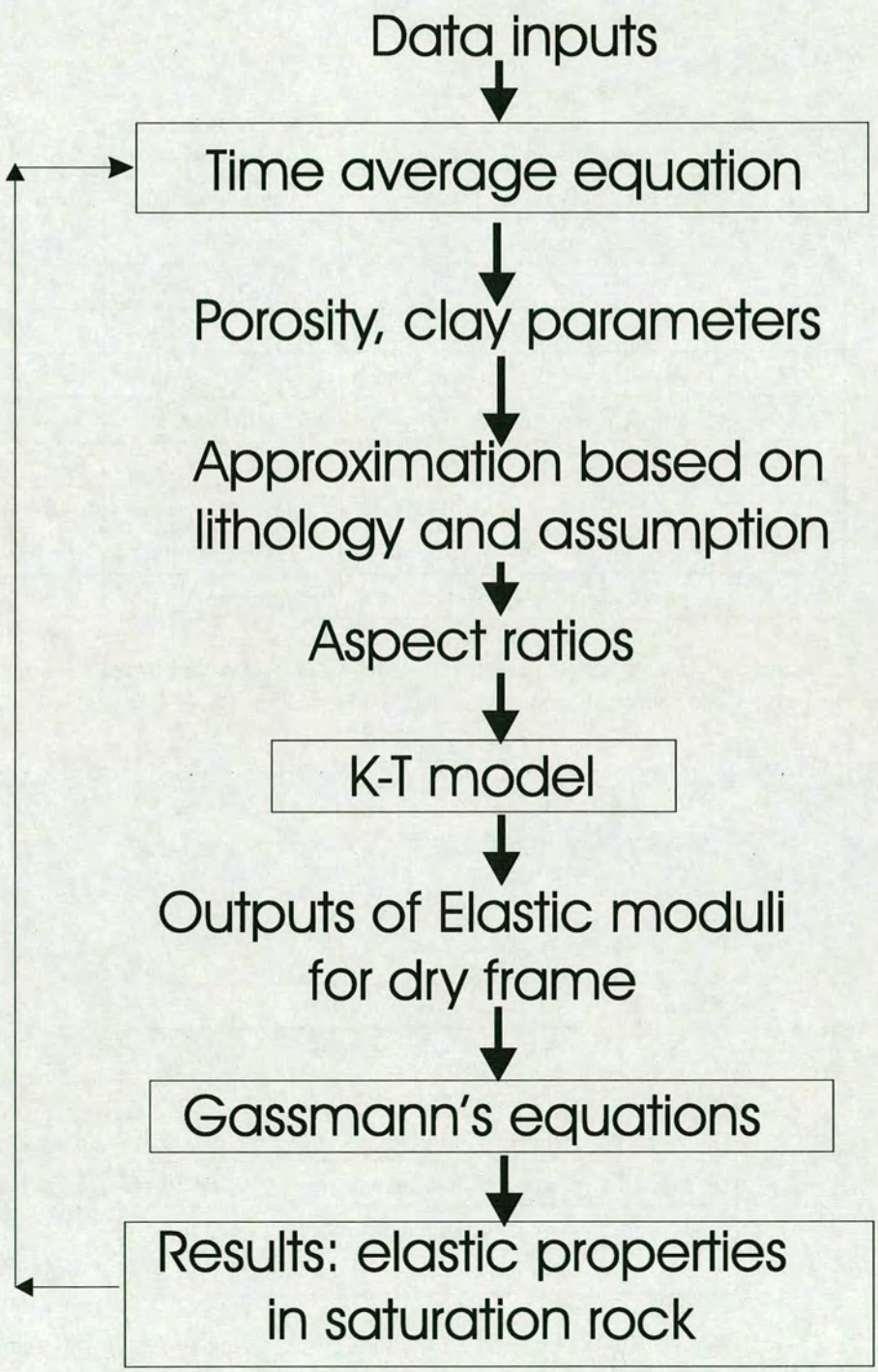

Figure 4.1: The flowchart of Xu-White model. Porosity and aspect-ratio are divided into sand and clay related pores, and the Kuster-Toksöz and DEM theories are used to calculate elastic properties. Gassmann's equations are used for fluid substitutions.

Symbol	Parameter meaning	Brief description	Unit
ρ	rock bulk density value	value from log	g/cm^3
GR	rock gamma-ray value	value from log	api
ϕ	total effective porosity	intermediate result	%
ψ	clay volume	intermediate result	%
T_s^p	P-wave transit time of sand grains	elastic constant	$\mu s/m$
T_s^s	S-wave transit time of sand grains	elastic constant	$\mu s/m$
T_{sh}^p	P-wave transit time of clay	elastic constant	$\mu s/m$
T_{sh}^s	S-wave transit time of clay	elastic constant	$\mu s/m$
α_s	aspect-ratio for sand related pores	approximation	v/v
α_c	aspect-ratio for clay related pores	approximation	v/v

Table 4.1: Initial and intermediate parameters for inputs of Xu-White model. They include log data, rock constants and assuming data (e.g. aspect ratios)

Symbol	Brief description	Unit
K_d	bulk moduli for dry frame	$kg/m.s^2$
μ_d	shear moduli for dry frame	$kg/m.s^2$
K_m	bulk moduli for mixture	$kg/m.s^2$
μ_m	shear moduli for mixture	$kg/m.s^2$
V_p	P-wave velocity for saturated rock	m/s
V_s	S-wave velocity for saturated rock	m/s

Table 4.2: The outputs of Xu-White model for prediction of rock properties in the clay-sand mixture. The velocities to be the final outputs of Xu-White model.

velocity relationship and loose clay filling in pores reduces velocity. So if clay is poorly compacted or poorly consolidated due to the low litho-static pressure, pores associated with clay particles are still open under such pressures, so that clay affects not only the elastic properties of the grain matrix but also the porosity-velocity relationship. In this case, the result no longer obeys the time-average equation. In general, two problems that arise in using the time-average equation are related to the estimation of the compressional velocity, saturating fluid velocity, and the range of applicability. Velocities in the rock matrix and pore fluid are normally assumed because detailed lithology and pore fluid composition are not available at the time of log interpretation. This assumption often generates errors in the derived porosity. The time-average equation is often applied over its range of applicability. Because it is based on an oversimplified model, it does not work for rocks containing fluid of low velocities such as gas and live oil (oil with gas in solution), or rock with vuggy pores or fractures (e.g. soft and unconsolidated sand). In particular, the time-average equation cannot be used to study the effect of partial gas-saturation on velocity in rocks. Because vuggy pores tend to be big, spherical, and incompressible, P-wave velocity is very insensitive to pore fluid saturation, so using this equation under these conditions will severely underestimate the porosity.

In addition, the marked feature of Xu-White model based on Kuster-Toksöz model and effective medium theories is that there are only two major variables (porosity and aspect-ratio) among many parameters (clays, fluid, cement and pressure etc.). In fact, the assumption of two fixed aspect-ratios allows estimation of the elastic moduli approximately and is only suitable for 'single media' formation. There is evidence showing that the aspect-ratio significantly controls the elastic behaviour of sand and clay mixtures. Therefore the aspect-ratio of pores plays the same significant role as those of porosity in velocity determination. Owing to the fact that aspect-ratio can only be

measured by core special spectrum analysis from laboratory or by modelling result (such as Kuster-Toksöz model). It can not obtained directly by the tool of well-logging, and it is difficult to derived from conventional methods or approaches. According this, the value of aspect-ratio is usually assumed to be constant for practical use. For instance, in Xu-White model the aspect-ratios for sand and clay related pores are defined as 0.1 and 0.03 respectively; both these values are often used as an approximation of aspect-ratios at large depth intervals.

Due to the computing error from velocity prediction, the raw data from logs cannot be used as the model input directly. Thus, the correction and editing of log curves need to be done before using them as inputs (the details will be presented in Chapter 6).

To overcame these weakness mentioned above, a new model will be presented in this chapter. The advantages of this new model include (1) an extended time-average equation is used to replace the Wyllie's time-average equation for building the relationship between porosity and velocity, (2) a back-propagation neural network is used to invert aspect-ratios faction using well-logs, and (3) the varying aspect-ratios will then be fed into the Kuster-Toksöz and DEM equations to determine elastic moduli and velocities.

4.4 Isotropic dual porosity model

This model can be incorporated in the scheme that is similar to Xu and White (1995a, b; 1996) model to predict elastic moduli and velocities based on the properties of randomly distributed sand grains, clay content and two varying aspect-ratios. Because this model is an extension of Xu-White model, it may be called 'improved Xu-White model' or 'isotropic dual porosity (IDP) model' (the related anisotropic dual porosity model (ADP) will be developed in the next chapter). Figure 4.2 illustrates the work flow of the isotropic dual porosity (IDP) model. Comparing with the Figure 4.1, the difference is the extended time-average equations and varying aspect-ratios are used for

the determination of elastic moduli and velocities.

4.4.1 Modification of time-average equation

Wyllie's (1956) equation is based on dual phase media, its weakness is that it cannot accurately estimate the relationship between porosity and velocity when clay is present in a sand formation. Also it is only suitable for porosity range between 15 and 30% (Raymer *et al.* 1980). Wyllie *et al.* (1956) suggested that the total rock should include pore and sand matrix as shown in Figure 4.3, the travel time can be expressed as

$$T = (1 - \phi)T_m + \phi T_f, \tag{4.1}$$

where ϕ is effective porosity of rock, T, T_{ma}, T_f are the travel times for the bulk rock, solid matrix and fluid, respectively.

Time-average equation gives a simple relationship between total travel time (velocity) and porosity in a two-component composite. The velocity derived from seismic inversion and synthetic data can be used to estimate porosity. Therefore, using this equation we can obtain formation or rock velocity based on porosity (for example, using sonic log or density log). On the other hand, we can invert porosity from velocity if we have velocity measurement (for example, using measurements from the dipole sonic log or VSP data).

Angeleri and Carpi (1982) proposed the use of a new time average equation for three-phase media. They suggested that the clay content is an independent component. Unfortunately, the clay content is unknown in the region beyond the immediate area of the well when velocity is obtained from seismic data, so that in real application this method cannot be effectively used to estimate porosity.

In this section, a new concept of an extended time-average model has been proposed as an equivalent model. The sand formation containing clay may be equivalent to a

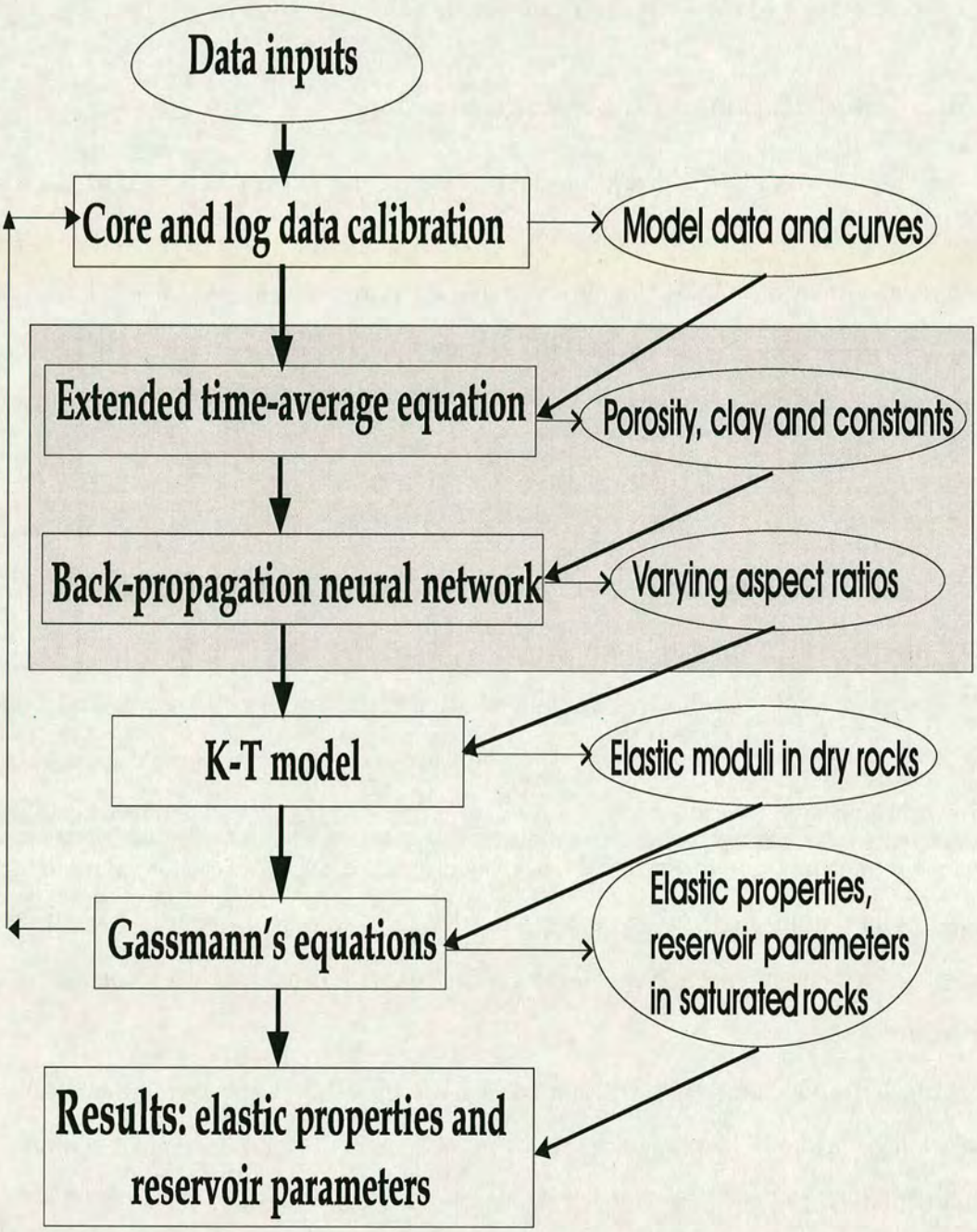

Figure 4.2: Work flow of the isotropic dual porosity model for predicting rock properties. The main improvements are: the both extended lithology and physical properties equations are used to replace the time average equation, and a back-propagation neural network is used to estimate aspect-ratios to replace fixed aspect-ratio for the whole depth range.

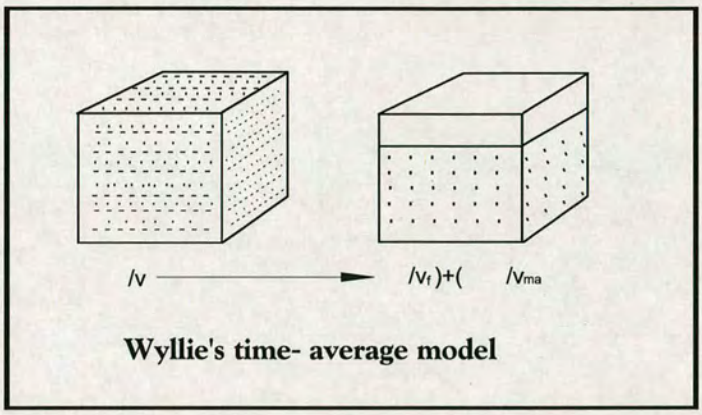

Figure 4.3: Traditional model to build the relationship between velocity and porosity, which is called time-average equation by Wyllie *et al.* (1956).

two-unit model (Figure 4.4), which includes clean sand and clean clay. According to the principle of the time-average equation of Wyllie (1956), we may build a lithology properties equation to account for clay content in sand formation based on velocity, and also we can build another physical property equation to estimate porosity containing clay influence.

In the lithology properties part, we have

$$1 = \psi + (1 - \psi), \tag{4.2}$$

where the unit rock volume is 1, ψ is clay particles, $(1-\psi)$ represents clean sand volume. By transferring this equation to travel time, we have

$$T = T_\psi + T_s, \tag{4.3}$$

where T is the travel time through the whole rock volume, T_ψ is the travel time in the clay particles and T_s is the travel time in the clean sand. Because

$$T = \frac{d}{V}, T_\psi = \frac{d \cdot \psi}{V_\psi}, T_s = \frac{d \cdot (1 - \psi)}{V_s},$$

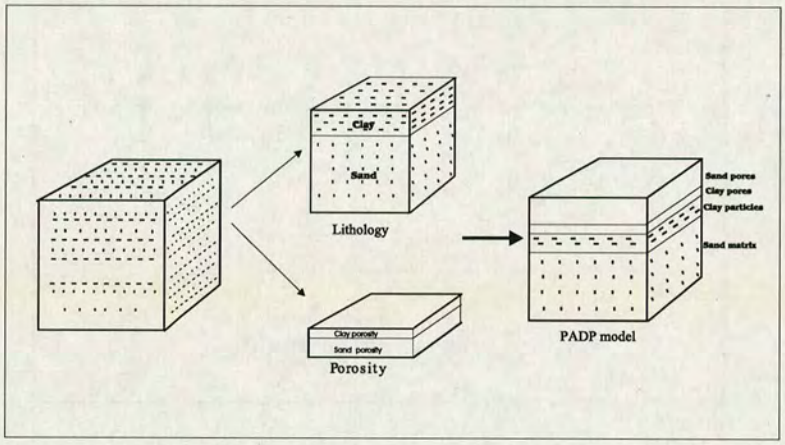

Figure 4.4: Extended time-average model. The rock is divided into both clean sand and clean clay. The total porosity is divided into sand porosity and clay porosity. The time through the whole rock volume is equal to the total travel time through sand, clay, clay pore and sand pore.

where d is the total distance in unit rock volume, based on equation (4.3), we have

$$\frac{1}{V} = \frac{\psi}{V_\psi} + \frac{1-\psi}{V_s}, \tag{4.4}$$

where V is P-wave velocity, V_ψ and V_s are P-wave velocities of clean clay and clean sand respectively, ψ is the clay content. From Figure 4.4 we can see that the physical properties can be sub-divided into sand pore, clay pore, clay particles and rock matrix respectively. Therefore, the effective porosity should include two parts as

$$\phi = \phi_s + \phi_\psi, \tag{4.5}$$

so, we have

$$1 = \phi + \psi + m_a, \tag{4.6}$$

for travel time, we have

$$T = T_f + T_\psi + T_{ma}, \tag{4.7}$$

where ϕ is the total porosity, ϕ_s is the sand porosity, ϕ_ψ is the clay porosity, T is travel time in the whole rock, T_f is travel time in pore space filled by fluid, T_ψ is travel time through clay particles and T_{ma} is travel time for rock matrix. Using the method similar to the time-average equation of Wyllie (1956), we have:

$$T = \frac{d}{V}, T_s = \frac{d \cdot (1-\psi)}{V_s}, T_\psi = \frac{d.\psi}{V_\psi}, T_{ma} = \frac{d \cdot (1-\phi-\psi)}{m_a},$$

where d is the total distance in unit rock volume, based on equation (4.7), we have

$$\frac{1}{V} = \frac{\phi}{V_f} + \frac{\psi}{V_\psi} + \frac{1-\phi-\psi}{m_a}, \tag{4.8}$$

according to equations (4.4) and (4.8), we can obtain extended lithology-physical property equations as follows

$$\begin{cases} \frac{1}{V} = \frac{\psi}{V_\psi} + \frac{1-\psi}{V_{sand}}, \\ \frac{1}{V} = \frac{\phi}{V_f} + \frac{\psi}{V_\psi} + \frac{1-\phi-\psi}{m_a}, \end{cases} \tag{4.9}$$

where V_f is the fluid velocity inside sand pore (m/s), V_{ma} is the rock matrix velocity (m/s), the equation (4.9) can be written based on P-wave travel time as

$$\begin{cases} T^p = \psi T_\psi^p + (1-\psi) T_s^p, \\ T^p = \phi T_f^p + \psi T_\psi^p + (1-\phi-\psi) T_{m_a}^p. \end{cases} \tag{4.10}$$

where T^p is total transit time of P-wave in sand-clay mixture T_ψ^p, T_s^p, T_f^p and $T_{m_a}^p$ are the P-wave velocities for clay particles, clean sand, fluid inside pore space and rock matrix, respectively.

Using equation (4.9) or equation (4.10), the porosity containing effect of the clay will be obtained. P-wave and S-wave velocities are given by

$$V_p = \left(\frac{\lambda_m + 2\mu_m}{\rho_m} \right)^{1/2}, \tag{4.11}$$

and

$$V_s = \left(\frac{\mu_m}{\rho_m} \right)^{1/2}, \tag{4.12}$$

where V_p and V_s are the P- and S-wave velocities, μ_m is the shear modulus and ρ_m is the bulk density, that

$$K_m = \lambda_m + \frac{2}{3}\mu_m, \tag{4.13}$$

where λ is the Lame's constant, based on equations (4.11), (4.12) and equation (4.13), so we can obtain

$$K_m = (V_p^2 \rho_m - 2\mu_m) + 2\mu_m - \frac{4}{3}(V_s^2 \rho_m), \tag{4.14}$$

and

$$K_m = \rho_m (V_p^2 - \frac{4}{3} V_s^2). \tag{4.15}$$

The bulk and shear moduli of the sand-clay mixture are calculated from its transit time using

$$K_m = \rho_m \cdot \left[\frac{1}{(T_m^p)^2} - \frac{4}{3(T_m^s)^2} \right], \tag{4.16}$$

and

$$\mu_m = \rho_m \cdot \left[\frac{1}{(T_m^s)^2}\right]. \tag{4.17}$$

Based on equation (4.10), we have

$$T_m^p = \phi T_f^p + \psi T_\psi^p + (1-\phi-\psi)T_{ma}^p, \tag{4.18}$$

$$T_m^s = \phi T_f^s + \psi T_\psi^s + (1-\phi-\psi)T_{ma}^s, \tag{4.19}$$

T_m^p, T_f^p, T_ψ^p and T_{ma}^p are the P-wave travel times for mixture, fluid, clay and matrix, respectively. T_m^s, T_f^s, T_ψ^s and T_{ma}^s are the S-wave travel times for mixture, fluid, clay and matrix, respectively.

4.4.2 Inversion of aspect-ratios

I have mentioned that Xu and White (1995a, b; 1996) used two fixed effective aspect-ratios in their model. This is because the use of effective aspect-ratios are valid, but in practice, the determination of aspect-ratios has two major difficulties:

(1) The assumption of an idealized ellipsoidal pore shapes can hardly be expected in real rock.

(2) Description of the hypothetical pore spaces associated with the sand and clay using just two fixed aspect-ratios over a large depth range is obviously a simplification.

To overcome the problems above, a back propagation neural network is used to estimate aspect-ratio on the basis of measured results and well-logs for the large depth range (Yan *et al.* 2002). This network consists of an input layer, an intermediate layer (hidden layer) and an output layer. The log data such as caliper log, gamma-ray log, self-potential log and density log are used as input values, and the measured aspect-ratios are used as the desired values. The connection nodes of inputs and outputs in

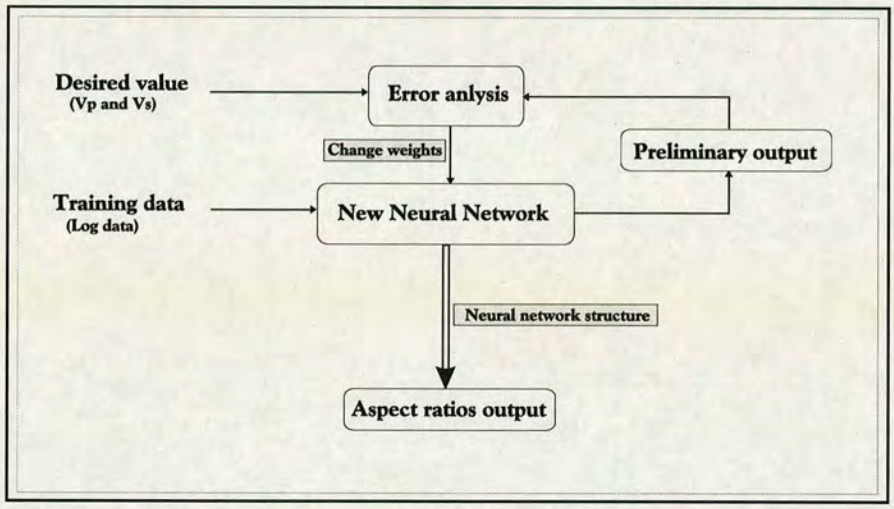

Figure 4.5: The work diagram for inversion of aspect-ratio using a back-propagation neural network. This network consists of an input layer, an intermediate layer (hidden layer) and an output layer. The connection nodes of inputs and outputs in the network are known, but the number of hidden nodes will be decided while data training.

the network are known, but the number of hidden nodes is unknown.

The range of numbers for hidden nodes is designed between 1 and 25 in this model, and its choice depends on various factors such as the number of samples, system error etc.. When the network is running, the outputs are used as original data to analyse the coherence and error of the network. If the coherence is larger, or when the error changes too fast, the value of the network will be adjusted. The results of inversion can integrate the response of many influencing factors. The output error propagates backwards through the network to modify the link weights of the network, and the mapping relationship between the input and desired output vectors is encoded in the weights with a distributed form.

The structure of neural network is shown in Figure 4.5. The main procedure used to invert aspect-ratio may be described below:

- (1) The measured velocities from dipole sonic log are used as the desired (expected) values. The predicted velocity from Xu-White model is used as the esti-

mated values. Choosing the first depth point and using Xu and White model via error comparison of velocity, a value of aspect-ratio may be determined by the minimal velocity error. This value will be chosen as a sample (standard value) of aspect-ratio in the neural network. Repeating this procedure, the second value of aspect-ratio will be determined at the next depth until enough samples are obtained.

- (2) The sample aspect-ratios are chosen based on the above are regarded as the standard values, they will be used as the desired values for the network.
- (3) Logs data (such as GR, SP, DEN) at related depth are chosen as inputs for network.
- (4) Assigning a suitable weight value to this network.
- (5) Running network for data training.
- (6) Calculating error based on the predicted aspect-ratios and desired aspect-ratios.
- (7) Making adjustment of the weight values to reduce the error between predicted values and expected values.
- (8) After correction of the weight values, network starts to compute the whole error, which is the total error sum of single training pattern.
- (9) If the error is larger than the tolerance, repeating the steps (3) to (7).

The process is iterated many times, until the error reduces to the expected accuracy, and a BPNN is established. To calculate the average value of error (ΔE_n) for the aspect-ratio, the input is presented to an initially randomized BPNN, and the weights values are adjusted based on the previously determined values until all training sets are

exhausted, and it is necessary to adjust the learning rate (η) during training. Note that the BPNN used in this chapter is the same with my previous empirical model (refer to Chapter 3).

4.4.3 Estimation of bulk and shear moduli in dry rocks

Kuster and Toksöz (1974) derived their model from the scattering theory (hereafter referred to as KT model). KT model assumes that

- the effective medium is composed of two phases of different properties.
- one phase(the matrix) forms a continuum and the other phase is the inclusion embedded randomly.
- the inclusions (pores) are so dilute that they do not interact or overlap with each other.
- the wavelength is much larger than the size of the inclusions.

These assumptions can also be extended to macroscopically homogeneous effective media, and imply that the pores are isolated and the effective medium has porosity but no permeability. It also assumes that multiple scattering effects are negligible. The KT model for spheroidal inclusions and a fluid-saturated rock produces the following equations:

$$K_d = \frac{K_m + 4A\mu_m}{1 - 3A}, \tag{4.20}$$

and

$$\mu_d = \mu_m \frac{1 + B(9K_m + 8\mu_m)}{1 - 6B(K_m + 2\mu_m)}, \tag{4.21}$$

where

$$A = \frac{1}{3}\left(\frac{K' - K_m}{3K_m + 4K\mu_m}\right) \sum_{l=s,c}^{N} \phi_l T_{iijj}(\alpha), \tag{4.22}$$

$$B = \frac{1}{25} \frac{(\mu' - \mu_m)}{\mu_m(3K_m + 4\mu_m)} \sum_{l=s,c}^{N} \phi_l \left(T_{ijij}(\alpha) - \frac{T_{iijj}(\alpha)}{3} \right). \tag{4.23}$$

K_d, K_m and K' are the bulk moduli of dry frame, mixture and fluid. μ_d, μ_m and μ' are the corresponding shear moduli of dry frame, mixture and fluid. The bulk and shear moduli of dry frame (K_d and μ_d) can be determined by equations (4.20) and (4.21), the bulk and shear moduli of the mixture (K_m and μ_m) also can be obtained from equations (4.15) and (4.17) and the bulk and shear moduli of fluid ($K^{'}$ and $\mu^{'}$) are zero when computing the moduli of the dry frame (with empty pores). The scalars $T_{iijj}(\alpha)$ and $T_{ijij}(\alpha)$ are functions of the aspect-ratio (the ratio of short-axis to long-axis), and they are given by Kuster-Toksöz (1974) (Appendix A).

KT model shows that the effective elastic moduli of a two-phase medium depend not only on the intrinsic moduli and the concentration (porosity for rocks) but also on the shape of the inclusions. A small concentration of low aspect-ratio pores in a rock can greatly reduce the effective moduli, a prediction which is in agreement with the experimental results of Nur and Simmons (1969).

4.4.4 Prediction of velocities in saturated rocks

I have reviewed Gassmann's (1951) model in Section 2.4.1.1. This model relates the elastic moduli of a fluid saturated porous rock to elastic moduli of the rock in its dry state (rock frame), and the moduli of solid grain matrix and pore fluids. Fluid saturated bulk modulus K is given by

$$K = K_d + \frac{\left(1 - \frac{K_d}{K_m}\right)^2}{\frac{\phi}{K'} + \frac{1-\phi}{K_m} - \frac{K_d}{K_m^2}}. \tag{4.24}$$

Since shear modulus of the rock is not affected by fluid saturation, so

$$\mu = \mu_d,$$

and

$$\rho_b = (1 - \phi)\rho_m + \phi\rho' \tag{4.25}$$

where μ_d is the frame (dry) shear modulus of the rock. The density of the saturated rock is ρ_b, ρ_m is the density of the rock matrix and ρ' is the density of the fluid.

Gassmann's equation is normally used together with the auxiliary equations (expressing the P- and S-wave velocities, Vp and Vs, in terms of the elastic moduli) and equation (4.25) (relating bulk density ρ_b to porosity). Velocities can be obtained from equations (4.11) and (4.12). In the original derivation of the Gassmann equation, following basic assumptions were made.

(1) all the pores are interconnected or communicating,

(2) the pores are filled with a viscous fluid (liquid or gas),

(3) the relative motion between the solid and the fluid is negligible small compared to the motion of the saturated rock,

(4) the pore fluid does not interact with the solid matrix in a way that would change the shear rigidity of the frame (hardening or softening),

(5) the rock or porous medium (both the matrix and the frame) is macroscopically homogeneous and isotropic.

Thus, Gassmann equation can be used to predict the S-wave velocity from the P-wave velocity if a relationship between the bulk and the shear moduli in the dry state is assumed. This assumption is consistent with experimental data from different authors. Hence Gassmann's equation provides the theoretical justification for the use of seismic attributes which measure estimations of velocity, White (1965) formulated the Gassmann model for the P-wave velocity (V_p) as:

$$V_p = \left\{ \frac{1}{\rho_b} \left[K_d + \frac{4}{3}\mu_d + \frac{\left(1 - \frac{K_d}{K_m}\right)^2}{\frac{(1-\phi)}{K_m} + \frac{\phi}{K_f} - \frac{K_d}{K_m}} \right] \right\}^{\frac{1}{2}}, \tag{4.26}$$

and for the S-wave velocity (Vs) as:

$$V_s = \left\{ \frac{\mu_d}{\rho_b} \right\}^{\frac{1}{2}}. \tag{4.27}$$

Direct application of equations (4.26) and (4.27) requires knowledge of the moduli of the dry rock frame, which can be reasonably assumed to be equivalent to the moduli of the gas saturated rock. Also required are the elastic moduli of the grain matrix for the pore fluid and porosity.

4.4.5 Model implementation

4.4.5.1 *Work flow*

Implementation of the isotropic dual porosity (IDP) model can be roughly divided into seven steps (refer to the next section), which include data inputs, processing and result outputs. Based on the structure of IDP model and its function, the work flow for the implementation of IDP model can be summarized as Figure 4.6:

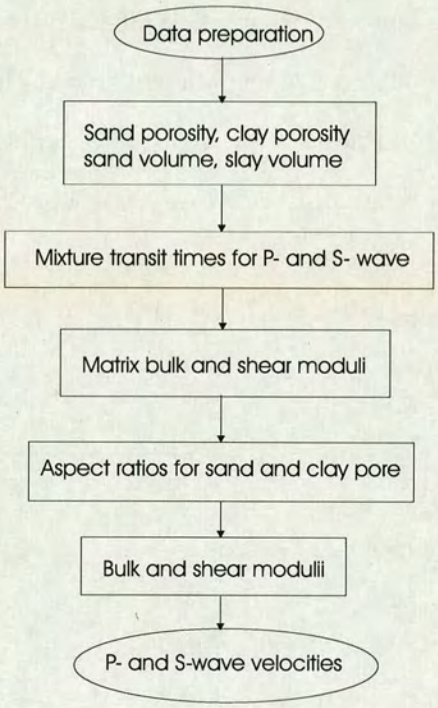

Figure 4.6: The workflow of the implementation of IDP model.

4.4.5.2 *Step by step*

Using well-log, lithology data and core analysis results, the rock elastic moduli and velocities may be predicted by the steps below:

- ***Step 1: Correction and calibration for input data***

Log data correction and data calibration will be discussed in next chapter (refer to Sections 6.2 and 6.3 in Chapter 6)

- ***Step 2: Estimation of reservoir and rock parameters***

i) Pore volumes and clay volume: The dual porosity means that the sum of the pore volumes related to sand grains ϕ_s, and related to clay content ϕ_ψ, is equal to the total pore space of the mixture by equation (4.5). We have

$$V_s = 1 - \phi - V_\psi \,, \tag{4.28}$$

where ϕ_s and ϕ_c are therefore approximated by the following equations:

$$\phi_s = V_s \frac{\phi}{1-\phi} \,, \tag{4.29}$$

and

$$\phi_\psi = V_\psi \frac{\phi}{1-\phi} \,, \tag{4.30}$$

where ϕ is total effective pore, ϕ_s is pore volume related to sand grains, ϕ_ψ is pore volume related to clay content, V_s is sand volume and V_ψ is shale volume which can be estimated by GR log or a combination of the neutron and density logs (refer to Section 3.3.3 in Chapter 3)

ii) P- and S-wave transit times: The P- and S-wave transit times (T_m^p and T_m^s) can be determined by equations (4.18 and 4.19). Note that T_m^p, T_f^p, T_ψ^p and T_{ma}^p are the P-wave travel times for mixture, fluid, clay and matrix, respectively. T_m^s, T_f^s, T_ψ^s and T_{ma}^s are the S-wave travel times for mixture, fluid, clay and matrix, respectively.

- ***Step 3: Calculation of elastic moduli for clay-sand mixture***

Elastic bulk and shear moduli of the mixture of sand grains and clay are calculated from P- and S-wave transit times by equations (4.16) and (4.17). The mixture density (ρ_m) can be obtained directly from density log (DEN).

- ***Step 4: Inversion of aspect-ratio of sand and clay***

Aspect-ratios (α_s, α_ψ) are estimated here from artificial neural network (BPNN), which needs log data as the inputs to BPNN, and aspect-ratios are the outputs (predicted values). This procedure may be simplified as:

Training: GR, SP, DEN, AC—> α_s, α_ψ (for samples).

Predicting: GR, SP, DEN, AC—> α_s, α_ψ (for large depth).

Note that the aspect-ratios will be used as the inputs to the equations of $T_{iijj}(\alpha)$ and $T_{ijij}(\alpha)$ in order to obtain the functions of the aspect-ratio (Appendix A).

- ***Step 5: Determination of elastic properties for dry rocks***

The next step is to evaluate the bulk and shear moduli (K_d, μ_d) for dry rocks in isotropic porous rocks using Kuster and Toksöz (1974) model by equations (4.20), (4.21),(4.22) and (4.23). The scalars $T_{iijj}(\alpha)$ and $T_{ijij}(\alpha)$ are functions of the aspect-ratio given by Kuster-Toksöz (1974).

- ***Step 6: Fluid substitution***

The Gassmann (1951) model is used to simulate the effect of fluid relaxation. P- and S-wave velocities (V_p and V_s) in fluid saturated rocks are estimated using equations (4.26) and (4.27). The saturated rock (ρ_b) is expressed as equation (4.25), ρ_m is the density of the rock matrix, $\rho^{'}$ is the density of the fluid.

- ***Step 7: Outputs***

The outputs include rock elastic parameters and predicted velocities.

4.5 Modelling and results analysis

4.5.1 The impact of porosity and clay

There is much laboratory evidence to demonstrate that porosity and clay content can affect P-wave and S-wave velocities (Han *et al.* 1986; Klimentos 1991 and Marion *et al.* 1992). Although each of the above studies has a different physical basis, all results have illustrated to a general trend that increasing clay content in sandstones systematically

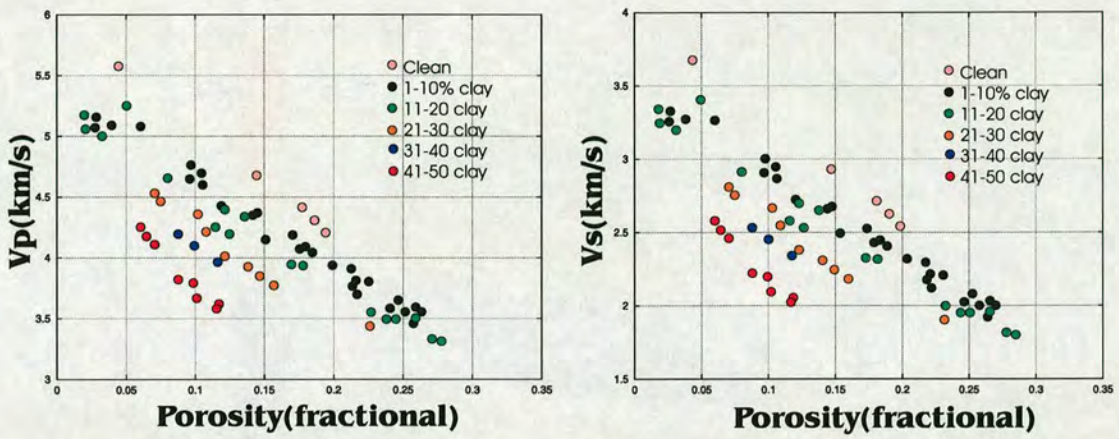

Figure 4.7: Measurement of the observed variation of velocities with porosity and clay content. (left) P-wave and (right) S-wave velocities versus porosity for the sandstone samples at 40 MPa confining pressure and 1 MPa pore pressure. The porosities of the samples range from 2 to 30 percent, and the clay contents by volume fraction range from 0 to 50 percent (measured data are from Han *et al.* 1986).

decreases wave velocities in both well-consolidated and poorly consolidated sandstones. In other words, these results proved that clay minerals may significantly affect the elastic moduli and velocities of sandstones.

Han *et al.* (1986) measured compressional velocity Vp and shear velocity Vs as a function of pressure by varying clay contents and porosities. The compressional velocity Vp and shear velocity Vs versus porosity ϕ for all samples are shown in Figure 4.7 (left) and (right). A clear trend is that both Vp and Vs decrease with increasing porosity.

The measured results of Han *et al.* (1986) is at 40 MPa confining pressure and 1 MPa pore pressure. The range of clay content is from 0 to 50 percent; if it is a clean sandstone (Vcl = 0) or with less than 20% clay content, the varying trend of velocity versus porosity approximates to a linear relationship, which is consistent with the Wyllie time-average equation in a clean formation. However, when clay content is more than 20% in sandstone (in particular more than 30%), there is an obvious difference between the predicted velocities and the measured velocities (Han *et al*, 1986).

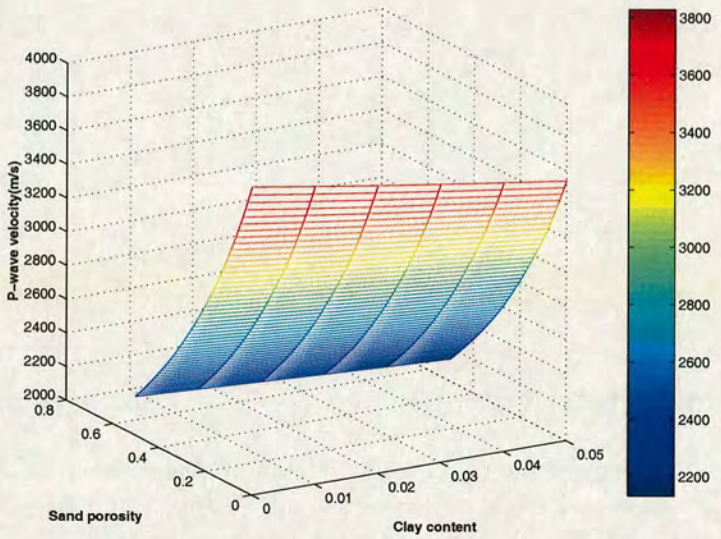

Figure 4.8: The modelling 3D relationship between velocity, porosity and clay content using the IDP model in clay-sand mixture.

The modelling result is used to study the relationships between velocity, porosity and clay content. Figure 4.8 indicates that velocity decreases with increasing porosity, and these results depend upon the clay content (in order to fit velocity, we have to account for the effect of clay content). The modelling results indicate that the velocity begins to rise rapidly when the clay content reaches 30%, the clay will fill low aspect-ratio pores and it can affect velocity prediction.

4.5.2 The effects of pore aspect-ratios

According to the IDP model described above, the pores are assumed to be spheroidal and their shape is characterized by their aspect-ratios. The total pore space is divided into two parts, with one associated with sand grains and the other associated with clay. Two varying aspect-ratio curves will replace both fixed values of aspect-ratio. The sand-related pore aspect-ratio is assumed to be 0.12, and 0.03 for clay-related pore aspect-ratio in Xu-White model; Table 4.3 shows these fixed aspect-ratios and other

Lithology	$T_P(\mu s/m)$	$T_s(\mu s/m)$	Density(g/cm^3)	aspect-ratio
Sandstone	171	256	2.65	0.12
Shale	341	584	2.45	0.03
Limestone	161	311	2.60	
Salt	220	348	2.00	
Brine	623		1.10	

Table 4.3: Aspect of ratios used in Xu and White (1995) model for the modelling to predict velocities in clay-sand mixture.

parameters used by Xu and White (1995).

As we can see in Table 4.3, when the sand-clay mixture contain thin-bed or other lithologies (e.g. limestone), the fixed values of aspect-ratio will fail to match the variability and possibly result in obvious error in elastic parameter prediction. This is because pore aspect-ratios in rock are not simply distributed, which has been illustrated by the validation of the physical model. The high effective pressure closes pores with very small aspect-ratio like micro-cracks, leaving large aspect-ratio pores open. In effect, the mean aspect-ratio can increase with confining pressure. The detailed discussion has already been given by Nur and Simmons (1969); and Murphy (1993). In summary, aspect-ratio may be affected by many factors, such as fluid property, lithology, formation pressure and micro-cracks etc.. In particular, if porosity is low or cracks are abundant, pressure plays a much more important role than others factors. Figure 4.9 shows the aspect-ratio variation under experimental pressure in the laboratory. Initially the experimental samples were dominantly populated with cracks (0.45% and 0.2% pore porosity). As differential pressures reached 10 *MPa*, these cracks in the sample continued to collapse until almost all original cracks with small aspect-ratios were closed; the large aspect-ratio pores and cracks became dominant with an average aspect-ratio as high as 0.01. When pressure reached 20 *MPa*, large aspect-ratio cracks continued to

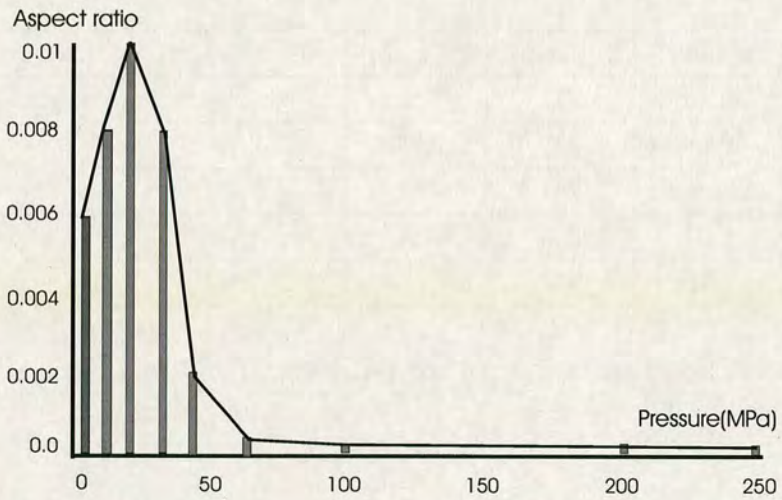

Figure 4.9: The relationship between aspect-ratios and pressure, derived from granite velocity measurements, performed by Nur and Simmons (1969).

collapse and pores began to deform into cracks. When the pressures reached 40 *MPa*, all the original cracks were fully closed and pores were deformed to become cracks with low aspect-ratio. Above 40 *MPa*, newly-formed cracks deformed the rock and at 70 *MPa*, the average aspect-ratio is lower. At pressures of 100 *MPa* and above, most new cracks are closed and the lowest aspect-ratio is reached.

The modelling result of Figure 4.10 shows a relationship between aspect-ratios and dry moduli, which gives the changed range of aspect-ratio from 0.01 to 1.0. In practice, the main varying range is approximate from 0.05 to 0.35 for a formation of clay-sand mixture, therefore, the fixed value of 0.1 for sand used by Xu-White just represents a special case, the possible reasons leads to variable aspect-ratio is (1) The high pressures resulted in the closure of the most compliant pores, thus increasing the effective aspect-ratio. (2) The aspect-ratio for the quartz component is determined from pure sandstones for the core data and ignores clay effects. (3) The effects of lithology, thickness of layer, inclusion and others factors are not considered.

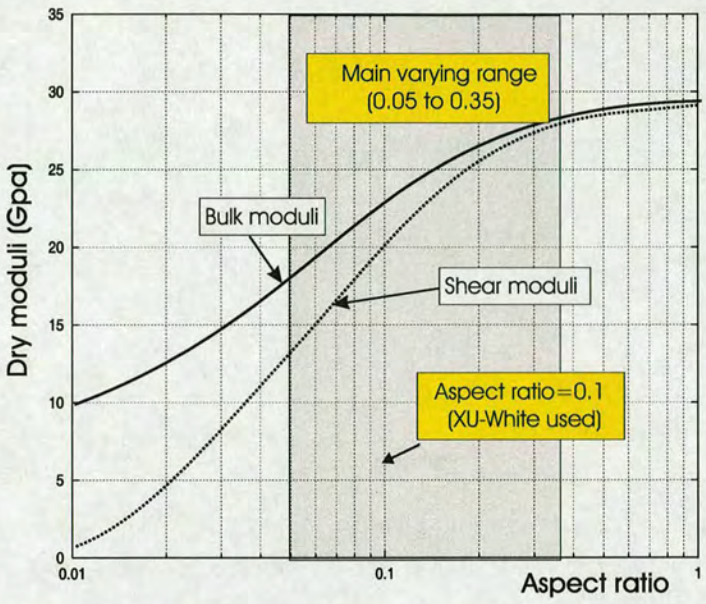

Figure 4.10: Modelling results for bulk and shear moduli as a function of aspect-ratio, the range from 0.05 to 0.35 is the main distribution for aspect-ratios in sand related pore, which indicates that the value of 0.1 is just a special case, representing the average value.

4.5.3 Velocities and elastic moduli in dry rocks

Murphy *et al.* (1993) measured the elastic moduli of clean sandstones over a wide range of porosities at ultrasonic frequencies and high pressures (>50 MPa). They use empirical equations to fit these data. Vernik (1997) used the method of Kachanov *et al.* (1994) to model elastic moduli also from ultrasonic measurements at high pressures. The data modelled by Vernik (1997) are compared with the data of Murphy *et al.* (1993). The two datasets are similar but with systematic differences at high porosities. Figure 4.11 shows the modelling results. As we can see that for high porosity both Xu-White model and PADP model have a good agreement, for low porosity area, there is an obvious different between Xu-White model and PADP model.

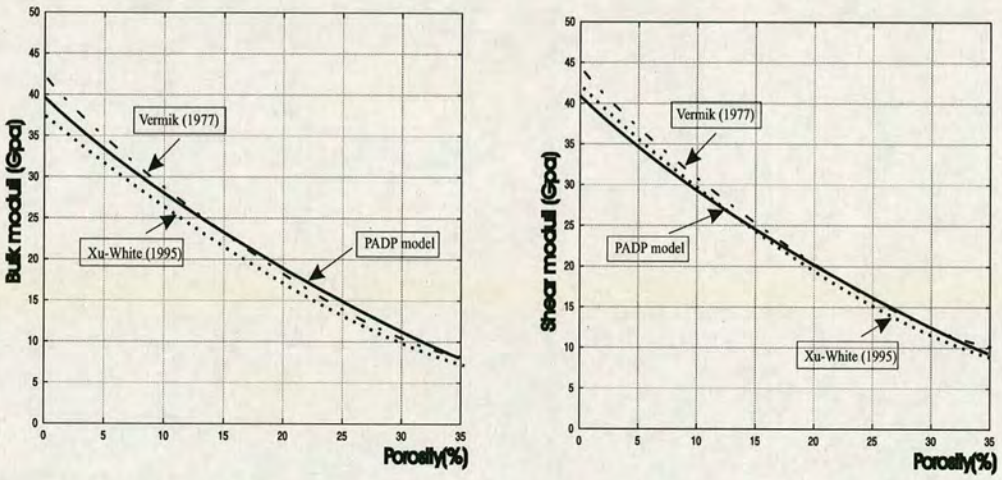

Figure 4.11: The relationship between bulk and shear moduli and porosity in dry rocks. The figures compared the relationship between elastic modulus and porosity from Xu-White and PADP model.

4.5.4 Velocities and Vp/Vs ratio in saturated rocks

We often use seismic data to obtain P- and S-wave velocities and hence the Vp/Vs ratio in an isotropic porous medium. This is because the velocity ratio Vp/Vs is a very useful parameter for the indication of rock properties, thus these results in turn can be used for the prediction of lithology and fluid substitution.

Many studies have been conducted to build the relationship between lithology, porosity, and Vp/Vs ratio. Castagna *et al.* (1985) showed that the velocity ratio for water-saturated clay-sand formations depends upon both porosity and clay by a least-squares regression, which can be expressed in a general form as:

$$V_p/V_s = a + b\phi + c\psi$$

where a, b, and c are the regression coefficients, ϕ and ψ are porosity and clay content. This relationship shows that an increase in porosity or clay content will increase Vp/Vs and the velocity ratio is more sensitive to porosity changes. The sand with high clay

content has velocity ratios which are similar to those in carbonate rocks. Thus, the resulting ambiguity in the interpretation of velocity data may be resolved by the combined use of the velocity and velocity ratio, and this provides an useful tool for reliable lithology discrimination. The following examples are used to prove this further:

Referring to Section 2.3.4 in Chapter 2, Castagna *et al.* (1985) found that shear velocity is nearly linearly related to compressional velocity for water saturated elastic silicate sedimentary rocks; the relations is

$$V_s = 0.862V_p - 1.172.$$

Referring to previous Chapter 2 and Chapter 3, Han *et al.* (1986) also showed that Vs is nearly linearly related to Vp, with some different coefficients from the equation above, and the best linear least-squares fit yields

$$V_s = 0.783V_p - 1.178,$$

Figure 4.12 shows the relationship between Vp/Vs, porosity and clay content in 3D based on the results of ADP model. The porosity is assumed to change from 10 to 50%, and the clay content also is assumed to change from 0 to 50%. The modelling results showed that the velocity ratio for water saturated clay-sand mixture depends on both porosity and clay content,. The variation of Vp/Vs ratios shows an increase range varies between 1.58 and 1.82.

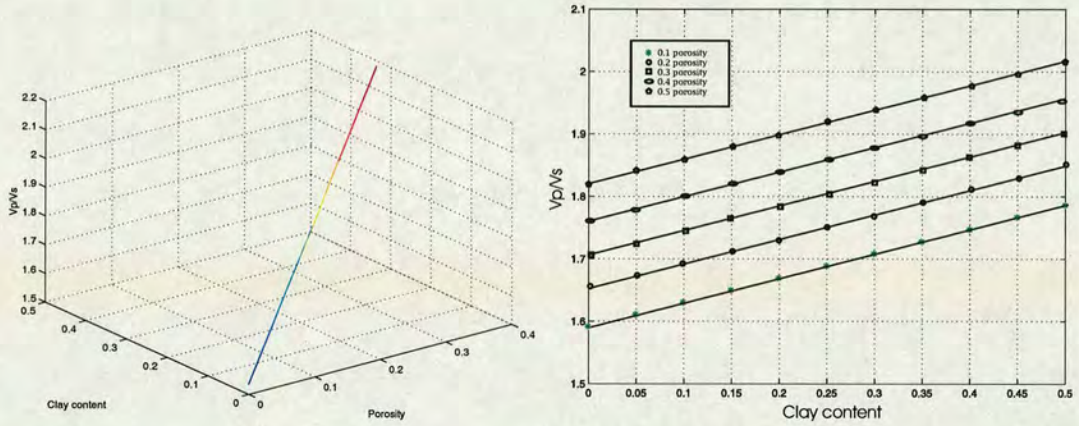

Figure 4.12: The modelling results using ADP model: The relationship between Vp/Vs, porosity and clay content (left hand figure); the changes of Vp/Vs at porosity ranging from 10% to 50% versus clay content (right hand figure).

4.6 Applications

4.6.1 Field data

Using the isotropic dual porosity model described above we firstly need to estimate the reservoir parameters, such as porosity, shale content and oil saturation. Figure 4.13 shows an example of the key reservoir parameter as: Panel 1 and Panel 2 show input log data, they are Grammar-Ray log, Caliper log and GR log and bulk Density log. Panels 3 to 5 show derived key reservoir parameters from the input logs, the outputs include the effective porosity, clay content and fluid saturation respectively. The method for key parameters determination will be discuss in the sections of reservoir parameters (Section 7.5 and 7.6, Chapter 7).

I applied the results of BPNN for large depths to predict pore aspect-ratio. Figure 4.14 shows an example from real data. This result shows that the changed range of aspect-ratios related to sand pores is between 0.05 to 0.35, and with those for clay related pores is between 0.01 to 0.02.

Figure 4.15 shows predicted velocities from the IDP model. The first curve is the

predicted P-wave velocity, the second curve is the predicted S-wave velocity, and also estimated is a related lithology based on the interpretation from log data.

Figure 4.16 (panel 4) is a result of the predicted S-wave velocity, which uses part of the training data to built the correlation to predict S-wave velocity for the whole depth in the same well. Panel 5 shows S-wave velocity measured from a sonic log, which can be used as the error comparison or analysis with the predicted result in panel 4.

4.6.2 Error analysis

Table 4.4 shows the predicted pore aspect-ratio for sand by neural network, column 1 shows 25 sample numbers, columns 2 to 5 are training input data from well-log, column 6 is training standard value by measurement (expected aspect-ratio values). Running this network, the predicted aspect-ratios can be obtained in column 7. Both columns 8 and 9 show the error values between the expected and the predicted aspect-ratios.

Figure 4.17 is an example of field data based on the comparison of different models for prediction of P-wave and S-wave. The panel 1 in Figure 4.17 displays the comparison of Vs from log measurements and Vs predicted by the Han *et al.* model; panel 2 is a comparison of the measured Vs and predicted Vs by the original Xu-White model and panel 3 is the measurement and prediction by the isotropic dual porosity model.

Figure 4.18 (top) shows the velocity error analysis from Xu-White model (both measured Vs and predicted Vs). Figure 4.18 (bottom) is the result from the IDP model. Comparing both of them by cross-plot analysis, we can see that the IDP model gives a better relationship than Xu-White model, because its scatter of result points is much smaller. In addition, the distribution range of error in the IDP model (the frequency distribution histogram) is between -200 and +200 m/s, and the peak value is 79.6% (error deviation is from -100 to 200 m/s). However for Xu-White model, its

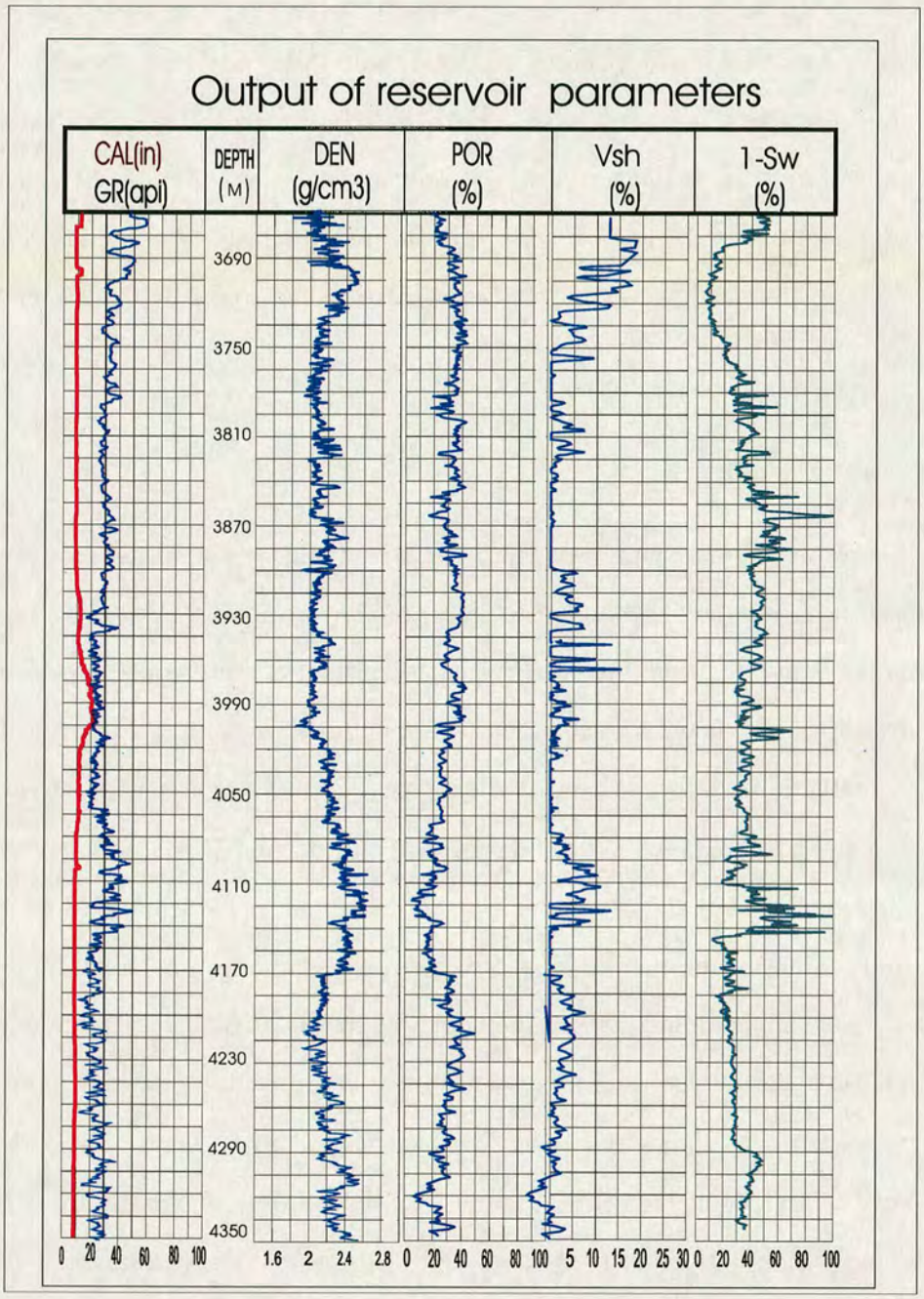

Figure 4.13: The key reservoir parameters. This example shows input log data, and using the method of parameters determination, the key reservoir parameters can be estimated, which include the effective porosity, clay content and fluid saturation respectively.

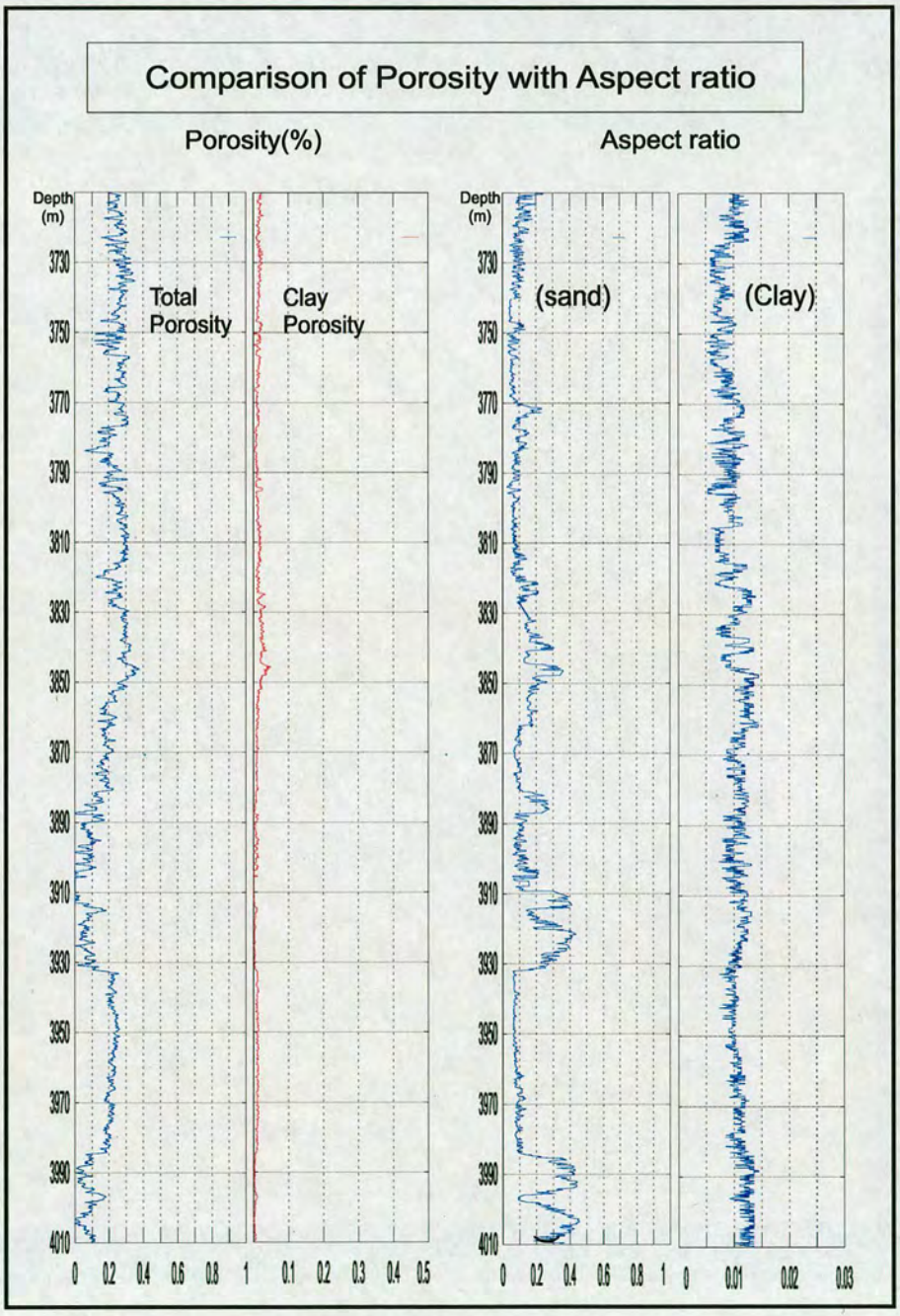

Figure 4.14: The example of output for aspect-ratios which are predicted using the IDP model. This result shows that the main distribution range of aspect-ratios for sand is between 0.05 and 0.35, and between 0.01 and 0.02 for clay. Therefore, the fixed values of 0.1 for sand and 0.03 for clay used in Xu-White model represent a simplification.

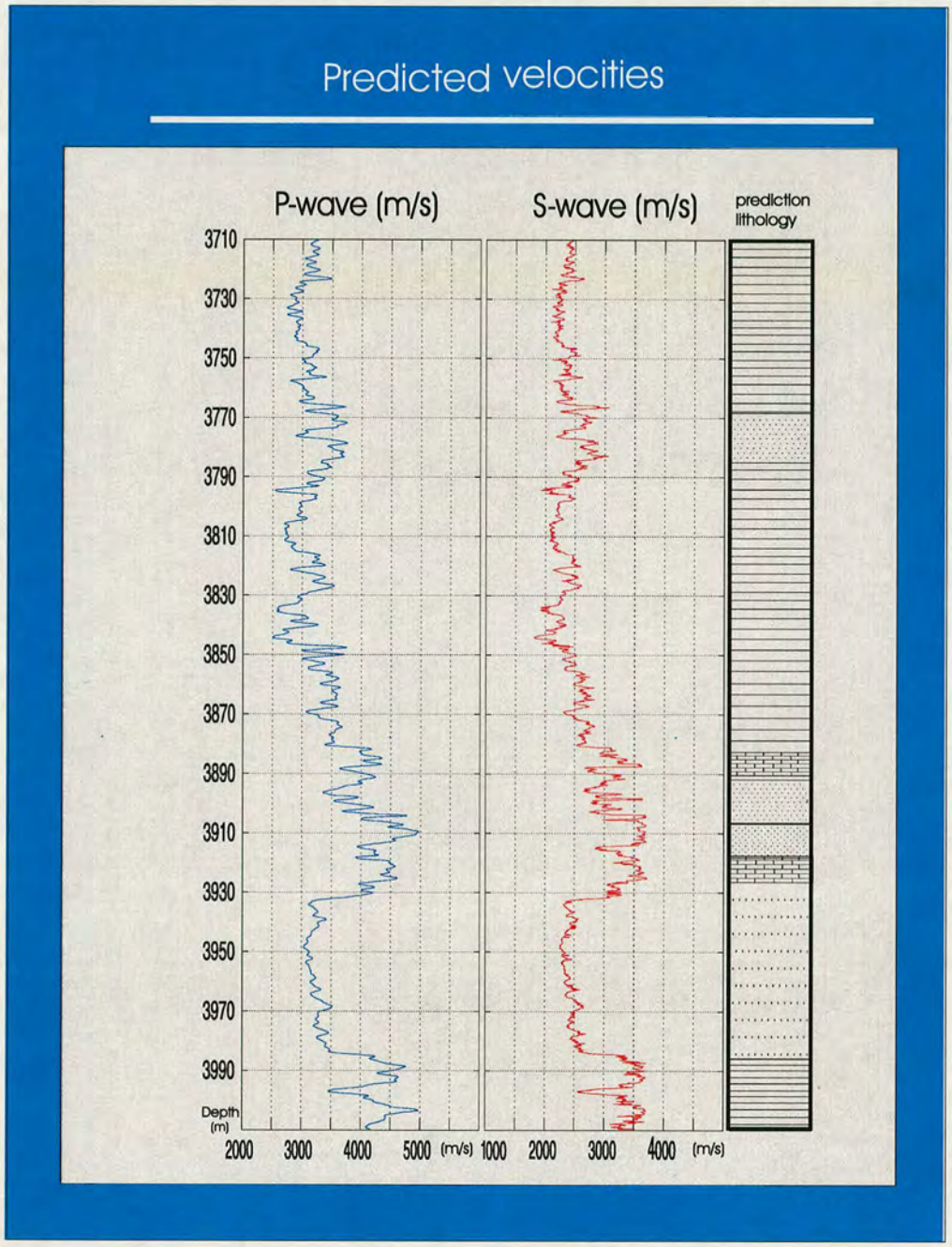

Figure 4.15: Predicted velocities using the isotropic dual porosity model (IDP). This result shows the relationship between Vp, Vs and lithology. As we can see that both Vp and Vs velocities show high values for a high density formation (depth between 3876m and 3928m). On the other hand, both velocities show low values in a loose formation (depth between 3790m and 3850m).

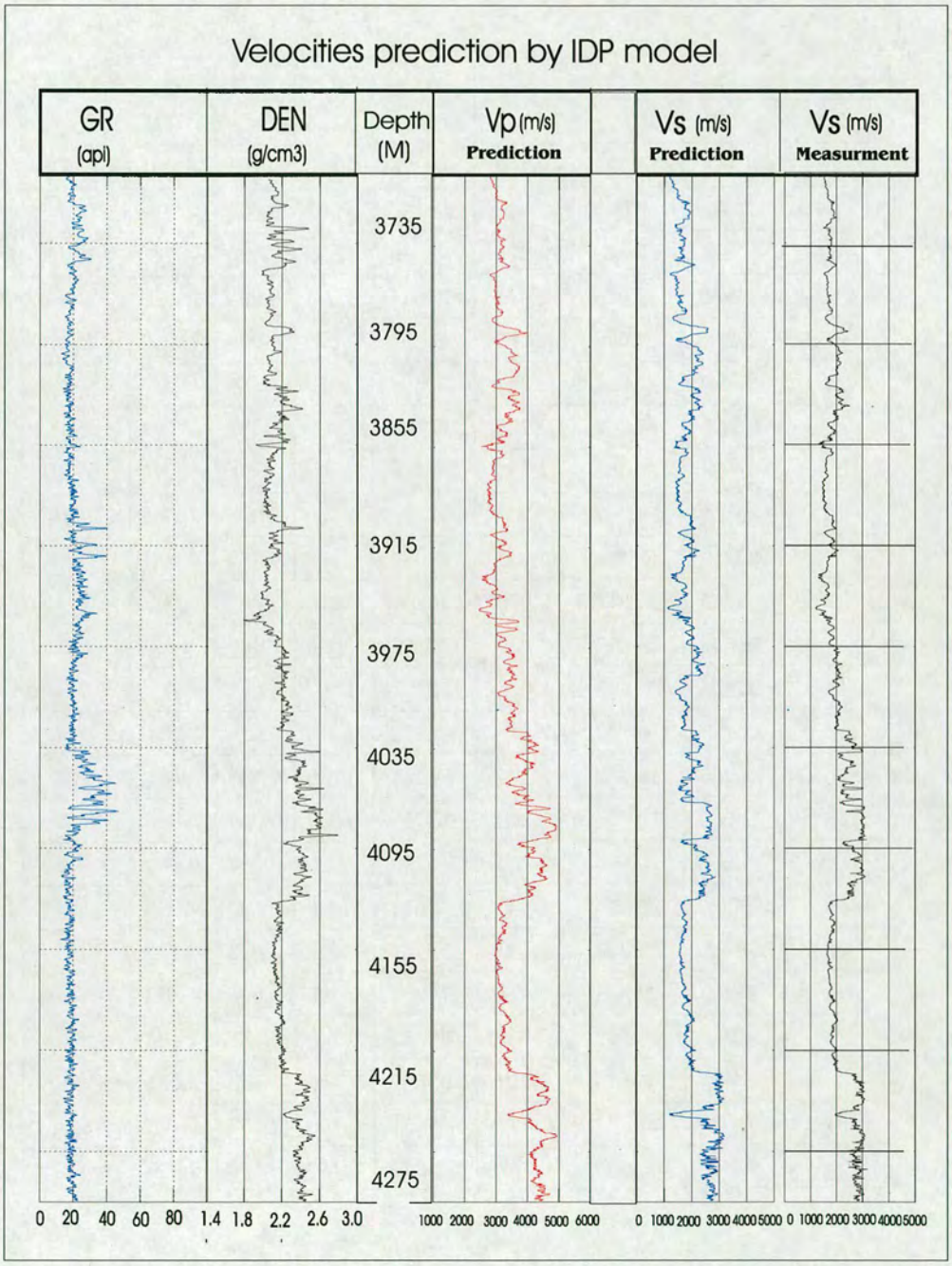

Figure 4.16: S-wave velocity predicted by isotropic dual porosity (IDP) model. Panel 3 shows predicted Vp, Panel 4 is a predicted Vs, and panel 5 is a measurement of Vs from log. Both predicted and measured S-wave velocities show a good agreement.

Samples	GR	SP	DEN	AC	α_s	$\alpha_s^{'}$	err_1	$err_2(\%)$
1	9.162	31.228	2.183	93.385	0.130	0.128	0.002	2.94
2	9.162	31.717	2.173	93.276	0.120	0.121	-0.001	-0.91
3	9.165	22.099	2.095	95.436	0.093	0.084	0.009	9.32
4	9.165	23.378	2.078	95.536	0.090	0.100	-0.01	-11.15
5	9.167	19.928	2.089	96.344	0.100	0.096	0.004	3.98
6	9.170	19.047	2.115	95.497	0.090	0.098	-0.008	-9.24
7	9.167	30.954	2.233	95.396	0.070	0.07	0.0	0.0
8	9.167	31.362	2.223	95.004	0.080	0.082	-0.002	-2.94
9	9.012	19.368	2.255	89.548	0.060	0.06	0.0	0.0
10	9.013	19.002	2.261	88.898	0.060	0.066	-0.006	-9.91
11	9.264	17.128	2.109	84.464	0.200	0.184	0.016	7.98
12	18.365	25.973	2.016	117.123	0.070	0.067	0.003	4.74
13	18.533	25.207	2.023	117.243	0.060	0.060	0.0	0.0
14	19.868	23.845	2.036	113.472	0.060	0.064	-0.004	-6.80
15	12.101	18.199	2.189	86.428	0.110	0.120	-0.01	-9.35
16	12.095	18.957	2.195	86.264	0.110	0.103	0.007	6.39
17	11.069	19.726	2.219	92.750	0.092	0.084	0.008	8.69
18	11.071	19.607	2.232	92.705	0.085	0.084	0.001	1.18
19	9.603 5	28.646	2.455	72.614	0.090	0.100	-0.01	-11.5
20	9.603	29.392	2.442	72.477	0.080	0.082	-0.002	-2.94
21	9.604	29.888	2.426	72.281	0.090	0.091	-0.001	-0.60
22	9.129	37.592	2.354 0	78.833	0.160	0.171	-0.011	-6.70
23	9.121	35.482 0	2.350	9.017	0.160	0.159	0.001	0.510
24	9.113	33.373	2.352	77.151	0.150	0.152	-0.002	-1.34
25	9.115	31.667	2.357	77.027	0.150	0.130	0.020	13.31

Table 4.4: Predicted pore aspect-ratio for sand formation by BPNN. *GR,SP*, *DEN* and *AC* are corrected log data, α_s is the target value of sand-pore aspect-ratio (expected), $\alpha_s^{'}$ is predicted aspect-ratio value, err_1 and err_2 are absolute and relative errors respectively.

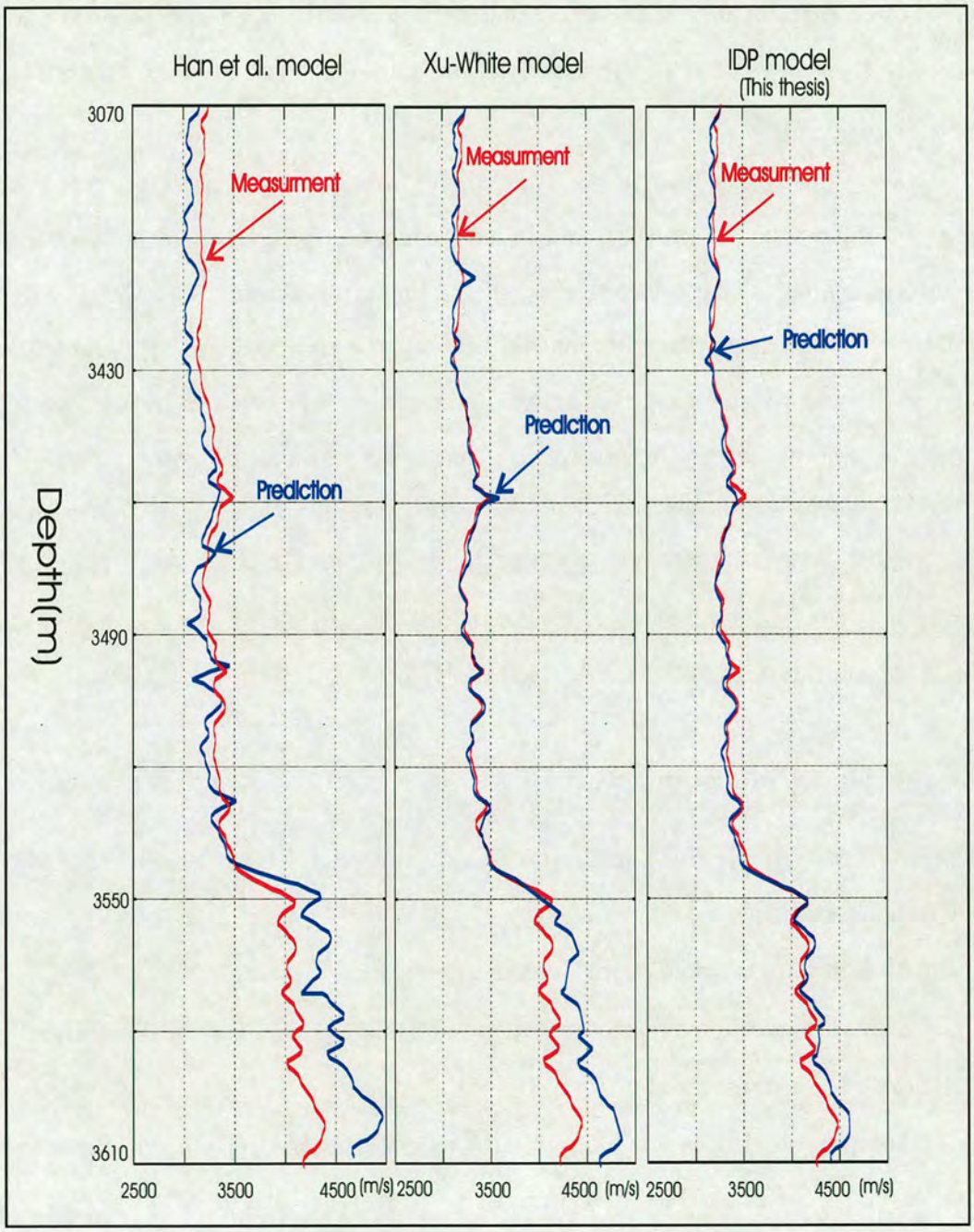

Figure 4.17: Comparison between predicted and measured S-wave velocities (Vcl $< 25\%$ and POR: 0.1 to 0.28). Predicted velocities were derived from the Han *et al.* model (panel 1), Xu-White model (panel 2) and my IDP model developed in this thesis (panel 3, also called PADP) respectively. We can see that the predict Vs from IDP model is closer to measured Vs than other models.

regression coefficient (R) is 0.683, the distribution of error is between -300 and +300 m/s, and its peak value is 52% (error deviation is from -100 to 200 m/s), which is lower than the IDP model.

Figure 4.20 displays sensitivity testing results from velocity, aspect-ratio and transit time. In Figure 4.20 (a1) to (b2), we can see that for a given transit time of sand grains or the clay minerals, the velocity changed as a linear relationship, and this causes the problems in establishing the relationship between the transit time and parameters of sand grains or clay minerals. For given aspect-ratios, the velocities are also affected, but there is no linear relationship between the velocity and aspect-ratios (Figure 4.20, c1 and c2). The variation of aspect-ratios with lithology may therefore affect the velocity prediction, The predicted precision will depend on the aspect-ratio. Because the variation is not linear, there is a hint that the use of fixed aspect-ratios is only suitable for small depth intervals with invariable lithologies.

4.6.3 Model validation: discussion

Because of the use of DEM theory and Gassmann's equations in the IDP model, the following assumptions have been made:

1) All pores are ellipsoids with random orientations.

2) All pores are interconnected, there are no isolated pores (permeable formation).

3) Rock is fluid saturated.

4) The pore fluid does not interact with the solid matrix (clay sand mixture, and there are no other mineral components).

This implies that the solution obtained from BPNN is only suitable for the similar lithology in the same formation or the same area. Otherwise, this model may not be used because obvious errors will appear. The Figure 4.21 shows two testing wells. Although, both wells have the similar lithology, and they also belong to the same geological group.

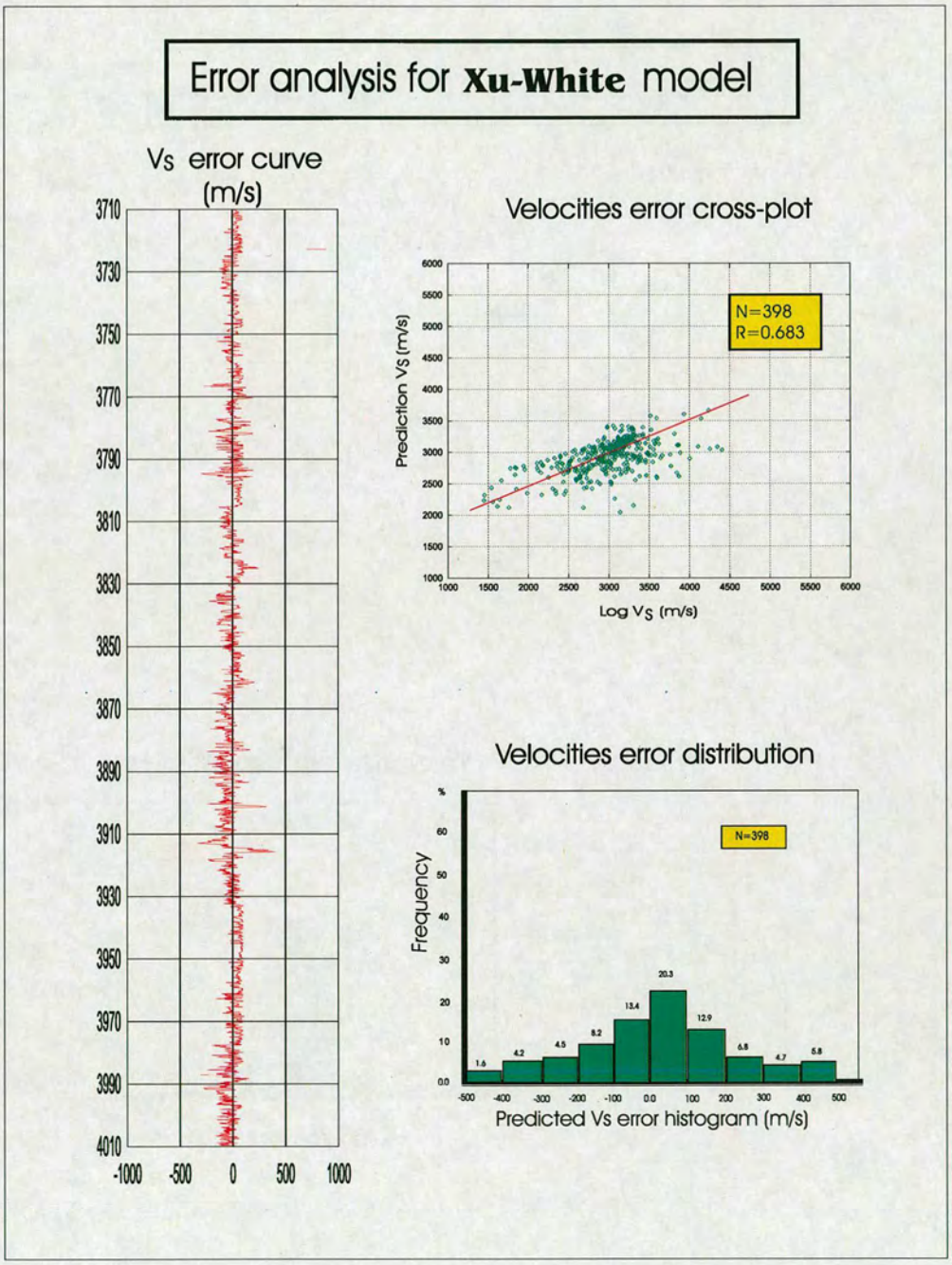

Figure 4.18: The comparison of error analysis between Xu-White model, which shows the error velocity by cross-plot, and it also gives an error distribution by histogram-plot.

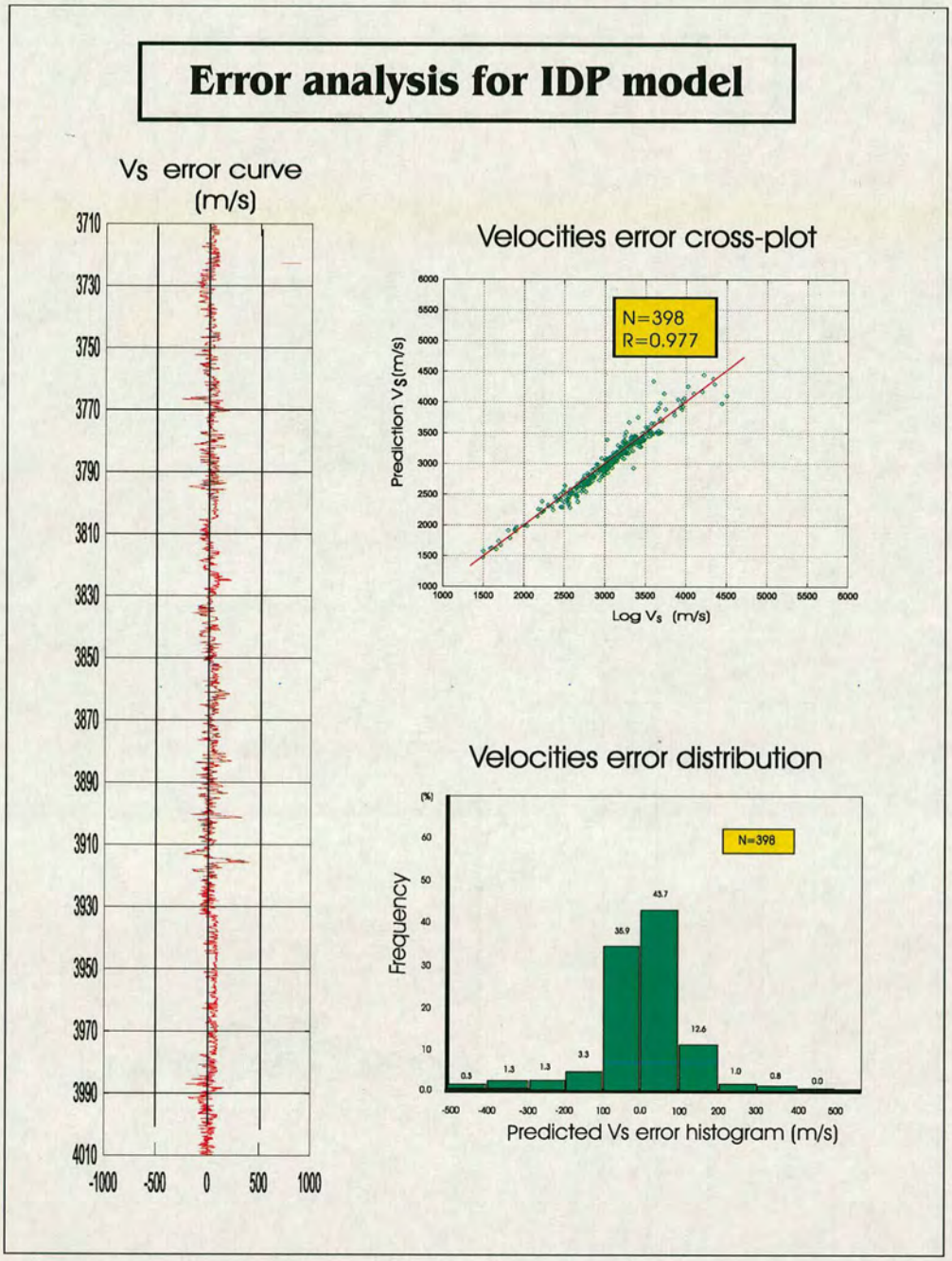

Figure 4.19: The comparison of error analysis for IDP (PADP) model, which shows the Vs error cross-plot, and error distribution by histogram-plot.

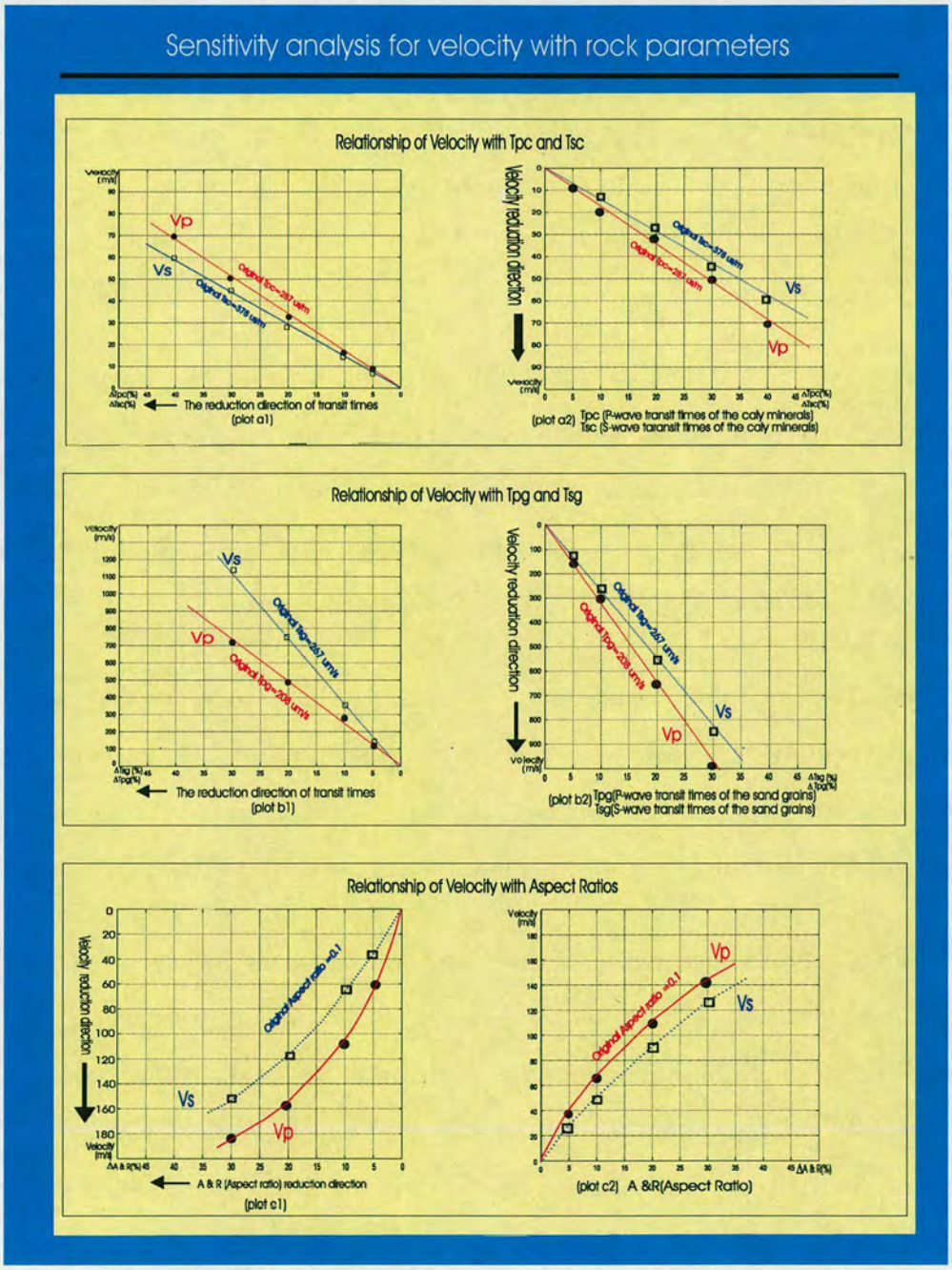

Figure 4.20: Sensitivity analysis between velocities, aspect-ratios and transit times. (The top figures show that a linear relationship between velocities and transit time of clay content. The middle figures show the velocities changed as a linear relationship with the transit time of sand grains. The bottom figures show the varying relationship between velocities and aspect-ratios).

Due to the presence of fault between the testing well-1 and the testing well-2, two wells are divided into different blocks (Black M and Black S), so the training data and model parameters built from the first well-1 cannot be used directly to the second well-2, a necessary data correction should be done for the testing well-2.

Figure 4.22 gives a further comparison. In this example, the training data was built from the testing well-1 and input them into IDP model, a better predicted shear velocity can be obtained. The left hand figure shows the comparison between predicted and measured *Vs*, and we can see that predicted *Vs* gives a good fit to the measured *Vs*, and the last panel shows an acceptable velocity error curve.

Using the same solution and input parameters to IDP model for the testing well-2. Unfortunately, the predicted *Vs* cannot fit the measured *Vs* satisfactorily, this comparison has been shown in the right hand in Figure 4.22, and the final panel also shows an obvious error curve, which is much larger than the test well-1.

Although, the testing well-2 is in the same area with the testing well-1, and both wells belong to the same geological group divided by geologists. Based on the core shale analysis and log data interpretation, the difference of both wells is their shale content, which causes different rock properties changes. Therefore, due to the effects of fault which causes different shale variability and rock properties in Black M and Black S, so that the model parameters and training data (solution) of the well-1 cannot be used to the well-2 directly. In this case, the model parameters and training data should be re-built based on the well-2 data itself. If the sample data is unavailable to build new relationship, I suggest that a suitable data correction is necessary for the IDP model application. Otherwise, other proper approaches should be considered to use.

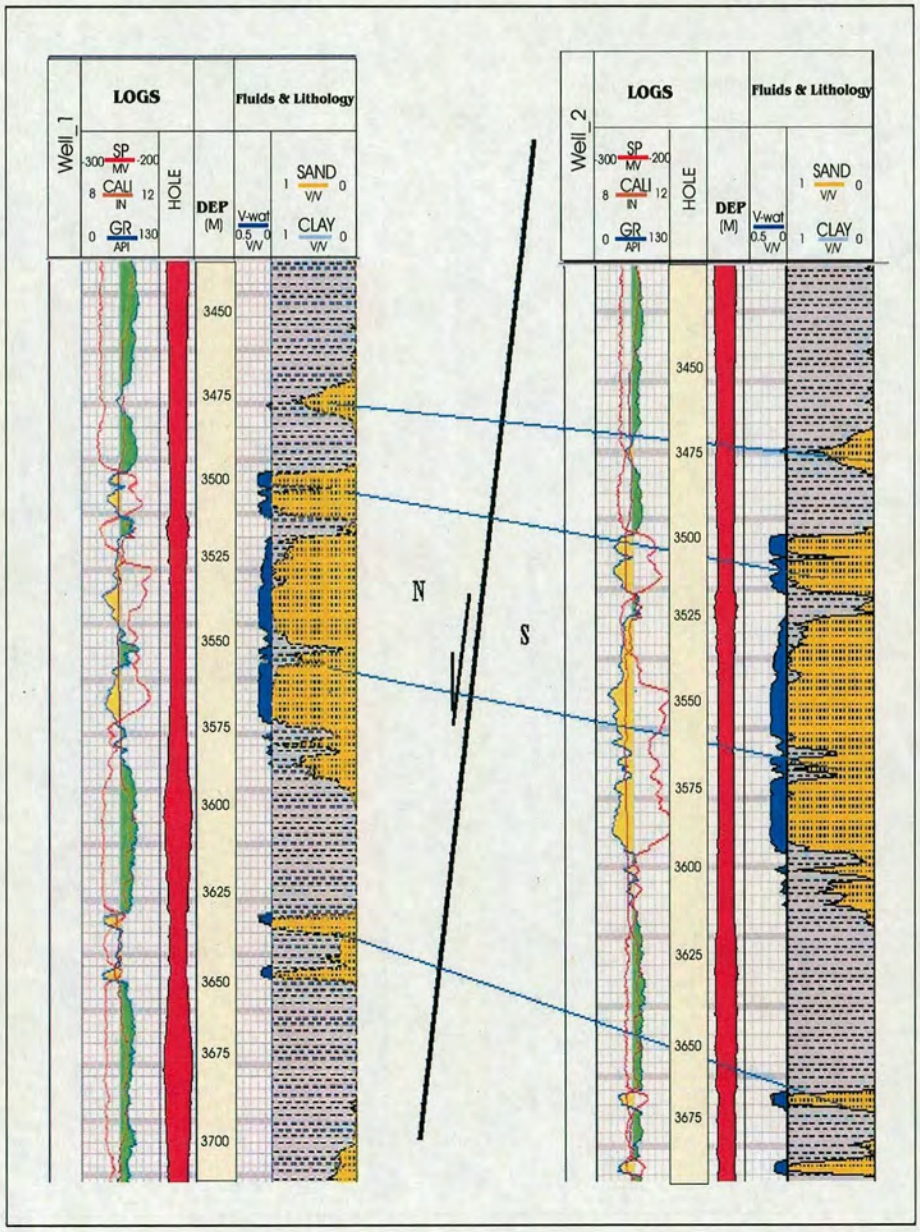

Figure 4.21: The presence of fault between testing well-1 and testing well-2, which divided this area into Black M and Black S. The first test well is located in the Black M, and the second test well is located in the black S.

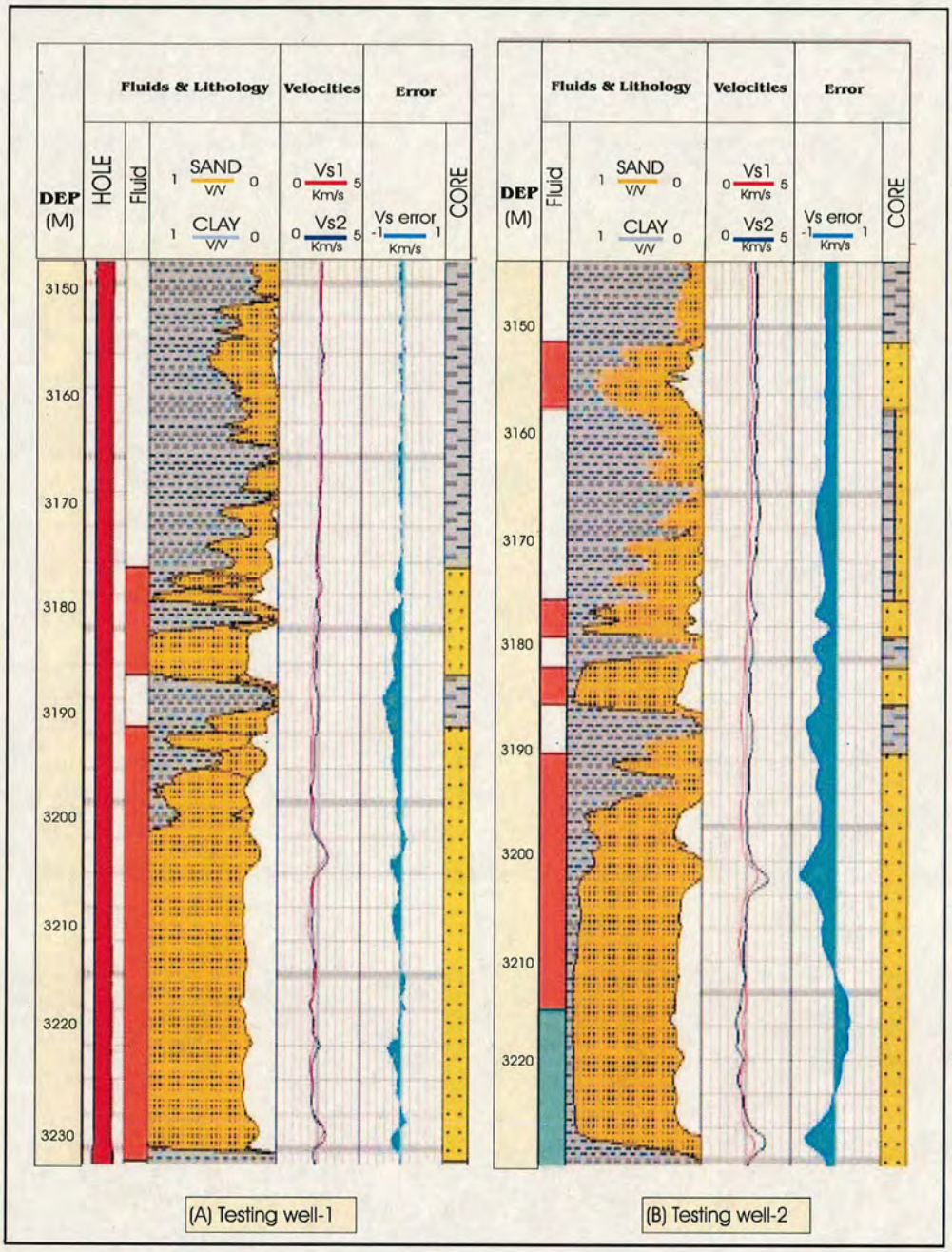

Figure 4.22: IDP model validation analysis, which proved that the training data and model parameters built from the first well-1, and the training result was used directly to the second well-2. As we can see that a data correction is needed for second well, this is because the testing well-1 (left hand figure) shows a satisfactory fit for predicted and measured *Vs*. But, in the right hand figure, the testing well-2 shows a larger error than the testing well-1).

4.7 Summary

In this chapter, I have improved Xu-White model (see Section 2.4.1.5) by the development of a new isotropic dual porosity model (IDP) for a two-phase medium which related both porosity and pore aspect-ratios to P- and S-wave velocities. The main improvements are as follows: an extended time-average equation based on lithology and physical properties is built, a back-propagation neural network is employed to invert pore aspect-ratios directly for the whole depth range, the Kuster-Toksöz and DEM theories are used to calculate elastic properties, and then Gassmann's equations are employed to predict velocities in the isotropic media for saturated rocks.

This new improved model has been tested using the field data. The accuracy of velocities is obviously enhanced compared with that of Xu-White model for the large depth range. This is confirmed by error and sensitivity analysis.

The isotropic dual porosity model provides a practical tool for estimating reservoir parameters and velocities, which is suitable for clay-sand formation. However, this improved model is still an isotropic model. In the next chapter, I will develop a model for anisotropic rock, which is basically an extension of the model developed in this chapter.

Chapter 5

ANISOTROPIC DUAL POROSITY MODEL

5.1 Introduction

In the previous discussion (Chapter 4) I have developed a new physical model to predict elastic and formation parameters in sand-clay mixtures. This model is based on Xu-White model using the theories of Kuster-Toksöz (1974) and Gassmann (1951).

Although the Isotropic Dual Porosity model (IDP) is well suited for consolidated formations, it cannot be used in anisotropic rocks. In particular, there are some difficulties in calculating elastic moduli if rocks contain high clay contents or aligned minerals, clay particles or cracks. In other words, the model in Chapter 4 is restricted to isotropic rocks and cannot take account of the clay platelet alignment which gives the Transverse Isotropy with a Vertical symmetry axis (TIV).

Some theoretical investigations have been made on elastic anisotropy caused by preferred pores and crack alignment (Anderson *et al.*, 1974; Griggs *et al.*, 1975; Hoenig, 1979), but the application of these methods needs some special conditions and assumptions. For example, Anderson *et al.* (1974) implicitly employed an equation given by Eshelby (1957) that is formulated for a dilute concentration of crack and pores, and most of the models mentioned above require the dry bulk and shear moduli as input parameters. This does not cause a serious problem for simulating laboratory measure-

ments since the dry rock frame moduli can be measured. However, when we construct models from well logs, the dry rock frame moduli are not measurable in practical application.

The purpose of this chapter is to develop a general model to estimate reservoir parameters and to predict rock properties in anisotropic porous media. To achieve this, we propose an Anisotropic Dual Porosity (ADP) model to calculate effective elastic moduli and elastic constants in rocks with randomly oriented inclusions and aligned inclusions. This new model is an extension of IDP model to anisotropic rocks, and is incorporated in a scheme similar to the IDP model. The ADP model extends my previous isotropic dual porosity model (IDP) by means of the equivalent medium concept of Nishizawa (1982), Brown and Korringa (1975) and Hornby *et al.* (1994).

5.2 Anisotropy in borehole data

5.2.1 Problems

Figure 5.1 shows the faster and slower S-wave velocity measurements from dipole sonic log. Comparing measured curves, we can see the differences between them, which caused by anisotropy. To give a quantitative description, the following relationship may be used to define the anisotropic coefficient.

$$m = \frac{V_{s2} - V_{s1}}{\overline{V}}, \tag{5.1}$$

where m is anisotropic coefficient, V_{s1} and V_{s2} are the velocities of shear-waves in X and Y directions, $\overline{V}$ is the average velocity of V_{s1} and V_{s2}. The anisotropic coefficient is shown on panel 4 in Figure 5.1.

The anisotropic response can be estimated from seismic data by using walk-away VSP. In addition the phase slownesses can be obtained from the first break travel

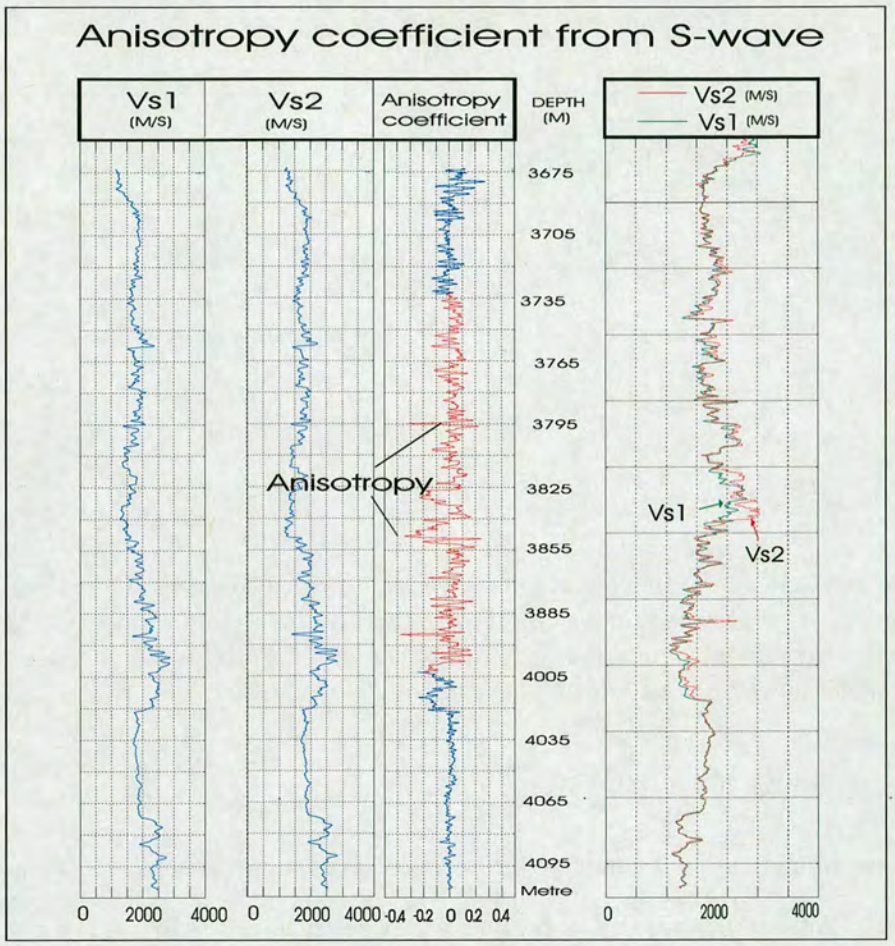

Figure 5.1: Anisotropic response from an oil field in the North Sea. It shows the velocity anisotropy presence between depths of 3740m and 4000m (panel 3 and panel 4). The last panel gives anisotropic coefficient (m) calculated by equation (5.1).

times. For a receiver array located in the vertical portion of a well, the common shot and receiver gathers give vertical and horizontal slownesses, respectively. These are required to estimate the desired elastic constants. (Ohlsen and MacBeth 1998). Figure 5.2 shows qP slownesses (Sz-vertical, Sh-horizontal) from walkway VSP data by first-break picking, it can be seen that the slowness surfaces are elliptical, indicating the presence of anisotropy.

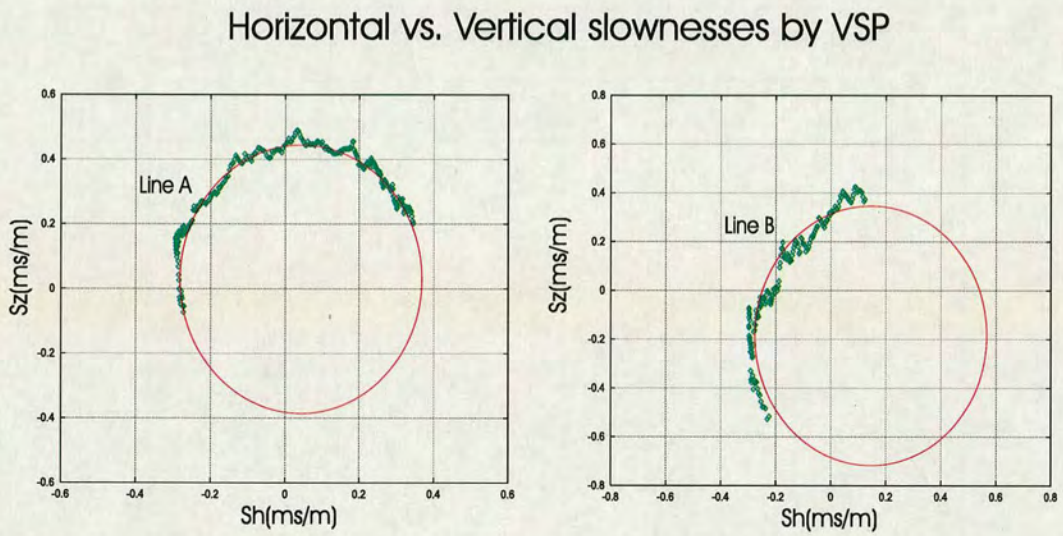

Figure 5.2: Horizontal versus Vertical slownesses after recovering the vertical slowness from the apparent slowness along the receiver array. Both plots show that the elliptical slowness curves are an indication of the presence of anisotropy, and the right plot (line B) shows the more obvious anisotropic phenomenon than left plot (line A).

5.2.2 Velocity anisotropy

A TIV medium is uniquely described in terms of five independent elastic constant (e.g., Thomsen, 1986) and in matrix notation we can write as:

$$C = \begin{bmatrix} C_{11} & C_{12} & C_{13} & 0 & 0 & 0 \\ C_{12} & C_{11} & C_{13} & 0 & 0 & 0 \\ C_{13} & C_{13} & C_{33} & 0 & 0 & 0 \\ 0 & 0 & 0 & C_{44} & 0 & 0 \\ 0 & 0 & 0 & 0 & C_{44} & 0 \\ 0 & 0 & 0 & 0 & 0 & C_{66} \end{bmatrix}, \tag{5.2}$$

where $C_{66} = (C_{11} - C_{12})/2$, and there exists a simple method of index translation between the tensor notation, C_{ijkl} and the matrix notation C_{mn} as:

Tensor	ij or kl	11	22	33	32=23	31=13	21=12
Matrix	m or n	1	2	3	4	5	6

If the angle between the arrival and the vertical direction is zero, and ρ is the density of media, we have the velocities of P-wave in the vertical direction and the SV-wave ($\theta = 0$) as:

$$V_p(0) = (\frac{C_{33}}{\rho})^{1/2}, \tag{5.3}$$

$$V_s(0) = (\frac{C44}{\rho})^{1/2}, \tag{5.4}$$

Thomsen (1986) introduced three parameters as:

$$\varepsilon = \frac{C_{11} - C_{33}}{2C_{44}}, \tag{5.5}$$

$$\gamma = \frac{C_{66} - C_{44}}{2C_{44}}, \tag{5.6}$$

$$\delta = \frac{1}{2C_{33}^2}[2(C_{13} + C_{44})^2 - (C_{33} - C_{44})(C_{11} + C_{33} - 2C_{44}]. \tag{5.7}$$

Both ε and γ are the anisotropic parameters (Thomsen 1986), Thomsen argued that most sedimentary rocks exhibit only weak anisotropy, so that ε, γ and δ are all small. Consequently, the velocity equations can be simplified for weak transversely isotropic rock to:

$$V_p^2(\theta) = V_{p0}^2[1 + \varepsilon \cdot sin^2\theta + D^*(\theta)], \tag{5.8}$$

$$V_{sv}^2(\theta) = V_{s0}^2[1 + \frac{V_{p0}^2}{V_{s0}^2}\varepsilon \cdot sin^2\theta + \frac{V_{p0}^2}{V_{s0}^2}D^*(\theta)], \tag{5.9}$$

$$V_{SH}^2(\theta) = V_{s0}^2[1 + 2\gamma \cdot sin^2(\theta)], \tag{5.10}$$

and

$$D^*(\theta) = \frac{1}{2}\left[1 - \frac{V_{s0}^2}{V_{p0}^2}\right] \cdot \left\{[1 + \frac{4\delta}{(1-V_{s0}^2/V_{p0}^2)^2} sin^2(\theta)cos^2(\theta) + \frac{4(1-V_{s0}^2/V_{p0}^2+\varepsilon)\varepsilon}{(1-V_{s0}^2/V_{p0}^2)^2} sin^2(\theta)]^{1/2} - 1\right\},$$

under the weak anisotropy assumption (e.g anisotropic parameters ε, δ <0.2), Thomsen (1986) also shows that

$$D^*(\theta) \approx \frac{\delta}{(1 - V_{s0}^2/V_{p0}^2)^2} sin^2(\theta)cos^2(\theta) + \varepsilon \cdot sin^2(\theta), \tag{5.11}$$

and similarly, the equations (5.8 to 5.10) can be approximated to

$$V_p(\theta) = V_{p0}[1 + \delta \cdot sin^2\theta cos^2(\theta) + \varepsilon \cdot sin^4(\theta), \tag{5.12}$$

$$V_{sv}(\theta) = V_{s0}[1 + \frac{V_{p0}^2}{V_{s0}^2}(\varepsilon - \delta) sin^2\theta cos^2(\theta)], \tag{5.13}$$

$$V_{SH}(\theta) = V_{s0}[1 + \gamma \cdot sin^2(\theta)], \tag{5.14}$$

and

$$\delta = \frac{1}{2}[\varepsilon + \frac{\delta}{(1 - V_{s0}^2/V_{p0}^2)}] = \frac{(C_{13} + C_{44})^2 - (C_{33} - C_{44})^2}{2C_{33}(C_{33} - C_{44})}, \tag{5.15}$$

as we discussed above, a transversely isotropic elastic material is defined in terms of the five components of the elastic constants relating stress and strain for the transversely isotropic medium as $C_{11}, C_{33}, C_{13}, C_{44}, C_{66}$ (refer to Appendix B)

These parameters are all zero for an isotropic medium and their deviation from zero represents the degree of anisotropy. The value of ε, which is alway positive, represents

the relative difference between the P-wave velocities propagating perpendicular (V_{p1}) and parallel (V_{p2}) to the axis of symmetry. The parameter γ describes the S-wave anisotropy. It is the relative difference between the faster S-wave (V_{s1}) velocity and the slower S-wave (V_{s2}) velocity. The parameters δ dominate the anisotropic response when the acoustic wave propagates in a plane which is parallel or approximately parallel to the axis of symmetry. It is independent of the seismic velocities of the medium perpendicular to the axis of symmetry and can take either positive or negative values.

5.2.3 The combination of SCA and DEM

To create a biconnected solid at all porosities to estimate the anisotropic properties, the expression for the effective compliances of the composite material is given by Hornby in 1994 below:

$$I - c^0 s^* = \sum_{n=1}^{N} v_n (c^n - c^0) K^n. \tag{5.16}$$

The equation (5.16) can be rewritten, and the expression for the effective compliances of the composite material is:

$$s^* = s^0 - \sum_{n=1}^{N} v_n (c^n - c^0) K^n, \tag{5.17}$$

where $c^n = \sigma^n / e^n$, and σ is stress tensor, e is local stress tensor, $v_n = V_n / V$, and V is volume of a material, V_n is the volume of the nth constituent, I is the unit tensor, s^* is the tensor of compliances of effective material and K is the tensor that related to the applied stress.

In the case of porous solids with connected fluid and solid phases, we replace the matrix material in the model with the effective material: i.e., we set $c^0 = c^{SCA}$. Then equation (5.16) becomes:

$$\sum_{n=1} v_n(c^n - c^{SCA})K^n_{SCA} = 0, \tag{5.18}$$

where K^{*n} depends on the solution, rearranging c^{SCA}, we get:

$$c^{SCA} = \sum_{n=1}^{N} v_n c^n K^{*n} \left\{ \sum_{p=1}^{N} v_p K^{*n} \right\}^{-1}. \tag{5.19}$$

This expression may be solved iteratively, by setting an initial value for c^{SCA}, computing K^{*n}, and reevaluating c^{SCA}, this equation can be rewritten as:

$$\underline{\mathbf{C}}^{SCA} = \sum_{n=1}^{N} \nu_n \underline{\mathbf{c}}^n (\underline{\mathbf{I}} + \hat{\underline{\mathbf{G}}}(\underline{\mathbf{c}}' - \underline{\mathbf{c}}^{SCA}))^{-1} \times \left\{ \sum_{p=1}^{N} \nu_p \left[\underline{\mathbf{I}} + \hat{\underline{\mathbf{G}}}(\underline{\mathbf{c}}^p - \underline{\mathbf{c}}^{SCA}) \right]^{-1} \right\}^{-1}. \tag{5.20}$$

Then more clay is added until the required porosity is reached using a differential effective medium (DEM) method. The SCA and DEM combination ensures the biconnectivity of both phase (Hornby 1994). The procedure is as follows. Beginning with an effective medium generated using the SCA at a value of the porosity where that approximation yields a biconnected solid (e.g., ϕ =50%), we compute the effective properties at other value of ϕ by successive operations of removing an infinitesimal subvolume of host material and replacing it with a corresponding sub-volume of the nth component. At each successive increment of component n, the previous step is taken as the host material. The actual change in the concentration, v_n , of the nth component is $\triangle v_n/(1 - v_n)$. To compute the properties of this new effective material based on equation (5.17). It was reformulated as a differential equation. For included material c^i and effective properties of the media at concentrations v give by $s^*(v)$ equation (5.17) gives:

$$\frac{d}{dv}(\underline{\mathbf{c}}^{DEM}(v)) = \frac{1}{(1-v)}(\underline{\mathbf{c}}^{i} - \underline{\mathbf{c}}^{DEM}(v)) \times \left[\underline{\mathbf{I}} + \underline{\hat{\mathbf{G}}}(\underline{\mathbf{c}}^{i} - \underline{\mathbf{c}}^{DEM}(v))\right]^{-1}, \tag{5.21}$$

where $c^i = \sigma^i/e^i$, and σ^i is stress tensor, e^i is local stress tensor, $v = V_n/V$, and V is volume of a material, V_i is the volume of the ith constituent, $\boldsymbol{I}$ is the unit tensor, $\boldsymbol{G}$ is the tensor related to the pore geometry (Nishizawa,1982).

5.2.4 Elastic contents in saturated rock

An equation was derived for the dependence of the elastic properties of a porous material on the compressibility of the pore fluid by Brown and Korringa (1975). In general, the elastic properties of a container of arbitrary shape are related to the compressibility of the fluid filling the cavity in the container. If the material is homogeneous, this equation is similar to the well-known Gassmann equation. For the other elastic properties, Brown and Korringa (1975) derived their theory relating the effective elastic moduli of an anisotropic dry rock to the effective moduli of the same rock containing fluid, so that they are often called the anisotropic Gassmann equations. This is given below:

$$S^{(dry)}_{ijkl} - S^{(sat)}_{ijkl} = \frac{(S^{(dry)}_{ij\alpha\alpha} - S^{0}_{ij\alpha\alpha})(S^{(dry)}_{kl\alpha\alpha} - S^{0}_{kl\alpha\alpha})}{(S^{(dry)}_{\alpha\alpha\beta\beta} - S^{0}_{\alpha\alpha\beta\beta}) + (\beta_{fl} - \beta_0)\phi}, \tag{5.22}$$

and

$$\beta_{fl} = S\beta_L + (1-S)\beta_G, \tag{5.23}$$

where $S^{(dry)}_{ijkl}$ is the effective elastic compliance tensor of dry rock, $S^{(sat)}_{ijkl}$is the effective elastic compliance tensor of dry rock saturated with pore fluid, $S^{0}_{ij\alpha\alpha}$ is the effective elastic compliance tensor of mineral material making up the rock, β_{fl} is compressibility of pore fluid, β_L is compressibility of the liquid phase, β_G is compressibility of the gas

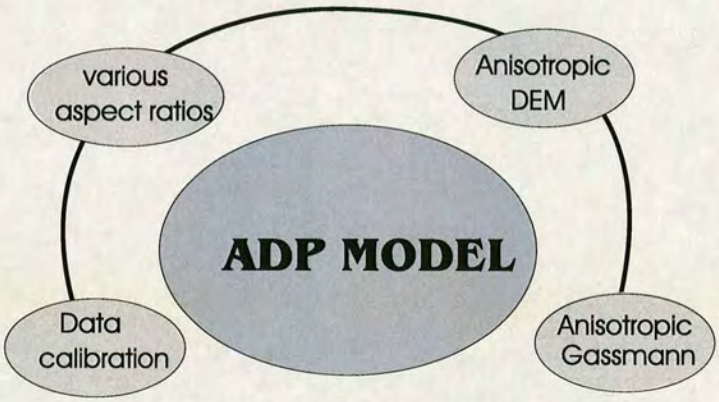

Figure 5.3: A general approach for reservoir parameter prediction in isotropic and anisotropic rocks.

phase, β_0 is compressibility of mineral material $S^0_{ij\alpha\alpha}$, S is the saturation and ϕ is the porosity.

Using Brown and Korringa's (1975) equations to perform fluid substitution and predict velocities in anisotropic media, the following assumptions are necessary: 1) low seismic frequencies with equilibrated pore pressures, 2) all minerals making up rock have the same moduli, and 3) fluid-bearing rock is completely saturated.

5.3 Construction of anisotropic dual porosity model

To build a model to predict reservoir parameters in anisotropic media, we divide the pore spaces (including clay and cracks) into two parts: the random pores giving rise to isotropic elastic constants and the preferentially aligned pores giving rise to anisotropic elastic constants. We refer to this model as Anisotropic Dual Porosity model (ADP). In essence, it can be regarded as an extension of the isotropic dual porosity model in Chapter 4.

The procedure to use ADP model is similar to that of the previous isotropic model in Chapter 4. The inputs include porosity, clay content and related parameters, for example, to determine elastic constants and velocities in dry rocks, the input parameters

lambda matrix(λ)	shear moduli(μ)	lambda inclusion (λ_f)
fluid inclusion (μ_f)	matrix density(ρ)	aspect-ratio(αr)
porosity (ϕ)	clay content(V_{sh})	

Table 5.1: Input parameters for modelling anisotropic case.

are those summarized in Table 5.1.

Figure 5.4 shows the schematic chart of ADP model, it can be summarized as follows:

- ***Data calibration***: This is used to correct original input data for estimating rock's porosity and clay content.
- ***Various aspect-ratios***: The various aspect-ratios are determined by using a BPNN.
- ***Anisotropic DEM and SCA:*** Anisotropic differential media theories and self-consistent approximation are used to calculate the elastic moduli for a dry rock frame of rocks with aligned pore distributions. The rock's anisotropic characteristics can been evaluated.
- ***Brown and Korringa theory***: Fluid substitution used Brown and Korringa theory, this theory is often called the anisotropic Gassmann theory, and it is used to estimate elastic constants in saturated anisotropic rocks.

5.4 Modelling and studies

Numerical simulations have been performed to investigate the effects of porosity, clay contents, pore shapes (aspect-ratios), orientation of pores and inclusions and velocities.

5.4.1 Effects of porosity and clay content

If S-wave velocity is not available from well-log and core data in the field or laboratory, the ADP model can be used to predict the S-wave velocity. The modelling results show

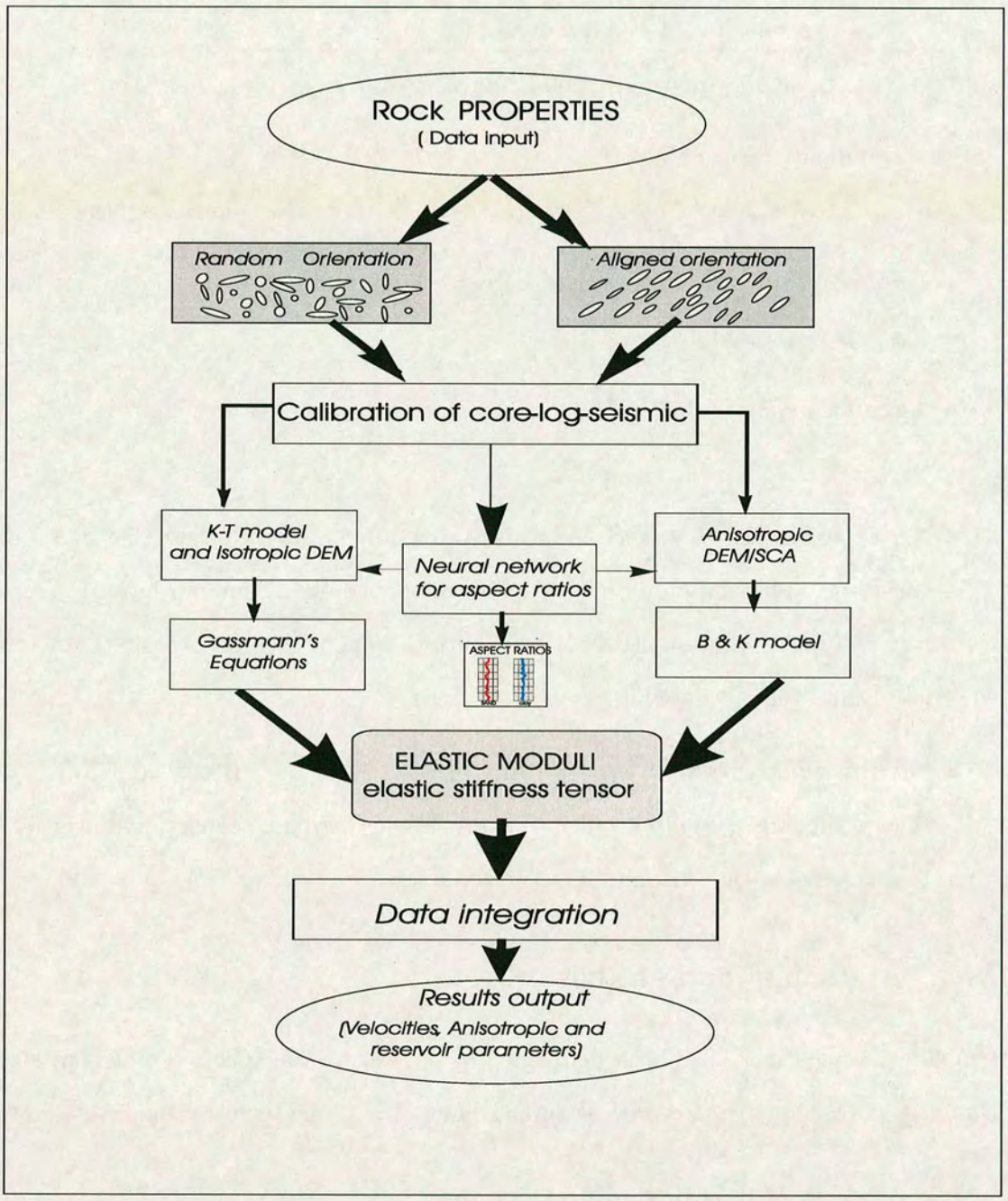

Figure 5.4: The schematic diagram for implementation of ADP model.

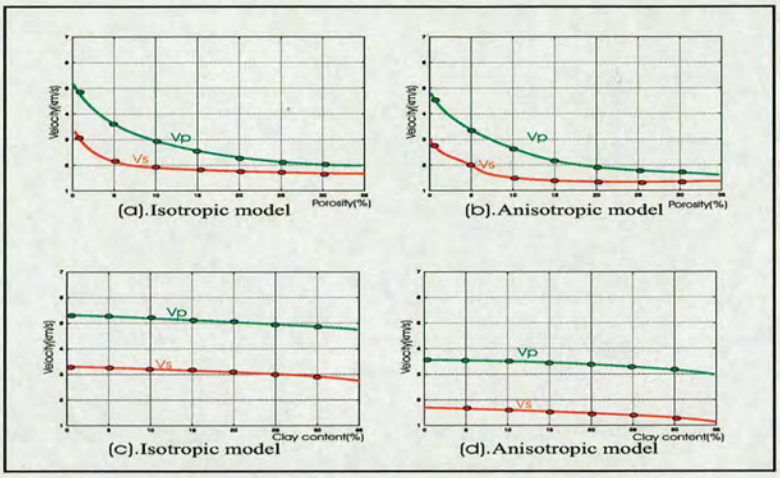

Figure 5.5: Vertical P-wave and S-wave velocities with porosity and clay content (a). isotropic case (velocities and porosity); (b). anisotropic case (velocities and porosity); (c). isotropic case (velocities and clay content); (d). anisotropic case (velocities and clay content).

that P-wave and S-wave velocities depend upon both porosity and clay content; this dependency is illustrated in Figure 5.5. One obvious observation from Figure 5.5 is that both Vp and Vs decrease as clay content increases, and that the velocities are sensitive to porosity change.

This is in agreement with the results of laboratory measurements by Marion *et al.* (1992) (Figure 5.6). As can be seen from the laboratory result, clay first fills the pores and reduces porosity, and the P-wave velocity at first decreases slightly with clay content. Once the pores are completely packed with clay, the effect of clays on the elastic moduli of the effective medium become important. When the clay content reaches the original porosity, the effective porosity is a minimum because all pores are completely filled by clays and their associated pores, the sand grains are held within the clay, and the porosity will increase if more clay is introduced, causing a reduction in the P-wave velocity.

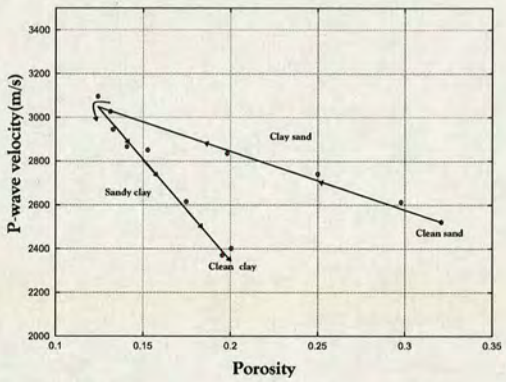

Figure 5.6: Laboratory measurement of the porosity-velocity trend: one for clay sand and the other for sandy shale (Marion *et al.* 1992). Arrows indicate the direction of increasing clay content.

5.4.2 Relationship between velocities and aspect-ratios

To model the effects of pore aspect-ratios on velocities, the P- and S-wave velocities and Thomsen's (1986) anisotropy parameters are calculated as a function of aspect-ratios for a solid permeated with aligned ellipsoid inclusions. In this study, the aspect-ratio of the inclusions varies from 0.001 to 0.3, 0.08 for porosity, 2.55 for density and 0.03 for clay content. As the result, Figure 5.7 shows a variation of velocities with rotated angle (from 0 to 90 degrees) and aspect-ratio (from 0.001 to 0.3). From the Figure 5.7 we can see when the rotation angles are fixed, velocities will change with the variation of pore aspect-ratios.

5.4.3 Effects of orientation distribution

If the pores and inclusions are aligned, the relationship between the velocities and pore orientation can be modelled as shown in Figure 5.8, in which the velocities are in transversely isotropic media shown in Figure 5.8 (right).

Figure 5.9 shows the correlation between velocities and aspect-ratios form different angles of the inclusion normal. Clearly, the values of velocity increase as the aspect-ratio decreases when aspect-ratio is larger than 0.08; the velocity will arrive at the lowest

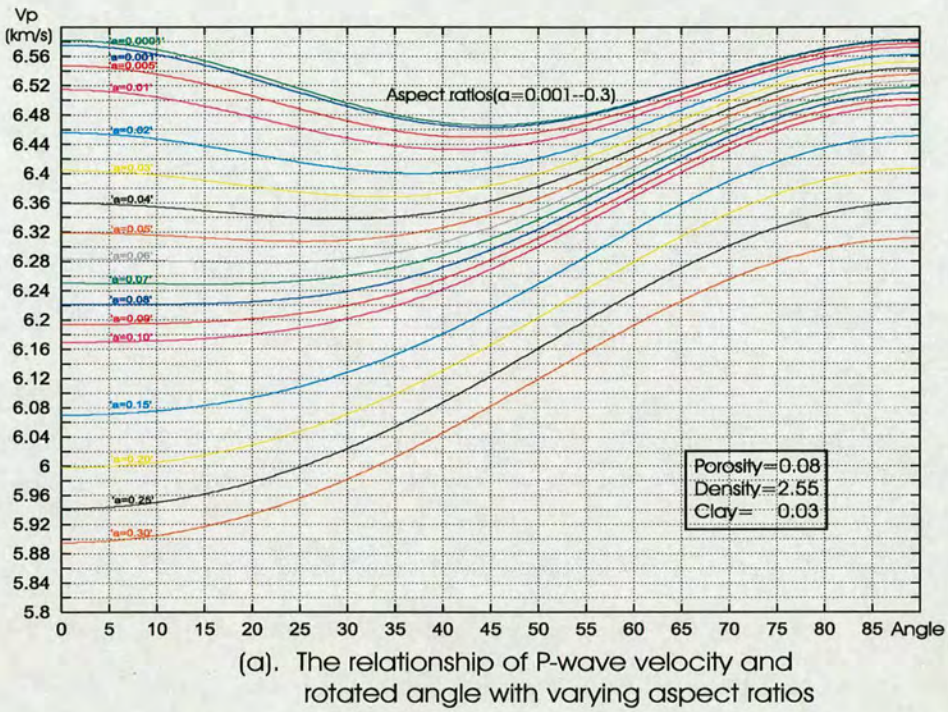

Figure 5.7: P-wave velocity as a function of rotation angle and pore aspect-ratios. The variation of velocities with rotated angle (from 0 to 90 degrees) and aspect-ratio (from 0.001 to 0.3).

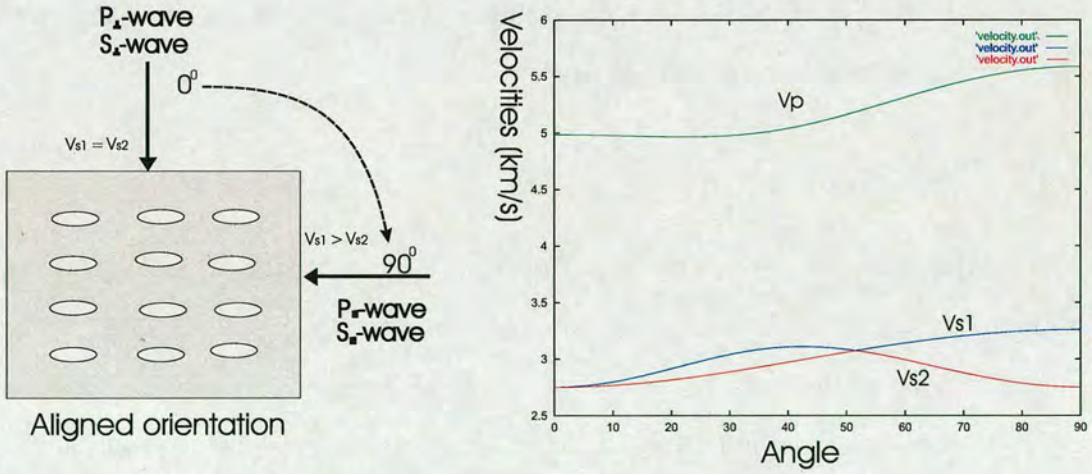

Figure 5.8: Modelling velocities in transversely isotropic effective media, which show the relationship of pore orientation (0 to 90 degree) and V_p (compression-wave velocity), V_{s1} (faster shear-wave velocity) and V_{s2} (slower shear-wave velocity).

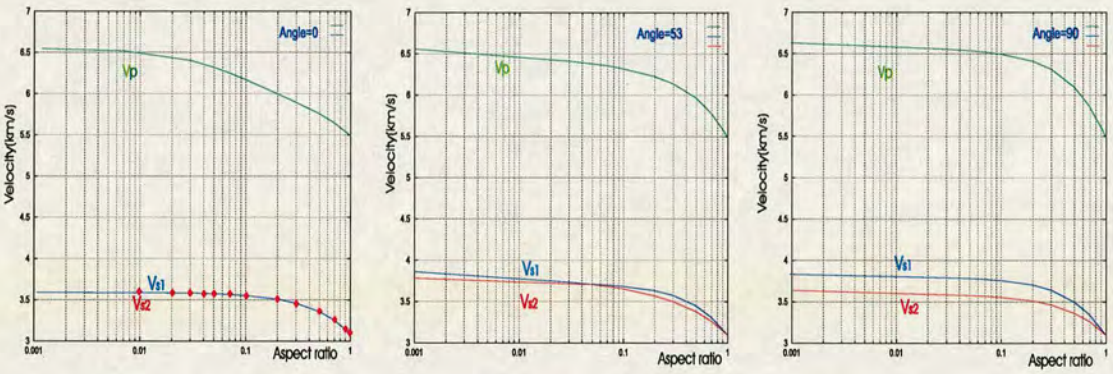

Figure 5.9: The relationship of velocity and aspect-ratio with different rotation angles of media distribution (variations are 0, 53 and 90 degree respectively).

point when aspect-ratio α=1, and the values of faster and slower S-wave velocities are equal. From this result we can also see that both P- and S-wave velocities have a non-zero constant value for a large range of small aspect-ratios, and they only tend to be a minimum for large aspect-ratios. Hence, for a large group of small aspect-ratios the resultant velocities are hardly affected by a change in aspect-ratio for the case when solid is permeated by inclusions, which indicates that there is also a constant difference between the two S-wave velocities propagating both parallel and perpendicular to the plane of cracks, for the same range of aspect-ratios.

5.4.4 Anisotropic parameters

Figure 5.10 shows the modelling results of Thomsen's anisotropic parameters. The isotropic background material is the same as that used by Nishizawa (1982). This result shows anisotropic parameters as a function of the pore aspect-ratio. When the aspect-ratio increases from 0.01 to 0.2, the P-wave anisotropy(ε) is increased, but the S-wave anisotropy (γ) is decreased.

ε is related to P-wave velocity, γ is related to S-wave velocity, and δ is related to the changes in the shapes of wavefront surfaces. For all the cases studied, the values of ε

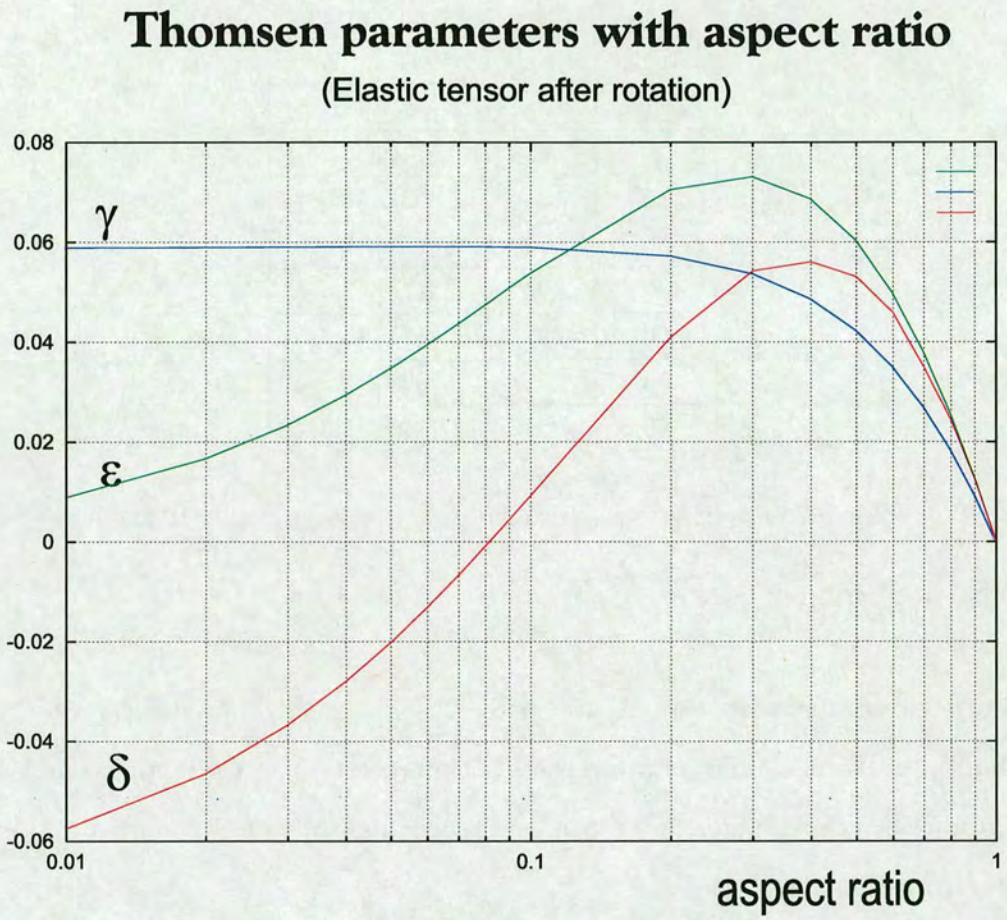

Figure 5.10: Thomsen anisotropy parameters as a function of aspect-ratio (ε is related to P-wave velocity, γ is related to S-wave velocity, and δ is related to the changes in the shapes of wavefront surfaces).

and γ are always positive, which indicates that the P-wave velocities (V_{p1}) propagating perpendicular to the axis of symmetry is always greater than V_{p2} propagating along a symmetry axis; and the S-wave velocities (V_{s1}) propagating perpendicular to the axis of symmetry is always greater than V_{s2} propagating along a symmetry axis.

Angle	Vp	$Vs1$	$Vs2$
$(degree)$	(km/s)	(km/s)	(km/s)
0	7.419	3.574	3.574
15	7.354	3.655	3.588
30	7.195	3.827	3.625
45	7.043	3.927	3.675
60	6.987	3.847	3.725
75	7.011	3.762	3.664
90	7.032	3.774	3.574

Table 5.2: Predicted velocities with angle changes by ADP mode.

5.5 Application

I have demonstrated that reservoir parameters may be affected by anisotropy due to the alignment of the minerals and pore spaces within rocks. Here, I will apply the ADP to perform velocity prediction and to compare the results with those from the IDP model presented in Chapter 4.

Figure 5.11 shows an output from the ADP model. These results include vertical and horizontal velocities for P- and S-waves and also three anisotropic parameters. When the angle of pore alignments changes from 0 to 90 degrees, the corresponding P- and S-wave (faster and slower) velocities are derived in Table 5.2, and anisotropic parameters are listed in Table 5.3.

These results are the summary of the associated anisotropy parameters, which shows changes that P-wave anisotropy parameter (ε) is approximately 5.07%, S-wave anisotropic (γ) is about 5.89% and anisotropic parameter (δ) is -13.97%. Additional parameters may be defined as (ε-δ), which is related to an-ellipticity, and indicates the deviation from elliptical of the wave surfaces. When (ε-δ)>0, the P slowness surface

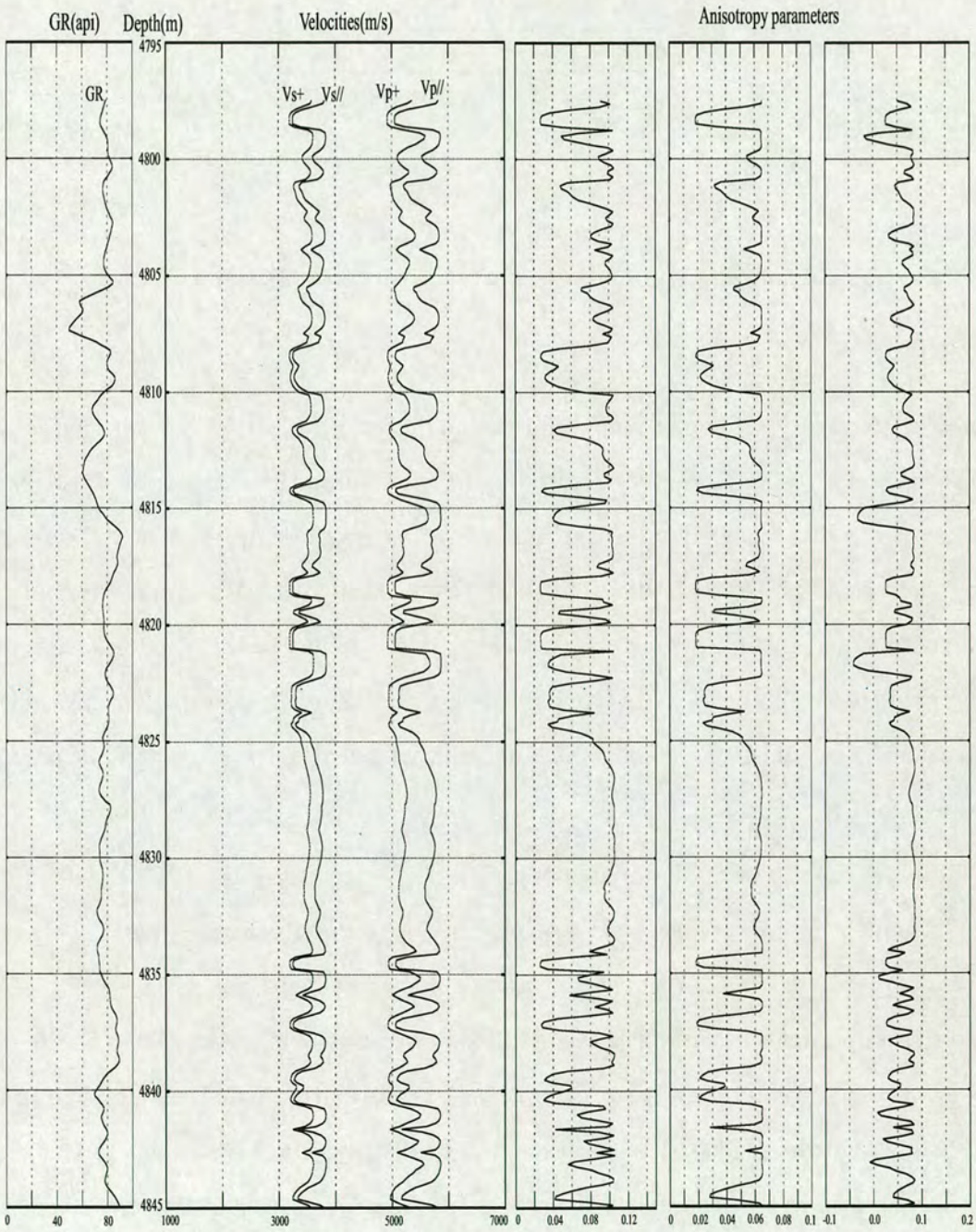

Figure 5.11: Prediction of velocities and anisotropic parameters by the ADP model (The results include vertical and horizontal velocities for P- and S-waves and also three Thomsen's anisotropy parameters, ε , γ and δ).

ε	γ	δ	$(\varepsilon - \delta)$
0.05068	0.0589	-0.1397	0.1904

Table 5.3: Predicted three Thomsen's anisotropic parameters by ADP model

will bulge out, and the Vs slowness surface will bulge in.

Comparing with different models for the prediction of velocities, we can see that the ADP model gives a satisfactory result. Figure 5.12 shows the comparison of predicted velocities using measured velocities in field data and the empirical model described in Chapter 3; the isotropic dual porosity (IDP, or called PADP) model described in Chapter 4; and the anisotropic dual porosity (ADP) model in this chapter. Note that the predicted results above are based on a part of training data to predict Vp and Vs for whole depth in the same well, which including the depth intervals where the training data is missing or un-available.

Figure 5.13 shows results of predicted S-wave velocity from the IDP model and the ADP model. As we can see that two velocities are similar generally, but the effect of anisotropy results in different velocity changes in some depth interval. Figure 5.14 is error cross-plot of measured and the predicted velocities. This result shows the P- and S-wave velocities and their error using an error distribution function. Comparing the measured and the predicted velocities and error distribution, I find that the scattering of ADP model and measurement is quite small, because their correlation coefficient of regression (R) is 0.893 for Vs and 0.947 for Vp respectively.

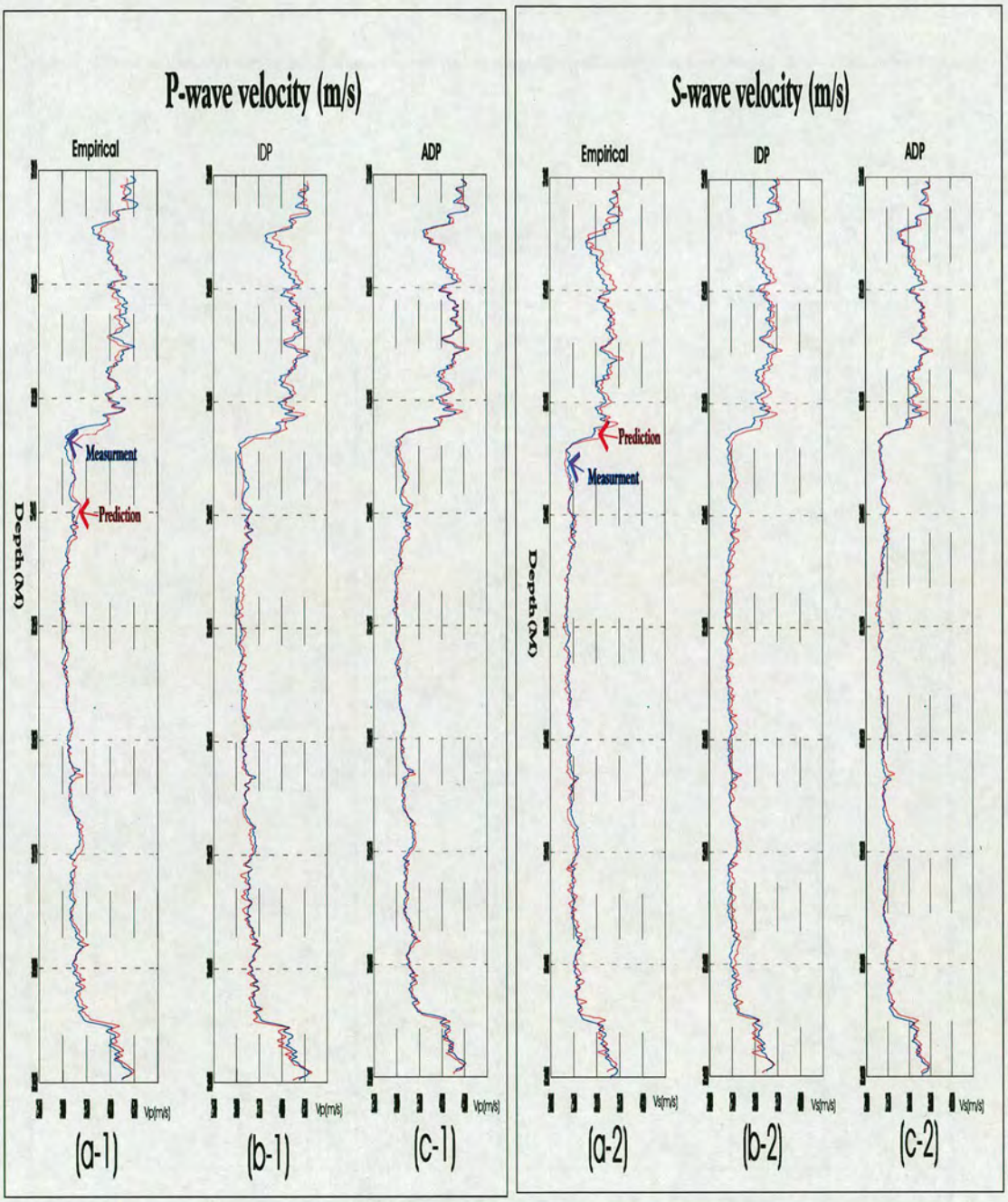

Figure 5.12: Comparison between predicted and measured P- and S-wave velocities using three models based on the same training datasets (The Figures (a-1) and (a-2) are the empirical model for Vp and Vs respectively; the Figures (b-1) and (b-2) are the IDP model for Vp and Vs respectively; the Figures (c-1) and (c-2) are ADP model for Vp and Vs, respectively).

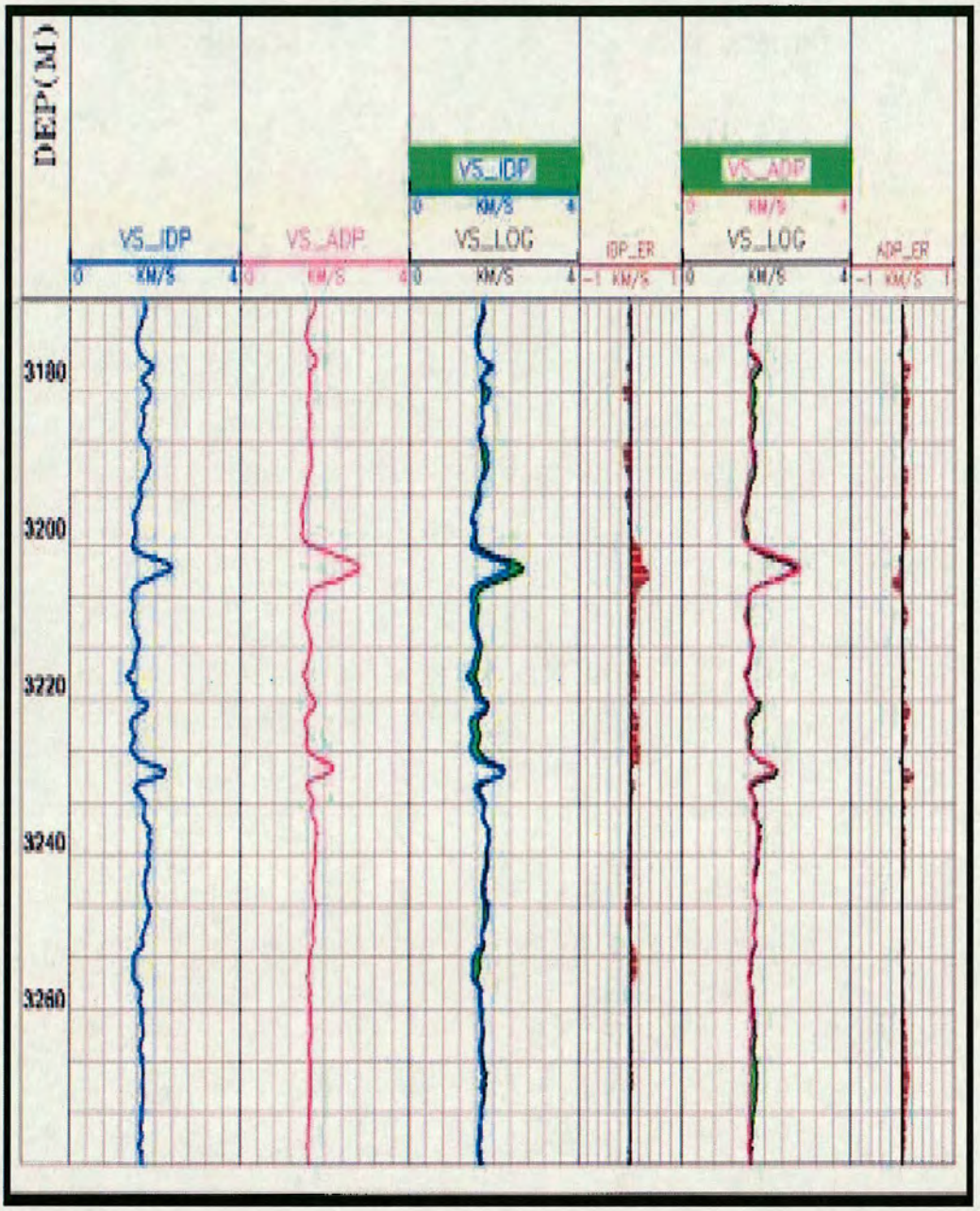

Figure 5.13: Comparison between predicted S-wave velocities using IDP model and ADP model. The velocity difference can be found from predicted velocity and measured velocity (Panel 3 and Panel 5), and Pane 4 and Panel 6 also show their calculated error curves.

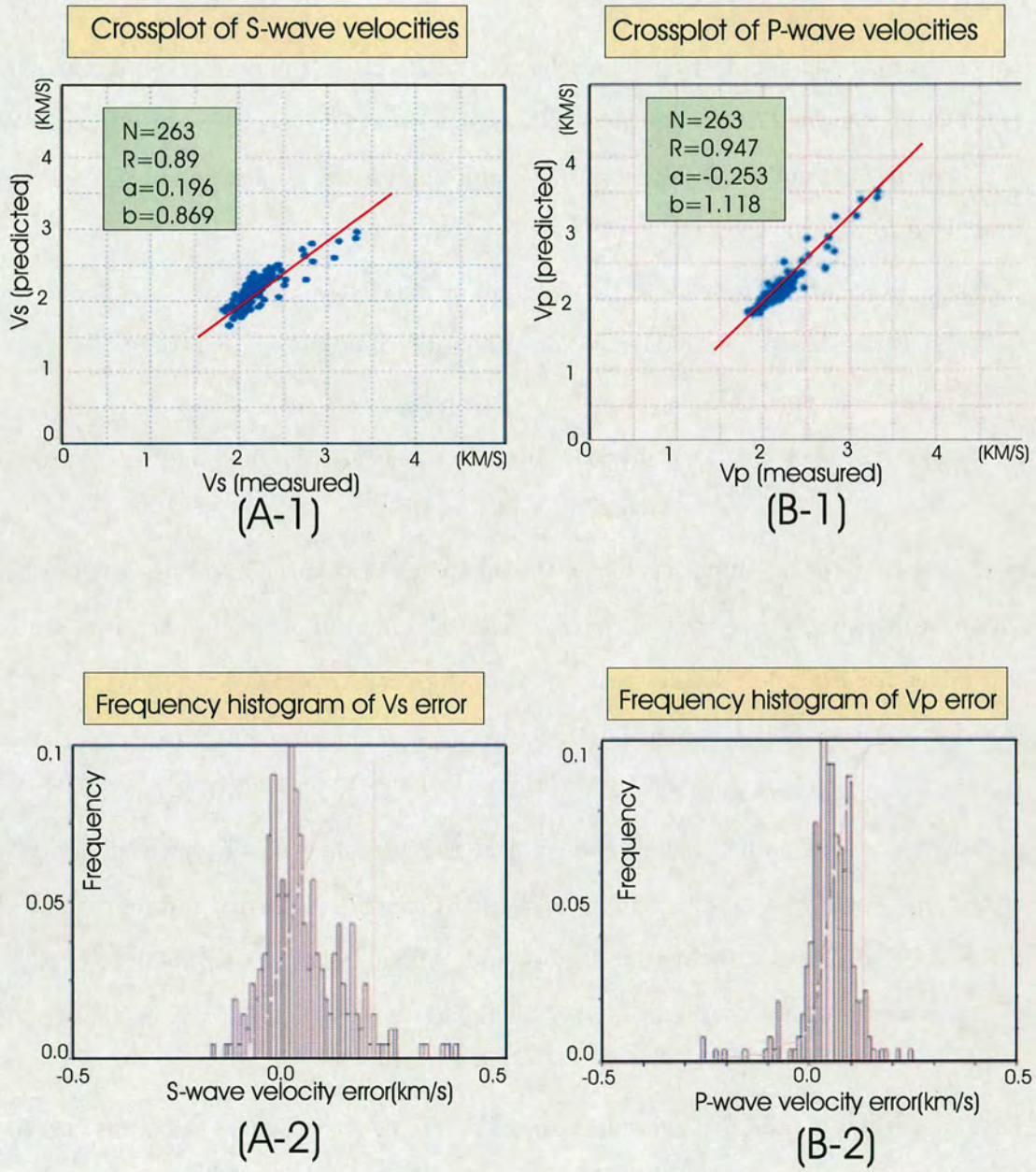

Figure 5.14: Error analysis of predicted and measured P-wave and S-wave velocities from the field data in the North Sea. The predicted velocities are determined from ADP model, the measured velocities are obtained from measured sonic log. Figure (A-1) and Figure (B-1) are the Vs and Vp error cross-plots between measured with predicted; Figure (A-2) and Figure (B-2) are Vs and Vp error distribution plots.

5.6 Summary

An anisotropic dual porosity model has been developed to estimate reservoir parameters of a rock containing distributed pores, clay, minerals and cracks. Because of the use of anisotropic DEM and SCA theories, the assumption for the application of ADP model should be addressed:

1) All pores are ellipsoid, and they are interconnected.

2) The pores are perfectly aligned or have a distribution of orientations .

3) The wavelength is large compared to the pore size.

4) There is no chemical or physical interaction between the fluid and rock frame.

Based on these assumptions above, this model can take account of preferred orientation of distributions of aligned pores, cracks, clay and other inclusions. In essence, this model has extended the clay-sand mixture model of Xu and White (1995a, b; 1996) to cover transversely isotropic media by means of the differential effective media theory and self-consistent methods.

To ensure that both the fluid and solid phases percolate at all porosities, Hornby (1994) and Nishizawa (1982) models are used to combine anisotropic formulations of the Self-Consistent Approximation (SCA) and Differential Effective Medium (DEM). Using this combination, we can predict the effective elastic properties in anisotropic media.

The method is valid for high pore concentration, as it introduces the pores into the system step by step. The application followed by anisotropic Gassmann model (Brown and Korringa, 1975) would be more consistent, which providing good connectivity for saturated rock in isotropy porous media.

Application of the ADP model to the field data from a reservoir in the North Sea, which indicates that reservoir parameters such as porosity, clay content, water satu-

ration, pore aspect-ratios, P- and S-wave velocities and anisotropy parameters can be satisfactorily obtained.

Chapter 6

DATA CONDITIONING AND CALIBRATION

6.1 Introduction

In the previous chapters (3, 4 and 5), I have presented detailed discussions about the model building. These include several empirical and physical models or methods used to estimate reservoir parameters in both isotropic and anisotropic rocks. These models or methods request the reconciliation of datasets from different measurements. Therefore, the measurement process, quality control, data correction, resolution matching and data calibration must be understood for each dataset.

Three datasets may be multiple measurements of the same physical parameter by different techniques. They are borehole core data (centimetre scale), well log data (centimetres to metre scale) and seismic data (metres to more than 10 metres scale).

Calibration is the process by which measurements are compared with known standards for the purpose of enabling the quantitative comparison of measurements, and it requires samples for which supposedly 'true' values are known in order that precision may be defined (Ruth and Pohjoisrinne, 1993). A practical calibration procedure is to assume that one of the datasets is correct and to adjust others to create a best fit; this is called core-log calibration or log-seismic calibration. Note that whilst laboratory determinations are the standards by which in situ log measurements are compared, each

method must be examined carefully to determine experimental limitations, accuracy and precision, as well as potential mineral alteration processes that can occur when a rock is sampled. At the same time, vertical seismic profiles (VSP) are studied in order to examine the relationship between well log and seismic data; thus demonstrating the validity of the log-seismic calibration.

The use of datasets from different sources involves the reconciliation of different observations which may be inter-related through their inherent property or physical basis. Because integrated data are obtained from coring, logging or seismic survey, which is carried out by different measurement system, if we predict petrophysical properties from these integrated data, we should consider a suitable method for data correction in order to have a satisfactory estimation for data calibration purposes.

The objective of this chapter is to identify an alternative, less subjective approach to integrate core, log and seismic data for data calibration. This is organized in two principal parts. The first part is dedicated to the data conditioning such as basic data description, the methods of data editing and correction. The second part deals with the problem of data matching and calibration between core and log, or log and seismic. To achieve this, firstly, a few basic principles will be introduced, which involves the data acquisition and interpretation through consideration of the measurement process and correction. Secondly, different data matching and calibration methods will be discussed, and several results and examples will be presented. More examples and detailed results will be shown in Chapter 7 (Integrated case study).

6.2 Core data analysis

Core analysis provides a great deal of information to geology, hydrocarbon exploration, well completion and evaluation of oil and gas reserves. This section provides an overview of the capabilities and approaches for core data analysis and processing.

6.2.1 What do we need for core analysis?

The application of core analysis plays an important role in exploration and reservoir evaluation. This is because core analysis makes it possible to recognize the structure of the reservoir trap, therefore we can obtain some important physical characteristics from reservoir parameters such as porosity, clay and shale content, and permeability. Additionally, in the field development stage, the core measurements are often employed to estimate hydrocarbon reserves, determine contacts between reservoir fluids such as water-oil contact line and their variations across the field, establish structural and stratigraphic correlations and define limits of the field.

The core data that we used in this study include routine core plug analysis (porosity, permeability and grain density), and special core analysis (shale, clay content, saturation and rock properties). The rock sample at reservoir conditions equilibrates the in situ brine with the salts deposited in small cracks or fissures and clay. The difficulty in making a core reach equilibrium under laboratory conditions is due to two main causes. Firstly, during coring, a fluid different from the native brine almost always comes in contact, with and at least partially saturates the core. Secondly, during core handling, salts are deposited and clays are partially or totally dehydrated if the core is allowed to dry out. In practice, all core analysis should be used only for qualitative purposes.

6.2.2 Coring methods

Core analysis makes it possible to recognize the structure of the formation trap, rock physical characteristics, as well as obtaining reservoir parameters. For simplicity, the coring techniques can be divided into the following three types:

• ***Conventional coring:*** This refers to core taken without regard to precise orientation, and encompasses a range of coring devices and core barrels. The main disadvantage of conventional coring is that coring equipment requires that the entire drill

string be pulled out to retrieve the core; however, the advantage is that large cores 7.62 to 12.7 cm, in diameter and 9.15 to 27.45 m in length, may be recovered.

• ***Wireline coring:*** The core may be retrieved without pulling the drill string out by using an overshot running down the drill-pipe on a wireline. The cores obtained by this method are small, approximately 2.54 to 5.08 cm, in diameter and 3.05 to 6.10 m in length. Other advantages include downhole durability and higher core recovery.

• ***Sidewall coring:*** Sidewall coring is necessary if it is desirable to obtain core samples from a particular zone that has already been drilled through, especially in soft rock zones where hole conditions are not conducive to open-hole drill-stem testing. The sidewall coring device contains a hollow tool which, when fired from an electric control panel at the surface, embeds itself in the formation wall.

The selection of coring and analysis methods are generally dictated by the type of reservoir rock and objectives of the core analysis. In fact, the conventional coring, which was used in many fields by the oil industry is still widespread.

6.2.3 Selection of core analysis methods

Various analytical methods are used, most of which are basic but provide results of a fairly good quality. Table 6.1 shows typical results obtained from core analysis. Porosity, permeability and shale or clay content are the most common parameters derived from core analysis in laboratory. Saturation of residual oil and initial water are measured routinely in cores access some hydrocarbon provinces. Additionally, electrical property measurements appear to be quite reliable although in practice they are seldom used (Graham, 1995).

A wide range of other analytical techniques is of course employed on cores, but usually as incidental further studies (geological, petrophysical and reservoir engineering)

Slabbed core	Small sample	Thin sections	Routine Plug	Special analysis
Photograph	Grain size	Pore structure	Porosity	Electrical properties
Sedimentology	Mineral	Diagenesis	Permeability	Capillary pressure
Lithology	X-ray& SEM	Porosity type	Grain density	Acoustic properties
Samples	Bio-dating	Environment	Saturation	Compressive props.
			Shale & clay	Specific tests

Table 6.1: Reservoir characteristics obtained from core analysis.

rather than as part of a structured core analysis programme. These include optical petrographic analysis of thin sections. These are usually restricted to descriptions of the main mineral phase, although some attention has been paid recently to the process in sediments, their relationship with depth, and their impact on reservoir quality (e.g. Sakhibgareev, 1989).

6.2.4 Core sample process and application

The preservation and preparation of core samples prior to analysis can have a significant effect on the quality of data subsequently generated. It is therefore vital that the optimum methods to be used are carefully planned prior to cutting the core or commencing the analysis programme. Generally, the preparation procedures can be subdivided into:

•**Applications:** Generally used in fractured reservoirs, vuggy carbonates, conglomerates and heterogeneous reservoirs where plug type analysis may not be representative. Analysis can be carried out on clastic rocks or carbonates.

•**Sample preparation:** Suitable sample diameters range from 6.35 to 12.7 cm. The sample should be at least as long as its diameter. The ends are squared off to produce right cylinders. It is recommended that all whole core samples are over-cored to reduce any effects of mud filtrate invasion.

•**Sample clearing and extraction:** Samples can be cleaned using similar methods for plug samples. An alternative option is to clean samples by gas driven solvent

extraction, and also the samples can be cleaned by the combined action of the solvent and the gas coming out of the solution.

•**Porosity and permeability measurements:** Normally, the porosity is measured using a Helium expansion porosimeter which operates using Boyle's Law. The porosimeter is calibrated at least once per day and the accuracy of results are checked by running standard check samples. Permeability is measured by the steady state method. All pressure measuring devices are calibrated regularly, and a range of standard check samples are run after each batch of whole cores.

•**The grain density, shale, clay content and other special core analysis:** The analysis of grain density, shale, clay and others is described in more details in *API* (American Petroleum Institute) recommended practice for core analysis.

6.3 Log correction

Well-log data provide an intermediate link between the small-scale, with high-resolution sedimentological and stratigraphical features visible at outcrops, and the large-scale data available from seismic sections. The well-logs are obtained from tools introduced into a borehole at the end of a cable. These tools measure physical parameters such as current flow, natural or induced radioactivity, wave propagation times and signal amplitude. The petrophysical characteristics of the formation are inferred from calibrations carried out on well logging tools. The measurements take account of a fairly small rock volume surrounding the tool. Because of this fact, the environmental conditions in the well (e.g. presence of mud, mud cake, caved sections, fractures, micro fissures etc.) can adversely influence the measurements. Therefore, we should realize that it is necessary to make log correction in order to match core and seismic data.

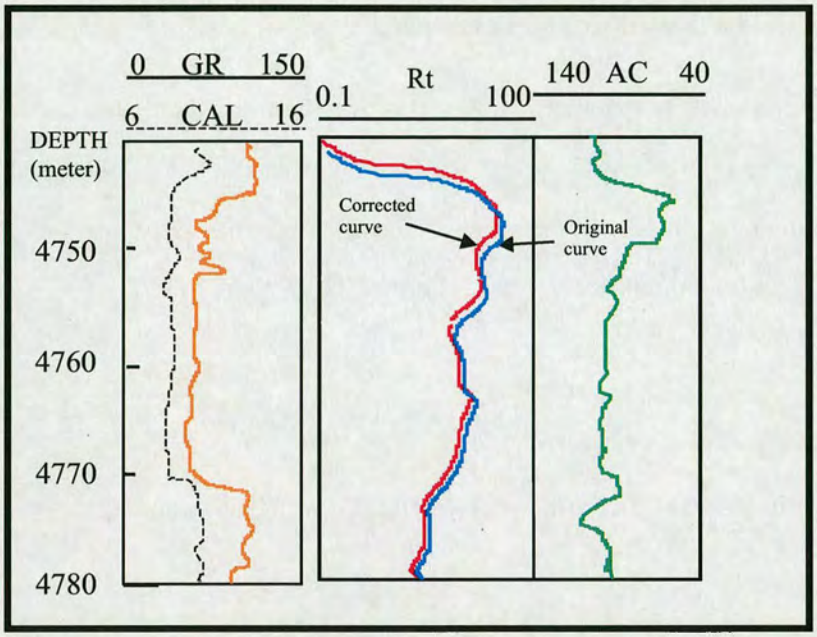

Figure 6.1: The example of log curve depth correction from the resistivity log (Rt). GR log gives a depth reference.

6.3.1 Log depth adjustment

It is very important to check the corrected depth to match two successive runs, and check whether there are missing log data between one run and another. The logging tools run into the well are subject to significant amounts of stretch due to tension and temperature effects. In normal and good borehole conditions, stretch is compensated for by the operator, however poor borehole conditions can easily cause depth errors that will need to be corrected before data interpretation.

The depth difference for two separate log measurements in the same depth interval should be adjusted. Recordings obtained in the same downhole run with combined tools are subject to the breakout of wall-rock during drilling, and stick-and-pull as logging tools are winched up the well. Figure 6.1 shows an example of depth adjustment for Rt log.

6.3.2 Deviated-well depth correction

For a deviated well, it is necessary to make a deviated-well correction from measured depth (MD) to true vertical depth (TVD). The method is to assume that the depth interval of deviated hole is a constant value, which is called curvature, and the variation of the angle of hole deviation (δ) with depth (h) is equal to

$$\frac{d\delta}{dh} = constant\,,$$

for a very small deviation (dh), we have the following relationship:

$$dz = dh \cdot cos(\delta), \tag{6.1}$$

where dz is the vertical distance, dh is deviation distance and δ is the angle of hole deviation.

Figure 6.2 is a sketch to show a correction of deviated depth into true vertical depth. We can see that point 1 is the position of deviation depth (h_1) and vertical depth (z_1), the angle of deviation is δ_1. In the same way, point 2 is the position of deviation depth (h_2) and vertical depth (z_2), the angle of deviation is δ_2. Assuming the rate of change of deviation angle between points 1 and 2 is a constant value, we have:

$$\frac{d\delta}{dh} = \frac{\delta_2 - \delta_1}{h_2 - h_1}, \tag{6.2}$$

the vertical distance between point 1 and 2 should be:

$$Z_2 - Z_1 = \int_{z_1}^{z2} dZ = \int_{h_1}^{h_2} cos\delta \cdot dh, \tag{6.3}$$

and

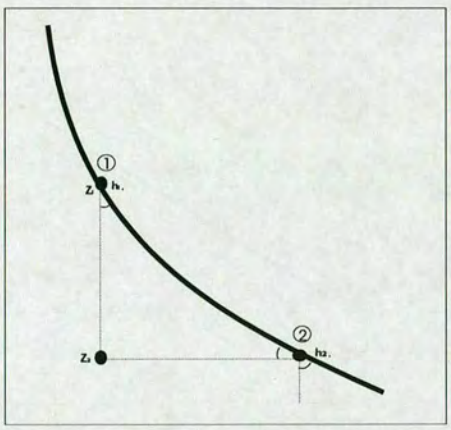

Figure 6.2: Correction of a deviated hole from measured depth (MD) to true vertical depth (TVD).

$$Z_2 - Z_1 = \int_{\delta_1}^{\delta 2} \frac{h_1 - h_2}{\delta_2 - \delta_1} cos\delta \cdot d\delta, \tag{6.4}$$

$$= \frac{h_1 - h_2}{\delta_2 - \delta_1}(sin\delta_1 - sin\delta_2), \tag{6.5}$$

where h_1 and h_2 are the starting and final depths for deviated hole, Z_1 and Z_2 are relative vertical depth intervals, and δ_1 and δ_2 are the angles of hole deviation.

Using this method, equation (6.5) is used to divide the deviated hole into several intervals, and using 1, 2...M points to divide the deviated hole into M-1 interval depths, we can obtain the vertical depth as shown in Figure 6.3.

6.3.3 Correction of abnormal log curve

If log data at a certain depth interval show abnormal variations, or are missing, a necessary replacement correction is normally done to find out a new relationship between

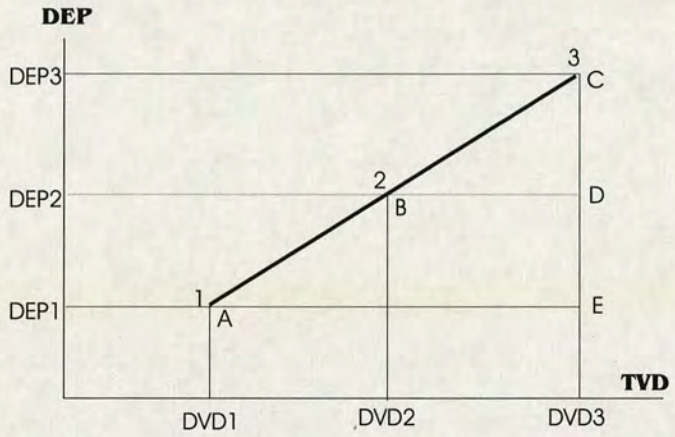

Figure 6.3: The relationship of deviated depth (DEP) and true vertical depth (TVD)

erroneous log data and other logs such as porosity (por), shale content (V_{sh}) or other log curves ($log_1, log_2...$). The new log curves ($log*$) will then be used to replace the abnormal interval based on the following function:

$$log* = f(por, Vsh, log_1, log_2...).$$

Figure 6.4(left) shows an example to correct abnormal GR log at the reservoir depth intervals. Using the available logs such as DT, SP and Rt, and choose the normal value of GR as the output, based on a suitable regression approach (for example, linear, non-linear or multi-regression etc.) to build a relationship between output (GR) and inputs (DT, SP and Rt). Therefore, a new GR log curve as a replacement of the abnormal log curve at the same depth can be obtained (Figure 6.4, right shows an example).

6.3.4 Resistivity log (Rt) correction

When drilling in a reservoir, mud water will invade the original formation. With increasing time, the volume of mud water will increase and invade the reservoir; the original fluid (oil, gas or water) will be pushed deeper into the formation. As a result, the original oil, gas or water in reservoir will be replaced by the invaded fluid (mud-water).

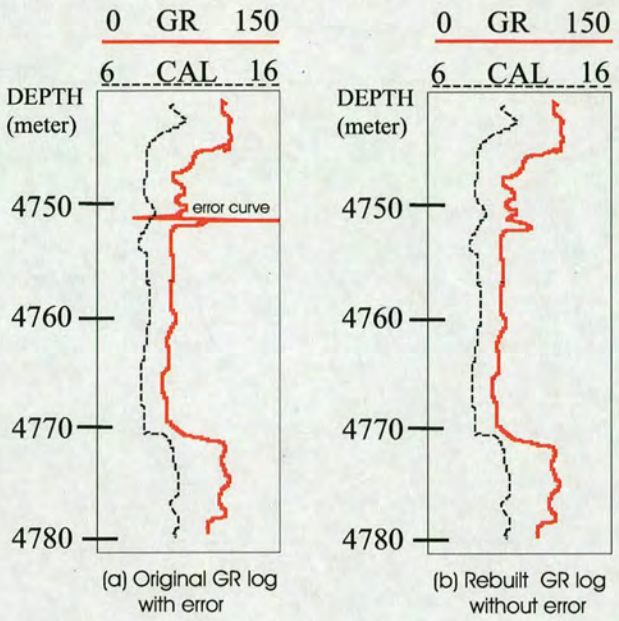

Figure 6.4: Comparison of the original log with abnormal interval (panel 1), and a new replacement of log curve (GR) is given by multi-linear regression method (panel 2).

Therefore the value of *Rt* log could be reduced in a reservoir containing oil or gas. On the other hand, the value of *Rt* log is probably increased if it is a water reservoir.

The value of *Rt* may affect fluid saturation estimation in petrophysics interpretation. Obviously, it is an important factor therefore we have to obtain an accurate value for *Rt* log from a reservoir. In this section, I used a practical correction method for *Rt* which is described as follows:

- for a new field, two logging runs should be taken for *Rt* correction,
- the first *Rt* value should be obtained soon from a key well (say, within 3 days of opening a reservoir), because this will give an original value for deep reservoir resistivity (Rt).
- after well completion, a second *Rt* logging should be taken.
- using both logging runs to build a relationship for correction (Figure 6.5).

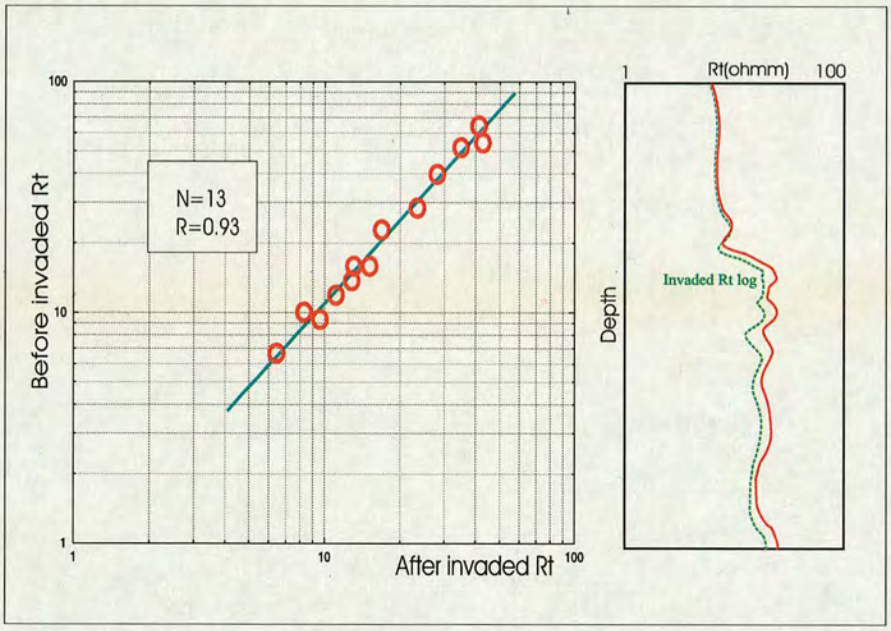

Figure 6.5: Correction of invaded Rt log plot, which is made by the correlation of the original resistivity log value ('true' value) and invaded resistivity value (logging after 10 days drilling) based on the North Sea data.

The following equation shows a relationship for data correction between the real log (first Rt: logging within 3 days drilling) and invaded log (second Rt: logging after 10 days drilling).

$$R_c = 1.326R_t - 0.021, \tag{6.6}$$

where R_c is the correction value, and R_t is the log measured value after 10 days drilling. In the same area or same research zone, we may use the oil-based mud coring data as a standard value for Rt checking and correction.

6.3.5 Fluid saturation correction

Using the relationship between oil saturation and oil-height based on capillary-pressure analysis, we can estimate the oil saturation to correct the Archie's equation for estima-

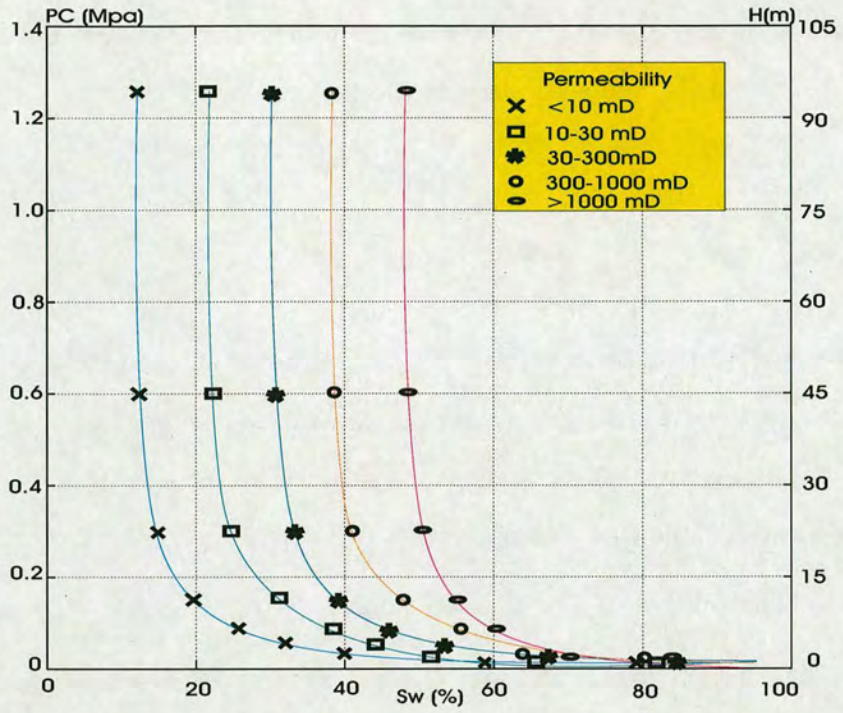

Figure 6.6: Using the relationship between capillary-pressure, oil-height and water saturation to correct Sw.

tion of fluid saturation. Figure 6.6 is the relationship between the capillary-pressure (PC), oil-height (H) and saturation (S_w), which provides a practicable method for Sw correction.

If Sw is affected by lithology or other factors, we may use a numerical method to correct the effects. The modelling method should combine with the practical data such as core analysis (in the well with oil based mud) to obtain the optimal correction results for saturation calculation.

6.4 Velocity estimation using vertical seismic profiles

A well velocity survey is a type of seismic well operation performed to determine the vertical propagation time of a wave emitted at the surface by a seismic source, and then recorded by a geophone. For well velocity shooting, an assumption can be made that

the ray-path is vertical from the source position to the reference plane, but it is oblique and rectilinear from the reference plane to the well geophone.

6.4.1 VSP data

The operation of Vertical Seismic Profiles (VSP) is very similar to a check shot survey (well velocity survey). The VSP is a downhole seismic operation where a seismic signal emitted at surface is recorded by a geophone situated successively at different depths, VSP survey has the following features:

a. If a well is drilled vertically, the source has a fixed position close to the wellhead.

b. If the well is deviated, the source has a variable horizontal position so as to maintain the transmitter and receiver on the same vertical depth.

c. The VSP can be regarded as an acoustic log at seismic frequencies. Its lateral resolution is limited to the diameter of the first zone, while the lateral investigation is a function of the source offset in relation to the well-head and the structural geometry of the strata.

d. In the case of a horizontal tabular medium, the lateral investigation is equivalent to the lateral resolution for a vertical well. For a deviated well, this lateral investigation is equal to well's deviation (see Figure 6.7).

A possible way of increasing the lateral investigation consists of offsetting the source in relation to the wellhead and downhole geophone. The choice of offset depends on the depth of the target. It is limited by the fact that incident waves must have an angle of incidence with the markers to satisfy the assumption of near-normal incidence for the calculation of the reflection coefficient and to avoid guided and refracted modes.

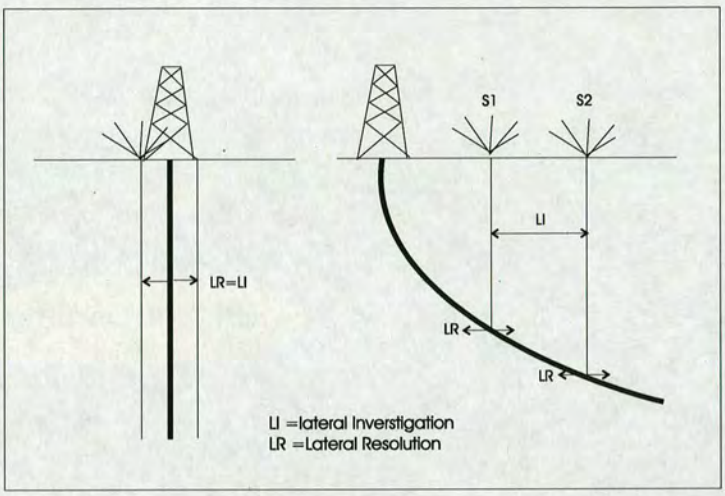

Figure 6.7: Lateral range of Investigation (LI) and Lateral Resolution (LR) in a vertical seismic profile.

6.4.2 Picking of first arrival times

A well velocity survey is carried out to establish the propagation time versus depth relation T = F(Z). It is also used to perform the sonic log calibration and to obtain sonic and density logs as a function of the vertical two-way travel time through the various formations.

A velocity survey with P- and S-waves are often required in order to establish the relationship between travel time and depth (Tp = Fp(Z) and Ts = Fs(Z)), but an incorrect estimate of the position of the shot points at the surface can yield erroneous propagation velocities. Particularly, in the case of an offshore VSP, the position of the source can vary in relation to the reference point. Variations may occur in both horizontal and vertical planes if the source is lowered in a hurry. This type of error can be avoided by monitoring the operation and noting every factor that might give rise to such errors, as well as by checking the arrival times at the reference receiver. The different picking techniques employed can be a source of discrepancy between the time measurements. In a well velocity survey operation, the picking is done by finding

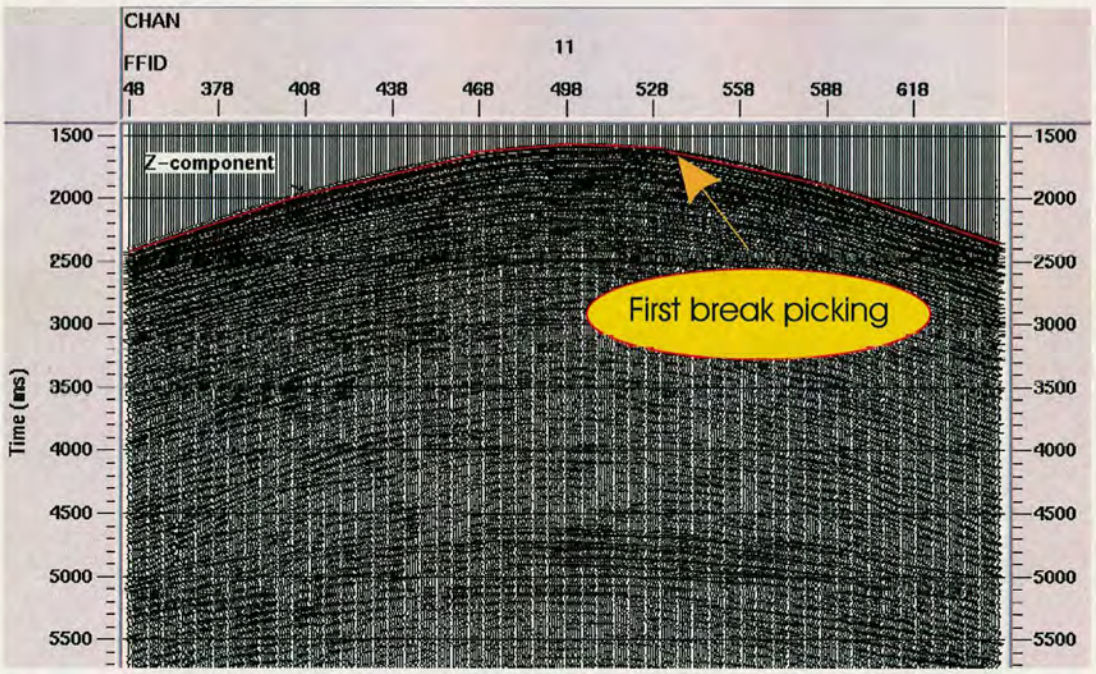

Figure 6.8: VSP data are used to pick the first breaks for velocity estimation. This velocity is then used to compare with the measured velocity from log data in order to build the correction of seismic velocity (VSP) and log velocity (DT). The aim is to use the measured velocity to calibrate the modelled velocity.

the first break (Figure 6.8), which recording the travel-times corresponding to the peak amplitudes of the first breaks.

6.4.3 Picking error

In order to obtain an accurate first break pick, the three-component recording from a zero-offset VSP is used to estimate seismic velocity, and the same depths of geophone were used to pick first break, the statistical interval transit time is obtained by picking travel time. The histogram (Figure 6.9) shows the effective value of interval transit times (Z and Y-components). The X-axis and Y-axis show respectively the interval transit time of the same depth and the statistics points, as we can see that the maximum deviation of interval transit time is about 0.3 ms, and the root-mean-square error can

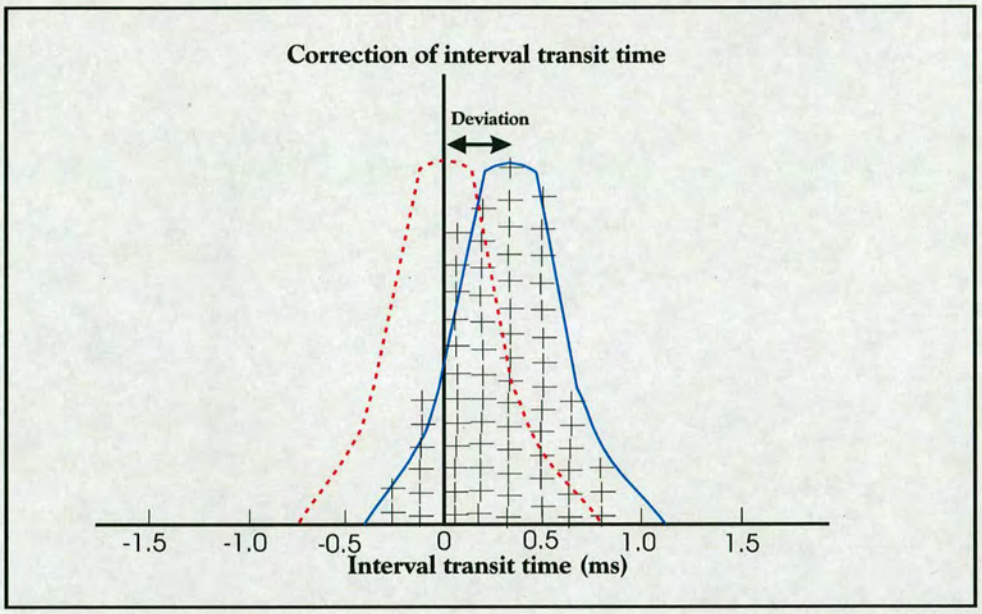

Figure 6.9: The interval transit times are shown by two peaks, which include a Z-component and a X-component.

be expressed by

$$\sigma^2 = [\frac{1}{n}\sum_{i=1}^{n}(m_i - \overline{m})^2])$$

6.5 Core-log calibration

Core-log calibration involves putting one dataset through some equalization procedure, whereby one dataset is assumed to be correct. Another scenario is where the two or more datasets are integrated through the selective addition of components to enhance the overall picture of the formation represented by both downhole measurements and in the recovered core. The process of calibration of logging tools concerns the production of a specific signal in response to known measurement values within a formation (Theys, 1991); thus the transformation of the raw measurement to usable values is designated separately as the tool response.

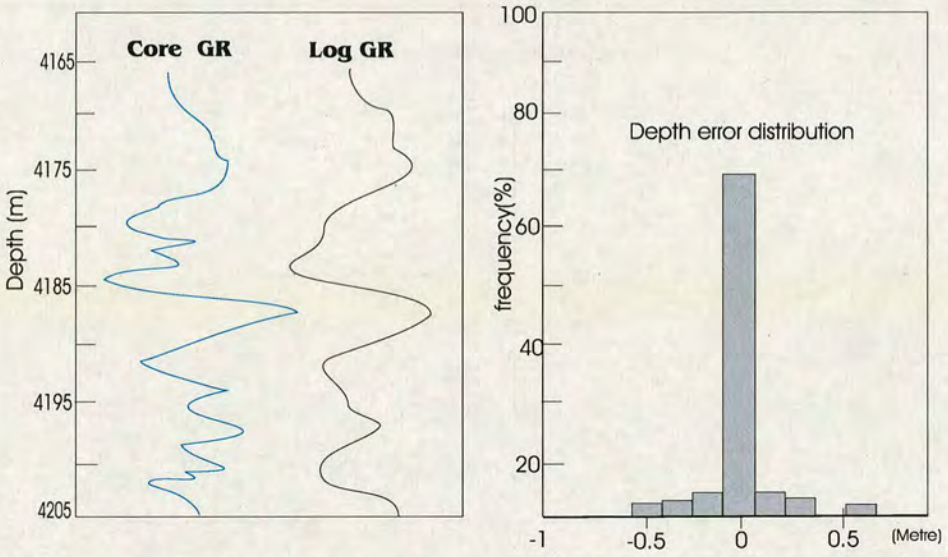

Figure 6.10: Using the gamma-ray at surface for core depth positioning. It shows using a gamma-ray measurement (Land GR) at surface to compare with a gamma-ray log measurement in hole (Log GR) for the purpose of core depth positioning. The left plot shows the error distribution of both land and log GR data.

6.5.1 Matching depth position

We may choose a depth interval in which the core recovery rate is more than 90% for depth matching. The following two methods have been adopted in this study:

- ***Positioning by gamma-ray tool:*** After obtaining cores, the cores are measured continually by a gamma-ray tool; the results of the measurement at surface will be compared with a downhole gamma-ray log (GR) curve at the same depth. The different values will be detected, and a core depth matching error may be identified based on this comparison. Through depth positioning, we can ensure that the GR log depth is equal to the depth of core samples. Figure 6.10 shows an example using a gamma-ray measurement at surface compared with a gamma-ray log measurement (GR) downhole for the purpose of core depth positioning.

- ***Positioning by density log:*** To match the depth of log and core data for the

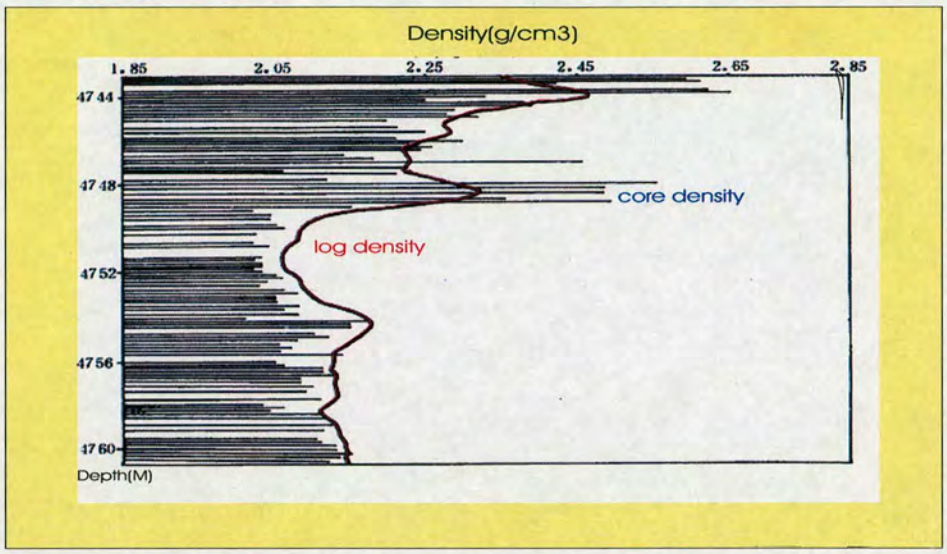

Figure 6.11: Log depth is used to adjust and correct the core depth, the core depth adjustment is based on the depth of density log (g/cm^3).

purpose of calibration, a bar-plot of depth-density can be made using both log and core density measurements (or transfer to porosity). Figure 6.11, a bar-plot is drawn on the basis of density measured in core samples and the density log in the same depth interval. We note that the depth of density log is normally regarded as the standard value to adjust core depth.

6.5.2 Curve normalization

For multi-well data, it is very common to have a different log reading for the same formation in the same area. A standard layer (normally, a thick shale layer) is defined as the normal layer for log normalization. Therefore, a normalization value in the standard layer is then used to correct log readings. Figure 6.12 is an example of normalization correction based on the sonic log, and we can see that three unusual points have been found.

If we choose two layers or beds as the normalized standard formations in the same

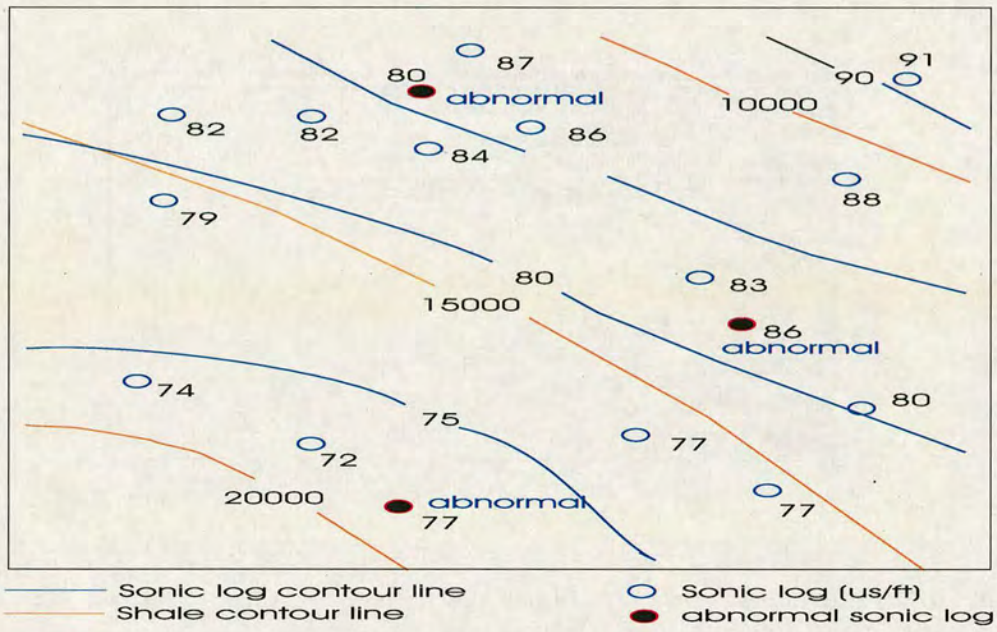

Figure 6.12: Normalization of sonic reading in the shale formation. Three unusual sonic points (values) can be found in this example.

research area, using the core sonic velocity we can recognize different lithologies. For example, a limestone is chosen as Log_l , and another sandstone is chosen as Log_s, a new normalized value (Log_{nor}) may be obtained based on the measured value (Log) using the following equation:

$$Log_{nor} = Log_s + \frac{Log - Log_l}{Log_s - Log_l} \tag{6.7}$$

Table 6.2 is an example for the statistics value of the same standard formation in sandstone. Normally, we should use the average value as the standard value for the curve calibration.

6.5.3 Resolution matching

In comparison of the resolution between log and core data, we know that the core data have higher resolution than the log measurement. Generally, the coring density are 5

Well	Depth	Thickness	Density(g/cm^3)	Density(g/cm^3)	Neutron(%)	Neutron(%)	Sonic($\mu s/m$)	Sonic($\mu s/m$)
	(M)	(M)	(range)	(peak)	(range)	(peak)	(range)	(peak)
Well A	4360-4365	5	2.21-2.27	2.23	27-30	28	75-91	87
Well B	4440-4445	5	2.21-2.33	2.25	24-30	27	79-89	84
Well C	4380-4385	5	2.23-2.33	2.25	25-31	28	75-95	89
Average				2.237		27.7		86.7

Table 6.2: The example of log normalization in the key wells for density, neutron and sonic logs.

to 10 plugs each metre, and this means that the core response in the measured range is between 0.2 and 0.1 metre. In contrast, we know that log resolution is far lower than 0.2 or 0.1 metre. For example, the density log records the bulk density of rock, which is a function of the density of the matrix and the density of the fluids in the pore space. Therefore, any attempt to construct a field density log with the same characteristics and resolution as the density log has to take into account the density of the matrix and the density of pore fluid. Its resolution will be decided by the distance of source to receiver of a log tool. For example, in an older single-detractor density log tool, the source distance is 0.36 metre, its vertical resolution is around 35 to 40 cm (Serra 1984), for a model two-detractor tool, the source distance is 25 cm. Comparison with other log tools, we can see that source distance for the Neutron log is 0.64 metre, Sonic log is 0.6 metre and *Rt* log is 1.02 metre. Based on their source distance, we may consider the use of an effective filtering technique to smooth core data in order to match log data. Therefore, a suitable window length of the resolution capability should be chosen on the basis of the source distance for different log tools. For example, if the coring density is between 5 and 10 plugs, a three-point filtering may be considered for matching density log, and a five-point filtering can be used to match neutron and sonic log. To match *Rt* log, we can employ a point-by-point equal weight filtering technique. If the coring

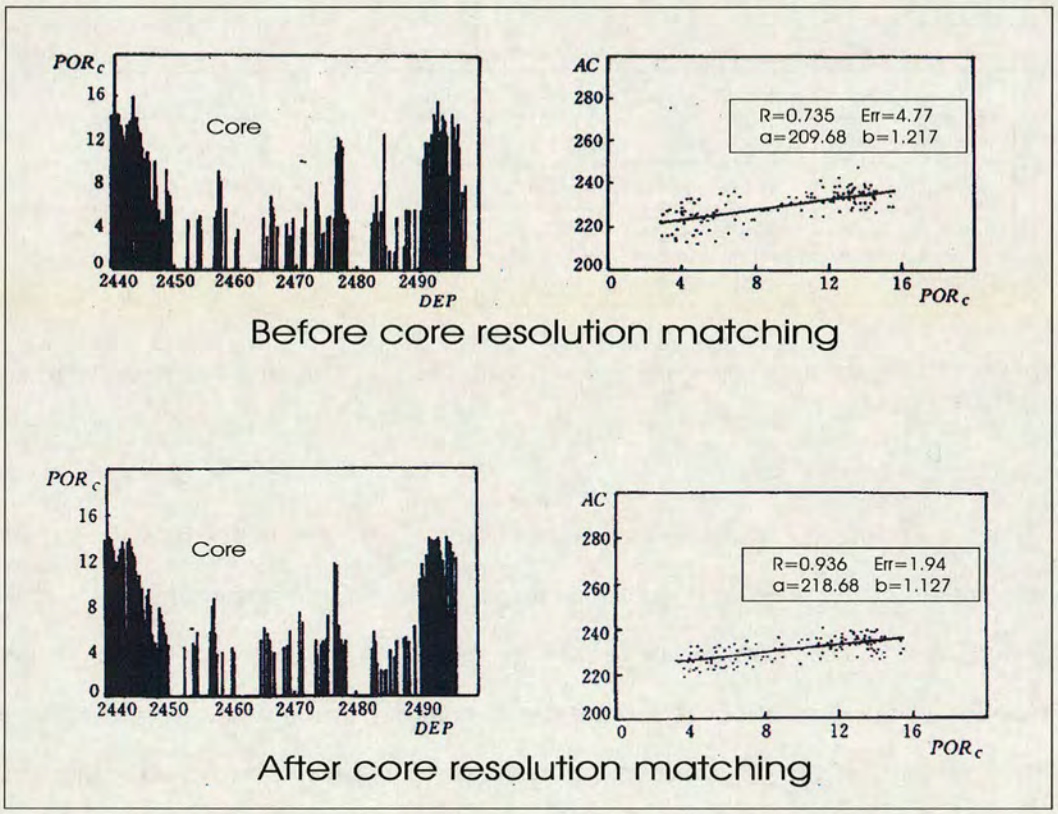

Figure 6.13: Filtering comparison between core data (core analysis porosity) and log data (sonic calculated porosity). In this example, a three point filtering is used for core analysis porosity, and gives a much better linear relationship between core and log data.

plug interval is not equal, we may use a quadratic function for non-linear interpolation processing. Assuming the core data is as COR, the core value after filtering at point K is:

$$COR(K) = \sum_{n=1}^{N} PAR(n) \times COR(K - \frac{N}{2} + n - 1), \tag{6.8}$$

where N is sampling number of filtering window, $PAR(n)$ is the array of n weight coefficient. Figure 6.13 shows a comparison of cross-plots from the core and log data. We find that a three-point filtering gives a much better linear fitting result, because the scattering of data points has been reduced significantly.

6.6 Log-seismic calibration

Compressional velocity is measured at all scales by log and seismic. It is therefore chosen as the most representative property for the analysis as an example of the average rock properties. Note that compressional velocity data for both log and seismic data are derived by different techniques; well-log data is provided from sonic velocity logging, and the seismic data is derived directly from the two way transit velocities from VSP.

6.6.1 Influence of surrounding media on measurements

Logs (sonic or density log) have a shallow depth of penetration (less than 1 metre, see Figure 6.14, left), so the analysis of a rock volume is limited to the immediate surroundings of the borehole in the flushed zone where mud has driven out the formation water and part of the hydrocarbons. This flushed zone is generally not very extensive (a few decimetres at the most). The seismic wave emitted at the surface is mainly propagated through the un-invaded formation before reaching the reservoir through the flushed zone. The velocity and density characteristics of geological media depend on fluid (mud, formation water and hydrocarbons) and hydrocarbon saturation. These fluid characteristics are therefore related to the geological media investigated by the survey. Correction for the sonic and density values can be envisaged through a complete logging interpretation. After correction, the acoustic and density logs can enable the calculation of the relationship with seismic velocity.

On the other hand, the sonic log does not necessarily give a travel time corresponding to the path taken by the seismic wave (Figure 6.14, right). Although the correction for well deviation (conversion to vertical times) minimizes this error, it does not take into account all the effects mentioned above and does not enable the recovery of time discrepancies. Only sophisticated simulations using available data are able to reduce the errors incurred in this way. However, this type of costly approach is not generally

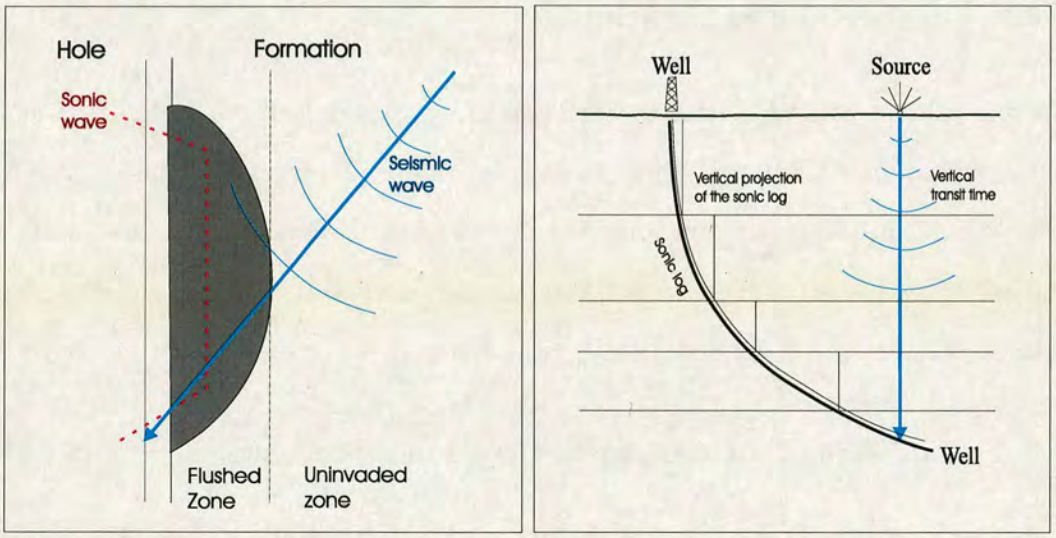

Figure 6.14: (left) Propagation media for seismic and well log wave. (right) Influence of well deviation on the estimation of vertical times.

adopted, at least for a simple sonic calibration; moreover, the precision of the applied correction is probably illusory considering the relative lack of knowledge of the geological media (with the exception of flushing and well deviation corrections).

6.6.2 Depth-to-time conversion

The calibration of sonic logs to seismic survey data consists of limiting the mismatches observed at the well velocity measurement depths. This is done by modifying the sonic log at given depth (generally at a thick depth interval) so as to establish a T=f(h) relation based on an integration of this re-calibrated log. Although the time-depth relation is compatible with the seismic data, it is based on a higher sampling rate comparable to that of the acoustic log. In the case of well seismic survey, the measurement of travel time is direct (from a source at the surface to a receiver in the well). However, the sonic log is calculated by the error on Δt accumulated progressively over the depth of the log. As we know, in VSP, the seismic wave is emitted from a shot point which does not lie vertically above the reception point, whereas in sonic well logging, the wave is

propagated along the hole axis.

The conversion of the measured seismic time to vertical time is merely an approximate correction since the ray-path is not always a straight line. In the case of deviated wells, re-plotting of the sonic time on a vertical axis only provides an approximate slowness log. In fact, this correction assumes a horizontal homogeneity of the formation along the entire deviation of the well.

The log data are recorded as depth sampling, and the seismic data were recorded as time sampling. To match both data together to allow the log and seismic data to be converted within the same record domain, a relation should be defined to convert depth logs to time logs with the seismic scale. The following equation (6.9) gives a formula for the depth-to-time conversion

$$T = T_{H_0} + 2\sum_{i=1}^{n} T_i \cdot \Delta H, \tag{6.9}$$

where T_{H_0} is the time of log starting depth, corresponding to the reflection time of seismic wave; T_i is interval transit time from sonic log or dipole log; ΔH is the depth sampling interval; T is the dual transit time, which is the integration of acoustic propagation time Δt measured by the sonic tool over the entire recording-depth interval (after correction for the media), and it is necessary to:

(1) Add a T_{H0} time corresponding to the transit time from the common reference depth to the beginning of the sonic log.

(2) Convert the times to a vertical scale in the case of a deviated well.

The integrated time obtained in this way is directly comparable with the well velocity corrected vertical time. This procedure provides the discrepancy D between these two times. Once corrected, the integrated sonic log leads to the calculation of a new Time versus Depth relation. This allows the conversion of sonic and other type of logs into sections as a function of time.

6.6.3 Correction of Δt *value*

- ***Block shift method***: The block shift method involves the uniform redistribution of the time losses or gains within each interval by applying a constant correction to the sonic log. In this method, it is assumed that the correction is distributed uniformly over the whole interval between two inflection points (see Figure 6.15, A); the Δt is corrected within the interval using a constant value $d\Delta t$ as follows:

$$\Delta t_{cor} = \Delta t + d\Delta t \tag{6.10}$$

$$d\Delta t = \frac{D_{2-1}}{Z_2 - Z_1}, \tag{6.11}$$

where: D_{2-1} is the time difference at the depth Z_2 and at the depth Z_1. Z_1 and Z_2 are depths.

This method can be used if there is a positive drift gradient (drift increasing with depth, $D_{2-1}>0$) or possibly a negative gradient but with very low Δt values.

- ***Minimum Δt value:*** In this method (see Figure 6.15, B), the adjustment is proportional to the value of Δt itself. Below a chosen minimum Δt no correction should be applied. Above this value, the correction is a function of Δt.

Since the overall correction in a zone between two "knees" separated by the distance $Z_2 - Z_1$ is defined as D_{2-1}, the shift required at each time or depth value may be obtained as follows:

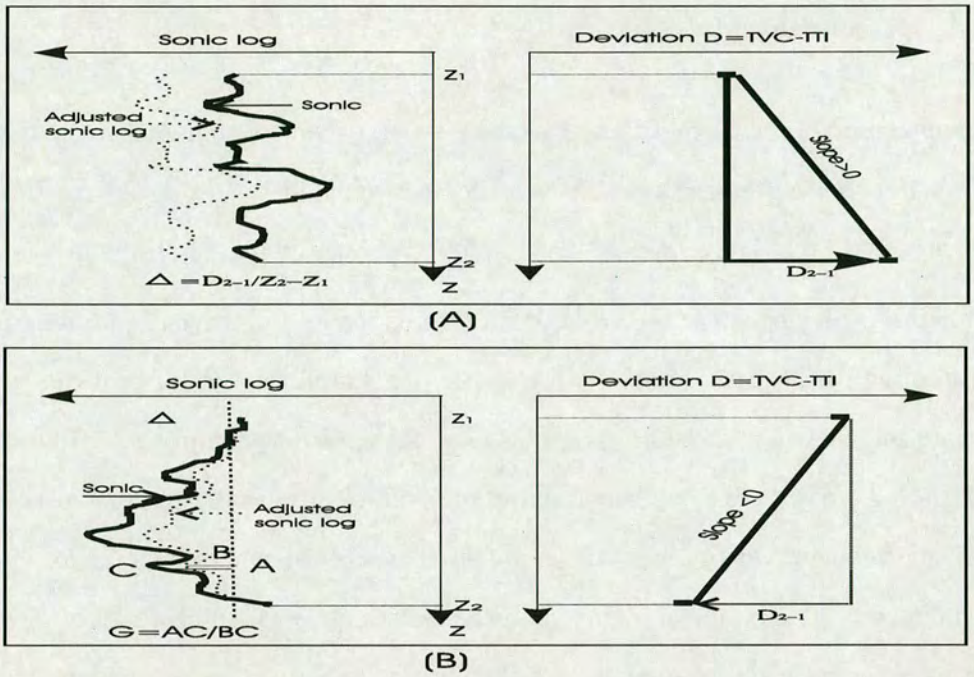

Figure 6.15: (A) Correction by the block shift method. (B) Δt correction by the minimum Δt method.

$$\Delta t_{cor} = G(\Delta t - \Delta t_{min}) + \Delta t_{min}\,, \tag{6.12}$$

where $G = 1 + (D_{2-1}/T)$ and $D_{2-1} < 0$

$$T = \int_{Z_1}^{Z_2} d\Delta t(z) dz\,, \tag{6.13}$$

where $d\Delta t = \Delta t - d\Delta t_{min} > 0$. The choice of Δt_{min} can identify zones in which there is no discrepancy between integrated time and the seismic velocity corrected time. It is well known that, in shales or poorly-cemented formations with high porosity, the sonic log tends to give high Δt. This method is utilized when there is a negative drift (negative D_{2-1} value) associated with a strong Δt.

6.6.4 Resolution matching

The comparison of the travel times of acoustic waves between two depth points obtained by two different methods (logs and seismic) can only be made if the conditions of propagation are relatively similar. Then an effective matching method is needed.

If depth of the log curve is converted into time, due to difference of sampling points, the sampling in the time domain will become the sampling of a different interval. To integrate log curve and seismic trace, we may obtain a new sampling of time domain from the log curve based on the sampling interval of the seismic trace. On the other hand, the frequency of the log data is higher than the seismic frequency, for example the sonic log is 20 kHz, much higher than the seismic wave (0-100 Hz). In other words, the wave frequency has an influence on the elastic characteristics of rock and the fluid they contain, so the differences in travel times between a high-frequency (sonic log) wave and a low-frequency (seismic) wave should be linked.

To match sonic log curves with seismic data so as to obtain the same resolution, an effective filtering technique may be used, which not only allows the log resolution to match that of the seismic wave, but also may keep their physical characteristics of reservoirs. The benefit is that it will choose the true values rather than the average values in data alignment, so that the different properties in different rock layers will be kept. The key is to choose a suitable filtering factor and sampling window length, so it can allow a high resolution log curve to match with a low frequency velocity, which can be expressed as:

$$d_1(z) = f(z) * d_h(z), \tag{6.14}$$

where $f(z)$ is the filtering factor which is decided by the response functions of the high resolution curve d_h and the low resolution curve d_1, and we have:

$$f(z) = F^{-1}\left(\frac{G_1(\omega)}{G_h(\omega)}\right). \tag{6.15}$$

Because, the frequency bandwidth of response function $G_h(\omega)$ is larger than $G_1(\omega)$, the value $\frac{G_1(\omega)}{G_h(\omega)}$ will not appear as a singular value within the frequency bandwidth of $G_1(\omega)$.

Strictly speaking, using equation (6.14) to carry out matching filtering, which may only achieve the same approximate resolution. In fact, d_1 in equation (6.14) is only d_{hf} of the same frequency. In order to match the numerical value of d_1 and d_{hf} within a certain interval, which can calculate the fitting coefficient using a last square criterion as α, β and γ, and obtain d_1 and d_e as:

$$d_e = \alpha + \beta d_{hf} + \gamma d_{hf}^2 \tag{6.16}$$

By using fitting coefficients α, β and γ, we may obtain a matching curve (d_e). This curve can reflect the characteristic of layer interface. Figure 6.16 shows a real example precessed for a sonic log curve.

Figure 6.17 shows the effect of different window lengths on the porosity curves, at 2, 5, 11, 18 metres respectively, and hence divide the log data into lithological units denoted B, C, D, E, F, G, H and I. From this result, I find that there are different responses with different window lengths, but all of them give consistent responses at the interface of layer between B/C, C/D, D/E,E/F and G/H. Figure 6.18 presents an example of log-seismic calibration. In the example, a zero-offset VSP data and sonic log are used. Both log velocity and seismic velocity have a satisfactory agreement after velocity matching.

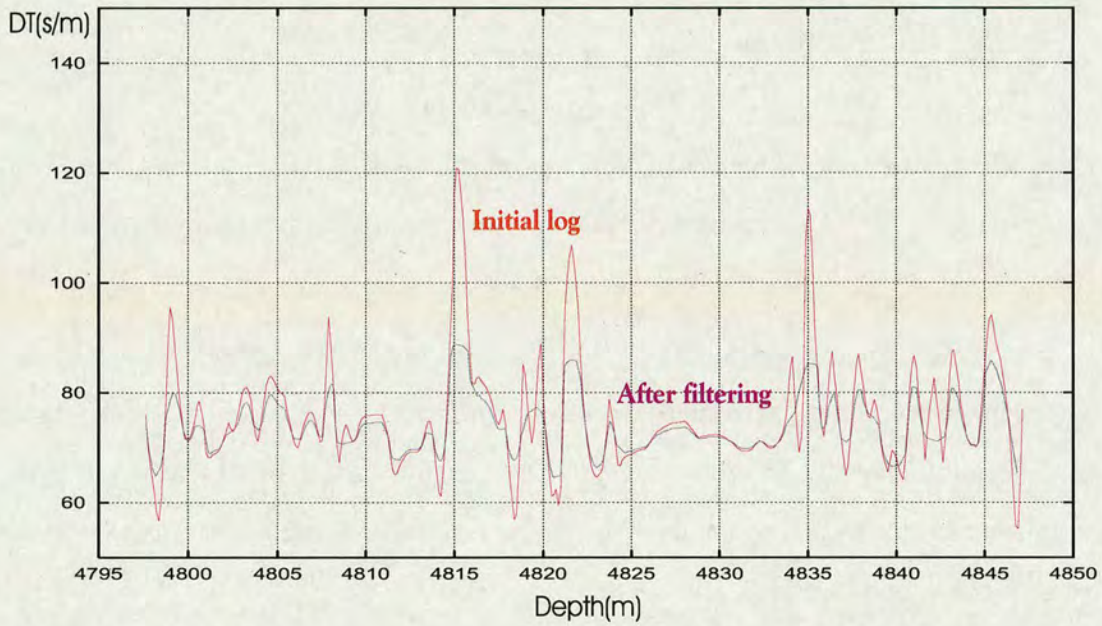

Figure 6.16: Comparison of an initial sonics log curve and its after filtering result. This result reflects the characteristic of layer interface.

6.7 Discussion and summary

Over the last decades, data (core, log and seismic) were often not integrated routinely within the exploration environment. There are a number of reasons, such as problems with the matching and calibration between different datasets, and the lack of understanding of core and log acquisition or the lack of confidence between logs and seismic data. These problems are often discussed as a preliminary step to the development of a strategy for improving data integration. Currently, enormous progress have been made in the understanding of the relationship between the physical properties of reservoir rocks, geological observations and geophysically measurements. For example, velocity versus porosity, Vp/Vs versus saturation and reservoir parameters versus lithology. Some of the key points have been the exploration of the effects of clay content, fluid

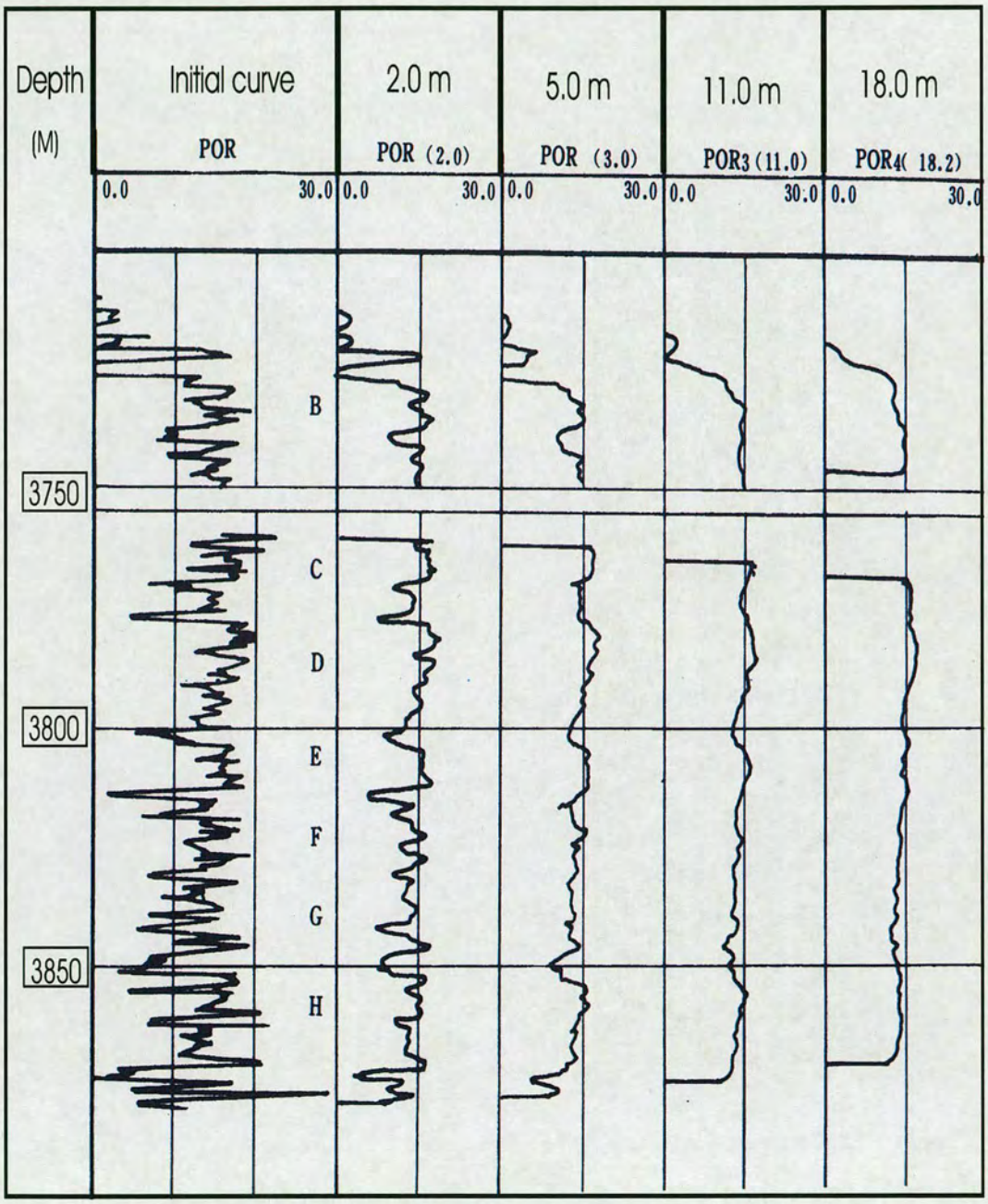

Figure 6.17: Comparison of different sampling window length for a porosity log, when choosing different window lengths, we can obtain the different responses from each layer interface.

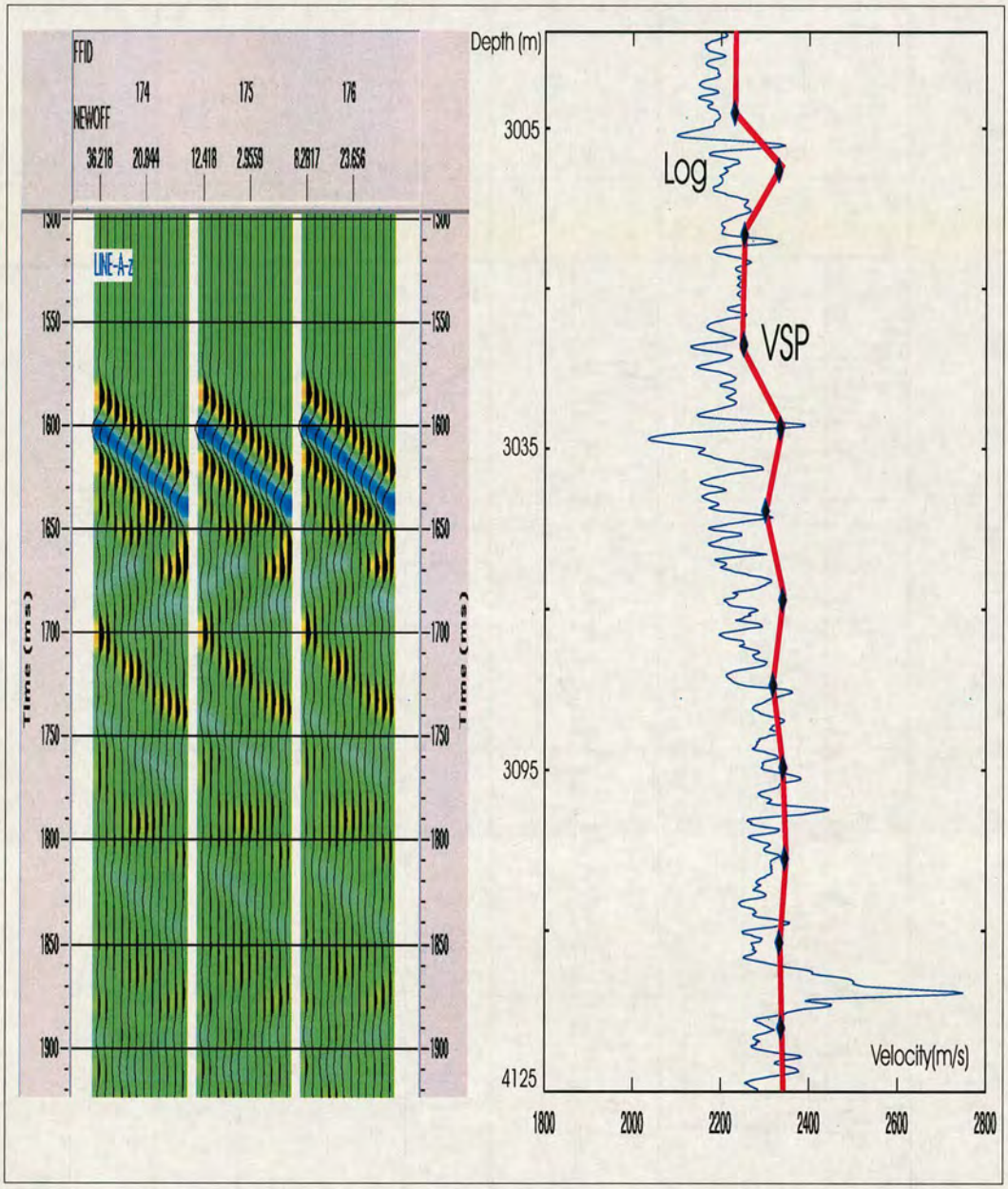

Figure 6.18: Zero-offset VSP for first break picking and velocity matching based on the real data from an oilfield in the North Sea. The left hand figure shows the real VSP data. Based on the way of first break picking, the VSP velocity can be obtained in the right hand figure. Using measured velocity from sonic log, a correction of VSP velocity and log velocity can be built.

type and saturation or pore pressure, and application of the advanced data integration technique in reservoir evaluation and description. The integration of disciplines actually means integration of all the aspects which constitute those disciplines. There is the aspect of integrating different pieces of work produced by different professionals, but also the aspect of integrating different geo-scientists belonging to different professional disciplines.

To obtain an accurate result, a number of physical factors for characterizing a core sample are required, such as irreducible fluid saturation, specific surface area, grain size distribution, grain shape, packing and layering, lithology and minerology, degree and type of cementing etc. The quality of core measurement is defined by the precision, accuracy and bias of the measurement (Murphy, 1969). A good quality measurement will be characterized by the precision and accuracy. Therefore we should keep in mind that correction is necessary for measured core data in order to obtain both an accurate and a precise result.

In this chapter I have discussed the key principles involved in data conditioning and interpretation. Based on the consideration of the measurement correction and process via velocities, there are three main factors for data calibration, they are:

a. Lithology factors such as the percentage of sand-clay mixture, lithology type and grain components.

b. Physical characteristic factors such as porosity, permeability and fluid pressure.

c. Fluid factors such as the oil, gas and fluid saturation or density.

Therefore, a series of suitable calibration approaches has been developed in this chapter, because the calibration of core, log and seismic data represents one of the many attempts to utilize geological data obtained by different measurements and at different scales. This use of data from different observations which are inter-related through their inherent properties or physical basis such as laboratory analysis, veloc-

ities or reservoir parameters, will involve the calibration of one dataset through some equalization procedure, in which one dataset is assumed to be corrected.

After correction of these effects mentioned above, the different datasets can then be calibrated using small scale core data, log data and large scale seismic data. The calibration through reconciliation of different measurements towards an optimized solution should yield the best interpretation.

Chapter 7

INTEGRATED CASE STUDY USING FIELD DATA FROM THE NORTH SEA

7.1 Introduction

An integrated reservoir study is by definition a complex process, which results from the integration of different disciplines and which has a definite objective. In this chapter, some of those aspects which are critical to such an integration process will be presented. Most of these aspects require a change of focus with respect to the traditional way of working. The conventional approach has been a sequential-type one, where geophysicists, reservoir geologists, petrophysicists and reservoir engineers work almost independently, and the results of each one are passed to the other without significant feedback. The process of integrating different disciplines to perform an integrated reservoir study requires a significant change. The new approach becomes multidisciplinary and the professionals work in an interacted way, where the feedback from other disciplines is fundamental to the validation of the work that is being performed. This process is illustrated in Figure 7.1.

The oil field studied here was initially discovered in 1970, when development started in 1978 with the installation of two platforms, Reservoir I and Reservoir II. First pro-

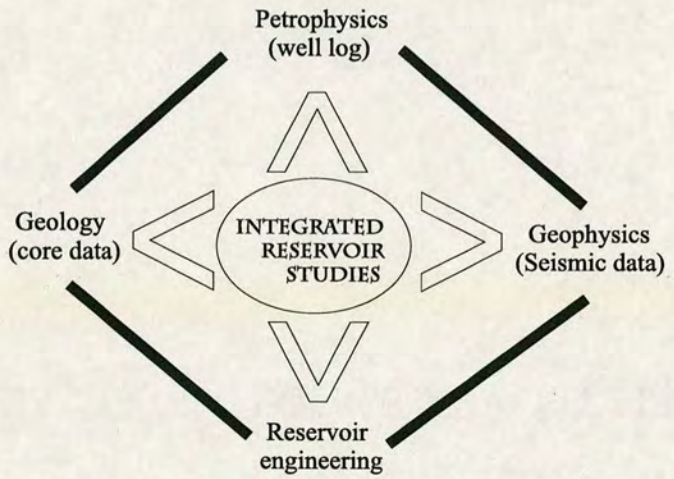

Figure 7.1: The links in the reservoir study based on integrated approach. It gives a simple relationship between different disciplines from geophysics, reservoir geology petrophysics and reservoir engineering.

duction came from the Reservoir I platform in 1979 with the Reservoir II platform joining production in 1980. The most productive reservoirs in this field has good porosity and extremely high live oil saturation. The porosities can be as high as 35% in some areas, however the permeability can be as low as 1 mD, because particles making up the matrix are very small and so both pores and pore throat sizes are also small. The datasets for this study contained the follows from the Reservoir I and Reservoir II:

- The reservoir structure maps.
- Petrophysical well logs data in digital format (LAS).
- Conversion data in deviated wells from MD to TVD.
- Formation water salinity data.
- Digital core data were supplied for a limited number of wells.
- DST, RFT and water (oil) testing data.
- Three components walkaway VSP data.

- Geological report from the operator.

In this chapter, I well apply the methods developed in the previous chapters to predict reservoir parameters and rock properties, and then I will make further reservoir evaluation and description based on the supplied data.

7.2 Background

The geological study carried out as part of the North Sea reservoir characterization effort consists of several integrated tasks. The main objective has been to ensure a robust description of the reservoir, with respect to both the structural framework and reservoir parameters. A study to provide data on the location of potential vertical barriers to flow was performed using all available log and test data. As production characteristics of this reservoir are closely related to litho-facies, and trend in litho-facies may indicate productivity, it was decided to use facies data to model the interior of the field, and extend the model to un-drilled flanks of the field. Litho-facies type described from core were translated into petrofacies using a combination of processing log curves.

Since the discovery of this oil field in 1978, numerous people have made lithological correlations as new wells have been drilled and logged. Because of the relative scarcity of easily recognized stratigraphic markers in the reservoir section, correlation of the various layers in the reservoir has been very difficult. In addition different criteria have been used by different people to make the correlation picks, and the end result has been a proliferation of inconsistencies in the top layer. The datasets provided contain VSP, log data and core measurements as shown in Figure 7.2.

One problem in attempting to correlate layer picks for this reservoir is the lack of easily recognizable horizons. I used the variations in clay content, expressed as events on a gamma-ray log as stratigraphic markers. Porosity and resistivity variations are also

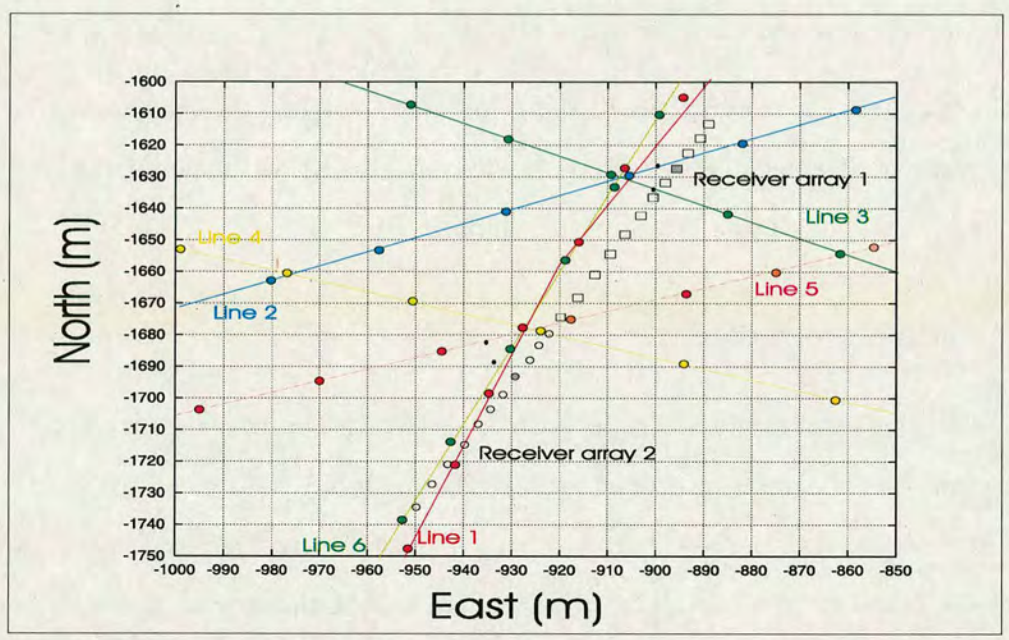

Figure 7.2: The location of the oil field in the North Sea. The datasets provided contain VSP, log data and core measurements.

commonly used to determine the positions of marker horizons in the well-bores. The generally low clay content, consistently high porosity, and high oil saturation reduced the variation in common well logs, and therefore, the number of correlation points are much reduced. Based on the geological interpretation, I adopted the following procedure for layer correlation.

- Linear modelling of well log response was used to generate a set of volume curves for each common mineral. The silica curve proved the most valuable in layer correlation.

- All layers were reinterpreted at all wells, resulting in a significant improvement in the consistency and confidence in interpreted layer tops.

7.3 Datasets

7.3.1 Core measurements

In addition to log data from wells and seismic data, the current study also used several types of data gained from the analysis of core in order to examine the validity of my methods. Although the amount of core samples recovered is relatively small, compared to the size of the field, the data from these cores is irreplaceable for constructing accurate models. The following is a discussion of the types of data from core measurements used in my study.

- **XRD analysis:** X-ray diffraction analysis of core mineralogy is the basis for the calculation of mineral content such as shale volume and clay content of the reservoir using log data.

- **Porosity measurements:** The study is able to build a database of porosity measurements from core plugs in key wells. This data is depth-shifted to match log curves. The porosity measurements from the cores are used to fine-tune the porosity calculation from the density, sonic, and neutron logs.

- **Permeability analysis:** The core permeability measurements are used to model the matrix and effective permeability using log data. The core permeability measurements are possibly the most important pieces of hard data available, at least from the standpoint of building an accurate geologic model and a reliable production simulation.

- **Litho-facies description**: Detailed core litho-facies description for the key wells are available for use in this study. For the most part, these descriptions are the results of work performed during this project. Therefore, the core litho-facies descriptions provided the basis for much of the petrofacies determinations.

Figures 7.3 and 7.4 are examples for core application in the key wells. They show the depth interval of coring, and general core porosity, core shale and core permeability.

7.3.2 Well-log data

The available well-log data include deep and medium-induction, spherically-focused log, porosity bulk density, interval transit time, gamma-ray logs, caliper and spontaneous potential log. Figures 7.5 shows a suite of raw well-logs curves with lithology description in sand-clay mixture.

It is important to apply quality control to edit and reconstruct the well-log curves for logs which exhibit anomalies, and therefore possibly incorrect responses. Logging instrument responses are adversely affected by breakout of wall-rock during drilling and stick-and-pull as logging tools are winched up the well. Based on log invasion experiment, the deep induction log records the formation true resistivity (Rt) when logged within three days after drilling. After three days, the oil layer resistivity of the deep induction log will gradually decreased, after up to 20 days this reduction may diminish to 25 per cent of the original value.

Because of measured errors in the field data, we would probably obtain different log readings from the same formation or the same rock in the same area. In this case, I define a standard formation (for example, a shale formation) to compare with the values of the same log data in the same formation or rock, and use the normalization method to correct log readings (described in Section 6.5.2 of Chapter 6)

There are a number of errors in the formation layering using log curves. One main reason is that different operators use different methods, and have different knowledge and data processing experience. To reduce error in this study I suggest here to use an automatic layering method based on curve extremal to divide layers and formations, and obtain automatically determined readings. To use automatic layering blocking,

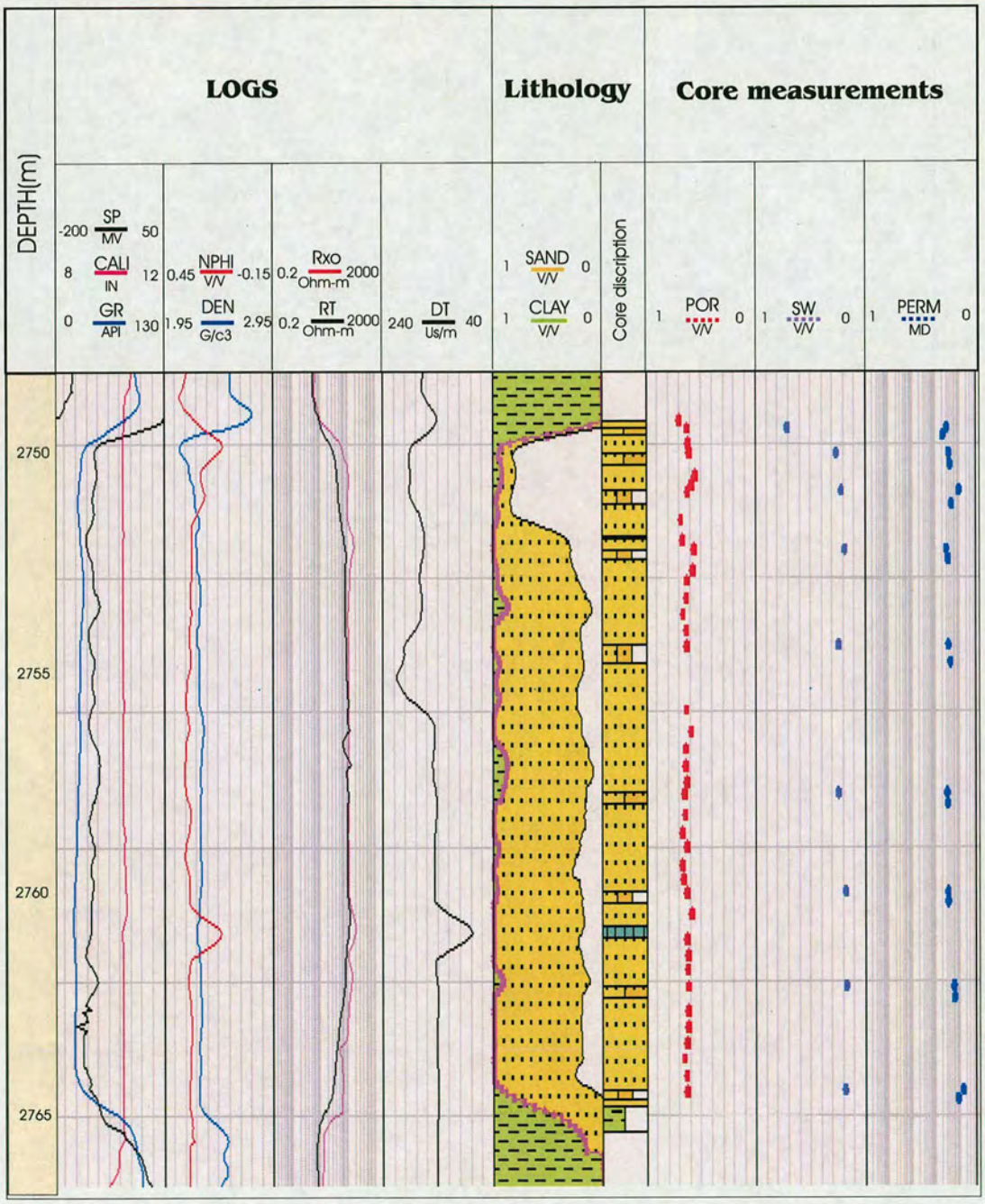

Figure 7.3: The example of core application in the key well A. This figure shows the depth interval of reservoir of well log data and lithology, and also shows core description (panel 6), core porosity (panel 7), core water saturation (panel 8) and core permeability (last panel).

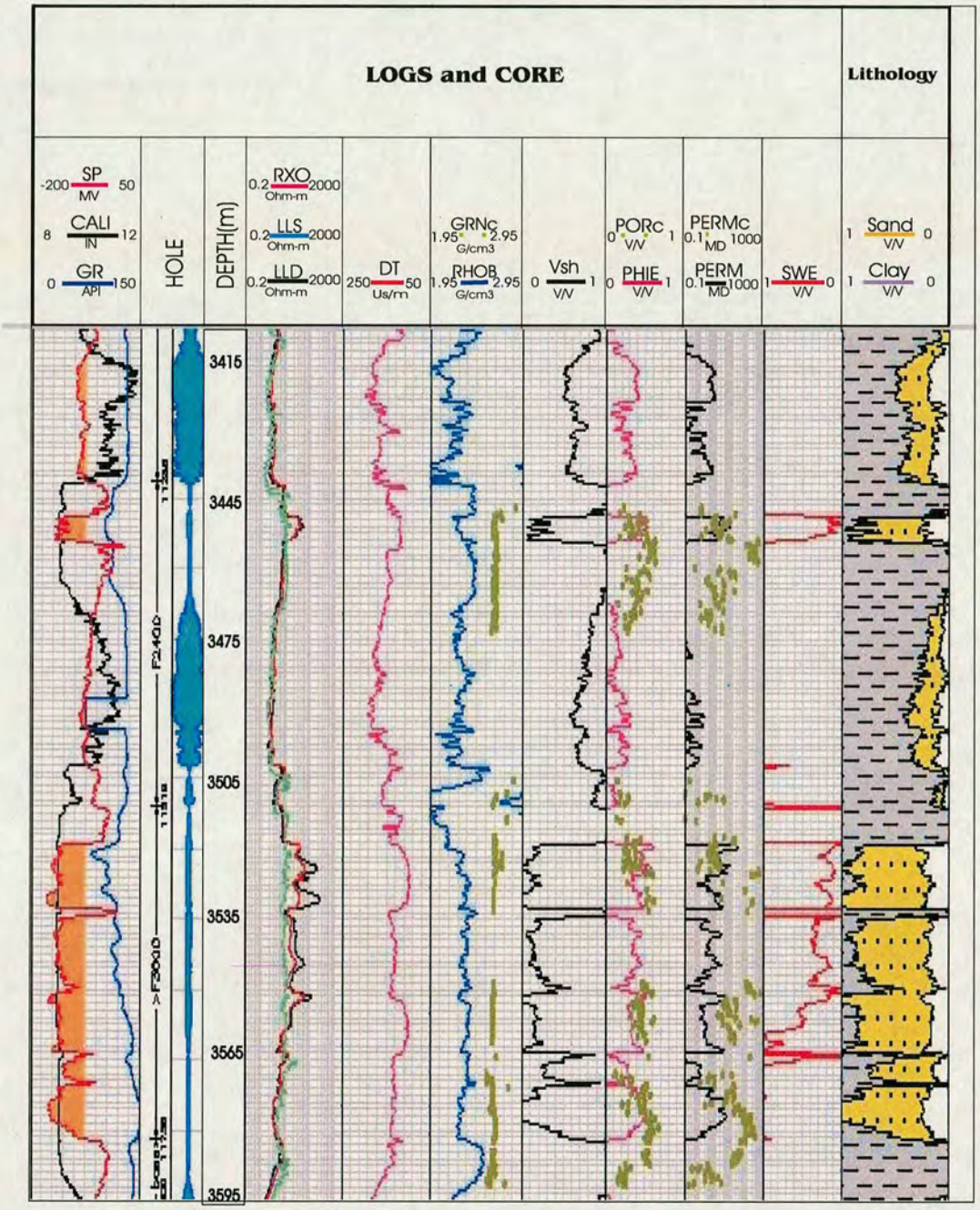

Figure 7.4: The example of core application in the key well B. This figure show derived logs and core analysis in main reservoir intervals. The comparison of core analysis results and predicted logs such as porosity (Panel 6) and permeability (Panel 7) are shown.

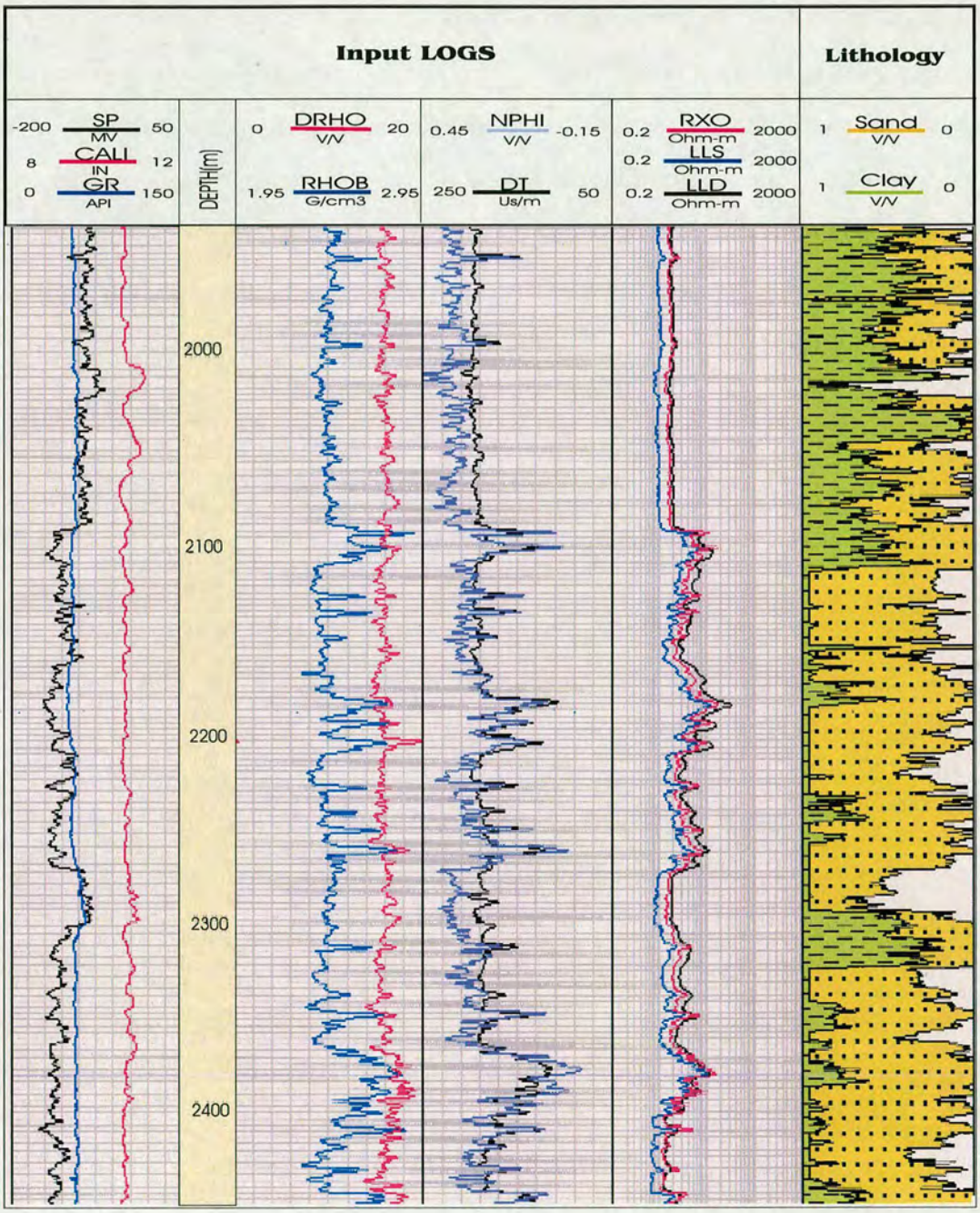

Figure 7.5: Original well-logs with lithology description in sand-clay mixture in the North Sea. The original input well-logs may be divided into three parts, i.e. (1) lithology logs (gamma-ray, caliper and spontaneous potential log in Panel 1), (2) porosity logs (density, neutron and sonics log in Panel 2 and Panel 3) and (3) fluid type logs (deep-induction, medium-induction and spherically-focused log in Panel 4).

firstly, a high resolution curve should be chosen as main layering curve, and then another curve possessing different physical characteristic and high resolution should be chosen as layering curve to assist in correcting the main layering curve. Because of this improvement, I can classify different log curves based on curve extremal variation to classify them into a set of groups; these groups should reflect the curve variation and they can represent lithological variation, which may be recognized as different curve elements through comparison of the elements of similar type and formation character. The pressures of automatic layering blocking are as follows;

- Self potential log (SP) or Gamma-ray log (GR) are chosen as main layering curve for large thickness formations of sand and clay mixture.

- Density log (DEN) or Micro-Spherically Focused Log ($MSFL$) is used to determine the top or bottom surface as assistant layering curve in permeable formations containing oil and gas.

- A suitable weight coefficient is assigned to the main layering curve in unusual thin formations to avoid layering confusion.

Figure 7.6 shows a layering result for Resistivity log and Gamma-ray log in real data, and we can see that the full formation is divided into different blocks, and log curves during the same depth also obtain respective readings, the results of automatic classification are shown in Table (7.1).

7.3.3 VSP data

The primary objective here is to provide a velocity model to link seismic results with well-log data. The well data utilized in geophysical interpretation completed in this study are sonic, density, velocity, shale volume, water saturation and effective porosity

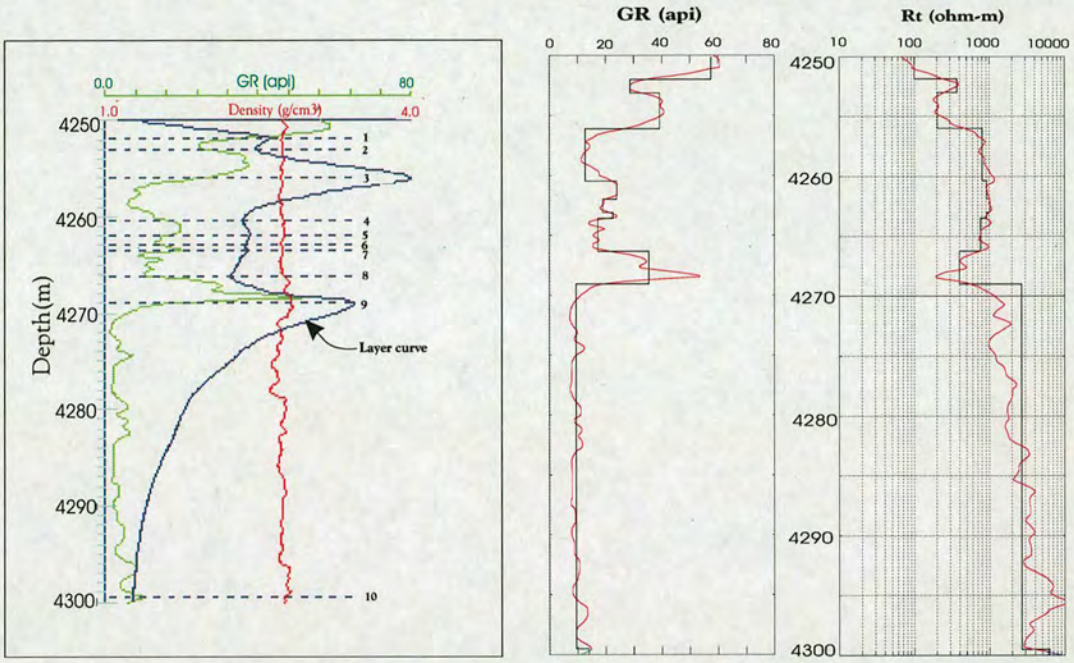

Figure 7.6: (left) Formation layering using extremal curves from *GR* and *DEN* curves. We can obtain layering results, which are shown by 10 small layers. (right) Layering blocks for two log curves, Gamma-Ray (*GR*) and Resistivity (*Rt*) log curves.

NO	DEPt	DEPb	Hd(M)	CAL	GR	DT	CNL	DEN	RLLD	RLLS
1	4250.000	4251.875	1.875	5.957	59.083	53.902	6.676	2.765	98.82	85.73
2	4251.875	4253.000	1.125	6.00	29.173	49.64	3.046	2.735	369.79	251.96
3	4253.000	4256.000	3.000	6.011	40.004	51.666	3.944	2.735	203.36	146.24
4	4256.000	4260.375	4.375	6.027	12.608	48.386	1.048	2.710	795.62	461.75
5	4260.375	4261.875	1.500	6.101	24.129	49.017	1.940	2.749	918.21	477.42
6	4261.875	4263.000	1.125	6.100	18.957	48.612	2.027	2.733	1016.55	480.67
7	4263.000	4263.500	0.500	6.100	22.714	48.215	1.953	2.729	916.56	398.67
8	4263.500	4266.250	2.750	6.068	17.237	48.751	1.401	2.715	755.42	360.66
9	4266.250	4269.000	2.750	6.07	35.992	50.498	2.88	2.771	397.22	217.40
10	4269.000	4299.500	30.50	6.233	9.25	48.250	1.385	2.733	2651.37	402.44
11	4299.50	4300.000	0.500	6.550	13.82	47.273	1.776	2.757	6212.49	1648.32

Table 7.1: The results of formation layering from well-log curves.

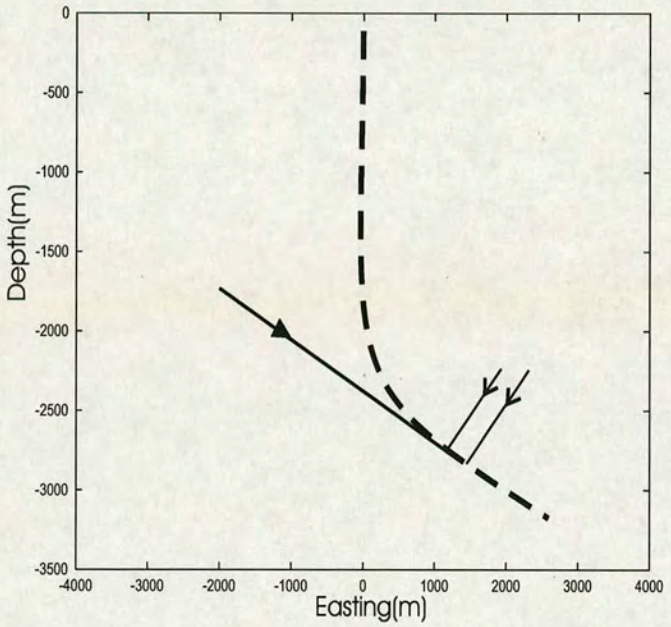

Figure 7.7: Vertical section showing well trajectory and the tool orientation. The seismic lines are oriented at 36^o angles with respect to one another, and intersect directly above the receiver array with its horizontal projection has an azimuth of 21^o with respect to the first line.

logs. These logs are used to generate synthetic seismograms in support of interpretation of seismic data for petrophysical inversion. A description of the data and the conditioning technique in these processes has already been presented in Chapter 6.

The VSP data consist of a three components zero-offset walkway VSP lines shot in a production well in the North Sea. In the deviated well, the twelve-receiver tools are placed at a depth with of an inclination of 57^o (Figure 7.7). Figure 7.8 shows the common receiver gather of the three top-level components for the first line.

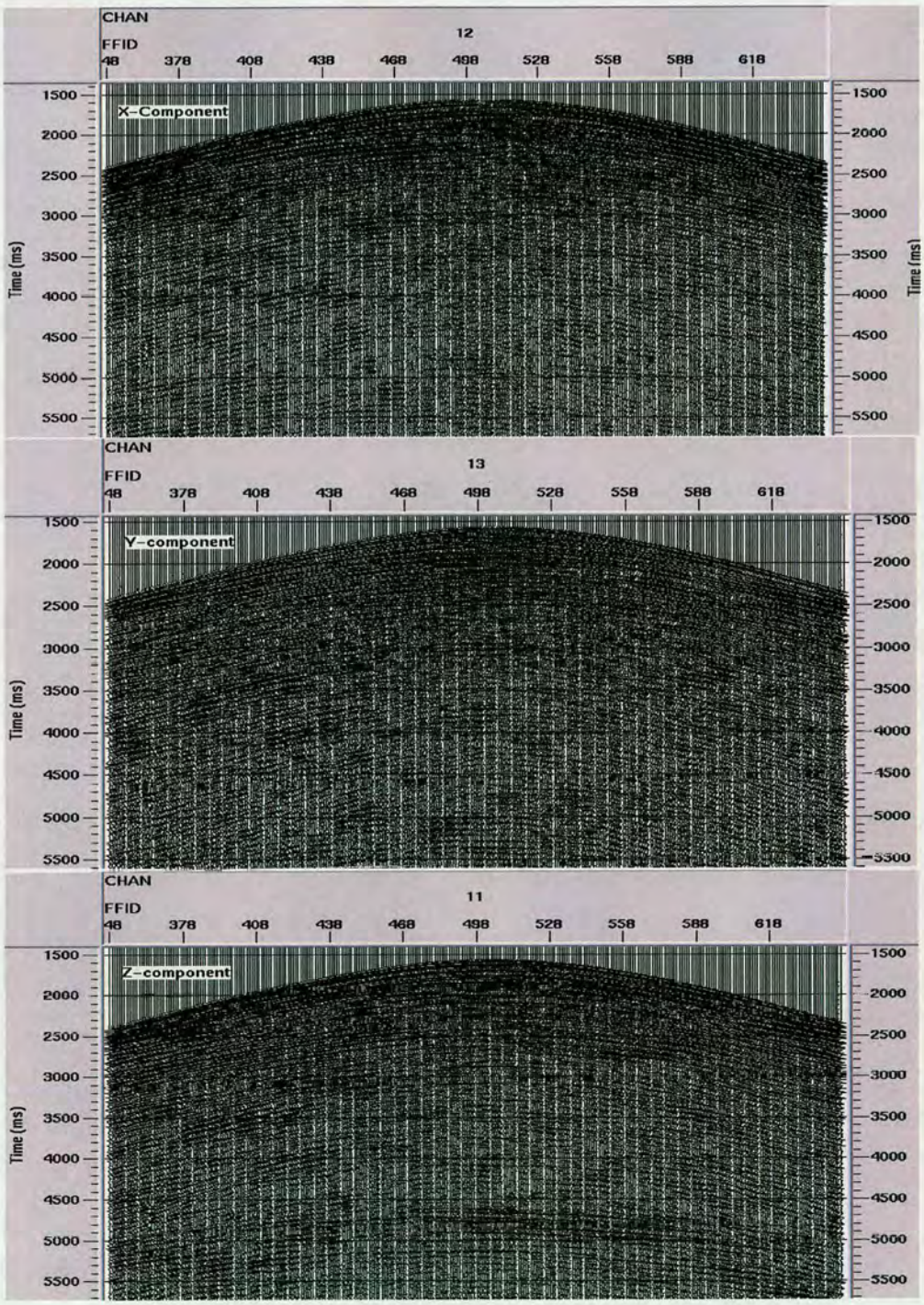

Figure 7.8: Common receiver gathers of the three top-level components for first line (from top downwards: horizontal component X, horizontal component Y and vertical component, there are 12 geophones, 330 shot points).

7.4 Data analysis

7.4.1 Velocity picking and prediction

The first break picking is used to determine the start time of down going wave for the recorded trace for each depth in the zero-offset VSP. The values of picking is used to build the correlation between time and depth, in turn to calculate the interval velocity, and then the interval velocity is used to calibrate a log curve such as sonic velocity log or density log. Figure 7.9 shows the zero-offset VSP of first break picking,

Table 7.2 shows the result of first break picking. Twelve-receiver tools are placed at depths between 2998.3m and 3087.7m, and the velocity varies between 1892 m/s and 2311 m/s. Figure 7.10 shows a comparison between predicted and measured velocities, and the results of ADP model developed in Chapter 5, The results prove to be an independent estimation of predicted velocities and lithology and he velocity ratios also are predicted. Table 7.3 is an example of rock properties using the project dataset.

Figure 7.11 shows a comparison of predicted and observed compressional wave velocities. Figure 7.12 shows a comparison of different models for predicting reservoir porosities. They consist of the traditional time-average equation, dual-porosity model (Chapter 4) and core measurements.

7.4.2 Anisotropic coefficient

From elastic moduli we can also predict shear-wave velocity, and the anisotropy coefficient in turn to build the velocity relationship of shear-waves in the horizontal and plane directions combined with the dipole sonic log (see Figure 7.13). An anisotropy coefficient (m) is determined using equation (7.1) based on Figure 7.13, (right), and have:

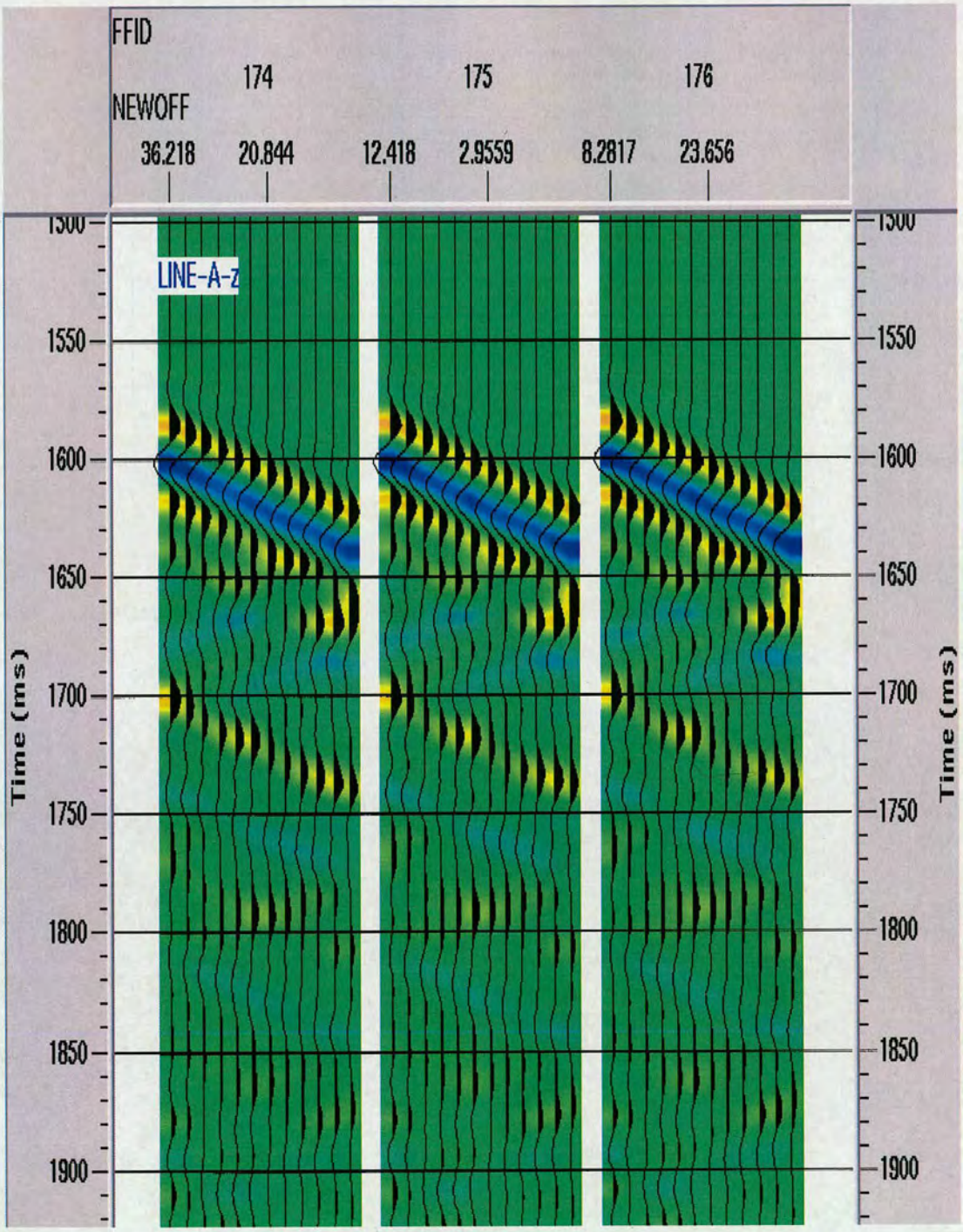

Figure 7.9: Zero-offset VSP with 12 geophones for first break picking. The offset distance is given by 2.956m, 20.844m and 23.656m separately, and twelve-receiver tools are placed at an appropriate depth between 2998.3m and 3087.7m.

Geophone	Depth (m)	Amplitude	velocity (m/s)	FFID
1	2998.3	0.507	1892	175
2	3006.5	0.607	2334	175
3	3014.6	0.61	2334	175
4	3022.8	0.59	2200	175
5	3030.8	0.63	2337	175
6	3039.1	0.55	2302	175
7	3047.3	0.611	2340	175
8	3055.4	0.513	2314	175
9	3063.5	0.71	2320	175
10	3071.5	0.48	2303	175
11	3079.6	0.59	2294	175
12	3087.7	0.797	2311	175

Table 7.2: Velocities obtained from first break picking from Zero-offset VSP, data from The North Sea (Line-A)

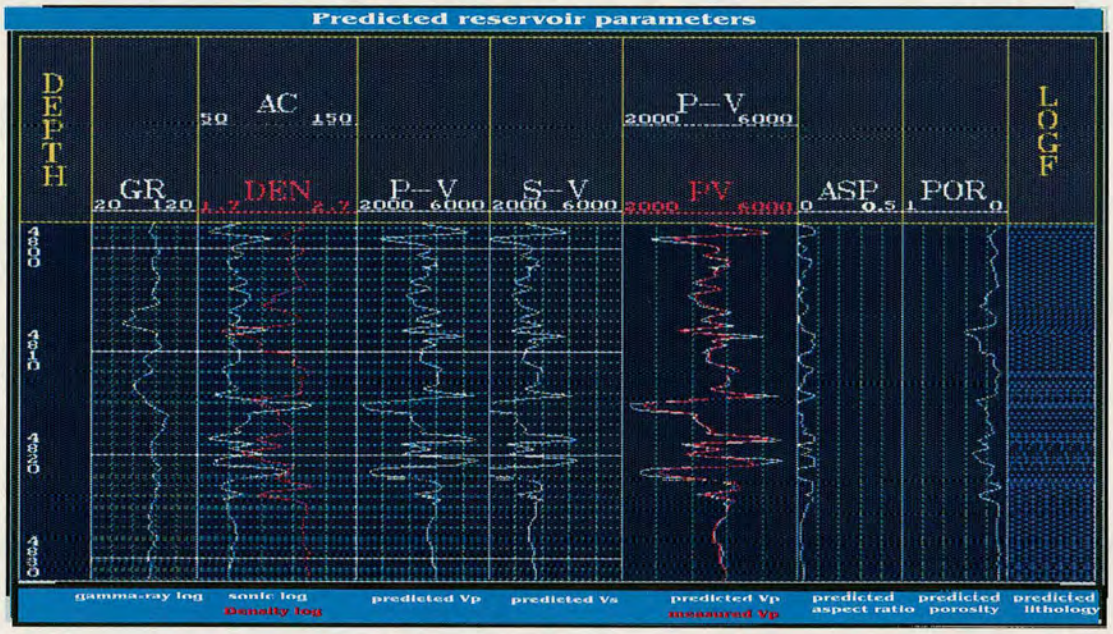

Figure 7.10: Predicted P-wave velocity (P-V) and S-wave velocity (S-V). The Panel 5 shows the comparison of measured velocity (PV) with predicted velocity (P-V).

Depth	Vp	1/Vp	Vp/Vs	Vs	1/Vs	Bulk Modulus	Shear Modulus
(ft)	(ft/s))	(/ft)	(ratio)	(ft/s)	(s/ft)	(GPa)	(Gpa)
12160.0	10430	95.88	1.81	5752	173.84	10.04597849	5.13950
12160.2	11788	84.83	1.97	5969	167.52	14.20610312	5.53460
12160.4	11334	88.23	1.77	6398	156.29	11.47657579	6.35875
12160.6	12280	81.44	2.33	5263	189.99	17.68797301	4.30278
12160.8	11988	83.42	2.33	5149	194.21	16.83303875	4.11840
12161.0	11120	89.93	2.03	5465	182.97	13.02258352	4.63941
12161.2	10715	93.33	1.95	5486	182.27	11.60125313	6.75140
12161.4	12070	82.85	1.95	6203	161.20	14.66129483	5.97704
12161.6	11444	87.38	1.90	6020	166.12	12.83801445	5.62958
12161.8	11632	85.97	1.99	5847	171.03	13.93713950	5.31067
12162.0	10780	92.76	1.91	5638	177.35	11.46808195	4.93779
12162.2	10846	92.20	2.49	4347	230.02	14.35970887	2.93536
12162.4	11015	90.78	1.88	5871	170.33	11.70829401	5.35435
12162.6	12366	80.87	2.05	6045	165.42	16.18569296	5.67643
12162.8	12322	81.15	2.00	6150	162.61	15.75173955	5.87534
12163.0	11297	88.52	1.54	7319	136.63	18.72988206	8.32121
12163.2	12409	80.59	1.99	6231	160.50	15.87825611	6.03113
12163.4	9303	107.4	1.96	4754	210.36	8.763008270	3.51076
12163.6	10308	97.01	1.67	6176	161.91	8.605459360	5.92512
12163.8	9686	103.24	2.01	4818	207.55	9.765879660	3.60592
12164.0	12676	78.89	2.04	6203	161.20	6.990785280	5.97704
12164.2	10399	96.16	1.95	5322	187.89	10.93194352	4.39980
12164.4	12453	80.30	2.05	6071	164.71	16.45586522	5.72537
12164.6	12586	79.45	2.06	6097	164.01	16.90765035	5.77451
12164.8	12280	81.44	2.05	5994	166.82	15.98361050	5.58106
12165.0	12111	82.57	2.01	6020	166.12	15.27858993	5.62958
12165.2	12586	79.45	2.05	6150	162.69	16.77321065	5.87534
12165.4	12676	78.89	2.07	6123	163.31	17.19502211	5.82387
12165.6	12861	77.76	1.87	6894	145.05	15.85022390	7.38288
12165.8	12497	80.02	1.97	6341	157.69	15.93228882	6.24595
12166.0	12029	83.14	2.03	5920	168.93	15.21839873	5.44410
12166.2	11155	89.65	1.98	5638	177.35	12.74585054	4.93779
12166.4	11748	85.12	2.05	5729	174.54	14.64135323	5.09848
12166.6	11788	84.83	2.05	5752	173.84	14.73290381	5.13950
12166.8	11988	83.42	2.06	5823	171.74	15.30136022	5.26716
12167.0	10338	96.73	2.09	4935	202.63	11.55759924	3.78318
12167.2	11947	83.70	2.11	5661	176.65	15.53424725	4.97816
12167.4	11947	83.70	2.11	5661	176.65	15.53424725	4.97816
12167.6	11866	84.28	1.86	6368	157.03	13.47316701	6.29925
12167.8	11786	84.85	2.10	5615	178.08	15.04812338	4.89759
12168.0	11746	85.13	2.07	5685	175.91	14.73807307	5.02046
12168.4	11591	86.28	1.98	5854	170.82	13.77226904	5.32339
12168.6	10511	95.14	2.01	5232	191.15	11.49247233	4.25224
12168.8	11477	87.13	1.76	6519	153.40	11.65957111	6.60154
12169.2	9723	102.85	2.15	4512	221.63	10.46875775	3.16243
12169.4	10837	92.28	1.82	5955	167.92	10.89832521	5.50867
12169.6	10205	98.00	2.02	5059	197.68	10.8765017	3.97569
12169.8	10938	91.42	2.09	5232	191.15	12.91518836	4.25224
12170.0	10205	98.00	2.02	5059	197.68	10.8765017	3.97569
12170.2	10000	100.00	2.19	4572	218.73	11.20453361	3.24710
12170.4	10000	100.00	2.06	4862	205.66	10.63788243	3.67208
12170.6	9944	100.5 0	2.41	4133	241.96	11.82254781	2.65346
12170.8	10116	98.85	2.07	4897	204.21	10.92961656	3.72514

Table 7.3: An example of prediction of rock properties in the North Sea.

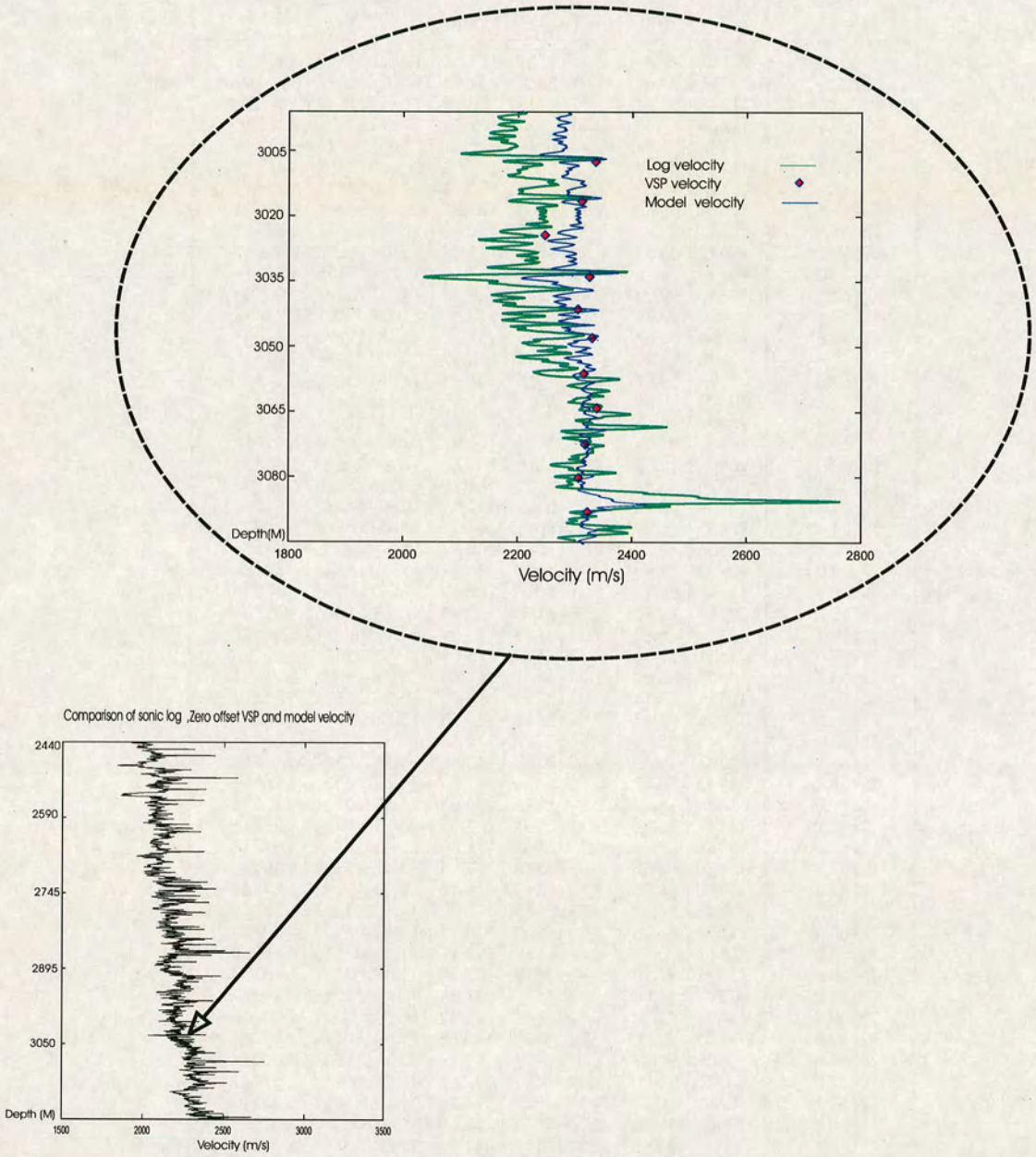

Figure 7.11: Three velocities comparison from measured velocity by log, first picking velocity by zero-offset VSP and predicted velocity by ADP model. This result also shows that the predicted velocity has a good agreement with the log measured velocity.

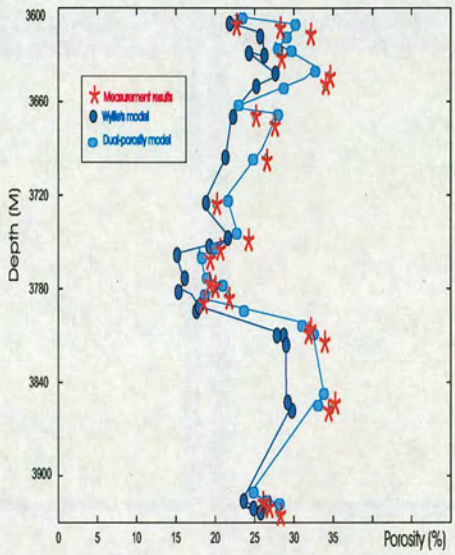

Figure 7.12: Comparison of between predicted porosity using the time-average model (blue curve), the isotropy dual porosity model (green curve) and core measurements (red curve). Three curves show a similar variation.

$$m = \frac{V_{s||} - \sqrt{2198 + 0.954V_{s||}^2}}{\overline{V_s}} \tag{7.1}$$

where $V_{s||}$ and $V_{s\perp}$ are the shear-wave velocities in the horizontal and plane directions, $\overline{V_s}$ is the average shear-wave velocity.

Using the equation (7.1), an anisotropic coefficient based on S-wave velocities can be predicted. This output may be called anisotropic detecting coefficient, which can be used to determine the presence of anisotropy in rocks. Figure 7.13 shows a real example for anisotropy detection.

If the solid grains and rock parameters are given as

λ_m= 39 GPa, μ_m=39 GPa, density ρ=2.70 g/cm^3 and K_f=2.25 GPa.

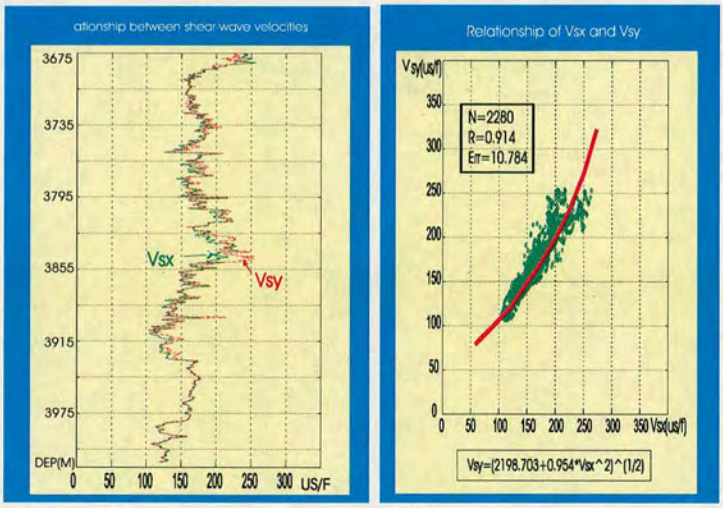

Figure 7.13: (left) Comparison of shear-wave velocities in the horizontal and plane direction. (right) The correlation of the horizontal shear-wave velocity and the plane shear-wave velocity, which shows a nonlinear relationship.

Using the ADP model in Section 5.2.2, Chapter 5, the Thomsen's anisotropy coefficients for the whole depth can be calculated. Therefore, the elastic stiffness ($C_{ijlk}^{(dry)}$) are obtained, and they can be used to determine the elastic constants for the dry rock frame. Using Brown and Korringa's (1975) relations for the fluid substitution problem in anisotropic rock, assuming the porosity (ϕ) to be 8%, and fluid density to be 1.05 g/cm^3, therefore we can obtain the elastic stiffness ($C_{ijlk}^{(sat)}$) in saturated rocks.

7.4.3 Synthetic seismograms

The models proposed in Chapters 4 and 5 are used to compute elastic moduli (K_d and μ_d, K_m and μ_m, K_f and μ_f), and P-wave and S-wave velocities are then predicted by the theoretical models (refer to Chapters 4 and 5). Based on the results obtained in previous chapters, such as prediction of elastic contents, aspect-ratios and anisotropy coefficients etc., the synthetic seismograms may be obtained by the use of the seismic software (ANALYSIS). Figure 7.14 is an example of synthetic seismograms, and shows a result with varying orientation.

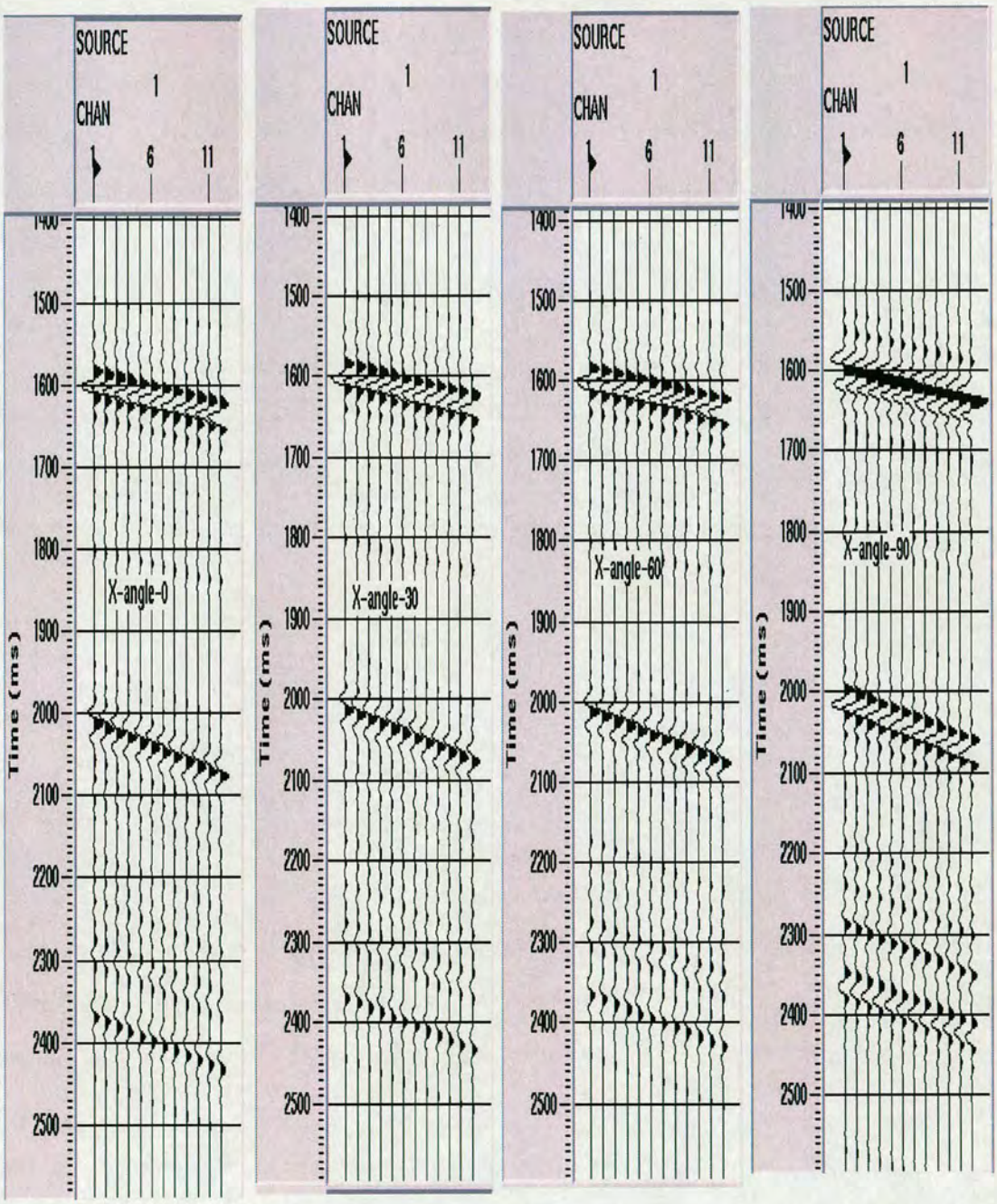

Figure 7.14: Synthetic seismograms using the modelling results of ADP model with the angle variations. The data from North Sea, the modelling software using ANISEIS (Panel 1: angle = 0 degree; Panel 2: angle = 30 degree; Panel 3: angle = 60 degree and Panel 4 = 90 degree, respectively).

7.5 Reservoir parameters

Reservoir complexity is typically related to spatial heterogeneity in porosity, permeability, clay content, and fluid saturation. The complexity of reservoir recovery processes is a direct consequence of this heterogeneity. The core and log data correction is described in Sections 6.2 and 6.3 of Chapter 6. The estimation of reservoir parameters based on the data from the North Sea may be described below:

- **Porosity:** The correlations of core porosity from density log and core porosity from sonic velocity log are built from core samples and logs for the zone in this study from the North Sea. The porosity correlation are derived from Figures 7.15. The density-porosity is estimated from correlation (7.2), and the sonic-porosity from correlation(7.3) as:

$$\phi = -65.359\rho + 174.85, \tag{7.2}$$

(N=79, R=0.934, Err=1.25)

$$\phi = 0.8532DT - 45.242. \tag{7.3}$$

(N=74, R=0.933, Err=1.25)

where ϕ is the total effective porosity from core analysis, ρ is the density log, and m and a are both lithological coefficients to be determined by least squares regression , and N is the number of samples, R is correlation coefficient, and Err is the root-mean-square error.

Figure 7.16 shows the porosity error comparison using cross-plot analysis. The X-axis represents the porosity measured from core samples with variation of 15 to 35%. The Y-axis represents the calculated (predicted) porosity using the model given above. As we can see from Figure 7.16, the predicted porosity is very close to the 45^o line, which shows that the calculated error is small to compare with the measurements.

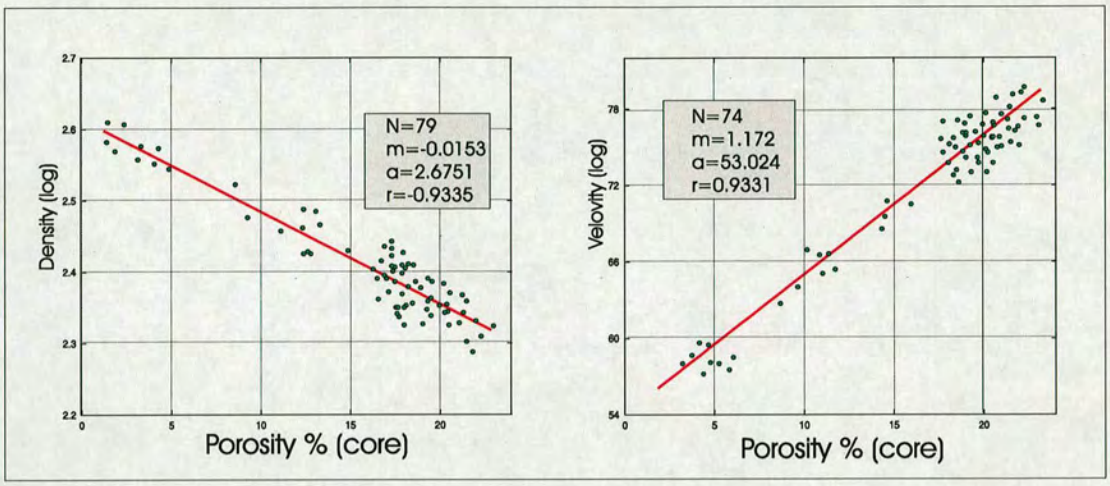

Figure 7.15: (left) The relationship of core porosity versus density log, and (right) the core porosity versus sonic log (data from the North Sea).

Generally, the porosity error from the time-average model is larger than IDP model, because the principal error distribution of porosity ranges from 2 to 6% in the time-average equation, its error peak value is 34.6 at 5%. However, using IDP model, the main error range of porosity is between 1 and 3%, and its error peak value is 57.7 at 2%.

- **Shale volume and clay content:** Figure 7.17 shows relationship derived by measurement and log (gamma-ray). Thus, the shale volume can be determined from equation (7.4) using real data from the North Sea:

$$V_{sh} = 10^{1.245*\Delta GR+0.6902}, \tag{7.4}$$

(N=79, R=0.870, Err=1.43)

and, clay content from equation (7.5) as:

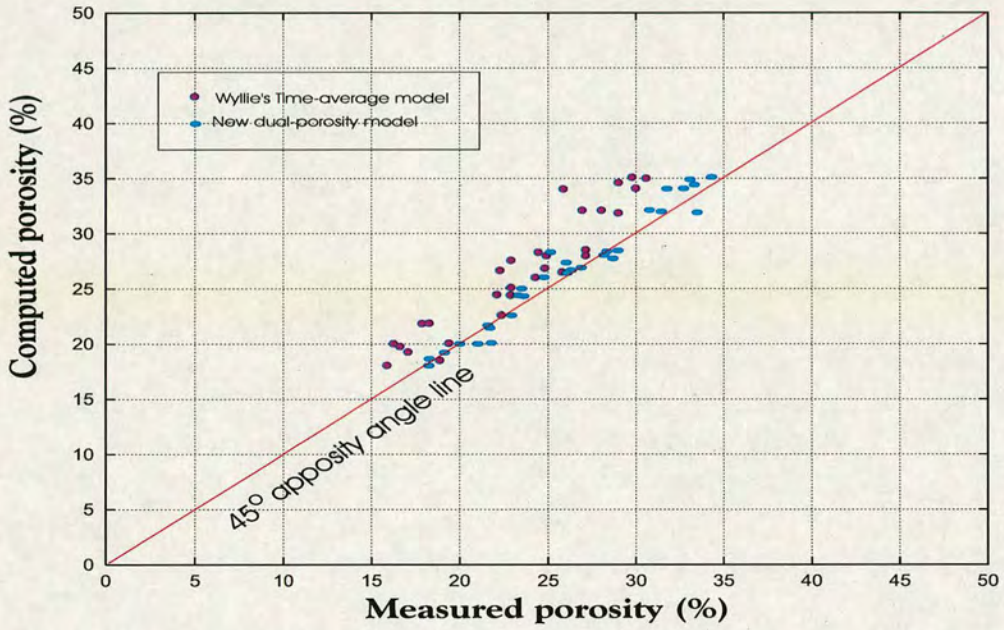

Figure 7.16: Comparison between measured and computed porosities by cross-plot, which shows both the time-average model and ADP model, the value of computed (predicted) porosity of the time average model is generally larger than ADP model.

$$V_{cl} = 10^{0.985*\Delta GR+0.35128}. \tag{7.5}$$

(N=53, R=0.855, Err=1.35)

- **Permeability:** Figure 7.18 shows the relationships between permeability-porosity measurements and permeability-shale content in a sandstone formation.

Based on the relationship derived from Figure 7.18, porosity and shale content are believed to control permeability in clay-sand mixtures. According to core analysis in the laboratory, the following regression for permeability (K) is found to be appropriate for the data of this study area:

$$K = 8.7096 \cdot 10^4 \frac{\Phi^{5.78}}{V_{sh}^{1.37}}, \tag{7.6}$$

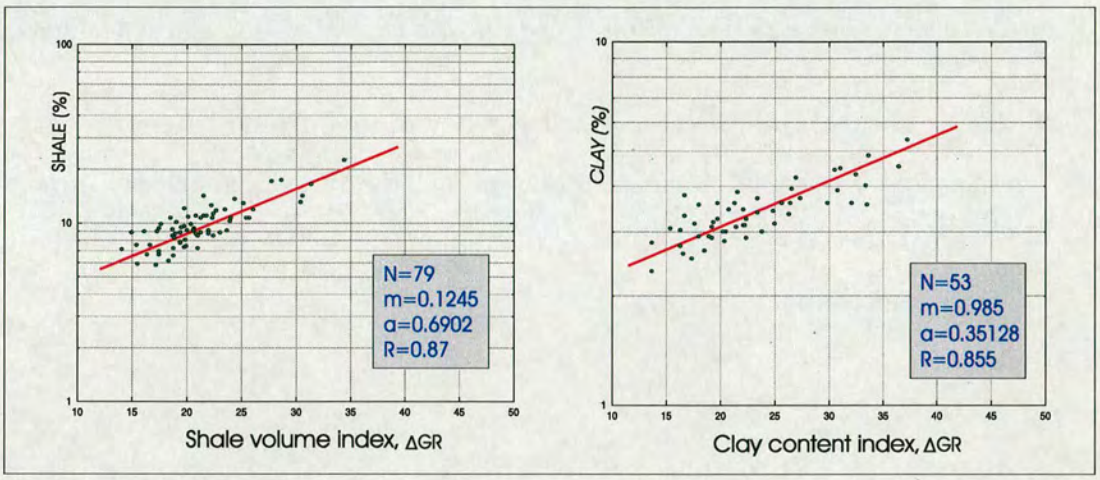

Figure 7.17: The relationship of shale and GR log (left), and the relationship of clay and GR log (right).

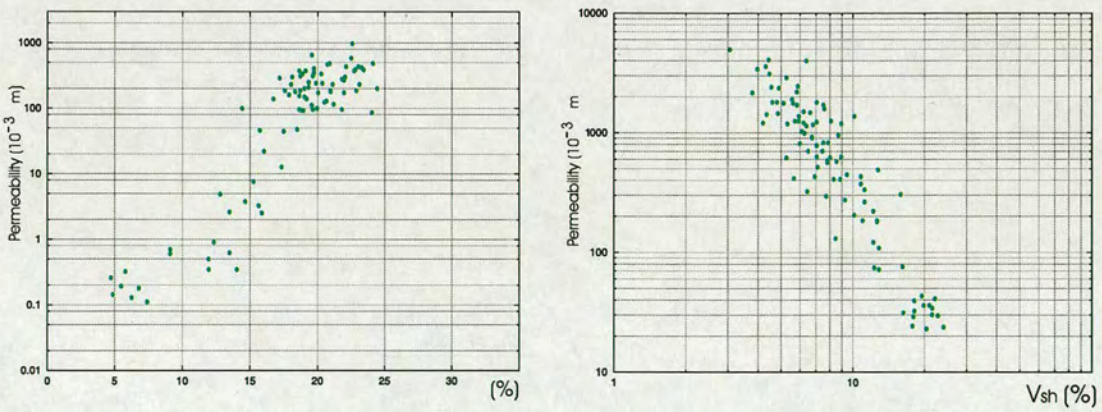

Figure 7.18: Permeability changed trend with porosity (left), and shale (right).

(N=53, R=0.833, Err=1.28)

where K is the permeability (mD), ϕ is the effective porosity and V_{sh} is the shale content. Figure 7.19 shows a comparison results between core-log calibration and modelling.

- **Water saturation:** Resistivity and porosity can be obtained from log curves, using analysis results of water saturation and the rock electrical properties in the laboratory, the saturation may be determined based on the water saturation formula in equation (7.7) as:

$$Sw = \left(\frac{0.902 R_w}{R_t \cdot \Phi^{2.142}}\right)^{\frac{1}{1.7}}, \tag{7.7}$$

where S_w is water saturation, R_t is the true resistivity of the formation(ohm-m), R_w is the water resistivity(ohm-m), ϕ is the porosity.

In order to obtain water saturation based on P-wave velocity, the Archie's equation and the relationship of formation resistivity (R_t) are used to combine the velocity to fit log data (Figure 7.20), and have:

$$\frac{1}{v_p} = 10^{c \cdot R_t^k}, \tag{7.8}$$

$$S_o = 1 - \sqrt[n]{\frac{a \cdot b \cdot R_w}{\left(\frac{lg\frac{1}{V_p}}{c}\right)^{\frac{1}{k}} \cdot \phi^m}}, \tag{7.9}$$

where S_o is the oil saturation, V_p is the P-wave velocity, R_t is the formation true resistivity, k and c are the regression coefficients derived from real data by a least square regression. In sand-clay mixture, a, b are approximately 0.85 and 1.0, and m, n

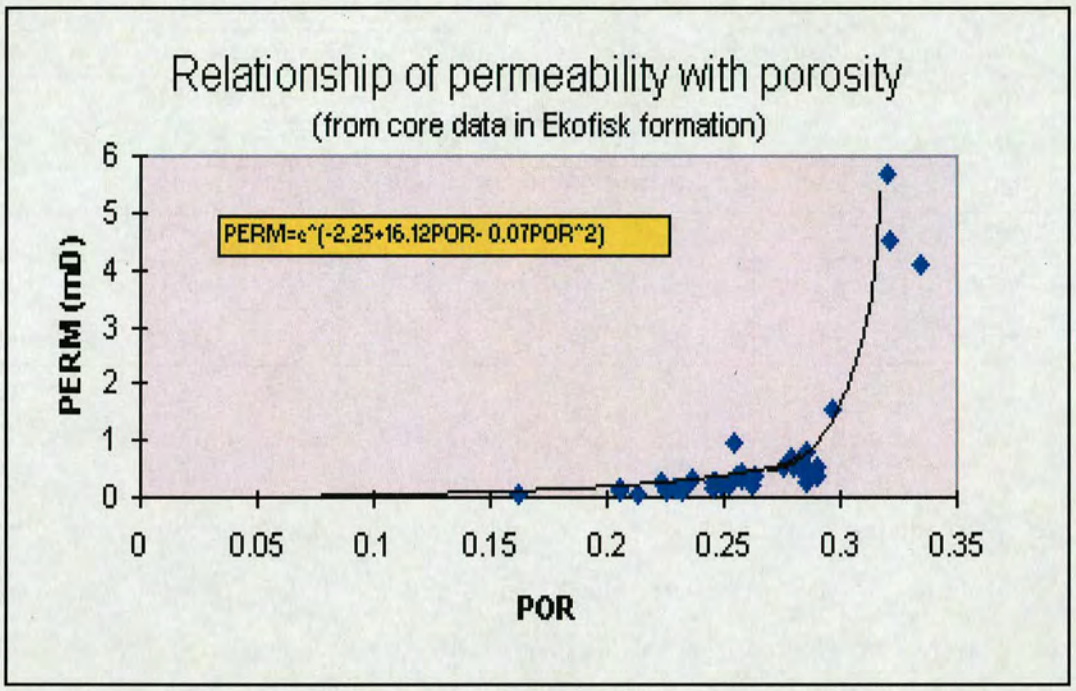

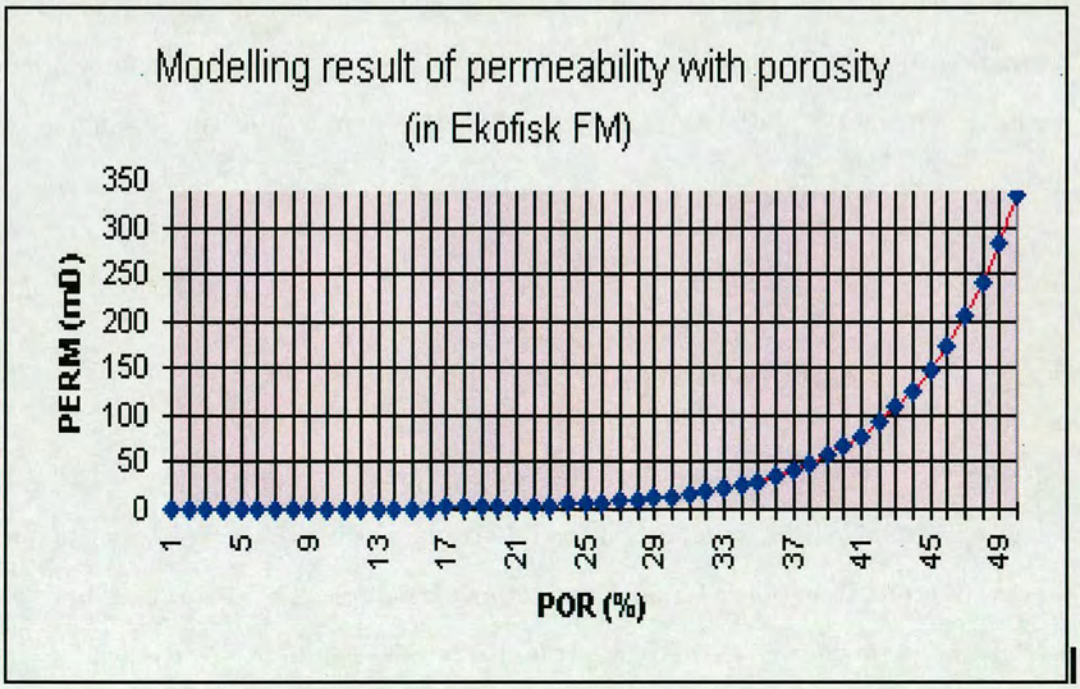

Figure 7.19: Permeability calculation based on core-log calibration. The top figure shows the relationship of K and ϕ. The bottom figure shows the result of modelling, which gives a comparison between core-log calibration and modelling.

Predicted Output	Equations or parameters	Description
Porosity (density)	$\Phi = -65.359\rho + 174.85$	N=79, R=0.934
Porosity (sonic)	$\Phi = 0.8532DT - 45.242$	N=74, R=0.933
Shale volume	$V_{sh} = 10^{1.245*\Delta GR+0.6902}$	N=79, R=0.870
clay content	$V_{cl} = 10^{0.985*\Delta GR+0.35128}$	N=53, R=0.855
Permeability	$K = 8.7096 \cdot 10^4 \frac{\Phi^{5.78}}{V_{sh}^{1.37}}$	N=53, R=0.834
Formation saturation	$Sw = \left(\frac{0.902R_w}{R_t \cdot \Phi^{2.142}}\right)^{\frac{1}{1.7}}$	m=2.142, n=1.7,a=1,b=0.902

Table 7.4: Practical equations for estimating reservoir parameters in the North Sea

are approximately 2.15 and 2.0. R_w is a fixed value depending on the water salinity of the formation, which can be determined from the resistivity (R_o) of a 100% saturation water layer or interpreted from the log data. Both Archie's equation and the expanded equation have a very good relationship, which suggests that the use of velocity to estimate water saturation is possible. Note that BPNN described in Chapter 3 is not required to predict S_o, because it is usually difficult to obtain sufficient S_o samples from the core analysis.

7.6 Formation evaluation

I have built a sequence of equations for reservoir parameter prediction in the study. These equations can be summarized in Table 7.4, which may be used for computer process interpretation (CPI) for a full formation evaluation. These equations have been used as the parameter models for reservoir characterization in the North Sea.

Figures 7.21, 7.22 and 7.23 show the results of reservoir evaluation for the case study. These include the log curves, core data and evaluated results (CPI). They can be divided into the following three parts:

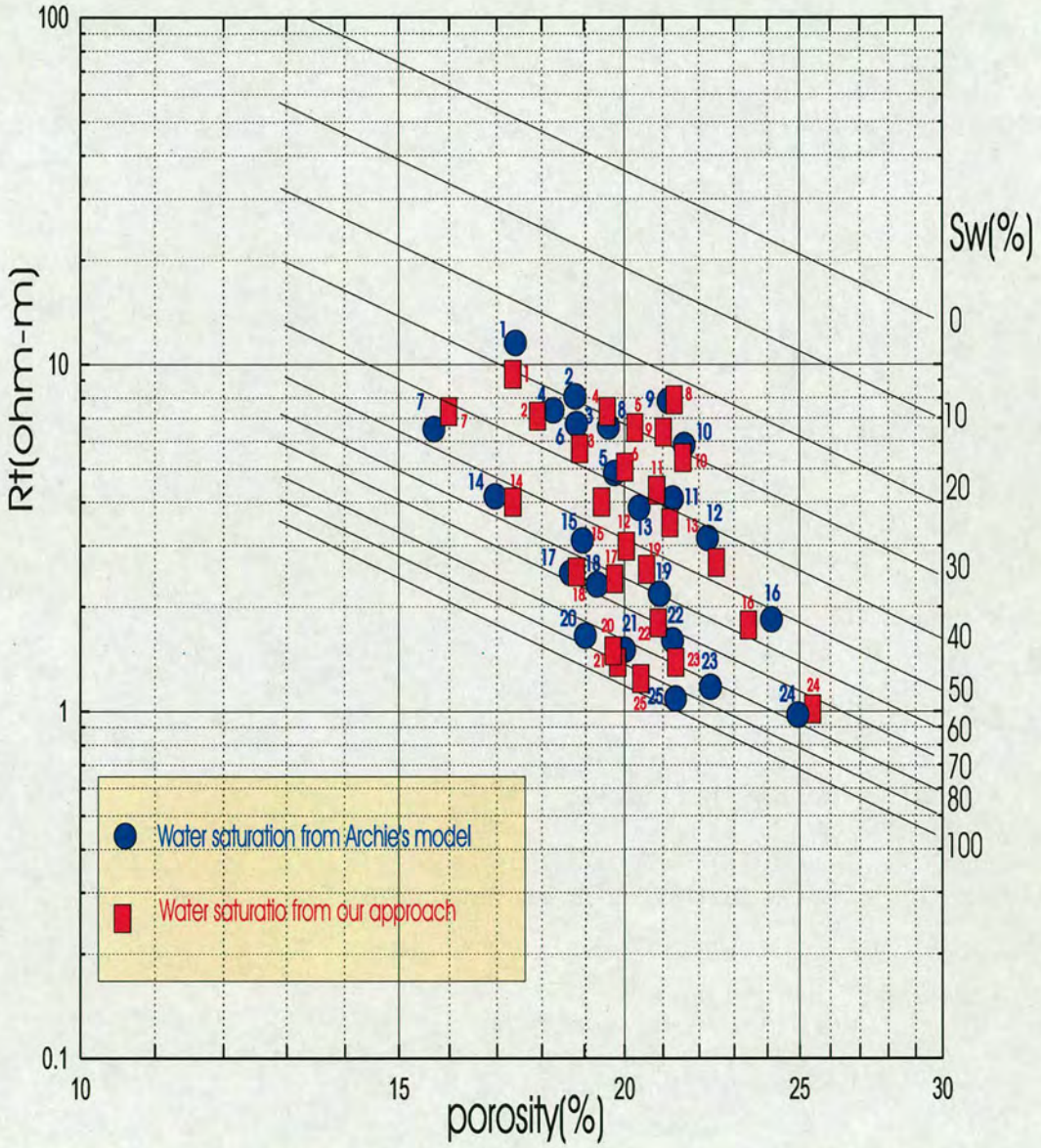

Figure 7.20: Estimation of water saturation (S_w) using the correlation of effective porosity(ϕ) versus P-wave velocity (V_p) by a cross-plot. The estimated results of water saturation is close to water saturation computed by Archie equation.

Log data are displayed as follows:

- *Panel 1: SP, GR* and *CAL* logs.
- *Panel 2: DEN* and *NEU* logs.
- *Panel 3: RT* and *RXO* logs.
- *Panel 4: DT* log.

Core analysis are shown as:

- *Panel 6:* Core porosity.
- *Panel 7:* Core saturation.
- *Panel 8:* Core permeability.
- *Panel 12:* Coring depth interval.

CPI outputs for calculating reservoir parameters:

- *Panel 6:* Calculated porosity.
- *Panel 7:* Calculated saturation.
- *Panel 8:* Calculated permeability.
- *Panel 9:* Calculated oil (gas) and water volume.
- *Panel 10:* Calculated shale volume, rock volume and porosity.

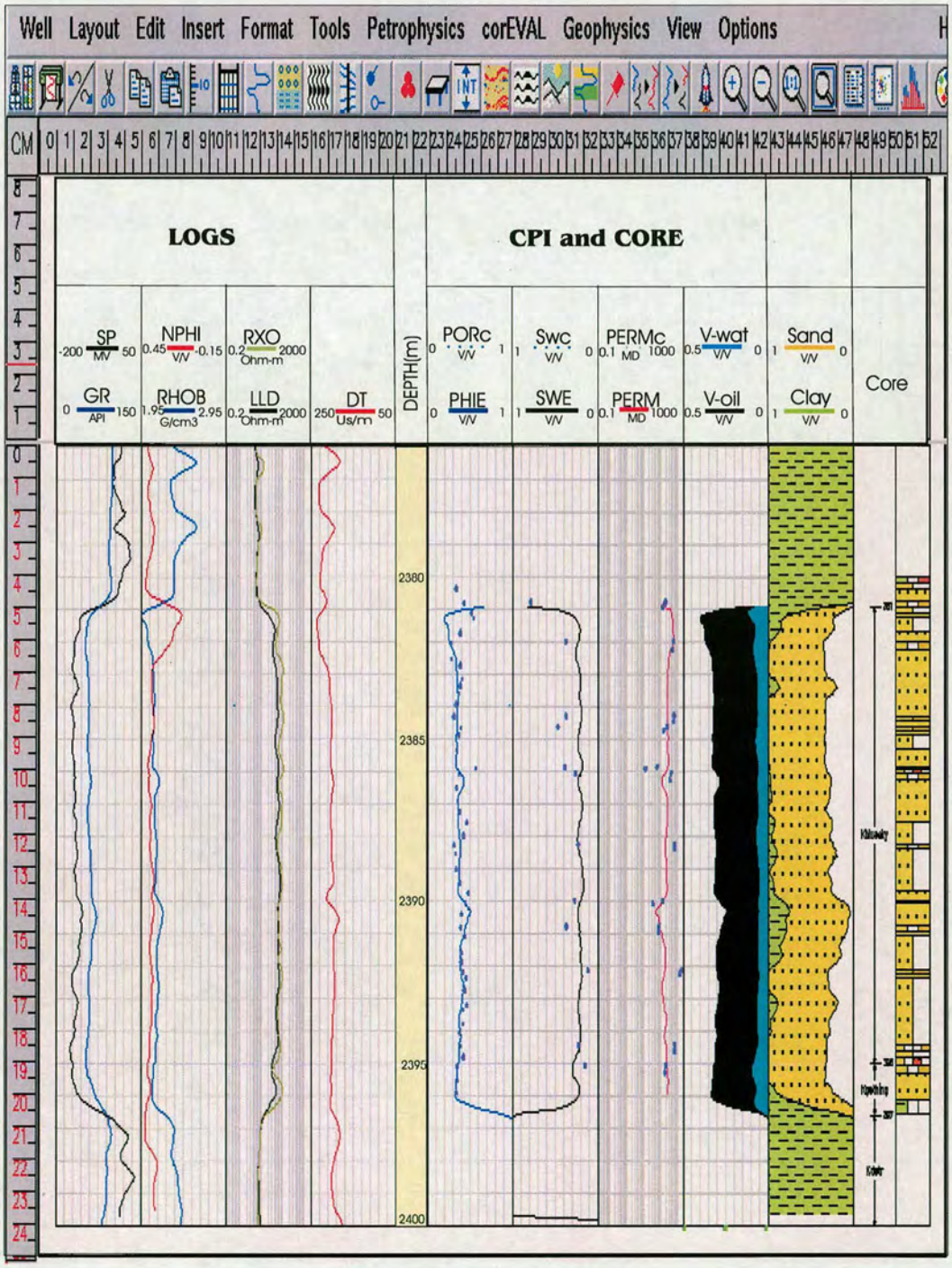

Figure 7.21: Integrated reservoir study for formation evaluation in Well A1 (This CPI plot shows predicted porosity, water saturation and permeability, also shows volume of gas, water and lithology).

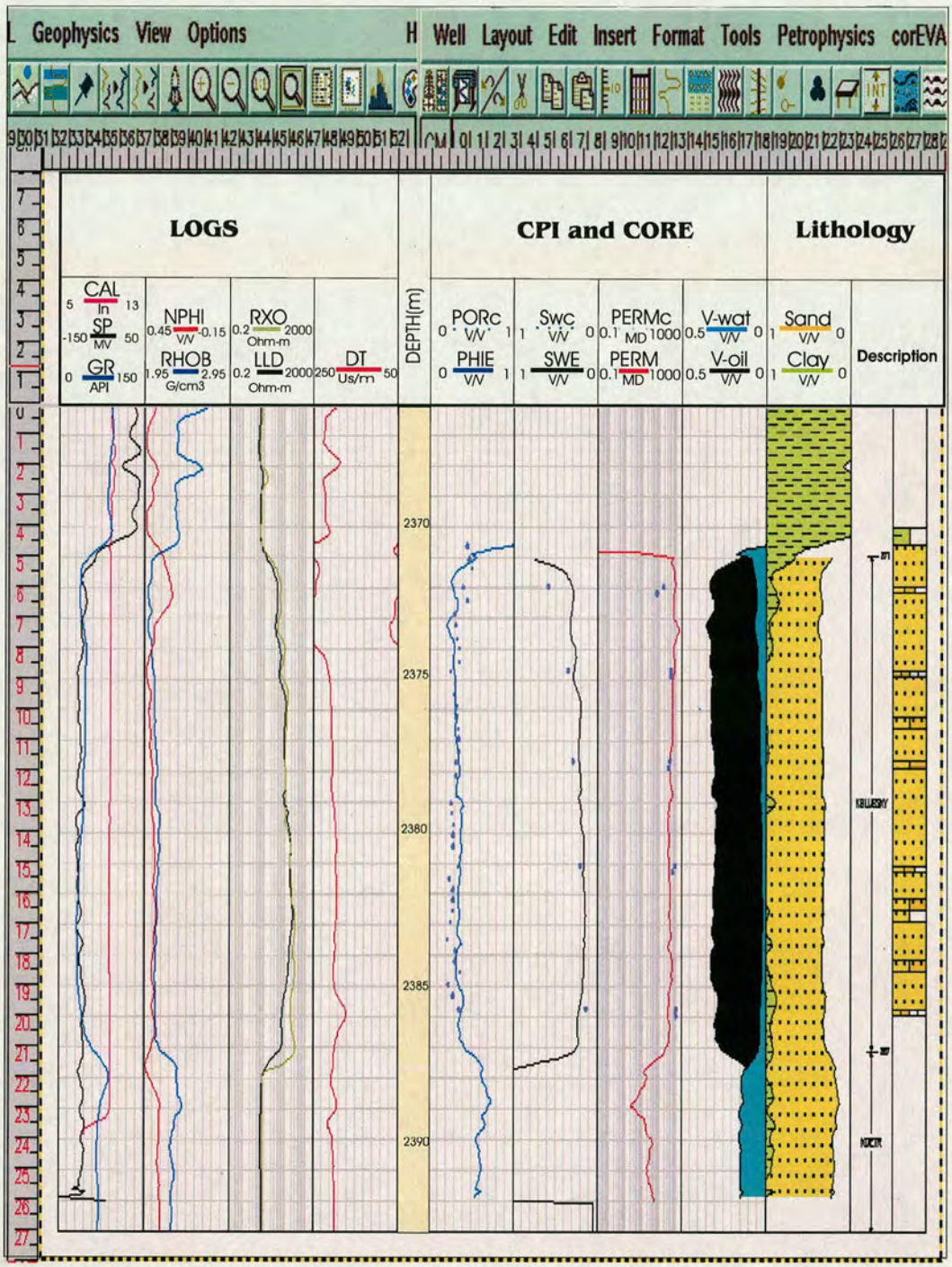

Figure 7.22: Integrated reservoir study for formation evaluation in Well A2 (This CPI plot shows raw logs in the left hand panels, and gives the CPI results in the right hand panels, they include porosity, water saturation and permeability, fluid types and lithology).

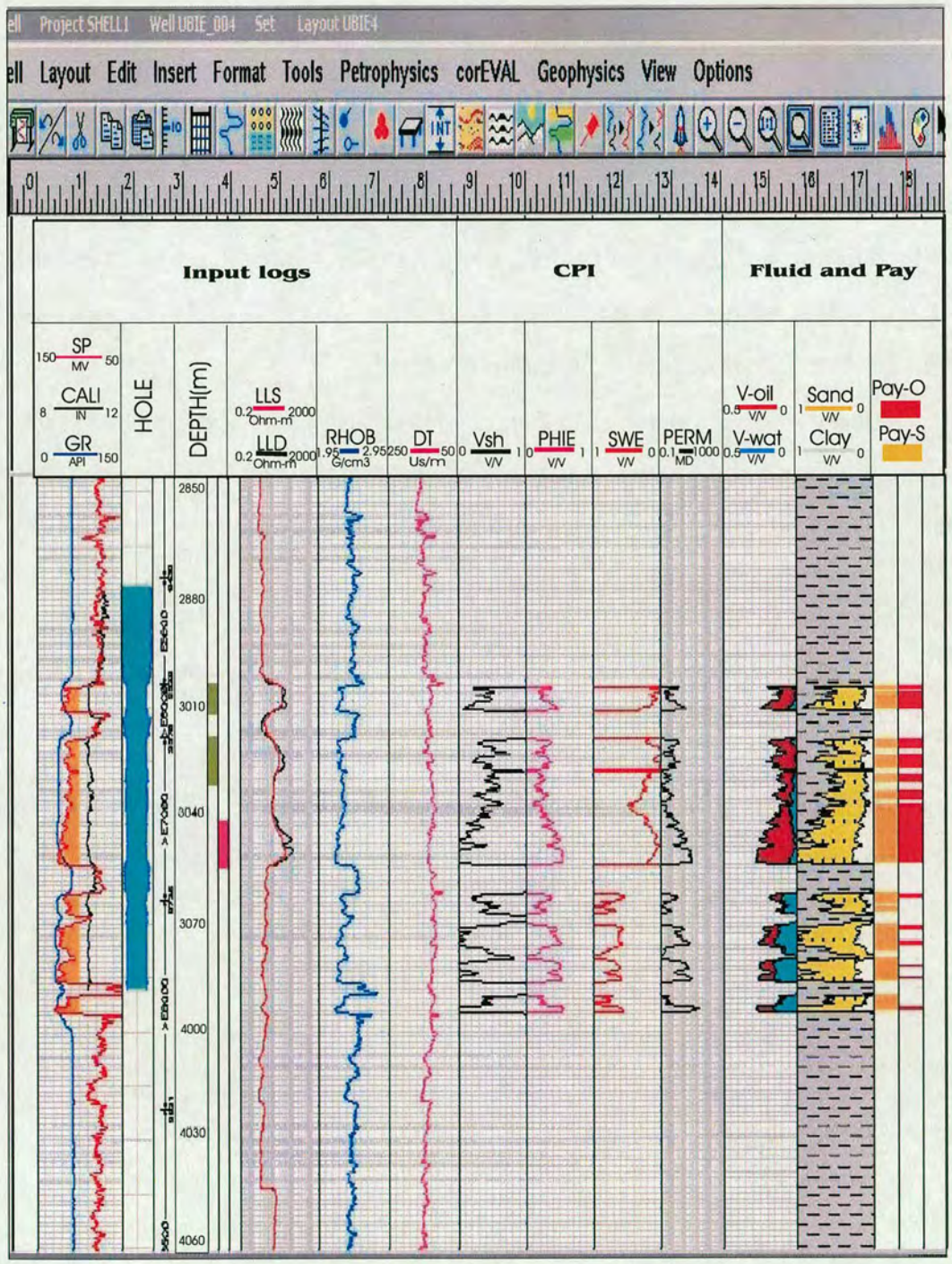

Figure 7.23: Integrated reservoir study for formation evaluation in Well A3 (This result shows key reservoir parameters, fluid types as well, the net sand and net pay flag in the last two panels).

7.7 Summary

In data integration study, I have completed the prediction of reservoir parameters, rock properties and formation evaluation based on real data from the North Sea. The wireline log data sources include raw and depth-matched open-hole log data. The routine core analysis from the laboratory is utilized, and fluid substitution algorithms are used for oil *API* values. Fluid data is available from well testing. The seismic data used to support the reservoir evaluation was a walkaway VSP.

This chapter covers practical techniques and methods for integration, ranging from basic laboratory and theoretical results to practical tool that can be immediately applied to the field data. The key procedures are summarized as follows:

- To establish the basis for calibration of core-log data, the first important step involves log curves editing and preliminary core processing, so that the log and core data can be matched properly.

- The selection of geostatistical methods (linear, non-linear, multi-linear regresses methods and filtering techniques) decides the accuracy of parameter prediction to compensate for the effects of lithology and other factors.

- The combination of reservoir parameters with seismic parameters (such as rock properties and velocities) extends the use of well-log, core and seismic data for reservoir characterization through an integration of petrophysical and mathematical modelling.

- Using predicted parameters and rock properties of reservoirs and cap rocks, it can help significantly in the identification of profitable areas in exploration where the hydrocarbon distribution and productivity in sand-clay mixtures of hydrocarbon reserves can be mapped out.

The study in this chapter has shown that detailed and careful data analysis is required. The success of the whole integrated work is determined by data quality at every stage. The application to the oilfield data from a North Sea reservoir shows that integrated approach presented in previous chapters can be satisfactorily applied to predict reservoir and rock parameters. This has been confirmed through error analysis and modelling performed based on the field data.

Chapter 8

SUMMARY

8.1 Conclusions from the thesis

Data integration for reservoir study is a challenging task to perform. Reservoir in reality is very complex in itself, which have to be characterized from a variety of viewpoints, with a large number of parameters and an acceptable degree of accuracy. In addition to the inherent complexity of the reservoir, we may also have man-induced errors to reservoir unknowns, e.g. inputs to reservoir parameter distribution, clay effects, and formation. As a consequence of these factors, studies always have a degree of uncertainty, which in turn can be considered as an (unknown) measure of in completeness of knowledge about reservoirs. Data integration is a two stage process involving data matching, reservoir evaluation and description. The strategy presented in this thesis has the potential to make core-log integration and log-seismic integration accurately and thus enable us to obtain the most data from core, log and seismic data.

The main aim of this thesis is to improve rock physical models for the integration of core, well-log and seismic data along with the specific application to reservoir characterization. The work includes prediction of important parameters such as porosity (ϕ), shale volume (V_{sh}), clay content (V_{cl}), water saturation (S_w), permeability (K), as well as rock properties such as elastic moduli (K, μ), aspect-ratios (α_{AR}), anisotropy coef-

ficients (m_s) and velocities (V_p and V_s). These parameters are then used for reservoir evaluation and description. The developed approach is applicable to both consolidated and unconsolidated formations, it can provide satisfactory results when applied for this objective. To start with, I have carried out an intensive literature review in Chapter 2, and searched for relevant studies on my project. One point is clear, that is, in today's oil and gas industry, the most successful methods used in core-log-seismic integration are still based on the empirical relationships (derived from laboratory experiments). In order to extract the reservoir parameters, many people have realized that there is a need to develop a consistent model that can be used to describe complex reservoir source rock. Despite many theoretical models present, no model has been found to be superior to others. This is because these models are based on particular assumptions about the rock properties and can only be used under specific circumstances.

In this study, I have extended Han *et al.*'s (1986) empirical model in Chapter 3 as the first step. This empirical method shows advantages in practical application, and give an accurate prediction of reservoir parameters based on the relationship between porosity, clay content and velocities, although it is difficult to be applied for formations with varied lithology. Han *et al.*'s (1986) empirical equations imply that P- and S-wave velocities are the functions of porosity and clay content. The differences in the least square regression obtained from studies of different formations under different conditions from many authors have proved, that extrapolation of this type of approach to cover other datasets does require calibration with a reasonable number of measurements. In this thesis, I have combined a back-propagation neural network with Han *et al.* model. This modified empirical model may be used to build and identify the relationship between velocities and reservoir parameters, which allows us to estimate porosity, clay content and aspect-ratios as well as velocities. Studies show that a neural network can be used to solve many problems in geophysics and petrophysics, and it is

especially suitable for applications to problems where some results are known but the manner, in which these results are obtained is not known.

The model developed by Xu-White is chosen as my starting point for building a physics based model, therefore an isotropic dual porosity model has been developed in Chapter 4. In this model, two famous classic theories are used and combined with the neural network in order to predict reservoir rock properties in clay-sand mixture. Briefly, it starts with Wyllie's (1956) time average equation and theory developed by Kuster and Toksöz in 1974 to compute the elastic properties of the rock frame (dry rock skeleton without fluid saturation). Gassmann's (1951) model is then used for fluid substitution. It is noted that Gassmann's model was published nearly 40 years ago and Kuster and Toksöz model was published more than 20 years ago, and both models are very popular in oil and gas industry. Therefore my new IDP model can be regarded as Wyllie-KT-Gassmann approach. In this model, two variable pore aspect-ratios are used to replace the fixed aspect-ratios in order to improve the accuracy of Xu-White model. There is strong evidence showing that fixed values of aspect-ratios fail to match the variability, and may result in error in elastic parameter prediction. Therefore I have argued that the aspect-ratios have a strong influence on Vp and Vs response to porosity. In practical applications, the fixed aspect-ratios are often misused or even 'abused'. This is because that pore aspect-ratios in rock are not uniformly distributed. They are controlled by the validity of physical factors, such as the high effective pressure, which tends to close pores with very small aspect-ratio such as micro-cracks, while leaving large aspect-ratio pores open. In effect, the mean aspect-ratio can increase with an increase of confining pressure. The IDP model therefore provides a practical tool for predicting elastic wave velocities. It is suitable for clay-sand formations, and particularly suitable for consolidated formations. This is confirmed by error and sensitivity analysis performed using field data.

The IDP model is useful for predicting S-wave velocity and reservoir parameters such as porosity, clay content etc., this model has several limitations associated with the integration of the CLS data (as discussed in Chapter 4), and there are some difficulties in calculating elastic moduli for rocks having a high clay content or aligned minerals, clay particles or cracks. Wyllie *et al.*'s (1956) time-average equation works well at great burial depth. However, when clay is poorly compacted or poorly consolidated due to the low litho-static pressure, pores associated with clay particles are still open under such pressures, so that clay affects not only the elastic properties of the grain matrix but also the porosity-velocity relationship, which results in this model invalid. In particular, the time-average equation is poor for studying the effect of partial gas-saturation on velocity. Because vuggy pores tend to be big, spherical, and incompressible, P-wave velocity is very insensitive to pore fluid saturation, so that this equation will severely underestimate the porosity.

In order to extend the IDP model to be used for anisotropic rocks, I noted that Hornby *et al.* (1994) combined two famous theories (SCA and DEM) in modelling the anisotropic nature of shale source rock successfully. A combination of SCA and DEM theories was first proposed by Sheng (1991) to model physical (electrical and elastic) properties of sediment rocks. The combination of SCA and DEM means that the model is now applicable to both consolidated and un-consolidated sediments. Another advantage of the combined model is its ability to model clay particle distributions, thus anisotropic characteristics of shale or shale-sand mixture that is believed to be a common feature of reservoir source rock. However, the model used by Hornby *et al.* (1994) is still limited as it does not consider the role of fluids. Like most other models, it is a static poroelastic model, i.e. zero-frequency approximation, and is not strictly valid for the CLS integration. What I have done is to extend this model to incorporate dynamic fluid-rock interaction using an anisotropic version of Gassmann's

model as developed by Brown and Korringa (1975). Therefore, my ADP model is a combination of SCA-DEM-BK. This new model substantially improved the existing model mentioned in Chapter 4, while retained its advantages, but overcame limitations of each individual model.

In my ADP model, I have extended the time-average equation and proposed an equivalent model for rock components. A sand formation containing clay can be equivalent to a two unit model, which includes pure sand and pure clay. According to the equal principle similar to Wyllie *et al.*'s equation, a lithology property equation is used to calculate clay content in sand formation based on velocity. The physical property equation is used to estimate porosity containing clay. On the other hand, the ADP model extends the IDP model by means of the SCA and DEM theories and models of Brown and Korringa (1975) and Liu *et al.* (2000). The results are similar to the IDP model for predicting elastic constants and velocities based on the aligned distributed inclusions, pores and clay. Therefore, we can say that the ADP model is basically an extension of the IDP model to anisotropic rocks, and is incorporated in a scheme similar to the IDP.

To apply the models mentioned above to field data, data conditioning and preprocessing should be done in advance. When we predict petrophysical properties from these integrated data, we have to consider suitable methods for data conditioning. The measurement process, quality control, data correction, resolution matching and data calibration must be appropriate for each dataset, The following methods have been suggested for these purposes:

(1) Measurements can be calibrated, either relatively (locally) or absolutely (globally). Caution must be taken since often this falls into inter-dataset comparison, and involves equalization, in which the modification of one dataset in preference to the other may negate additional benefits which integration may otherwise achieve.

(2) The best approach for core, log and seismic calibration is through judicious choice of interpretation target and a careful appropriate selection of measurement techniques, in order to obtain available data from data at different scale. So that the differences of scale in measurement sets may highlight geological features.

(3) One dataset should be assumed to be correct for data calibration. Core data are used to calibrate log data, and log data are then used to calibrate seismic (VSP) data. To ensure the log data is correct for building the relationship between core to log and log to seismic data, it is necessary to perform log data correction before data calibration.

Integrated studies for reservoir characterization from well-log, core and seismic data include prediction of reservoir parameters such as porosity (ϕ), shale volume (V_{sh}), clay content (V_{cl}), water saturation (S_w) and permeability (K), as well as rock properties such as elastic moduli (K, μ), aspect-ratios (α_{AR}), anisotropic coefficients (m) and velocities (V_p and V_s). It also needs to build the relationship between velocities and these parameters. These parameters have been used for reservoir evaluation and description to provide satisfactory results in the integrated study.

8.2 Suggestion for the future work

I am aware that many problems still exist in terms of data integration. For example, most theories available assumed static equivalent medium, which is not strictly valid for the purpose of data integration. Therefore, it would be interesting to extend static equivalent medium theory to dynamic equivalent medium theory. In addition, although the ADP model has introduced anisotropy to data integration due to presence of clay particle alignment, the anisotropy of cracked and fractured rock has not been properly addressed. The future work should bridge this gap, because reservoir characterization

in fractured rock, such as carbonate reservoirs is a complicated problem with no easy solutions. Furthermore, there are many factors affecting wave propagation and prediction of reservoir parameters in multi-phase media, such as partial saturation, pore pressure. Here, I suggest a few key issues for the future work:

- Carbonate reservoirs pose particular challenges. The use of Vp/Vs to determine lithology requires calibration, which can be done by core analysis to establish the best correlations between core and velocities. Therefore, we must make further investigation, if we use Vp/Vs to delineate a limestone reservoir, as Vp in limestone is found to be the least sensitive porosity indicator.

- Pore aspect-ratio appears to be influenced by gas, but the expected response may not occur in rocks with round pores. Therefore an integrated data analysis is required to study gas effects in the future.

- Permeability is one of the most important parameters in integrated reservoir study. The determination of permeability is problematic partly due to the complex nature of rock type. A physical model is needed to help us in understanding the factors controlling permeability.

- Horizontal drilling has been widely used in the oil industry. However, data integration of deviated and horizontal wells in the subject area of this thesis is still in its infancy. This is largely due to the lack of suitable physical models capable of handling the anisotropic behaviour of rock properties.

Appendices

A. Scalars in the Kuster and Toksöz (1974) theory

For ellipsoidal inclusions of arbitrary aspect-ratio, the scalars $T_{iijj}(\alpha)$ and $T_{ijij}(\alpha)$ which are used in the study are given by:

$$T_{ijij}(\alpha) = -\frac{3F_1}{F_2},$$

and

$$T_{ijij}(\alpha) - \frac{T_{iijj}(\alpha)}{3} = \frac{2}{F_3} + \frac{1}{F_4} + \frac{F_4 \cdot F_5 + F_6 \cdot F_7 - F_8 \cdot F_9}{F_2 \cdot F_4},$$

the parameters in the equations above are defined as follows;

$$F_1 = 1 + A[\tfrac{3}{2}(g+\phi) - R(\tfrac{3}{2}g + \phi - \tfrac{4}{3})],$$

$$F_2 = 1 + A[1 + \tfrac{3}{2}(g+\phi) - \tfrac{R}{2}(3g + 5\phi)] + B(3-4R),$$

$$-\tfrac{A}{2}(A+3B)(3-4R)[g + \phi - R(g - \phi + 2\phi^2)],$$

$$F_3 = 1 + \tfrac{A}{2}[R(2-\phi) + \tfrac{1+\alpha^2}{\alpha^2}g(R-1)],$$

$$F_4 = 1 + \tfrac{A}{4}[3\phi + g - R(g-\phi)],$$

$$F_5 = A[R(g + \phi - \tfrac{4}{3}) - g] + B\phi(3-4R),$$

$$F_6 = 1 + A[1 + g - R(g+\phi)] + B(1-\phi)(3-4R),$$

$$F_7 = 2 + \tfrac{A}{4}[9\phi + 3g - R(5\phi + 3g0] + B\phi(3-4R),$$

$$F_8 = A[1 - 2R + \tfrac{g}{2}(R-1) + \tfrac{\phi}{2}(5R-3)] + B(1-\phi)(3-4R),$$

$$F_9 = A[g(R-1) - R\phi] + B\phi(3-4R),$$
$$A = \frac{\mu'}{\mu} - 1, \quad B = \frac{1}{3}(\frac{K'}{K} - \frac{\mu'}{\mu}),$$
$$R = \frac{3\mu}{3K+4\mu}, \quad g = \frac{\alpha^2}{1-\alpha^2}(3\phi - 2),$$
$$\phi = \frac{\alpha}{(1-\alpha^2)^{3/2}}[cos^{-1}\alpha - \alpha(1-\alpha^2)^{\frac{1}{2}}].$$

Here, α denotes aspect-ratio; K_m and μ_m denote the bulk and shear moduli of the solid in which the pores are embedded; K' and μ' are the bulk and shear moduli of the inclusions (fluid).

B. Theoretical background of transverse isotropy

Hooke's law for a general anisotropic, linear elastic solid states that the stress σ_{ij} is linearly proportional to the strain ε_{ij} as expressed by:

$$\sigma_{ij} = C_{ijkl}\varepsilon_{kl} \quad (i, j, k, l = 1, 2, 3)$$

Based on Thomsen (1986), we have:

$$\begin{bmatrix} \sigma_{11} \\ \sigma_{22} \\ \sigma_{33} \\ \sigma_{23} \\ \sigma_{13} \\ \sigma_{12} \end{bmatrix} = \begin{bmatrix} C_{1111} & C_{1122} & C_{1133} & C_{1123} & C_{1113} & C_{1112} \\ . & C_{2222} & C_{2233} & C_{2223} & C_{2213} & C_{2212} \\ . & . & C_{3333} & C_{3323} & C_{3313} & C_{3312} \\ . & . & . & C_{2323} & C_{2313} & C_{2312} \\ S & Y & M & . & C_{1313} & C_{1312} \\ . & . & . & . & . & C_{1212} \end{bmatrix} \begin{bmatrix} \varepsilon_{11} \\ \varepsilon_{22} \\ \varepsilon_{33} \\ \varepsilon_{23} \\ \varepsilon_{13} \\ \varepsilon_{12} \end{bmatrix} \tag{8.1}$$

In the media with a cubic symmetry, these independent elastic constants are:

$$C_{1113} = C_{1112} = C_{2213} = C_{2212} = C_{3313} = C_{3312} = C_{2312} =$$

$$= C_{1312} = C_{1123} = C_{2223} = C_{3323} = C_{2313} = 0.$$

$$C = \begin{bmatrix} C_{1111} & C_{1122} & C_{1133} & 0 & 0 & 0 \\ C_{1122} & C_{2222} & C_{2233} & 0 & 0 & 0 \\ C_{1133} & C_{2233} & C_{3333} & 0 & 0 & 0 \\ 0 & 0 & 0 & C_{2323} & 0 & 0 \\ 0 & 0 & 0 & 0 & C_{1313} & 0 \\ 0 & 0 & 0 & 0 & 0 & C_{1212} \end{bmatrix}. \tag{8.2}$$

Thus it only has nine independent constants, Ox_3 is the symmetry axis, we also can prove

$$C_{1111} = C_{2222},\ C_{1133} = C_{2233},\ C_{2323} = C_{1313},$$

$$C_{1212} = \frac{C_{1111} - C_{1122}}{2}$$

We have:

$$C = \begin{bmatrix} C_{1111} & C_{1122} & C_{1133} & 0 & 0 & 0 \\ C_{1122} & C_{1111} & C_{1133} & 0 & 0 & 0 \\ C_{1133} & C_{1133} & C_{3333} & 0 & 0 & 0 \\ 0 & 0 & 0 & C_{2323} & 0 & 0 \\ 0 & 0 & 0 & 0 & C_{2323} & 0 \\ 0 & 0 & 0 & 0 & 0 & \frac{C_{1111} - C_{1122}}{2} \end{bmatrix}, \tag{8.3}$$

This elastic medium has a symmetry axis that is called transversely isotropic, which is the simple case in anisotropy. For a medium with transversely isotropic (hexagonal) symmetry, the wave slowness surface is always rotationally symmetric about the axis of symmetry. Based on the equation above, the relationship of stress and strain is given

as follows:

$$\begin{bmatrix} \sigma_{11} = C_{1111}\varepsilon_{11} + C_{1122}\varepsilon_{22} + C_{1133}\varepsilon_{33}, \\ \sigma_{22} = C_{1122}\varepsilon_{11} + C_{1111}\varepsilon_{22} + C_{1133}\varepsilon_{33}, \\ \sigma_{33} = C_{1133}(\varepsilon_{11} + \varepsilon_{22}) + C_{3333}\varepsilon_{33}, \\ \sigma_{23} = C_{2323}\varepsilon_{23}, \\ \sigma_{13} = C_{2323}\varepsilon_{13}, \\ \sigma_{12} = \frac{C_{1111}-C_{1122}}{2}\varepsilon_{12}. \end{bmatrix}, \tag{8.4}$$

therefore, we can calculate the velocities in any propagation direction as:

$$V_{p,V} = \sqrt{\frac{C_{3333}}{\rho}}, \quad V_{p,H} = \sqrt{\frac{C_{1111}}{\rho}},$$
$$V_{SV,V} = \sqrt{\frac{C_{2323}}{\rho}}, \quad V_{SV,H} = \sqrt{\frac{C_{2323}}{\rho}},$$
$$V_{SH,V} = \sqrt{\frac{C_{2323}}{\rho}}, \quad V_{SH,H} = \sqrt{\frac{C_{1111}-C_{1122}}{2\rho}}.$$

In geophysical context, we often assume hexagonal symmetry system which is called *Transverse Isotropy with an infinite-fold Vertical symmetry axis:* or TIV. The TIV system implies, in terms of velocity anisotropy, equal velocity in the azimuthal sense. The velocity varies with the angle of propagation in the vertical plane. The angular velocity dependence is the same in all vertical planes, i.e., a single vertical plane at any azimuth is representative of the entire medium. We may also say that any vertical plane is a symmetry plane. This system is particularly applicable to the case of horizontally stratified media, or to media with predominantly vertical stress directions, which in a geophysical study can be associated with the weight of the overburden.

There exists a simple method of index translation between the tensor notation, C_{ijkl} and the matrix notation C_{mn} (e.g. Winterstein, 1990):

Tensor	ij or kl	11	22	33	32=23	31=13	21=12
Matrix	m or n	1	2	3	4	5	6

A TIV medium is uniquely described in terms of five independent elastic constant (e.g., Thomsen, 1986) and in matrix notation we can write:

$$C = \begin{bmatrix} C_{11} & C_{12} & C_{13} & 0 & 0 & 0 \\ C_{12} & C_{11} & C_{13} & 0 & 0 & 0 \\ C_{13} & C_{13} & C_{33} & 0 & 0 & 0 \\ 0 & 0 & 0 & C_{44} & 0 & 0 \\ 0 & 0 & 0 & 0 & C_{44} & 0 \\ 0 & 0 & 0 & 0 & 0 & C_{66} \end{bmatrix}, \tag{8.5}$$

where $C_{66} = (C_{11} - C_{12})/2$. The phase velocities of three body waves with mutually orthogonal polarizations can be expressed in terms of the elastic constants (e.g., Thomsen, 1986). The phase velocity of a compressional wave is expressed by:

$$V_p(\theta) = \frac{\sqrt{C_{33} + C_{44} + (C_{11} + C_{33})cos^2\theta + D(\theta)}}{2\rho}. \tag{8.6}$$

The phase velocity of the shear wave with the vertical polarization direction (SV-wave) is expressed by:

$$V_{SV}(\theta) = \frac{\sqrt{C_{33} + C_{44} + (C_{11} + C_{33})cos^2\theta - D(\theta)}}{2\rho}. \tag{8.7}$$

The symbol $D(\theta)$, used in expressions for phase velocities of P- and SV-waves is given by:

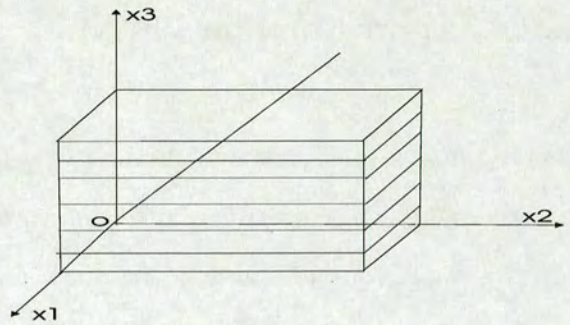

Figure 8.1: Transverse isotropy (Graphical illustration of a transversely isotropic medium. The axis of symmetry is the $OX3$ axis.

$$D(\theta) = \sqrt{(C_{33} - C_{44})^2 + 2[2(C_{13} + C_{44})^2 - (C_{33} - C_{44})E]cos^2\theta + [E^2 - 4(C_{13} + C_{44})^2]cos^4\theta}, \tag{8.8}$$

$$E = (C_{11} + C_{33} - 2C_{44}). \tag{8.9}$$

The phase velocity of the shear wave polarized in the horizontal direction (SH-wave) is expressed by:

$$V_{SH}(\theta) = \frac{\sqrt{C_{66}cos^2\theta + C_{44}sin^2(\theta)}}{\rho}. \tag{8.10}$$

ρ is the bulk density, θ is the angle between the axis of symmetry and the direction of wave propagation (Figure 8.1). The five components of the stiffness tensor for a transversely isotropic material are obtained from five velocity measurements: $V_p(0^o)$, $V_p(90^o)$, $V_p(45^o)$, $V_{SH}(90^o)$ and $V_{SH}(0^o) = V_{SV}(0^o)$.

The convention, contrary to the most geophysical descriptions where the phase angle is measured with respect to the vertical, i.e., colatitude, was chosen in order to facilitate the subsequent use of standard expressions of vector calculus in polar coordinates in subsequent.

C. Self-Consistent Approximation (SCA)

A relatively successful, and certainly popular, method to extend these specific geometry methods to slightly highly concentration of inclusion is the Self-Consistent Approximation (SCA). In this approach one still uses the mathematical solution for the deformation of isolated inclusions, but the interaction of inclusions is approximated by replacing the background medium with the as-yet-unknown effective medium. These methods were made popular following a series of papers by O'Connell and Budiansky (1974). Their equations for effective bulk and shear moduli, K^*_{sc} and μ^*_{sc}, respectively, of a cracked medium with randomly oriented dry penny-shaped cracks (in the limiting case when the aspect-ratio α goes to 0) are:

$$\frac{K^*_{sc}}{K} = 1 - \frac{16}{9}\left(\frac{1-\nu^{*2}_{sc}}{1-2\nu^*_{sc}}\right)\varepsilon, \tag{8.11}$$

$$\frac{\mu^*_{sc}}{\mu} = 1 - \frac{32}{45}\frac{(1-\nu^*_{sc})(5-\nu^*_{sc})}{(2-\nu^*_{sc})}\varepsilon. \tag{8.12}$$

K and μ are the bulk and shear moduli, respectively, of the un-cracked medium, and ε is crack density parameters, which is defined as the number of cracks per unit volume times the crack radius cubed. The effective Poisson ratio ν^*_{sc} is related to ε and the Poisson's ratio ν of the un-cracked solid.

Berryman(1980,1995) gives a more general form of the self-consistent approximations for N-phase composites:

$$\sum_{i=1}^{N} x_i(K_i - K^*_{sc})P^{*i} = 0, \tag{8.13}$$

$$\sum_{i=1}^{N} x_i(\mu_i - \mu_{sc}^*)Q^{*i} = 0. \tag{8.14}$$

where i refers to the ith material, x_i is its volume fraction, P and Q are geometric factors, and superscript $*i$ on P and Q indicates that the factors are for an inclusion of material i in a background medium with self-consistent effective moduli K_{sc}^* and μ_{sc}^*. These equation are coupled and must be solved by simultaneous iteration. Although Berryman's self-consistent method does not converge for fluid disks ($\mu_2 = 0$), the formulae for penny-shaped fluid-filled cracks are generally not singular and converge rapidly. However, his estimates for needles, disks, and penny cracks should be used cautiously for fluid-saturated composite materials. Dry cavities can be modelled by setting the inclusion moduli to zero. Fluid saturated cavities are simulated by setting the inclusion shear modulus to zero.

D. Differential Effective Medium (DEM)

The distribution of pores and inclusions is often assumed to be perfectly aligned. In reality, the pores, clay minerals and their associated pore space are not perfectly aligned and they have a distribution of orientations. Andrea *et al.* (1997) summarized three types of composite media in anisotropic rocks (Figure 8.2), which indicate that media with different orientation of inclusions require different effective medium theories. The anisotropy in sand-clay mixtures increases as the minerals and pores become more aligned (Hornby *et al.*, 1994). For the purpose of modelling, the DEM approach can be used to calculate the elastic properties of intermediate media with lens-shaped inclusions (Andrea *et al.*, 1997).

DEM theory models two-phase composites by incrementally adding inclusions of one phase (phase 2) to the matrix phase. The matrix begins as phase 1 (when concentration of phase 2 is zero) and is changed at each step as a new increment of phase 2 material is added. The processing is continued until the desired proportion of the constituents is reached. The resulting effective bulk and shear moduli K^* and μ^* in isotropic media are given by Berryman (1992) as:

$$(1-y)\frac{d}{dy}[K^*(y)] = (K_2 - K^*)P^{(*2)}(y), \tag{8.15}$$

$$(1-y)\frac{d}{dy}[\mu^*(y)] = (\mu_2 - \mu^*)Q^{(*2)}(y). \tag{8.16}$$

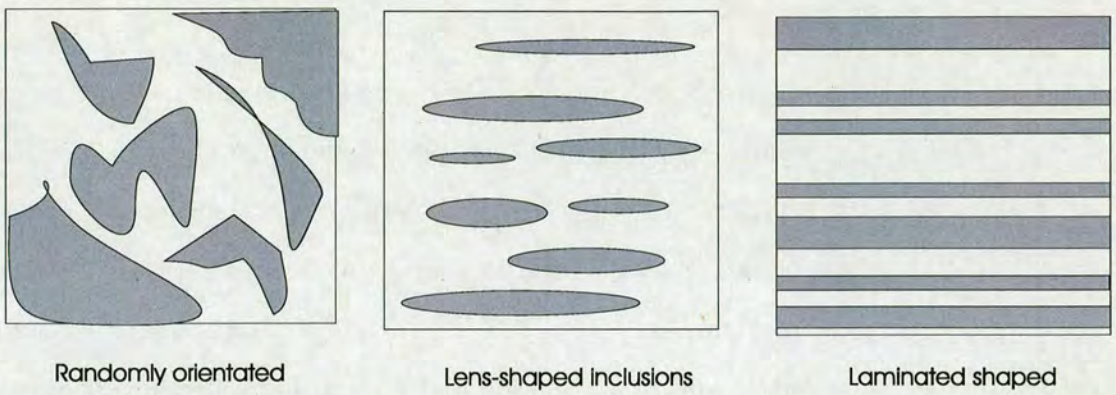

Figure 8.2: The media with different orientation of inclusions in anisotropic rocks.

The initial conditions are $K^*(0) = K_1$ and $\mu^*(0)=\mu_1$, where K_1 and μ_1 are the bulk and shear moduli of the initial host material (phase 1); K_2 and μ_2 are the bulk and shear moduli of the initial host material (phase 2); y is the concentration of phase 2 (for fluid inclusions and voids, y equals porosity (ϕ)); and Q and P are geometric factors which come from Eshelby (1957). For fluid filled inclusions and voids, y equals to the porosity (ϕ). The superscript ($*2$) in P and Q indicates that the factors are for an inclusion of material 2 with effective moduli K^* and μ^* in a background medium. Dry cavities can be modelled by setting the inclusion moduli to zero. Fluid-saturated cavities are simulated by setting the inclusion shear modulus to zero.

Because the cavities are isolated with respect to flow, this approach simulates very-high-frequency saturated rock behaviour appropriate to ultrasonic laboratory conditions. At low frequencies, when there is time for wave-induced pore pressure increments to flow and equilibrate, it is better to find the effective moduli for dry cavities and then saturate them with the Gassmann low-frequency relations. This should not be confused with the tendency to term this approach a low-frequency theory, as inclusion dimensions are assumed to be much smaller than a wavelength.

The derivation of the DEM equation as given above (Norris,1985; Berryman, 1992) assumes that, as each new inclusion (or pore) is introduced, it displaces on average

either the host matrix material or the inclusion material probabilities $(1-y)$ and y, respectively. A slightly different derivation by Zimmerman(1984) assumed that when a new inclusion is introduced, it always displaces the host material alone. This leads to similar differential equations with $dy/(1-y)$ replaces by dy. The effective moduli predicted by the Zimmerman version of DEM are always slightly stiffer (for the same inclusion geometry and concentration) than the DEM equations given above. They both predict the same first-order terms in y but begin to diverge at concentrations above 10 percent. The dependence of effective moduli on concentration varies as $e^{-2y} = (1-2y+2y^2-...)$ for Zimmerman's equations, whereas it behaves as $(1-y)^2 = (1-2y+2y^2-...)$ for the Norris version. In general for a fixed inclusion geometry and porosity, the Zimmerman DEM effective moduli are close to the Kuster-Toksöz effective moduli and are stiffer than the Norris-Berryman DEM predictions, which in turn are stiffer than the Berryman self-consistent effective moduli. For spherical inclusions, the Zimmerman estimates fall above the Hashin-Shtrikman upper bound for high concentrations. The equations for the corresponding anisotropic media are complicated and we shall not include them here (Nishizawa, 1982; Hornby *et al.*, 1994).

References

Anderson, D. L., Minster, B., and Cole, D., 1974, The effects of orientation on seismic velocities: J. Geophys. Res., 79, 4011-4015.

Andrea, M., Sams, M. S., Worthington, M. H., and King, M. S., 1997, Predicting horizontal velocity from well data: Geophysical Prospecting, 45, 593-609.

Angeleri, G. P., and Carpi, R., 1982, Porosity prediction from seismic data: Geophysical Prospecting, 30, 580-607.

Archie, G. E., 1942, The electrical resistivity log as an aid in determining some reservoir characteristics: Petroleum Technology, V. 5, 54-62.

Berg, R., 1970, Method for determining permeability from reservoir rock properties: Gulf Coast Association of Geological Societies.

Berryman, J. P., 1980, Long-wavelength propagation in composite elastic media II. Ellipsoidal inclusions: Journal of Acoustic Society of America, 68, 1820-131.

Berryman, J. G., 1992, Single-scattering approximation for coefficients in Biot's equations of poroelasticity: Journal of Acoustic Society of America, 91, 551-571.

Berryman, J. G., 1995, Mixture theories for rock properties, in a Handbook of physical Constants: American Geophysical Union, Washington, D. C., 205-228.

Biot, M. A., 1956a, Theory of propagation of elastic waves in a fluid saturated porous solid. I. low frequency range: Journal of Acoustic Society of America, 28, 168-178.

Biot, M. A., 1956b, Theory of propagation of elastic waves in a fluid saturated porous solid. II. Higher-frequency range: Journal of Acoustic Society of America, 28,

179-191.

Biot, M.A., 1962, Mechanics of deformation and acoustic propagation in porous media: J. Appl. Phys., 33, 1482-1498.

Bourke, L., Delfiner, P., Trouiller, J. C., Fett, T., Grace, M., Luthi, S., Serra, O., and Standen, E., 1989, Using formation micros-canner image: The Technical Review, 37, 16-40.

Bristow, J. F., and Demenocal, P. R., 1982, Evaluation of the quality of geochemical log data in hole 798B: Scientific Results, 127, 1021-1036.

Brown, R. J. S., and Korringa, J., 1975, On the dependence of elastic properties of a porous rock on the compressibility of the pore fluid: Geophysics, 40, 608-616.

Chapman, M., 2001, The dynamic fluid substitution problem: 71th SEG Expanded Abstracts, 1708-1711.

Castagna, J. P., Batzle, M. L., and Eastwood, R. L., 1985, Relationships between compressional-wave and shear-wave velocities in clastic silicate rocks: Geophysics 50, 551-570.

Carman, P. C., 1956, The flow of gases through porous media: Academic Press, Paris, 198 pp.

Charlez, P., 1999, Rock Mechanics-theoretical fundamentals: Petroleum application, Vol. 2, C4.

Cheng, C. H., and Toksöz, M. N., 1979, Inversion of seismic velocity for pore aspect-ratio spectrum of a rock: Geophy. Res., 84, 7533-7543.

Chiaruttini, C., and Salemi, G., 1993, Artificial intelligence techniques in the analysis of digital seismograms: Computers and Geosciences, 19, 149-156.

Clark, I., 1979, Practical Geostatistics. Elsevier, London.

Corbett, P. W. M., Jensen, J. L., and Sorbie, K. S., 1998, A review of up-scaling and cross-scaling issue in core and log data interpretation and prediction: The Geological

Society. Special Publications, London, 136, 9-16.

Dai, H. C., 1995, Analysis of local earthquake data using artificial neural networks: Ph.D thesis, University of Edinburgh.

Demuth, H., and Beale, M., 1993, Neural network toolbox for use with MATLAB: The math works, Inc, Natick, Massachusetts.

Dvorkin, J., and Amos, N., 1998, Time-average equation revisited: Geophysics. Vol, 63, 2, 460-464.

Dunn, D. A., Biart, B. M., and Johns, M.,1986, Physical properties data: Deep sea drilling project Leg 93, Sites 603, 604 and 605: Init. Reports Deep Sea Drill. Proj., 93, 445-464.

Eshelby, J. D., 1957, The determination of the elastic field of an ellipsoidal inclusion, and related problems: Proc. Royal. Soc. London, 241, 376-396.

Gardner, G. H. F., Gardner, L. W., and Gregory, A. R., 1974, Formation velocity and density- The diagnostic basics for stratigraphic taps: Geophysics, 39, 770-780.

Gassmann, F., 1951, Uber die elastizitat porous media: Vier. der Natur. Gesellschaft in Zurich, 96, 1-23.

Gist, G. A., 1994, Interpretation of laboratory velocity measurements in partially gas-saturated rocks: Geophysics, 59,1100-1109.

Goldberg, I., and Gurevich, B., 1998, A semi-empirical velocity-porosity-clay model for petrophysical interpretation of P- and S-velocities: Geophysical Prospecting, 46, 217-285.

Graham, B., 1995, Russian-style formation evaluation: The Geological Society, London, P4, 65-74.

Greenberg, M. L., and Castagna, J. P., 1992, Shear-wave velocity estimation in porous rocks: theoretical formulation, preliminary verification and applications: Geophysical Prospecting, 40, 195-209.

Griggs, D. T., Jackson, D. D., Knopoff, L., and Shreve, R. L., 1975, Earthquake prediction: Modelling the anomalous Vp/Vs source region: Science, 187, 537-540.

Hamilton, E. L., Shumway, G., Menard, H. W., and Shipek, C., 1956, Acoustic and other physical properties of shallow-water sediments off San Diego: Journal of Acoustic Society of America, 28, 1-15.

Han, D. H., Nur. A., and Morgan. D., 1986, Effects of porosity and clay content on wave velocities in sandstones: Geophysics, 51, 2093-2107.

Hashin, Z., and Shtrikman, S., 1963, A variational approach to the theory of the elastic behaviour of multiphase materials: J. Mech. Phys. Solids, 11, 127-140.

Heslop, A., 1974, Gamma-ray log response of shaly sandstones: 15th Ann. Symp., Soc. Prof. Well log Analysts, Mcallen. Texas.

Hill, R., 1952, The elastic behaviour of crystalline aggregate: Proc. Physical Soc., London, A65, 349-354.

Hoenig, A., 1979, Elastic moduli of non-randomly cracked body: Int. J. Solids Struct., 15, 137-154.

Hornby, B. E., Schwartz, L. M., and Hudson, J. A., 1994, Anisotropic effective-medium modelling of the elastic properties of shales: Geophysics, Vol. 59, 1570-1583.

Hudson, J. A., 1981, Wave speeds and attenuation of elastic waves in material containing cracks: Geophysics, 64, 133-150.

Hudson, J.A., 1994, Overall properties of a material with inclusions or cavities: Geophysics, 117, 555-561.

Jensen, J. L., Lake, L. W., Corbett, P. W. M., and Goggin, D. J., 1997, Statistics for petroleum engineers and geoscientists, Prentice-Hall: New Jersey.

Kachanov, M., Tsukrov, I., and Shapes, B., 1994, Effective moduli of solids with cavities of various shapes: Applied Mechanical Review, 1, 151-174.

Keys, R. R., and Xu, S. Y., 2002, An approximation for the Xu-White velocity

model: Geophysics, 5, 1406-1414.

Klimentos, T., 1991, The effects of porosity-permeability-clay content on the velocity of compressional wave: Geophysics, 56, 1930-1939.

Krief, M., Garat, J., Stellingwerff, J., and Ventre, J., 1990, A petrophysical interpretation using the velocities of P- and S-wave (full-waveform sonic): The log Analyst, 31, 355-369.

Kukal, G. C., and Hill, R. E., 1986, Log analysis of clay volume: an evaluation of techniques and assumptions used in an Upper Cretaceous sand-shale sequence: 27th Ann. Symp., Soc. Prof. Well Log Analysts. Houston.

Kuster, G. T., and Toksöz, M. N., 1974, Velocity and attenuation of seismic waves in two phase media: Part 1, Theoretical formulation: Geophysics, 39, 587-606.

Lindseth, R. O., 1979, Synthetic sonic logs: A process for stratigraphic interpretation: Geophysics, 44, 3-26.

Liu, E., Hudson, J. A., and Pointer, T., 2000, Equivalent medium representation of fractured rocks: Geophys. Res., 105, 2981-3000.

Lovell, M. A., and Jackson, P. D., 1991, Electrical flow in rocks: The application of high resolution electrical resistivity core measurements: 33nd Annual logging Symposium, Texas.

Mareen, J. E., Skiba, F. F., and Price, H. S., 1961. An evaluation of the significance of permeability measurements: Petroleum Technology, 13, 739-744.

Marion, D., Nur, A., Yin, H., and Han, D., 1998, Compressional velocity and porosity in sand-clay mixtures: Geophysics, 57, 554-563.

Mark, S. S., and Martijn, A., 2001, The effect of clay distribution on the elastic properties of sandstones: Geophysical Prospecting, 49, 128-150.

McCormack, M. D., Dunbar, J. A, and Sharp, W. W., 1984, A case study of stratigraphic interpretation using shear and compressional seismic data: Geophysics, 49,

509-520.

Miller, S. L. M., and Stewart, R. R., 1990, Effects of lithology, porosity and shaliness on P- and S-wave velocity from sonic logs: J. Expl. Geophys., 26, 94-103.

Mukerji, T., and Mavko, G., 1994, Pore fluid effects on seismic velocity in anisotropic rock: Geophysics, 59, 233-244.

Murphy, R. B., 1969, On the meaning of precision and accuracy: U.S. Department of Commerce National Bureau of Standards Special publication, Vol. 300, 357-360.

Murphy, W., Reischer, A., and Hsu, K., 1993, Modulus decomposition of compressional and shear velocities in sand bodies: Geophysics, 58, 227-239.

Nations, J. E., 1974, Lithology and porosity from acoustic shear and compressional wave transit time relationships: Soc. Porf. Well Log Analysts 15th Annual Symp.

Nelson, P. H., 1994, Permeability-porosity relationship in sedimentary rocks: The Log Analyst, May-June,1994.

Nishizawa, O., 1982, Seismic velocity anisotropy in a medium containing oriented cracks- Transversely isotropic case: J. Phys. Earth, 30, 331-347.

Norris, A. N., Sheng, P., and Callegari, A. J., 1985, Effective-medium theories for two-phase dielectric media: J. Appl. Phys., 57, 1990-1996.

Nur, A., and Simmons, G., 1969, Stress-induced velocity anisotropy in rocks- An experimental study: J. Geophys. Res., 74, 6667.

Nur, A., Mavko, G., Dvorkin, J., and Gal, D., 1995, Critical porosity: The key to relating physical properties to porosity in rocks: 65th Ann. Int. Meeting, Soc. Expl. Geophys. Abstracts, 878-881.

O'Connell, R. J., and Budiansky, B., 1974, Seismic velocities in dry and saturated cracked solids: J. Geophys. Res., 79, 4626-4627.

Ohlsen, F., and MacBeth, C., 1998, Fracture estimation from walkway VSPs recorded in a deviated well: 1998 BGS Internal Reports.

Pardus, Y. C., Conner, J., Schuler, N. R., and Tatham, R. H., 1990, Vp/Vs and lithology in carbonate rocks: A case study in the scrip trend in southern Michigan: 60th SEG Expanded Abstracts, 169-172.

Parmmer, M. G., and Drack, E. D., 1996, Measurements of clay bound water and total porosity by magnetic resonance logging: The Log analyst, 1996.

Picket, G. R., 1963, Acoustic character logs and their applications in formation evaluation: J. Petr. Tech., 659-667.

Pirson, S. J., 1963, Handbook of well Log Analyst: Prentice-Hall Inc.

Rafavich, F., Kendall, C. H., and Todd, T. P., 1984, The relationship between acoustic properties and the petrographic character of carbonate rocks: Geophysics, 49, 1622-1636.

Raymer, L., Hunt, E. R., and Gardner, J. S., 1980, An improved sonic transit time to porosity transform: 21th SPLWA annual logging symposium.

Reuss, A., 1929, Berechnung der fliessgrense von mischkristallen auf grund der plastizitatsbedingung fur einkristalle: Zeitschrift fur Angewandte Mathematik and Mechanik, 9, 49-58.

Rider, M. H., 1986, The geological interpretation of well-logs: Blackie and Son Limited: 27th SPLWA annual logging symposiums.

Robertson, J. D., 1987, Carbonate porosity from S/P traveltime ratios: Geophysics, 52, 1346-1354.

Ruth, D., and Pohjoisrinne, T., 1993, The precision of grain volume porosimeter: The log analyst, 34, 29-36.

Sakhibgareev, R. S., 1989, Secondary alteration of reservoir during the formation and destruction of oil accumulations: Nedra, Leningrad.

Sams, M. S., and Andrea, M., 2001, The effect of clay distribution on the elastic properties of sandstones: Geophysical Prospecting, 49, 128-150.

Schlumberger, 1985, Sedimentary environments from wireline Logs: Houston, Schlumberger Well Services, Inc.

Schlumberger, 1994, Log interpretation manual and principles: Schlumberger well survives, Inc.

Serra, O., 1984, Fundamentals of well-log interpretation for the acquisition of logging data: Developments in Petroleum Science,15A. Elsevier, Holland.

Shakeel, A., and King, M. S., 1998, Acoustic wave anisotropy in sandstones with systems of aligned cracks: The Geological Society, Special publication,136, 173-183.

Sheng, P., 1991, Consistent modelling of the electrical and elastic properties of sedimentary rock: Geophysics, 56, 1236-1243.

Sheriff, R. E., and Geldart, L. P., 1982, Exploration seismology volume 1: History, theory and data acquisition, Cambridge University press.

Shumway, G., 1960, Sound speed and absorption studies of marine sediments by a resonant method, Part I: Geophysics, 25, 451-467.

Skopec, R. A., 1992, Recent advances in rock characterization: The Log Analyst, 33, 270-285.

Tao, G., and King, M. S., 1993, Porosity and pore structure from acoustic well-logging data: Geophysical Prospecting, 41, 435-451.

Theys, P., and Woodhouse, R., 1994, Society of professional well log analysts topical conference on quality: The Log Analyst, 35, 71-81.

Thomsen, L., 1986, Weak elastic anisotropy: Geophysics, 51, 1954-1966.

Timur, A., 1968, An investigation of permeability, porosity and residual water saturation relationships for sandstones reservoirs: The Log Analyst, 9, 4-10.

Vernik, L., 1997, Predicting porosity from acoustic velocities in siliciclastics- A new look: Geophysics, 62, 118-128.

Voigt, W.,1928, Lehrbuch der Kristallphysik: Teubner, Leipzig.

Wang, Z., and Nur, A., 1990, Dispersion analysis of acoustic velocities in rocks: Journal of Acoustic Society of America, 87, 2346-2395.

Wang, Z., and Nur, A., 1992, Seismic and acoustic velocities in reservoir rocks: Theoretical and model studies: Soc. Expl. Geophy., Geophysics Reprint Series, Vol. 2, 457.

Warren. J. B., 1961, A new analysis of attenuation in partially melted rock: J. Geophys. Res., 74, 4333.

White, J. E., 1965, Seismic Waves: Radiation, Transmission, and Attenuation: McGraw-Hill Book Co.

Willis, J. R., 1977, Bounds and self-consistent estimates for the overall properties of anisotropic composites: J. Mech. Phys. Solids, 25, 185-202.

Wilkens, R., Simmons, G., and Caruso, L., 1984, The ratio of Vp/Vs as a discriminant of composition for siliceous limestone: Geophysics, 49, 1850-1860.

Winkler, K.W., 1983, Contact stiffness in granular porous materials: Comparison between theory and experiment: Geophys. Res. Lett., 10, 1073-1076.

Winsauer, W. O., Shearin, H. M., Masson, P. H., and Williams, M., 1952, Resistivity of brine-saturated sands with the pore geometry: American Association of Petroleum Geologists, V. 36, 253-277.

Wood, A. W., 1930, A textbook of sound: The Macmillan Co., New York, 360 pp.

Worthington, P. F., 1989, Reservoir characterization at the microscopic scale: 1989 SPWLA Annual Logging Symposium, Canada.

Wyllie, M.R., Gregory, A.R., and Gardner, L.W., 1956, Elastic wave velocities in heterogeneous and porous media: Geophysics, 21, 41-70.

Xu, S., and White, R. E., 1995a, Pore-elasticity of elastic rock: A unified model: 36th Annual Logging Symposium, Paris, France.

Xu, S., and White, R. E., 1995b, A new velocity model for clay-sand mixtures:

Geophysical Prospecting, 43, 91-118.

Xu, S., and White, R. E., 1996, A physical model for shear-wave velocity prediction: Geophysical Prospecting, 44, 687-717.

Yan, J., 2002, Reservoir parameters estimation from well log and core data: a case study from the North Sea: Petroleum Geoscience, Vol. 8, 63-69.

Yan, J., Liu, E., and Li, X.-Y., 2000, Determine reservoir parameters from log and core data: A case study from the North Sea: 2002 EAGE, Expanded Abstracts, P-27.

Yan, J., MacBeth, C., and Li, X.-Y., 2000, Estimating pore aspect-ratio from velocity prediction: 62nd Internat. Mgt., Euro. Asso. Geosci. Eng., Expanded Abstracts, P-159.

Yan, J., Li, X.-Y., and Liu, E., 2002, Effects of pore aspect-ratios on velocity prediction from well-log data: Geophysical Prospecting, 50, 289-300.

Yangjian, O., 1995, Interpretation of well-logging and description of reservoir rocks: Petroleum Industry, P. 54-109.

Zamora, M., and Poirier, J. P., 1990, Experiment study of acoustic anisotropy and birefringence in dry and saturated Fontainebleau sandstone: Geophysics, 55, 1455-1465.

Zimmerman, R.W., 1984, The elastic moduli of a solid with spherical pores: New self-consistent method: Int. J. Rock Meth., Min. Sci. Geomech. Abs., 21, 339-343.

List of publications

1. Yan, J., 2002, Reservoir parameters estimation from well log and core data: a case study from the North Sea: *Petroleum Geoscience*, Vol. 8, 63-69.

2. Yan, J., Li, X.-Y., and Liu, E., 2002, Effects of pore aspect-ratios on velocity prediction from well-log data: *Geophysical Prospecting*, 50, 289-300.

3. Yan, J., Liu, E., Li, X.-Y., and Chapman, M., 2001, Estimation of reservoir parameters using an anisotropic dual porosity model: *71nd SEG, Expanded Abstracts*, 1796-1799,USA.

4. Yan, J., Liu, E., and Li, X.-Y., 2001, Seismic anisotropy in sediments with clay-sand mixture: *63rd EAGE, Expanded Abstracts,* P-039, Amsterdam, The Netherlands.

5. Yan, J., Liu, E., and Scrutton, R., 2001, Petrophysical inversion of well-log and VSP data using a dual porosity model: *63rd EAGE, Expanded Abstracts*, P-195, Amsterdam, The Netherlands.

6. Yan, J., Liu, E., and Scrutton, R., 2000, Using a Semi-Empirical Approach for Petrophysical Inversion: *70nd SEG, Expanded Abstracts,* 1899-1902, Canada.

7. Yan, J., Liu., E., and Li, X.-Y., 2000, Determining of Reservoir Parameters from Log and Core Data: *62nd Internat. Mgt., Euro. Asso. Geosci. Eng., Expanded Abstracts*, P-27, UK.

8. Yan, J., MacBeth, C., and Li., X.-Y., 2000, Estimating Pore aspect-ratio from Velocity Prediction: *62nd Internat. Mgt., Euro. Asso. Geosci. Eng., Expanded Abstracts,*

P-159, UK.

9. Liu, T. Y., and Yan, J., 1999, An Oil Reservoir that Contains Pyrite: Low Resistivity Response and Interpretation: *1999 Canadian Petroleum Society*, P. 145-158.

Statistics of PhD study

PhD programs:

- Post -Graduate study starting on 08 January 1998 (Edinburgh University)
- English qualification passed on 22, June 1998 (EPTB: 45.4, IELTS: 6.5)
- PhD registration on 01, July 1998 (Edinburgh University)
- PhD transfer report on 03 October 1999 (Edinburgh University)
- PhD work completed on 31 August 2001 (Edinburgh University and BGS)
- Employed by oil and gas company on 03 September 2001 (Fugro-Robertson, UK)
- Thesis submitted on 14 February 2003 (Edinburgh University)
- Oral examination passed on 26 August 2003 (Edinburgh University)

PhD supervisors:

- Dr. Roger Scrutton (The University of Edinburgh)
- Dr. Enru Liu (British Geological Survey)
- Professor Xiang-Yang Li (British Geological Survey)
- Professor Colin MacBeth (In my first year PhD, Heriot-Watt University)

PhD viva examiners:

- Internal examiner: Professor Ian Main (The University of Edinburgh)
- External examiner: Dr. Shi-Yi Zheng (The Heriot-Watt University)

Publications during PhD:

- 2 publishes in "Petroleum Geoscience" and " Geophysical Prospecting"
- 7 publishes in SEG and EAGE
- 3 Reports in EAP (1999, 2000)

This thesis statistics:

- Thesis pages: 262
- Total text words: 48,528
- Figures: 93
- Tables: 15
- References items used: 116

Reservoir parameters estimation from well log and core data: a case study from the North Sea

Jun Yan

British Geological Survey, West Mains Road, Edinburgh EH9 3LA, Scotland, UK and Department of Geology and Geophysics, University of Edinburgh, UK (e-mail: yjun@bgs.ac.uk)

(Present address: Robertson Research International Ltd, Llandudno LL30 15A, UK)

ABSTRACT: In this paper we present an integrated approach to derive reservoir parameters from core and well-log data in clay–sand mixtures. This method is based on matching core and log data, and the linear and non-linear regressions are then used to build respective relationships between core and log data to determine formation parameters such as porosity, shale volume, clay content, permeability and fluid saturation. This information is then fed into a velocity prediction model to estimate seismic parameters such as elastic moduli, shear wave velocity and anisotropy coefficients. Finally, we test the method on real data from the North Sea and show that reservoir parameters can be accurately predicted.

KEYWORDS: *log calibration, reservoir characteristic, velocity logging, sand–shale ratio, North Sea*

INTRODUCTION

Various theoretical models have been proposed to model the fluid–solid interaction in reservoir rocks for the purposes of lithology prediction and fluid substitution (e.g. Gassmann 1951; Kuster & Toksöz 1974; Brown & Korringa 1975; Han *et al.* 1986; Tao & King 1993 and Gist 1994). However, most of these theories have some drawbacks and can only be applied under certain conditions, and some require specific parameters that are not easily obtainable. Recently, Xu & White (1995, 1996) proposed a method for velocity prediction in clay–sand mixtures; this model uses the time-average equation (Wyllie *et al.* 1956) to estimate porosity and clay content in consolidated formations, and the theory of Kuster & Toksöz (1974) and Gassmann models (1951) are used to predict elastic moduli and P- and S-wave velocities. Because of the use of the time-average equation, this model cannot be used in rocks with a loose matrix, or in the case of containing fluids, such as gas or oil.

In this paper, we propose an alternative approach that provides a satisfactory prediction for reservoir parameters and is applicable to both consolidated and unconsolidated formations. Our model is based on the calibration of core and well-log data. First, well-log and core data are edited and corrected before they can be used. Second, linear and non-linear regression are employed to derive porosity, shale volumes, clay contents, permeability and fluid saturation, so that the effects of lithology, fluid, temperature, pressure and other factors can be compensated for. Finally, we modify the original model developed by Xu & White (1995, 1996) which is based on the theories of Kuster & Toksöz (1974) and Gassmann (1951), to predict compressional and shear-wave velocitie sas well as anisotropy coefficient in clay–sand mixtures. A basic flow chart describing the above procedure is given in Figure 1. Our method requires log data and core data as inputs, and the outputs are reservoir parameters. We test our method on field data from a North Sea reservoir and obtain satisfactory results.

CALIBRATION OF LOG AND CORE DATA

In general, the available well-log data include deep- and medium-induction, spherically focused log, bulk density, interval transit time, gamma-ray, caliper and spontaneous potential log data. The core data derived from the laboratory measurements include porosity, shale content, permeability and fluid saturation. In order to calibrate well-log and core data, the following steps are necessary.

Log depth correction

Some well logs exhibit anomalous, and possibly incorrect data, so it is important to apply quality control when one edits and reconstructs well-log curves. Logging instrument responses are adversely affected by breakout of wall-rock during drilling, and stick-and-pull as logging tools are winched up the well. Gamma-ray log instrument response, in particular, is affected where the borehole is enlarged and distorted by shale breakout. In addition, there are difficulties in correlating depths among various separately run surveys. The depth errors of curves in our study are matched to within a range of 0.7 ft (0.2 m).

Deviated well correction

For a deviated well, the following equations are taken for deviation correction from measured depth to true vertical depth (Yangjian 1995).

$$\begin{aligned} Z_2-Z_1&=\int_{Z_1}^{Z_2} dZ=\int_{h_1}^{h_2} \cos\delta \cdot dh, \\ Z_2-Z_1&=\int_{\delta_1}^{\delta_2} \frac{h_1-h_2}{\delta_2-\delta_1} \cos\delta \cdot d\delta \\ &=\frac{h_1-h_2}{\delta_2-\delta_1}(\sin\delta_1-\sin\delta_2), \end{aligned} \tag{1}$$

where h_1 and h_2 are the start and end depth for a deviated hole, $Z_1$and Z_2 are relative vertical depth intervals, $\delta_1$and δ_2 are the

1354-0793/02/$15.00

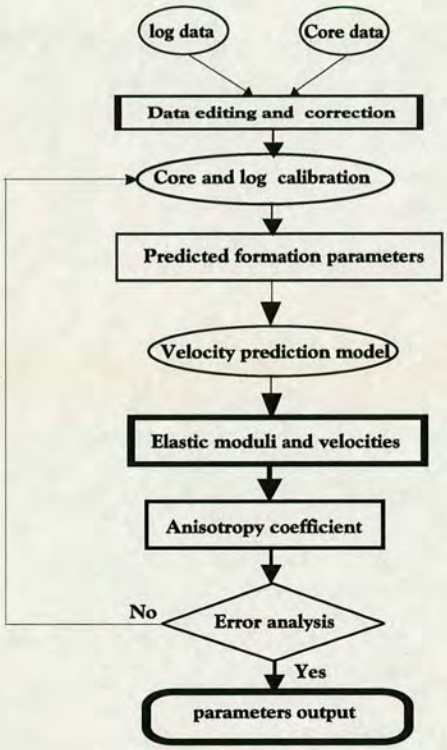

Fig. 1. Work flow for reservoir parameters estimation using well-log data and core data.

angles of hole deviation. We use points 1, 2...*M* to divide the deviated hole into *M*-1 intervals, then do the above correction. Figure 2 is a sketch showing correction of deviated depth into true vertical depth.

Rebuild log curves

When log data at certain depths show abnormal variations or are lost, a correction is normally done by finding a new relationship between erroneous log data and other logs for porosity (*Por*), shale content (V_{sh}) or other log curves (log1, log2...). The new log curves (log*) will then be used to replace the abnormal interval (Schlumberger 1994) based on the following relationship.

$$log^*=f(Por,\ V_{sh},\ log1,\ log2...) \qquad (2)$$

Curve normalization

For a multi-well data, it is very common to have different log readings for the same formation or rock types in the same area. A standard formation (normally, a shale formation) is defined to compare with the same log data in the same formation, and a normalization method is then used to correct log readings. Figure 3 is an example of correction of sonic log curve by the polynomial trend surface analysis; we can see that three unusual points have been found using this method.

Core re-position

To integrate log and core data, a comparison of depth can be made between log and core measurements. A bar-line plot is drawn on the basis of density or porosity measured in core samples to calibrate the density log in the same depth interval. Depth from the density log is regarded as accurate and can be used to calibrate core depth (see Fig. 4).

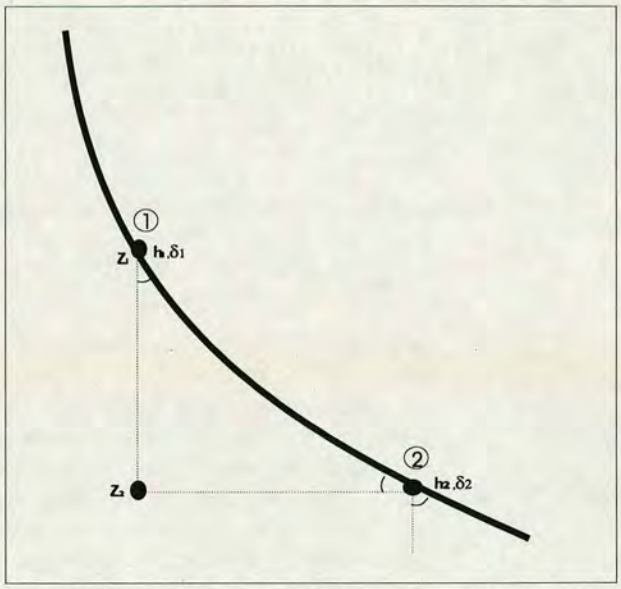

Fig. 2. Correction of a deviated hole from measured depth to true vertical depth.

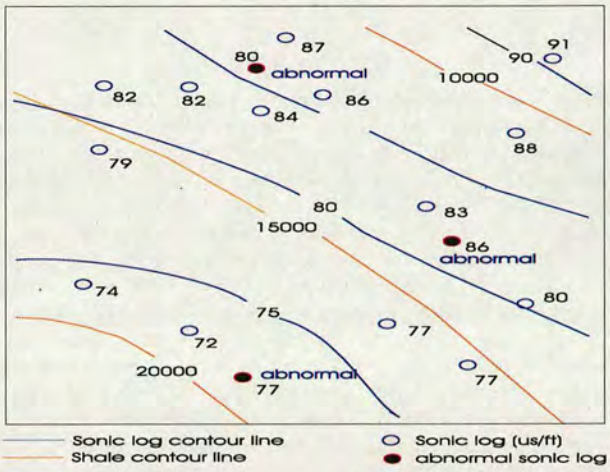

Fig. 3. Correction of sonic reading in the shale formation by polynomial trend surface analysis. Three unusual sonic points (values) can been found.

Core matching

The vertical resolution from core data is normally higher than that from log data. A smoothing technique is used here to match the vertical resolution of core data with log data, and the distance from the source to the receiver of a log instrument is used to decide a suitable filtering method. Figure 5 shows a comparison of cross-plot analysis for core and log data. We find that using a three-point filtering technique gives a better linear fit than the result before filtering, and that the scattering is much smaller.

ESTIMATION OF RESERVOIR PARAMETERS

Once core to log calibration is completed, a linear or non-linear regression method is employed to estimate the reservoir parameters, and the procedures are described below.

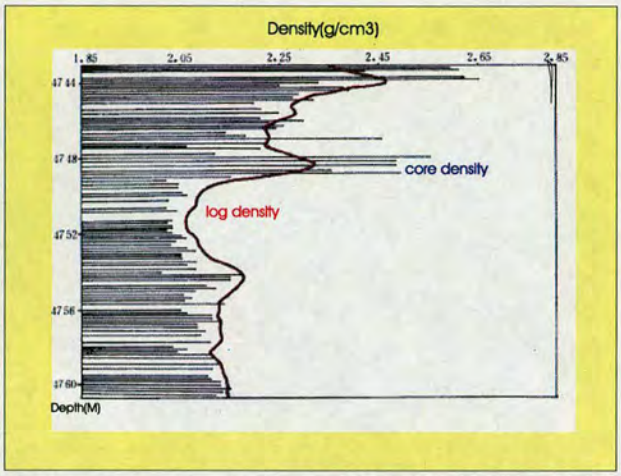

Fig. 4. Core re-position (density), which corrects the depth point of core samples based on the density log (in g cm^{-3}).

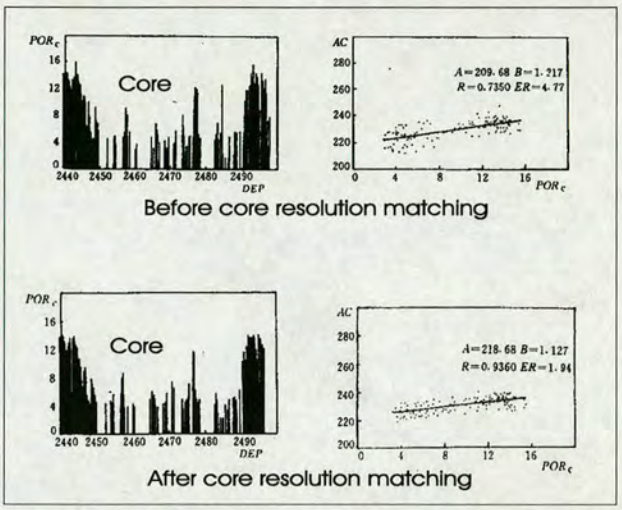

Fig. 5. Filtering comparison between core data (porosity) with log data (sonic log), the use of three-point filtering gives a much better linear relationship.

Porosity

Extracting porosity from log requires information on lithological fractions, core data and experimental information from the laboratory, such as the properties of the grain matrix and pore fluid. In this research, a simple and powerful approach of core-log calibration is proposed to estimate porosity, and a linear regression is used to determine the relationship of core porosity to log density by geostatistical method.

$$\rho = -m \cdot \varphi + a, \tag{3}$$

where φ is the total effective porosity from core analysis in the laboratory, ρ is the density log, and both m and a are lithological coefficients to be determined on the basis of the least squares regression. The example below uses 79 and 74 core porosity samples respectively to build the relationship of core porosity to density log and core porosity to sonic velocity log. Their equations are as follows (see Fig. 6a, b).

$$\varphi = -65.359\,\rho + 174.85 \tag{4}$$

(for density log), and

$$\varphi = 0.8532\,DT - 45.242 \tag{5}$$

(for sonic log).

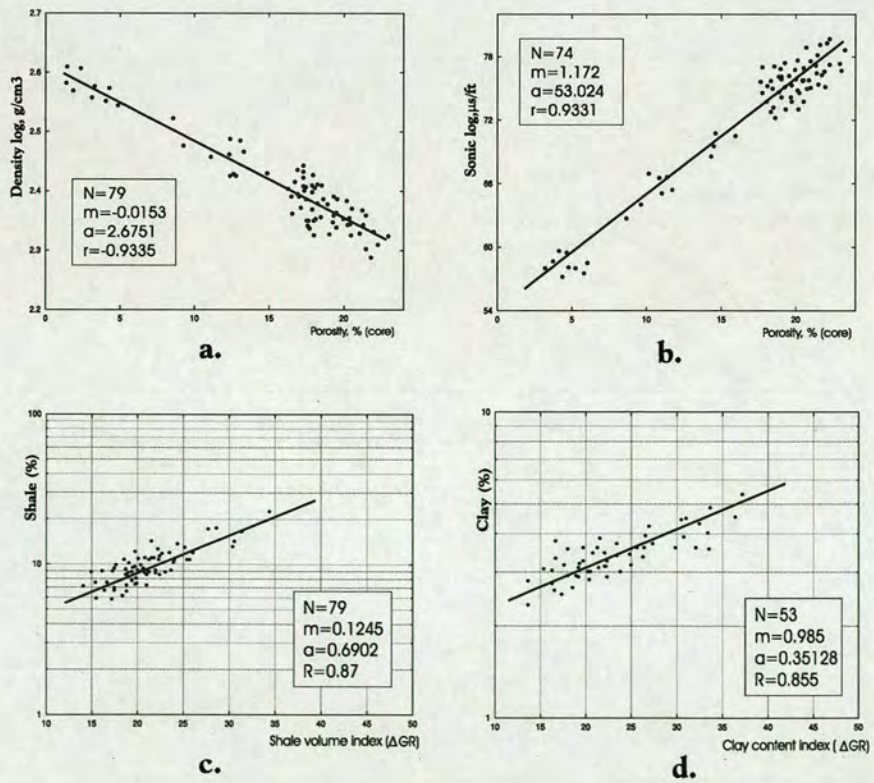

Fig. 6. The relationship of core with log: (**a**) core porosity and density log; (**b**) core porosity and sonic velocity log; (**c**) shale volume and index of gamma-ray log; (**d**) clay content and index of gamma-ray log.

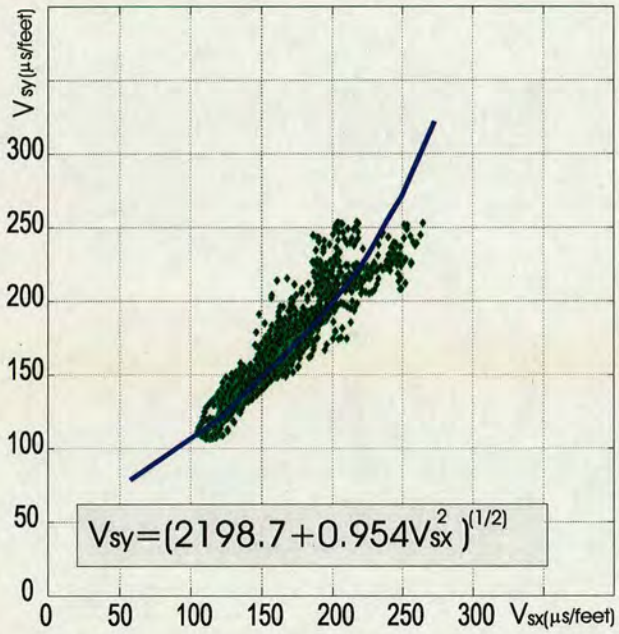

Fig. 7. Relationship of S wave velocities in the X and Y directions (data are from a North Sea reservoir).

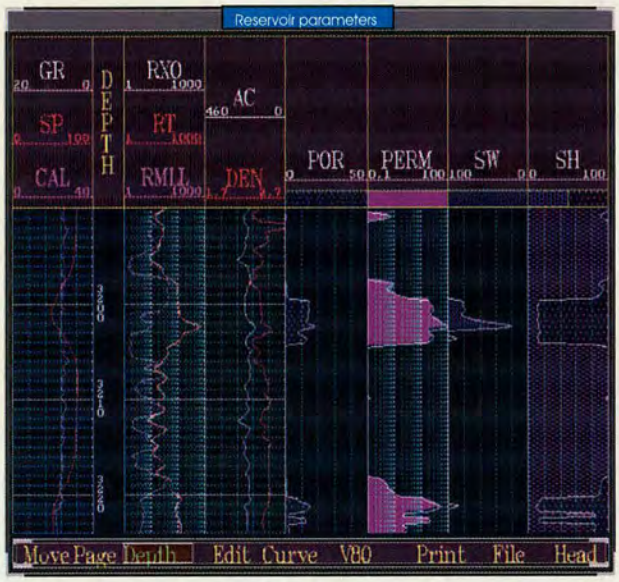

Fig. 8. Predicted formation parameters by well-log and core data calibration: porosity (panel 4), permeability (panel 5), water saturation (panel 6) and shale volume (panel 7).

When the shale value is more than 15%, a cut-off value will be used to correct porosity; the following equation is used for shale correction (Yangjian 1995).

$$\varphi^*=\frac{\rho_{ma}-\rho}{\rho_{ma}-\rho_w}-(V_{sh}-V_{cut\text{-}off})\frac{\rho_{ma}-\rho_{sh}}{\rho_{ma}-\rho_w}, \quad (6)$$

where φ^* is the corrected porosity, ρ_{sh} is the shale density, V_{sh} is the shale content, ρ_{ma} is the matrix density, ρ_w is the fluid density and $V_{cut\text{-}off}$ is the shale cut-off value.

Shale volume

When grain size is less than 0.063 mm it is defined as shale volume in this study area, and the shale volume may be obtained in the laboratory. The relationship between shale volume V_{sh} and gamma-ray log (GR) is determined using a non-linear regression which is similar to porosity equations based on a geostatistical method (see Fig. 6c).

$$V_{sh}=10^{c*\Delta GR+d} \quad (7)$$

where c and d are coefficients to be determined from this non-linear regression, and the shale volume index (ΔGR) can be estimated by gamma-ray values (GR).

$$\Delta GR=\frac{GR-GR_{clay}}{GR_{sand}-GR_{clay}} \quad (8)$$

Clay content

When grain size is less than 0.03 mm it is defined as clay content. Using a method similar to the shale volume (equation 7), (see Fig. 6d), the clay content V_{cl} is found to be

$$V_{cl}=10^{e*\Delta GR+f}, \quad (9)$$

where both e and f are non-linear regression coefficients to be determined.

Table 1. *Real equations for estimation of reservoir parameters*

Predicted output	Equations or parameters	Description
Porosity (density log)	$\varphi_{=-65.359\,\rho+174.85}$	$N=79$, $R=0.934$, $Err=1.25$
Porosity (sonic log)	$\varphi = 0.8532DT - 45.242$	$N=74$, $R=0.933$, $Err=1.25$
Shale volume	$V_{sh} = 10^{1.245*\Delta GR+0.6902}$	$N=79$, $R=0.870$, $Err=1.43$
Clay content	$V_{cl} = 10^{0.985*\Delta GR+0.35128}$	$N=53$, $R=0.855$, $Err=1.35$
Permeability	$K = 8.7096 \cdot 10^{\varphi^{5.78}/V_{sh}^{1.37}}$	$N=53$, $R=0.834$, $Err=1.28$
Water saturation	$S_w = \left(\frac{0.902 \cdot R_w}{R_t \cdot \varphi^{2.142}}\right)^{1/1.7}$	$m=2.142$, $n=1.7$, $a=1$, $b=0.902$
Effective elastic moduli	K, μ V_p and V_s	By velocity model
Anisotropy coefficient	$m_t = \frac{V_{f=}-\sqrt{2198+0.954 \cdot V_{f=}^2}}{\overline{V_s}}$	$\overline{V_t} = \frac{V_{f\perp}+V_{f=}}{2}$

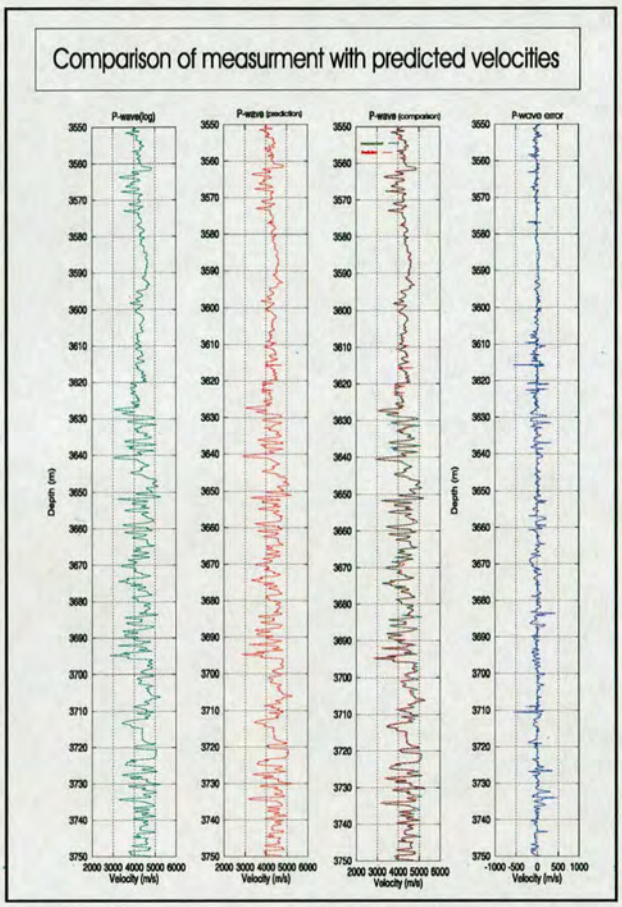

Fig. 9. Comparison of measured P-wave velocity and predicted P-wave velocity with velocity error.

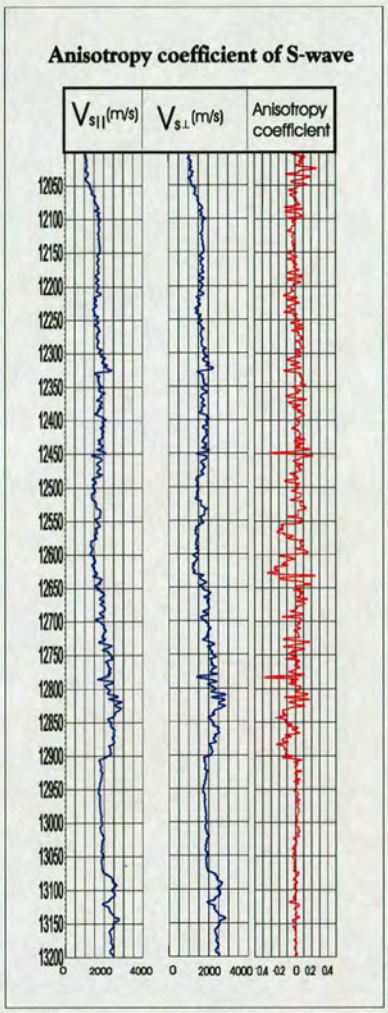

Fig. 10. Using shear-wave velocities for X and Y directions to estimate anisotropy coefficient in anisotropic porous rocks.

Permeability

Porosity and shale content are believed to control permeability in clay–sand mixtures. According to the core analysis in the laboratory, the following regression for permeability (K) is found to be appropriate for this study area

$$K=G\cdot 10^{4}\frac{\varphi^{g}}{V_{sh}^{b}}, \tag{10}$$

where G, g and b are the coefficients to be determined by non-linear regression.

Saturation

Resistivity and porosity can be obtained from log curves, using analysis results of water saturation and analysis of the electrical properties of rock in the laboratory, the saturation coefficients may be determined; they include a_1, b_1, n and m. The water and oil saturation are estimated based on Archie's (1942) formula as follows

$$S_w=\left(\frac{a_1\cdot b_1\cdot R_w}{R_t\cdot\varphi^{m}}\right)^{\frac{1}{n}}, \tag{11}$$

where S_w is water saturation, R_t is the true resistivity of the formation (ohm-m), R_w is the water resistivity (ohm-m) and φ is the porosity.

Elastic moduli and velocities

The model proposed by Xu & White (1995, 1996) based on the scattering theory of Kuster & Toksöz (1974) is used to compute elastic moduli (including K_d and μ_d, bulk and shear moduli for dry frame respectively, K_m and μ_m, bulk and shear moduli for mixture, K_f and μ_f, and bulk and shear moduli for fluid). P-wave and S-wave velocities are then calculated using Gassmann's (1951) equations:

$$V_p=\left\{\frac{1}{\rho_b}\left[K_b+\frac{4}{3}\mu_d+\frac{\left(1-\frac{K_c}{K_m}\right)^2}{\frac{(1-\varphi)}{K_m}+\frac{\varphi}{K_f}-\frac{K_c}{K_m}}\right]\right\}^{\frac{1}{2}}, \tag{12}$$

$$V_s=\left(\frac{\mu_d}{\rho_b}\right)^{\frac{1}{2}}, \tag{13}$$

where $\rho_b=\rho_m(1-\varphi)+\rho_f\varphi$, ρ_b, ρ_m and ρ_f, and are the density of bulk, matrix and fluid, respectively.

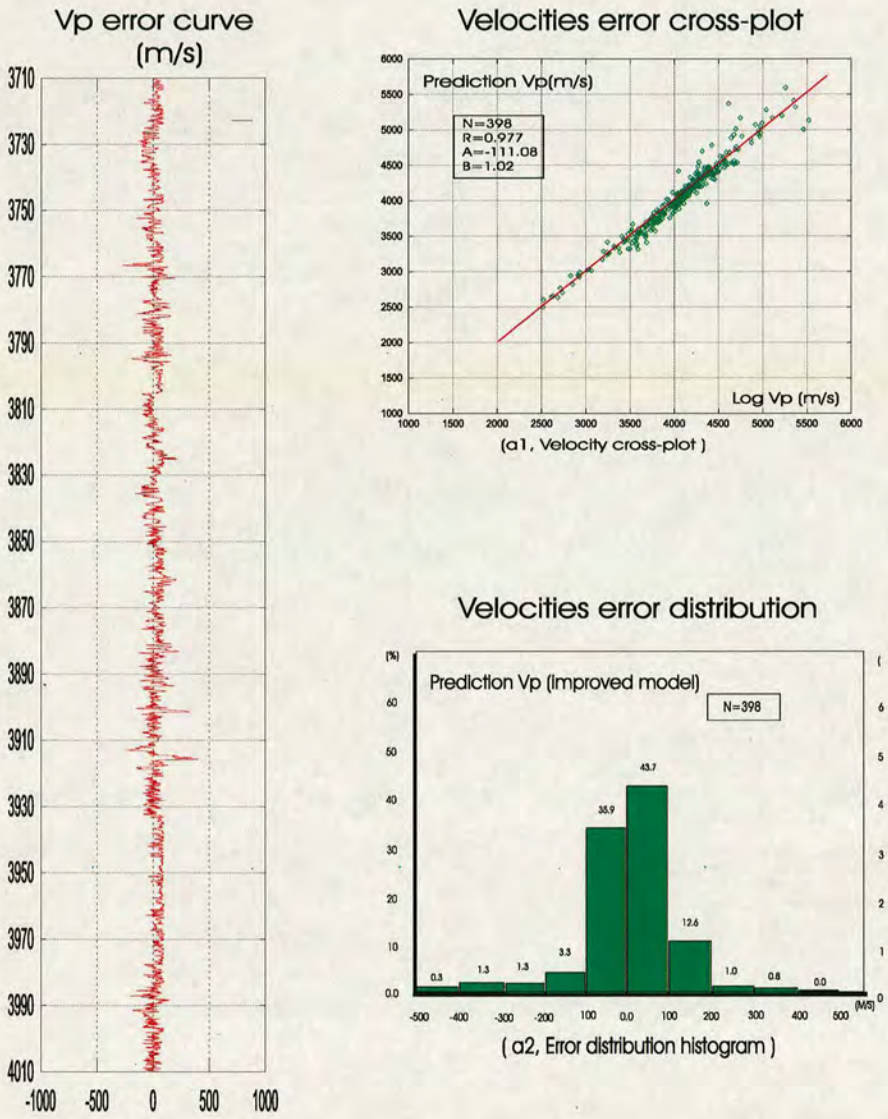

Fig. 11. Error analysis of P wave velocity using cross-plot and histogram plot between measured and predicted velocities.

Anisotropy coefficient

From elastic moduli we can also predict shear-wave velocity, and the anisotropy coefficient in turn can be estimated using the velocity relationship of shear-wave in the horizontal and plane directions, combined with the dipole sonic log (see Fig. 7). The anisotropy coefficient (m_s) is determined using the following equations:

$$V_{s\perp}=\sqrt{j+k\cdot V_{s=}^2}, \tag{14}$$

$$m_s=\frac{V_{s=}-V_{s\perp}}{\overline{V_s}}, \tag{15}$$

where $V_{s=}$ and $V_{s\perp}$ are the shear-wave velocities in the horizontal and plane directions, $\overline{V_s}$ is the average shear-wave velocity, and j and k are the regression coefficients on the basis of Figure 7.

RESULTS AND APPLICATIONS

The real field data – well-log data, core measurements with electrical property results – were from an oil field in the North Sea. The log data consisted of caliper, gamma-ray, density, resistivity and sonic logs, and the core measurements included porosity, shale volume, clay content and rock-electric analysis for water or oil saturation.

Using the relationship between the core and log data based on the field data, we can build a sequence of equations for reservoir parameter prediction (see Table 1 and Fig. 6). As an example, the density log was chosen to predict porosity, and we can see that the number of core samples (N) is 79, the correlation coefficient (R) is 0.934 and the rms error (Err) is 1.25 (Table 1). The regression coefficients and the relationship of core porosity and density log can be found from Figure 6a.

Using the methods mentioned above, others reservoir parameters, such as shale, clay, permeability, saturation and anisotropy coefficient, can also be determined. The elastic moduli and velocities can be obtained from the theoretical velocity model (equations 12 and 13). Table 1 summarized the application equations for the data we study. Figure 8 shows a parameters prediction result, which includes porosity (panel 4), permeability (panel 5), water saturation (panel 6) and shale volume (panel 7). Figure 9 shows a result of predicted velocity with the comparison of measurement and prediction (panel 3), and error curve (panel 4). Figure 10 is the output of estimated

anisotropy coefficient (m_s) based on shear wave velocities and Equations 14 and 15.

In order to prove predicted accuracy, Figure 11 shows an error analysis for compressional wave velocities. Comparing the measured and the predicted velocities in the cross-plot and error distribution (Fig. 11), we find that the scattering of prediction with measurement is quite small, and the correlation coefficient of regression (R) is over 0.97, which gives a satisfactory result for velocity prediction.

CONCLUSIONS

This paper presents an integration technique from well-log and core data to determine reservoir parameters. These parameters include reservoir porosity (φ), shale volume (V_{sh}), clay content (V_{cl}), water saturation (S_w), permeability (K), as well as seismic parameters such as elastic moduli (K_m, μ_m, K_d, μ_d) and anisotropy coefficients (m_s). The approach is applicable to both consolidated and unconsolidated formations, and can provide satisfactory results for reservoir characterization. The key procedures of this approach are summarized.

1. To establish the basis for calibration of core-log data, the first important step involves editing of log curves and preliminary processing of cores, so that the log and core data may be matched and integrated successfully.
2. The selection of geostatistical methods (different regressions technique) decides the accuracy of parameter prediction to compensate the effects of lithology and other factors.
3. The combination of reservoir parameters with a seismic velocity model (such as that in Xu & White 1995) extended the use of well-log, core and seismic data for reservoir characterization with an integration of petrophysics and mathematical modelling.

The application to the oil field data from a North Sea reservoir shows that this approach can satisfactorily predict reservoir and seismic parameters in porous rocks, and this is confirmed by error analysis performed on the data.

I am grateful to Dr Enru Liu (BGS), Dr Xiang-Yang Li (BGS), Dr Roger Scrutton (University of Edinburgh), Prof. Colin MacBeth (Heriot-Watt University) and Mr Frank Ohlsen (Jason Geosystems) for their valuable guidance and useful discussion. Thanks also go to Phillips Petroleum Company, Norway for providing some of the field data, and for permission to publish the data. This work was supported by the Natural Environment Research Council of UK and the industrial sponsors of the Edinburgh Anisotropy Project (EAP): Agip, BGS, BPAmoco, Chevron, Conoco, Norsk Hydro, PGS, Phillips, Schlumberger, Shell, Texaco, Trade Partners UK and Veritas DGC. This paper is published with the approval of the director of the British Geological Survey (NERC) and the EAP Sponsors.

REFERENCES

Archie, G.E. 1942. The electrical resistivity log as an aid in determining some reservoir characteristics. *Petroleum Technology*, **5**, 54–62.

Brown, J.S. & Korringa, J. 1975. On the dependence of the elastic properties of a porous rock on the compressibility of the pore fluid. *Geophysics*, **40**, 608–616.

Gassmann, F. 1951. Elasticity of porous rocks. *Vierteljahrschrift der Naturforschenden gesellschaft in Zurich*, **96**, 1–21.

Gist, G.A. 1994. Interpretation of laboratory velocity measurements in partially gas-saturated rocks. *Geophysics*, **59**, 1100–1109.

Han, D.H., Nur, A. & Morgan, D. 1986. Effects of porosity and clay content on wave velocities in sandstones. *Geophysics*, **51**, 2093–2107.

Kuster & Toksöz, M.N. 1974. Velocity and attenuation of seismic waves in two phase media: part 1: Theoretical formulation. *Geophysics*, **39**, 587–606.

Schlumberger 1994. *Log interpretation manual and principles*, **1**. Schlumberger Well Survives, Inc., Houston.

Tao, G. & King, M.S. 1993. Porosity and pore structure from acoustic well-logging data. *Geophysical Prospecting*, **41**, 435–451.

Wyllie, M.R., Gregory, A.R. & Gardner, L.W. 1956. Elastic wave velocities in heterogeneous and porous media. *Geophysics*, **21**, 41–70.

Xu, S. & White, R.E. 1995. A new velocity model for clay–sand mixtures. *Geophysical Prospecting*, **43**, 91–118.

Xu, S. & White, R.E. 1996. A physical model for shear-wave velocity prediction. *Geophysical Prospecting*, **44**, 687–717.

Yangjian, O. 1995. *Interpretation of well-logging and description of reservoir rock*. The Petroleum Industry Press (China), 54–109.

Received 18 September 2000; revised typescript accepted 30 July 2001

Geophysical Prospecting, 2002, 50, 289–300

Effects of pore aspect ratios on velocity prediction from well-log data

Jun Yan,[1,2]* Xiang-Yang Li[2] and Enru Liu[1]

[1]*British Geological Survey, Murchison House, West Mains Road, Edinburgh EH9 3LA, and* [2]*Department of Geology and Geophysics, University of Edinburgh, West Mains Road, Edinburgh EH9 3JW, UK*

Received June 2000, revision accepted October 2001

ABSTRACT

We develop a semi-empirical model which combines the theoretical model of Xu and White and the empirical formula of Han, Nur and Morgan in sand–clay environments. This new model may be used for petrophysical interpretation of P- and S-wave velocities. In particular, we are able to obtain an independent estimation of aspect ratios based on log data and seismic velocity, and also the relationship between velocities and other reservoir parameters (e.g. porosity and clay content), thus providing a prediction of shear-wave velocity. To achieve this, we first use Kuster and Toksöz's theory to derive bulk and shear moduli in a sand–clay mixture. Secondly, Xu and White's model is combined with an artificial neural network to invert the depth-dependent variation of pore aspect ratios. Finally these aspect ratio results are linked to the empirical formula of Han, Nur and Morgan, using a multiple regression algorithm for petrophysical interpretation. Tests on field data from a North Sea reservoir show that this semi-empirical model provides simple but satisfactory results for the prediction of shear-wave velocities and the estimation of reservoir parameters.

INTRODUCTION

Many theoretical models have been proposed in an attempt to establish a link between formation parameters and compressional- and shear-wave velocities in reservoir rocks (e.g. Kuster and Toksöz 1974; Xu and White 1995, 1996). These theoretical models are very useful for reservoir parameter estimations. However, they were formulated under certain assumptions, which means that they can be used only under certain conditions or they require specific input parameters. On the other hand, a number of authors have derived empirical relationships between velocity and porosity or other rock parameters (e.g. Han, Nur and Morgan 1986; Klimentos 1991; Goldberg and Gurevich 1998). Although these empirical models may give a reasonably good estimation of shear-wave velocities or other reservoir parameters, most models are applicable only under certain conditions, and they can be used for velocity prediction only over a very limited range of porosity and clay contents.

In the theoretical and empirical models mentioned above, both porosity and clay content are treated as important factors in the determination of the elastic parameters of the rock, but the varying pore aspect ratio (the ratio of the short to the long axis for sand grain and clay particles) is considered to be constant over the whole depth range. In fact, the porosity and clay content are not the only parameters affecting velocities; there are also other factors. For example, pore geometry (the pore aspect ratio) can explain most of the scatter in the porosity–velocity relationship, which has been considered to be an important parameter in velocity prediction (Xu and White 1995).

Xu and White (1995, 1996) not only considered that the aspect ratio can explain most of the scatter in porosity–velocity relationships, but also pointed out that the aspect ratio may significantly affect elastic moduli and velocities. Unfortunately, aspect ratios cannot easily be obtained from field data or laboratory measurements. Although Cheng and

*E-mail: yjun@bgs.ac.uk

Toksöz (1979) showed how to estimate aspect ratios from laboratory measurements, it is still difficult to obtain an independent estimate of aspect ratios from well-log data. Therefore, fixed values of aspect ratios are often used in velocity prediction or numerical modelling (Xu and White 1995, 1996; Goldberg and Gurevich 1998). On the other hand, Han *et al.* (1986) used an empirical formula to express the relationship between porosity, clay content and velocity, based on real field data and laboratory measurements. Han *et al.* (1986) showed that the empirical formula can give a satisfactory velocity prediction, even if the formation contains a loose matrix or fluids. Unfortunately, the weakness of Han *et al.*'s (1986) model is that the empirical equations produce obvious errors in varying lithology and thin formations.

In order to overcome these weaknesses and to develop a general model for velocity prediction, we propose a semi-empirical model which combines the theoretical model of Xu and White (1995, 1996) and the empirical formula of Han *et al.* (1986) via the aspect ratio. Our model differs from previous models in at least two aspects: (i) our model allows depth-dependent variation of pore aspect ratios which are inverted from well-log data using an artificial neural network; (ii) our model combines the two well-known models of Xu and White (1995) and Han *et al.* (1986) and can be used for reservoir parameter estimation. We first give a brief review of the theoretical background and problems of velocity and lithology prediction, then we present details of our approach, followed by a field data example from the North Sea.

THEORETICAL BACKGROUND AND THE PROBLEMS

Kuster and Toksöz (1974) developed a model for a two-phase medium which relates porosity and pore aspect ratios to P- and S-wave velocities. The derivation of the model is based on scattering theory. According to this model, the pores are assumed to be spheroidal and their shapes are characterized by their aspect ratios. Xu and White (1995, 1996) proposed a model to predict shear-wave velocities based on the Kuster and Toksöz (1974) model, differential effective medium (DEM) theory and Gassmann's (1951, 1952) theory. The Xu and White (1995, 1996) model divides the total pore space into two parts – one associated with sand grains and the other associated with clay platelets – and it requires density and gamma-ray logs as inputs. Additional inputs include the elastic moduli of the sand grains, clay particles and pore fluid, porosity, clay content and two aspect ratios (one for sand grains and one for clay platelets). The bulk and shear moduli for dry frame (K_d and μ_d), mixture (K_m and μ_m) and fluid (K_f and μ_f) are calculated on the basis of Kuster and Toksöz's (1974) model and DEM theory, and then Gassmann's (1951, 1952) equations are used for prediction of P- and S-wave velocities (V_P and V_S) in saturated rock. The main relationships between pore aspect ratios and elastic moduli are given by

$$K_d = \frac{K_m + 4A\mu_m}{1 - 3A}, \tag{1}$$

$$\mu_d = \mu_m \frac{1 + B(9K_m + 8\mu_m)}{1 - 6B(K_m + 2\mu_m)}, \tag{2}$$

$$A = \frac{1}{3}\left(\frac{K_f - K_m}{3K_m + 4K\mu_m}\right) \sum_{l=s,c}^{2} \phi_l T_{iijj}(\alpha), \tag{3}$$

$$B = \frac{1}{25} \frac{(\mu_f - \mu_m)}{\mu_m(3K_m + 4\mu_m)} \sum_{l=s,c}^{2} \phi_l \left(T_{ijij}(\alpha) - \frac{T_{iijj}(\alpha)}{3}\right), \tag{4}$$

where K_d and K_m are the bulk moduli of dry frame and mixture, μ_d and μ_m are the corresponding shear moduli of the dry frame and mixture, ϕ is the total effective pore space occupied by sands and clays, K_f and μ_f are the bulk moduli and shear moduli of fluid, and $T_{iijj}(\alpha)$ and $T_{ijij}(\alpha)$ are both functions of the aspect ratios for sand and clay (see the Appendix).

In the equations above, porosity can be divided into components, one associated with the clay fraction and the other with the sand fraction, and these fractions have different aspect ratios ($T_{iijj}(\alpha)$ and $T_{ijij}(\alpha)$). As aspect ratios cannot be measured directly from field data, in previous applications the aspect ratios were always chosen to be fixed. These fixed values are often used for large depth intervals of up to several hundred metres. In Xu and White's (1995, 1996) model, the aspect ratio for sand-related pores is set at 0.1 and for clay-related pores it is 0.03 (see Table 1).

Table 1 Rock properties (Xu and White 1995)

Lithology	T_P (μ s/m)	T_S (μ s/m)	Density (g/cm^3)	Aspect ratio
Sandstone	171	256	2.65	0.12
Clay	341	584	2.45	0.03
Limestone	161	311	2.60	–
Salt	220	348	2.00	–
Brine	623	–	1.10	–

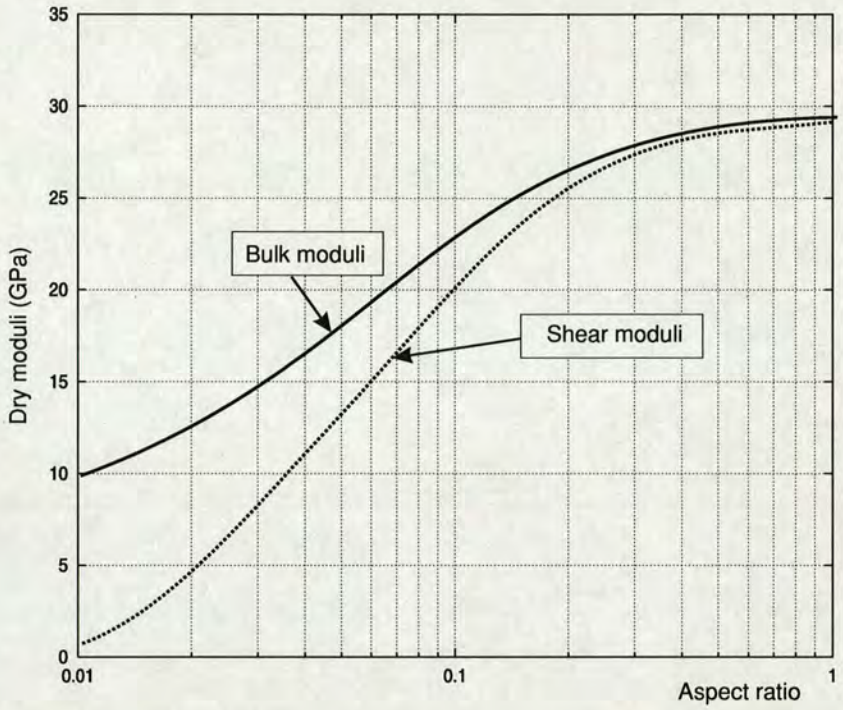

Figure 1 The relationship between aspect ratio and elastic moduli based on Kuster and Toksöz's (1974) model.

In fact, pore aspect ratios in real rock are not expected to be uniformly distributed, and their variations obviously affect the determination of elastic moduli. Figure 1 shows an example of the variation of elastic moduli with pore aspect ratio using the model of Kuster and Toksöz (1974). We can see that the variations of the elastic moduli with aspect ratio are not linear, which indicates that the use of fixed aspect ratios may be suitable only for small depth intervals at which lithology may be regarded as stable.

Pore aspect ratios are affected by many factors, such as fluid, lithology, formation pressure, microcracks, the environment of deposition and the diagenesis history, etc., and related discussions have already been given by Nur and Simmons (1969), Brown and Korringa (1975) and Murphy (1982). When porosity is low or microcracks are abundant, pore pressure plays a more important role than other factors. Figure 2 shows the aspect ratio variation with the experimental pressure (following Nur and Simmons 1969; Sun and Goldberg 1998). The results suggest that initially the samples were predominantly populated with cracks (0.45% and 0.2% pore porosity). As the differential pressure reached about 10 MPa, cracks in the sample continued to collapse until almost all the original cracks with small aspect ratios were closed and the large aspect ratio pores and cracks became predominant with an average aspect ratio as high as 0.01. When the pressure reached 20 Pa, large aspect ratio cracks continued to collapse and pores began to deform into cracks. When the pressures reached 40 MPa, almost all the original cracks were fully closed and pores were deformed to become cracks with a low aspect ratio. Above 40 MPa, newly formed cracks deformed the rock and at 70 MPa, the average aspect ratio was low. At pressures of 100 MPa and above, most new cracks were closed, and the lowest aspect ratio was reached.

When using conventional methods to determine aspect ratio directly, there are two major difficulties:

1 It is usually assumed that the pore shape is perfectly ellipsoidal, which can hardly be expected in real rock.

2 Describing the hypothetical pore spaces associated with sand and clay using just two fixed aspect ratios over a large depth range is obviously a simplification.

In order to model velocities of sedimentary rocks accurately, the influence of lithology, fluid, fractures, pressure and other factors should be considered.

DATA PREPARATION

Firstly, the well-log and core data are used to build a petrophysical model to derive the porosity and clay content on the basis of core-to-log calibration. Secondly, we use Xu

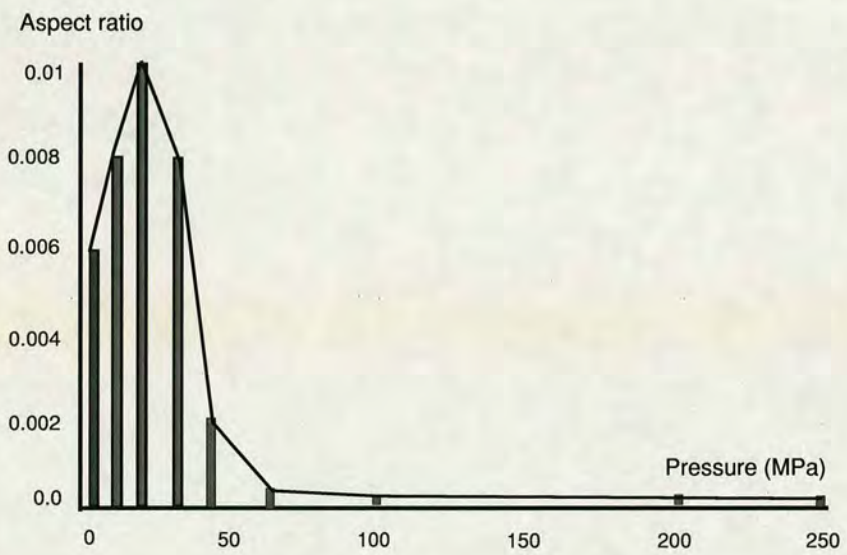

Figure 2 The relationship between aspect ratio and pressure, derived from granite velocity measurements (Nur and Simmons 1969; Sun and Goldberg 1997).

and White's (1995, 1996) model to estimate the elastic moduli and we combine it with a back-propagation neural network (BPNN) to invert the pore aspect ratios directly for sand grains and clay minerals. Finally, we use these variable aspect ratios to link with Han *et al.*'s (1986) empirical equations by means of a multiple regression algorithm and obtain a new semi-empirical equation for petrophysical interpretations. The main procedures are summarized as follows:

Core-to-log calibration

To decrease systematic computing errors, we cannot use the original log data as input directly, and the following corrections are necessary for data preparation.

1 *Log depth correction.* The depth correction for each log curve is matched to within a range of 0.2 m (0.7 ft).

2 *Correction of deviated well.* Deviation of the well is corrected from the measured depth to the true vertical depth.

3 *Log curve editing.* Log data editing enables the curves with abnormal variations to be corrected or replaced by new curves. Note that careful quality control is necessary to edit the log curves.

4 *Core reposition.* A histogram plot, drawn on the basis of core data, is used to calibrate the density log in the same depth interval.

5 *Core matching.* A smoothing technique is used to match the vertical resolution of the core data with the log data.

Estimating porosity and clay content

The estimation of porosity from the density log requires information about lithological fractions in the rock, such as the density of the grain matrix and the pore-fluid density. Here we propose a simple and useful approach, based on core analysis in the laboratory, to estimating porosity, using the following formula (Yang 1995):

$$POR = aDEN + b, \tag{5}$$

where POR denotes porosity, DEN denotes density log and the coefficients a and b are determined using a least-squares regression method (see Fig. 3, left).

Because the P-wave velocity initially increases with increasing clay content as clay particles fill the pore space, Xu and White (1995) suggested that a maximum P-wave velocity is reached when the clay content is equal to the initial porosity of the clean sandstone (more than 20–40% clay content). To obtain an accurate porosity value, we propose a cut-off value for clay content. This is because when the clay content is higher than 20–40%, equation (5) cannot be used to estimate porosity from the density log and, in this case, a cut-off value should be used to obtain the accurate porosity (Wyllie, Gregory and Gardner 1956; Yang 1995). The equation used is

$$POR_c = \frac{DEN_{ma} - DEN}{DEN_{ma} - DEN_w} - (V_{cl} - CUT_{off})\frac{DEN_{ma} - DEN_{cl}}{DEN_{ma} - DEN_w} \times 0.01, \tag{6}$$

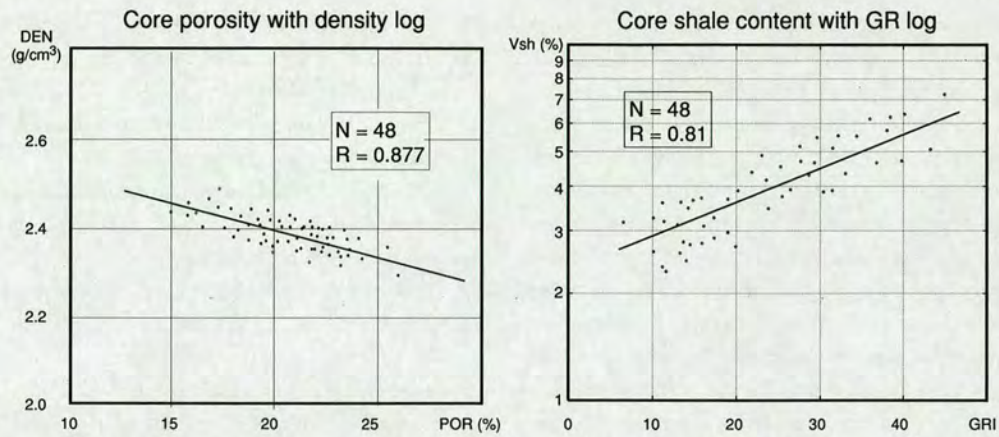

Figure 3 Core calibrated log using a regression method. Left: relationship between core porosity obtained from core measurements in the laboratory and density log. Right: relationship between clay content obtained from core measurements and gamma-ray log.

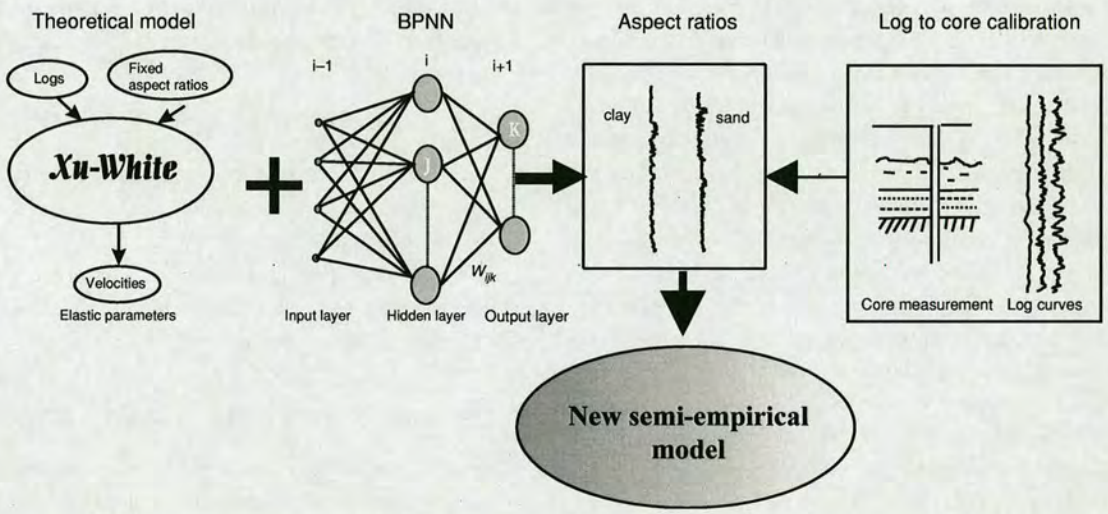

Figure 4 Schematic diagram showing the flow chart of the semi-empirical model for petrophysical interpretation.

where POR denotes the corrected porosity, DEN_{cl} denotes clay density, V_{cl} denotes clay content, DEN_{ma} denotes matrix density, DEN_w denotes fluid density and CUT_{off} denotes the cut-off value of the clay content.

Gamma-ray (GR) counts are the measurements most widely used to estimate clay fraction. Given a linear relationship between clay content and total radioactive counts, the clay volume index (GRI) can be estimated from the gamma-ray values:

$$GRI = \frac{(GR - GR_s)}{(GR_c - GR_s)}. \tag{7}$$

Based on the value of the GRI and the measurement of cores in the laboratory, a relationship between V_{cl} and GRI is proposed,

$$V_{cl} = 10^{c(GRI)+d}, \tag{8}$$

where V_{cl} denotes the clay content, GR_s and GR_c are the gamma-ray counts for sand and clay, respectively, and the coefficients c and d are determined using a least-squares regression method (see Fig. 3, right).

Estimation of pore aspect ratios using a neural network

We use the combination of Xu and White's (1995) model and a back-propagation neural network or BPNN to invert pore aspect ratios over a depth range (Dai and MacBeth 1994). Figure 4 illustrates this new approach. The aim of this

method is firstly to obtain an independent estimation of the aspect ratios from the log data and the P-wave velocity, and then to obtain the relationship between the aspect ratio and other reservoir parameters, such as porosity and clay content. Finally a semi-empirical model for shear-wave velocity prediction is proposed.

The BPNN is based on simple linear processing elements exhibiting complex non-linear behaviour, and it can learn to recognize patterns in data and to develop its own generalizations. The results can be used to integrate the response of many influencing factors. The output error propagates backwards through the network to modify the link weights of the network, and the mapping relationship between the input and desired output vectors is encoded in the weights with a distributed form. The main procedure is summarized as follows:

1 The measured P-wave velocities from the sonic log are used as the desired (expected) values. The predicted P-wave velocities from Xu and White's model are used as the estimated values. The first depth point is chosen and then by using Xu and White's model to compare the velocity errors, a value of aspect ratio is determined from the minimum velocity error. This value is used as a sample (standard value) of the aspect ratio in the neural network. This procedure is repeated and the value of the aspect ratio is determined at the next depth, until enough samples have been obtained.

2 Suitable samples of aspect ratios are regarded as the standard values, and are used as the desired values of the aspect ratios for the network.

3 Suitable log data (such as *GR*, *SP*, *DEN*) with their related depths are chosen as inputs for the network.

4 A suitable weight value is given to this network.

5 The network is run for training aim.

6 The error is calculated, based on the predicted aspect ratios and desired aspect ratios.

7 The weight values are adjusted to reduce the error between predicted values and expected values.

8 After correction of the weight values, the network starts to compute the whole error, which is the total sum of the errors of a single training pattern.

9 If the error is larger than the permitted range, steps (3) to (7) are repeated to reduce the error.

The process is iterated many times. Once the error signal is reduced and it reaches the expected accuracy, the iteration is stopped, and a BPNN is established. To calculate the average value of the error (ΔE_n) for the aspect ratio, the input pattern is first introduced into an initially randomized BPNN and the weights values are adjusted, based on the previously determined values, until all training sets are exhausted, and it is necessary to adjust the studying rate (η) during training. This gives

$$\Delta w_{ijk}(n+1) = \eta \delta_{jk} o_{ij} + \alpha \Delta w_{ijk}(n), \tag{9}$$

where Δw_{ijk} is the variation of weight connection, η is the learning rate, α is the momentum rate, o_{ij} is the output and δ_{ik} is the change in error.

The work flow diagram for the inversion of the pore aspect ratios, based on the neural network, is shown in Fig. 5, and the result is shown in Fig. 6.

NEW SEMI-EMPIRICAL FORMULAE

Once the procedure of data preparation is completed, a linear or non-linear regression method is employed to

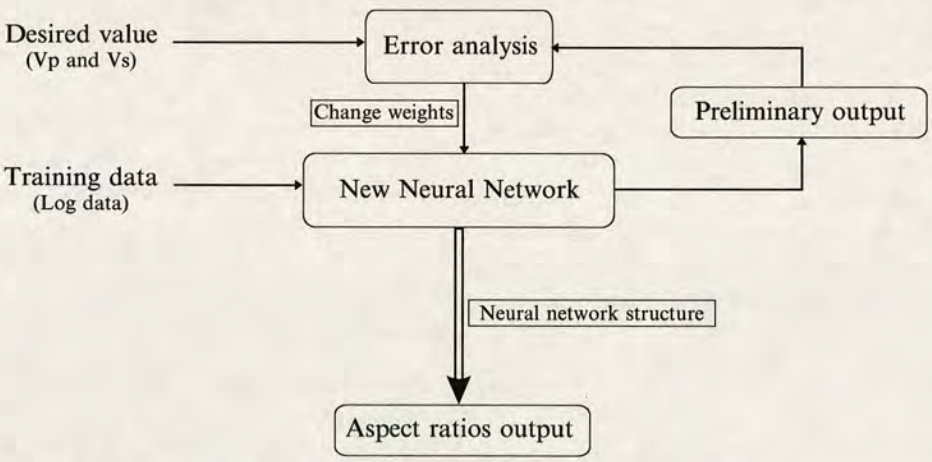

Figure 5 The work flow diagram for inversion of the aspect ratio using a back-propagation neural network.

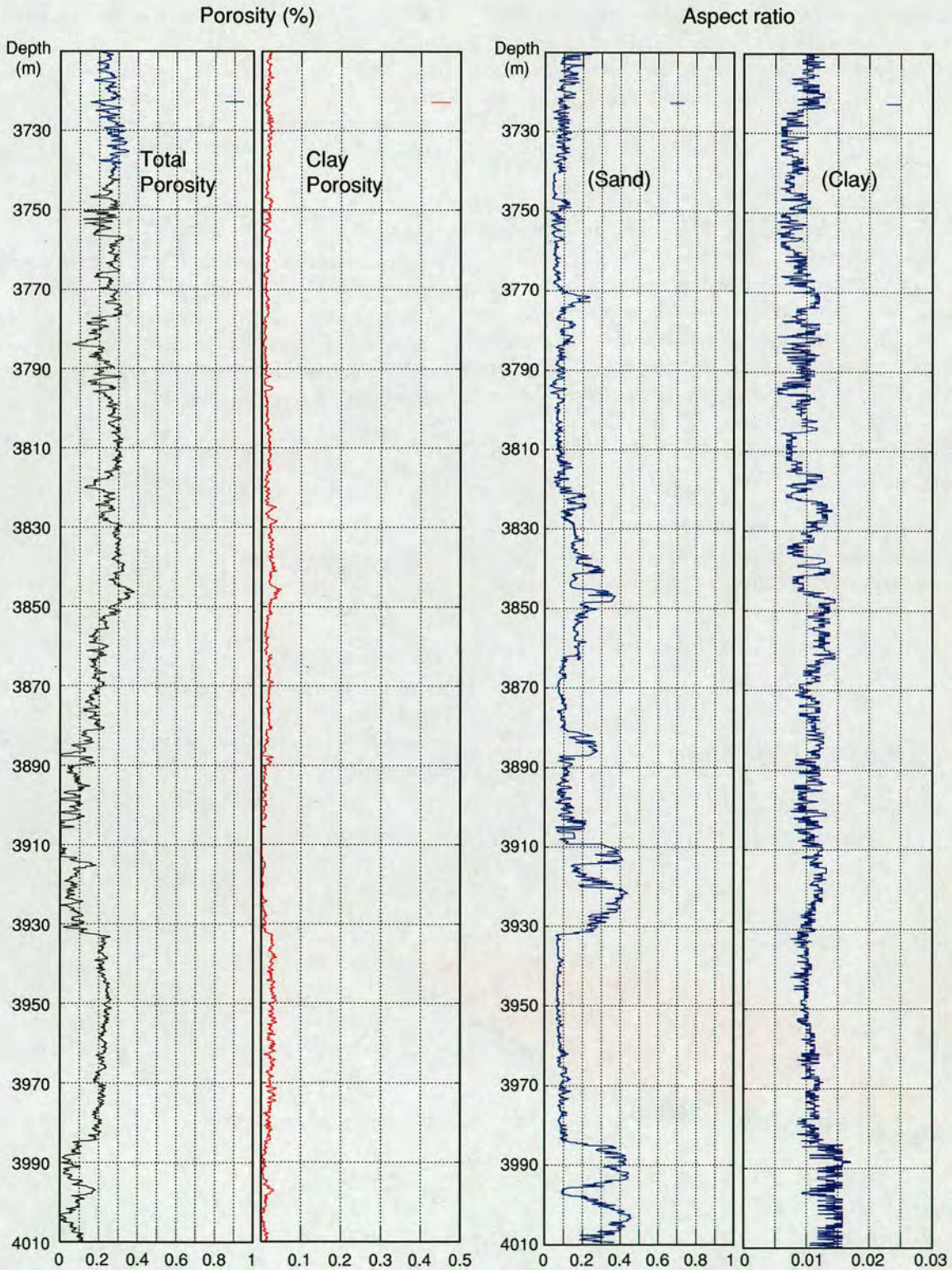

Figure 6 Aspect ratio output obtained with the back-propagation neural network.

estimate porosity and clay content. To estimate the effects of porosity (ϕ) and clay content (V_{cl}) on velocity (V), Han *et al.* (1986) used a least-squares linear fitting to a series of laboratory data and found the best fit to a polynomial in the form of

$$V = a + b\phi + cV_{cl}. \tag{10}$$

This equation indicates that P- and S-wave velocities are a linear function of porosity and clay content, and that they increase with increase in porosity and clay content. Han *et al.*'s (1986) model may be used to predict P- and S-wave velocities, but it will not give accurate results in varying lithology and thin formations. To improve this, we propose a forward segmentation multiple regression method to extend the empirical model of Han *et al.* (1986), and we combine it with the theoretical model of Xu and White (1995, 1996) via the aspect ratio as follows:

$$V = f[\phi, V_{cl}, T(\alpha)]. \tag{11}$$

Thus velocity, porosity, clay content and aspect ratio are combined as the whole regression elements, and we then obtain optimum fitting equations of the P-wave velocity (V_P) and the S-wave velocity (V_S) as follows:

$$V_P = A_0 + A_1\phi + A_2V_{cl} + \sum_{l=s,c} A_lT_l(\alpha) \tag{12}$$

and

$$V_S = B_0 + B_1\phi + B_2V_{cl} + \sum_{l=s,c} B_lT_l(\alpha), \tag{13}$$

where $\sum_{l=s,c} T_l(\alpha)$ are aspect ratios of sand grains and clay particles, respectively, and the coefficients A_0, A_1, A_2, A_l and B_0, B_1, B_2, B_l are determined by a multiple linear regression procedure. Figure 7 shows the relationship between sand aspect ratio, porosity and clay content when velocity values are fixed.

APPLICATIONS TO FIELD DATA

We applied our method to the field data from a North Sea reservoir. Well-log data contained caliper, gamma-ray, density, self-potential and dipole sonic. Core data consisted of porosity (ϕ) and clay content (V_{cl}). After application of a multiple linear regression to equations (12) and (13), we obtained the following equations:

$$V_P = 4.198 - 4.17\phi - 1.64V_{cl} + [2.99T_s(\alpha) - 4.05T_c(\alpha)], \tag{14}$$

$$V_S = 3.199 - 3.24\phi - 1.42V_{cl} + [2.64T_s(\alpha) - 3.32T_c(\alpha)], \tag{15}$$

with

$$\phi = -0.607DEN + 1.53, \tag{16}$$

$$V_{cl} = 10^{0.985(GRI)+0.35128}, \tag{17}$$

where V_P denotes P-wave velocity (in km/s), V_S denotes S-wave velocity (in km/s), ϕ denotes the effective porosity, ρ denotes density log (in g/cm^3), V_{cl} denotes clay content, $T_s(\alpha)$ denotes the aspect ratio for sand grains and $T_c(\alpha)$ denotes the aspect ratio for clay particles.

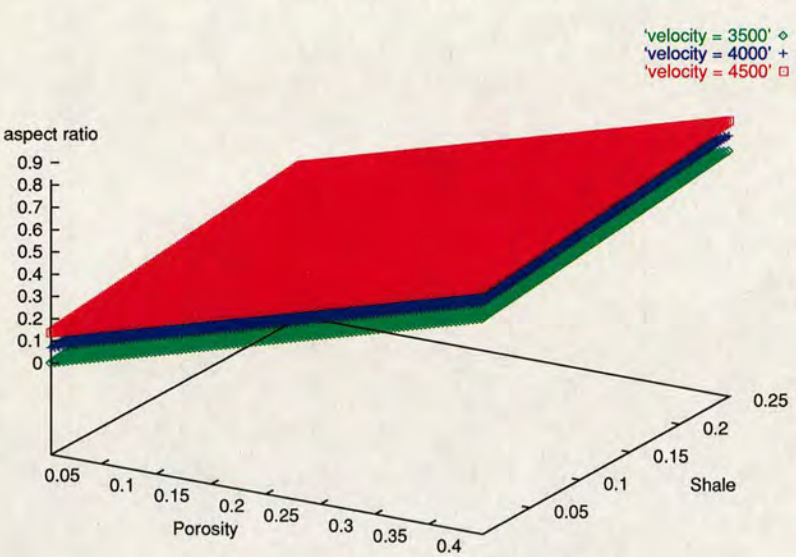

Figure 7 The relationships between aspect ratio, porosity and clay content for velocities of 3500, 4000 and 4500 m/s.

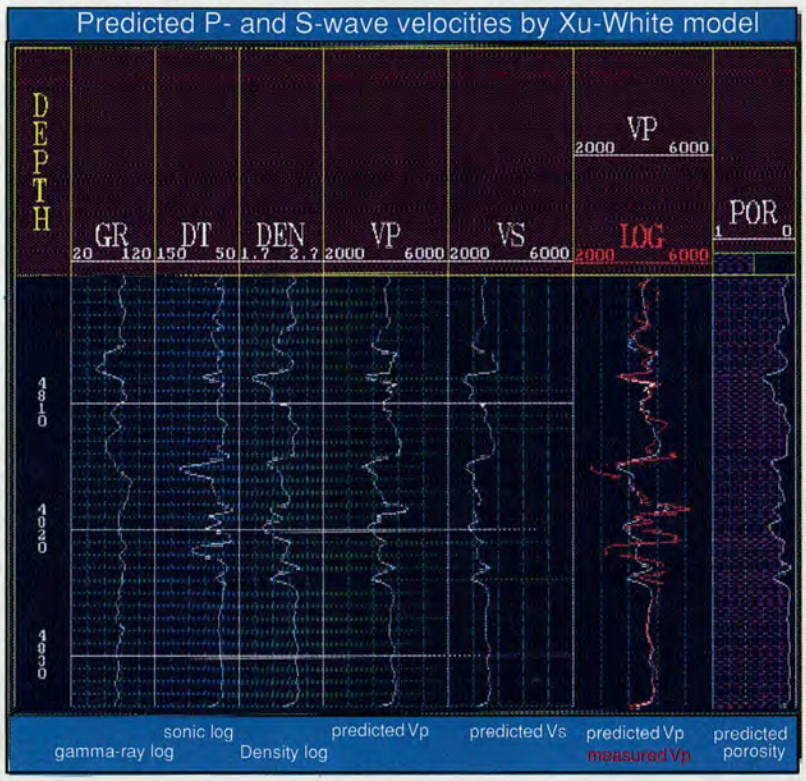

Figure 8 Predicted velocities using Xu and White's (1995, 1996) model. Panel 1: Gamma-ray log. Panel 2: P-wave sonic log. Panel 3: Density log. Panel 4: Predicted V_P using Xu and White's model. Panel 5: Predicted V_S using Xu and White's model. Panel 6: Comparison of predicted and measured V_Ps; Panel 7: Predicted porosity.

Figures 8 and 9 show the variation of P- and S-wave velocities using Xu and White's model and our semi-empirical model, respectively. Compared with Xu and White's (1995, 1996) model for the prediction of P- and S-wave velocities, we can conclude that our semi-empirical model gives a satisfactory result for velocity prediction (see Fig. 9). Figure 10 shows the errors between predicted and measured P- and S-wave velocities for Han *et al.*'s (1986) empirical model, Xu and White's (1995) model and our semi-empirical model. Figure 11 shows the cross-plot of measured and predicted velocities, and we find that our approach gives a satisfactory result. We can also see that the scattering is much smaller than that from Xu and White's (1995) model and from Han *et al.*'s (1986) model, and the correlation coefficient of regression (R) is larger than the other approaches. The results show that our semi-empirical model is at least as accurate as the other two models.

CONCLUSIONS

We have developed an approach to velocity prediction and reservoir parameter estimation. Our method is based on a combination of the theoretical model of Xu and White (1995, 1996) and the empirical model of Han *et al.* (1986). The model uses pore aspect ratios to characterize the compliance of the sand and clay components, so that the effects of lithology, fluid saturation, temperature, pressure and other factors can be compensated. This approach can be used for S-wave velocities and to invert pore aspect ratios from well-log and core data. The validity of this approach is confirmed by the analysis of field data from a North Sea reservoir.

ACKNOWLEDGEMENTS

J.Y. thanks Colin MacBeth (Heriot-Watt University) and Roger Scrutton (Edinburgh University) for their valuable guidance. We are grateful to Shiyu Xu (Exxon Mobil), Frank Ohlsen (Jason Geosystems), and Hengchang Dai (BGS) for useful discussions. We thank Dr Diephuis (Associate Editor) and one anonymous reviewer for their constructive comments which greatly improved the readability of this paper. Our thanks also go to Brackin A. Smith of the Phillips Petroleum Company, Norway for providing the field data. This work was supported by the Natural Environment Research Council (UK) and the industrial

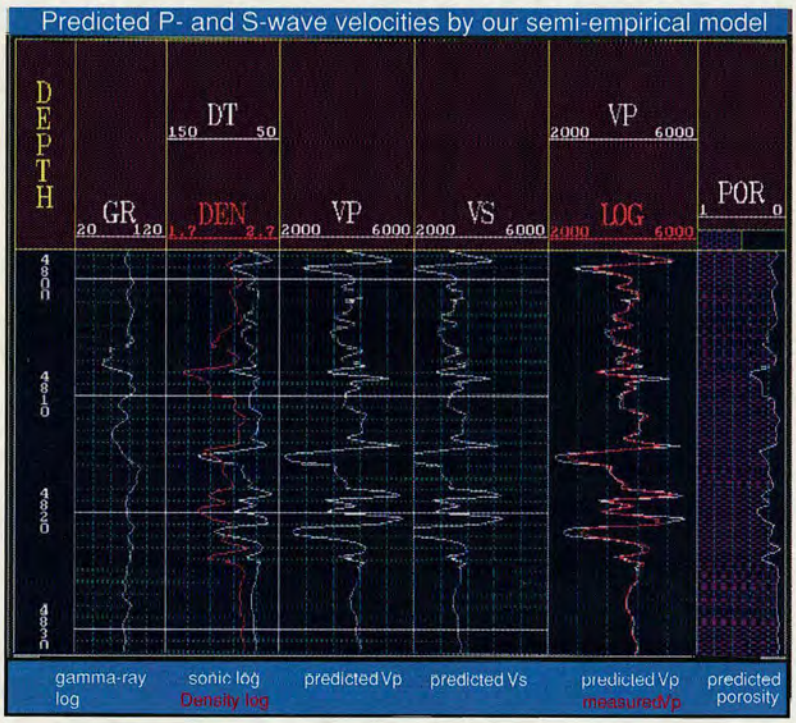

Figure 9 Predicted velocities using our semi-empirical model. Panel 1: Gamma-ray log. Panel 2: P-wave sonic log and density log. Panel 3: Predicted V_P using our semi-empirical model. Panel 4: Predicted V_S using our semi-empirical model. Panel 5: Comparison of predicted and measured V_PS. Panel 6: Predicted porosity.

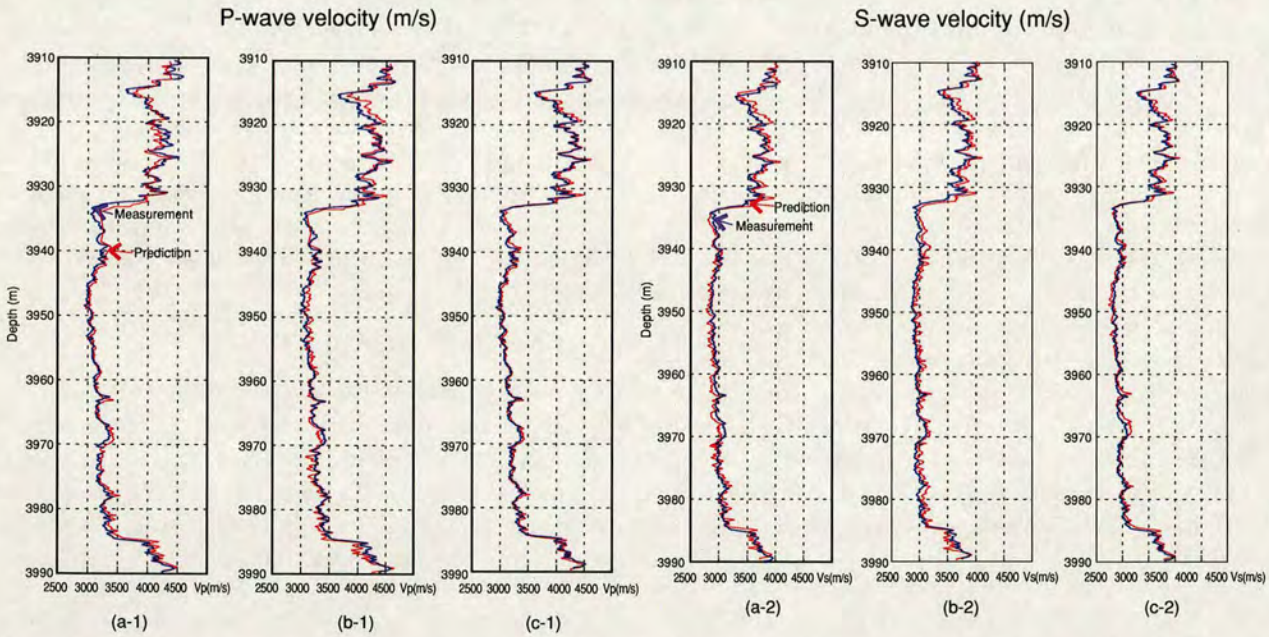

Figure 10 Comparison of predicted and measured P- and S-wave velocities in different models. (a-1) and (a-2) use Han *et al.*'s model for V_P and V_S, respectively; (b-1) and (b-2) use Xu and White's model for V_P and V_S, respectively; (c-1) and (c-2) use our semi-empirical model for V_P and V_S, respectively.

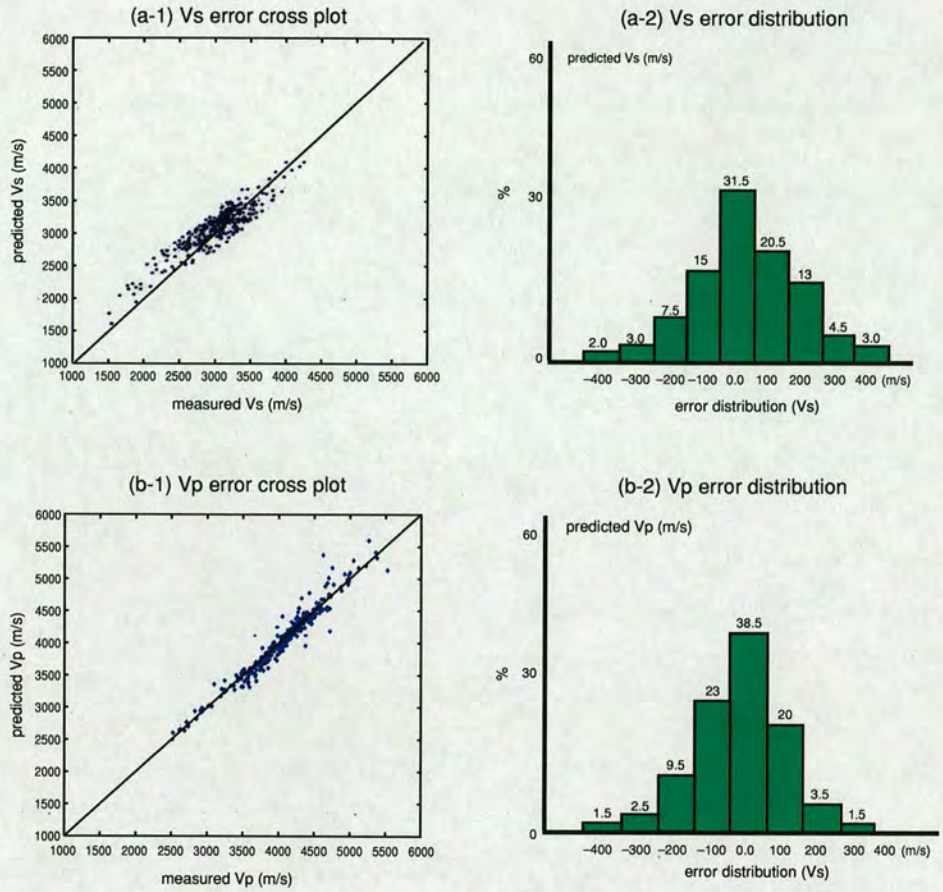

Figure 11 Error analysis of predicted and measured P- and S-wave velocities from the field data in the North Sea. The predicted velocities are determined from our semi-empirical model, the measured velocities are obtained from a dipole sonic log. (a-1) V_S error cross-plot; (a-2) V_S error distribution; (b-1) V_P error cross-plot; (b-2) V_P error distribution.

sponsors of the Edinburgh Anisotropy Project (EAP): Agip, BP, Chevron, Conoco, ExxonMobil, PGS, Phillips, Norsk Hydro, Schlumberger, Shell, Texaco, Trade Partner UK (DTI) and Veritas DGC. This paper is published with the approval of the Executive Director of the British Geological Survey (NERC) and the EAP sponsors.

REFERENCES

Brown J.S. and Korringa J. 1975. On the dependence of the elastic properties of a porous rock on the compressibility of the pore fluid. *Geophysics* **40**, 608–616.

Cheng C.H. and Toksöz M.N. 1979. Inversion of seismic velocities for the pore aspect ratio spectrum of a rock. *Journal of Geophysical Research* **84**, 7533–7543.

Dai H. and MacBeth C. 1994. Split shear-wave analysis using an artificial neural network. *First Break* **12**, 605–613.

Gassmann F. 1951. Elasticity of porous rocks. *Vierteljahrschrift der Naturforschenden Gesellschaft in Zürich* **96**, 1–21.

Gassmann F. 1952. Elastic waves through a packing of spheres. *Geophysics* **16**, 673–685.

Goldberg I. and Gurevich B. 1998. A semi-empirical velocity-porosity-clay model for petrophysical interpretation of P- and S-velocities. *Geophysical Prospecting* **46**, 217–285.

Han D.H., Nur A. and Morgan D. 1986. Effects of porosity and clay content on wave velocities in sandstones. *Geophysics* **51**, 2093–2107.

Klimentos T. 1991. The effects of porosity-permeability-clay content on the velocity of compressional wave. *Geophysics* **56**, 1930–1939.

Kuster G.T. and Toksöz M.N. 1974. Velocity and attenuation of seismic waves in two phase media: Part 1: Theoretical formulation. *Geophysics* **39**, 587–606.

Murphy W. 1984. Acoustic measures of partial gas saturations in tight sandstones. *Journal of Geophysical Research* **89**, 11549–11559.

Nur A. and Simmons G. 1969. The effect of saturation on velocity in low porosity rock. *Earth Planetary Science Letters* **7**, 183–193.

Sun Y.F. and Goldberg D. 1997. *Estimation of Aspect-Ratio Changes with Pressure from Seismic Velocities*, pp. 131–139. Geological Society Special Publication No. 122.

Wyllie M.R., Gregory A.R. and Gardner L.W. 1956. Elastic wave velocities in heterogeneous and porous media. *Geophysics* **21**, 41–70.

Xu S. and White R.E. 1995. A new velocity model for clay–sand mixtures. *Geophysical Prospecting* **43**, 91–118.

Xu S. and White R.E. 1996. A physical model for shear-wave velocity prediction. *Geophysical Prospecting* **44**, 687–717.

Yang J.O. 1995. *Interpretation of Well-Log Data for Reservoir Description*, pp. 54–79. The Petroleum Industry Press, Beijing (in Chinese).

APPENDIX

Scalars in Kuster and Toksöz (1974)

The scalars $T_{iijj}(\alpha)$ and $T_{ijij}(\alpha)$, which are used in the text, are given by

$$T_{iijj}(\alpha) = \frac{3F_1}{F_2}$$

and

$$T_{ijij}(\alpha) - \frac{T_{iijj}(\alpha)}{3} = \frac{2}{F_3} + \frac{1}{F_4} + \frac{F_4F_5 + F_6F_7 - F_8F_9}{F_2F_4},$$

where

$$F_1 = 1 + A\left[\frac{3}{2}(g+\phi) - R\left(\frac{3}{2}g + \phi - \frac{4}{3}\right)\right],$$

$$F_2 = 1 + A\left[1 + \frac{3}{2}(g+\phi) - \frac{R}{2}(3g+5\phi)\right] + B(3-4R) - \frac{A}{2}(A+3B)(3-4R)[g+\phi - R(g-\phi+2\phi^2)],$$

$$F_3 = 1 + \frac{A}{2}\left[R(2-\phi) + \frac{1+\alpha^2}{\alpha^2}g(R-1)\right],$$

$$F_4 = 1 + \frac{A}{4}\left[3\phi + g - R(g-\phi)\right],$$

$$F_5 = A\left[R\left(g+\phi-\frac{4}{3}\right) - g\right] + B\phi(3-4R),$$

$$F_6 = 1 + A[1 + g - R(g+\phi)] + B(1-\phi)(3-4R),$$

$$F_7 = 2 + \frac{A}{4}\left[9\phi + 3g - R(5\phi+3g)\right] + B\phi(3-4R),$$

$$F_8 = A\left[1 - 2R + \frac{g}{2}(R-1) + \frac{\phi}{2}(5R-3)\right] + B(1-\phi)(3-4R),$$

$$F_9 = A[g(R-1) - R\phi] + B\phi(3-4R),$$

with A, B and R given by $A = (\mu'/\mu) - 1$, $B = [(K'/K) - (\mu'/\mu)]/3$, $R = 3\mu/(3k+4\mu)$, and $g = \alpha^2(3\phi - 2)/(1-\alpha^2)$, $\phi = \alpha[\cos^{-1}\alpha - \alpha(1-\alpha^2)^{1/2}]/(1-\alpha^2)^{3/2}$. Here α denotes the aspect ratio; K and μ denote the bulk and shear moduli of the solid in which the pores are embedded; K' and μ' are the bulk and shear moduli of the inclusions.